Structural design and analysis of a 50kW wind turbine blade

GJ Kriel

20716524

Dissertation submitted in fulfilment of the requirements for the degree *Magister* in *Mechanical Engineering* at the Potchefstroom Campus of the North-West University

Supervisor: Dr AS Jonker

Co supervisor: Dr JJ Bosman

November 2015

ABSTRACT

Aero Energy, in conjunction with the North-West University and Stellenbosch University, is supplying small-scale wind turbines with power capacities of 1kW, 3kW and 10kW. The design of a 50kW blade is intended to serve as the next logical step in the process ladder to design even larger wind turbines, and at the end, reach the goal to design and manufacture wind turbines in the megawatt range. The design of the 50kW blade is thought to be rational as it lies near the boundary in distinguishing between small- and large-scale wind turbines. This project therefore covers the structural design, hence the design of the thickness distribution and topology of the structural subcomponents of the blade.

The structural design is performed by applying the loads from IEC 61400-2 to the aerodynamic shape obtained from a previous design. The loads are calculated according to IEC 61400-2's simplified load calculation method. The blade is divided into 10 sections and the loads are applied to the blade similar to the BEM method. A preliminary design is performed to determine the thickness distribution and topology of the structural subcomponents of the blade. These subcomponents consist of the blade's outer skin, spar caps and shear webs. The maximum stress criterion is used in the preliminary design due to the simplicity in its calculation and to validate the FEA model. The load-carrying spar caps' topology is optimised by determining the smallest cross-section area at each section of the blade that satisfies the design-required safety factor. This optimisation is performed to minimise the weight of the blade.

The thickness distribution and topology of the blade's subcomponents as obtained from the preliminary design are used to validate the FEA model performed with the commercially available software package Patran. Safety factor distribution results from performing an FEA on the blade, with the preliminary design thickness distribution and topology compared well with the design calculations. Thus, the application of the material properties, loads, layup sequence, layup orientation and meshing on the FEA model was validated.

The detailed structural design is performed by adjusting the thickness and topology of each of the subcomponents at each section of the blade to satisfy the design requirements. Safety factor and tip deflection are set as the design requirements for the blade. The detailed structural design is performed through several FEAs from which the results are analysed to perform the necessary adjustments. The results presented a relatively lightweight blade compared to those currently available in the market. The structural design process is verified by comparing the results obtained from performing the same analysis procedure on an existing composite propeller blade to that obtained from full-scale tests. The results from this FEA compared well with the full-scale test

results, therefore the structural design and analysis of the 50kW wind turbine blade are assumed to be adequate.

Key terms: Structural design, Finite element analysis, Wind turbine blade

ACKNOWLEDGEMENTS

Firstly, all praise to my heavenly Father for the strength He has given me during the duration of this study.

I would like to thank my family – parents Louis and Debbie, my sister Mariska and brother-in-law David – for their continued support and motivation throughout the duration of this study.

Thanks are also due to:
Dr Attie Jonker for his valuable advice as supervisor and for the financial support required to complete this study.

Dr Johan Bosman for his support as co-promoter of my study.

Mr Sarel van der Merwe and Mr Thabo Diobe for their help with the experimental setup of the propeller blade.

Mr Pieter Brand for his support throughout this study.

Michael Hindley, Christiaan Erasmus, Christopher Booysen and Mattie van Heerden for their motivation throughout the phase that I was completing this project on a part-time basis, and for the support with the finite element analysis of the blade.

Finally, to all my friends who continuously supported and motivated me to finish this project in times when my self-motivation was low.

TABLE OF CONTENTS

LIST OF FIGURES

LIST OF TABLES

LIST OF ABREVIATIONS

BEM	: Blade Element Momentum
BID	: Bi-directional
CAD	: Computer Aided Design
CFD	: Computational Fluid Dynamics
DMO	: Discrete Material Optimisation
FEA	: Finite Element Analysis
FEM	: Finite Element Method
FMB	: Failure Mechanism Based
GA	: Genetic Algorithm
GUI	: Graphic User Interface
LAP	: Laminate Analysis Program
PSO	: Particle Swarm Optimisation
SF	: Safety Factor
UD	: Unidirectional
VEPSO	: Vector Evaluated Particle Swarm Optimisation
NWU	: North-West University

LIST OF SYMBOLS

$A_{proj,B}$	:projected area of the blade	[m^2]
B	:number of blades	[-]
C_d	:drag coefficient	[-]
C_f	:force coefficient	[-]
C_{l_max}	:maximum lift coefficient	[-]
C_m	:pitching moment coefficient	[-]
C_T	:thrust coefficient	[-]
d_1	:distance from the point where the maximum bending moment is calculated to the first bearing on the blade root	[m]
F_a	:actual axial bearing load (see Figure D-1),	[kN]
$F_{cent,max}$	:maximum centrifugal force as calculated in Chapter 3	[kN]
F_i	:Force at section I of the blade	[N]
$F_{r,i}$	:actual radial load of bearing i (see Figure D-1)	[kN]
F_R	:reaction force at the root of the blade due to the loads on the blade	[N]
$F_{shear,max}$	:maximum shear force as calculated in Chapter 3	[kN]
F_{xB}	:force on the blade in the x-direction	[N]
F_{yB}	:force on the blade in the y-direction	[N]
F_{zB}	:force on the blade in the z-direction	[N]
G	:ratio between rated torque and short circuit torque for a generator	[-]
g	:acceleration due to gravity 9.81	[m/s^2]
I_B	:mass moment of inertia of the blade about the blade root flap axis	[kgm^2]
L_{rt}	:distance between the rotor axis and the yaw axis	[m]
m_B	:mass of the blade	[kg]
M_{brake}	:torque on the low speed shaft caused by the brake	[Nm]
M_i	:bending moment at section I of the blade	[Nm]
M_{max}	:maximum bending moment as calculated in Chapter 3	[Nm]
M_R	:total reaction moment at the root of the blade due to all the loads acting on the blade	[Nm]
$M_{x-shaft}$	:torsion moment on the rotor shaft at the first bearing	[Nm]
M_{xB}	:moment at the root of the blade about the x axis (edgewise bending moment)	[Nm]
M_{yB}	:moment at the root of the blade about the y-axis (flapwise bending moment)	[Nm]
M_{zB}	:moment at the root of the blade about the z axis (pitch moment about ¼ chord)	[Nm]
n_{design}	:design rotor speed	[rpm]
n_{max}	:maximum rotor speed	[rpm]

P_{design}	:design electrical power rating	[W]
P_0	:equivalent static bearing load	[kN]
Q_{design}	:design rotor torque	[Nm]
R	:radius of the rotor	[m]
R_{cog}	:radial distance between the centre of gravity of a blade and the rotor centre	[m]
V_{ave}	:annual average wind speed at hub height	[m/s]
V_{design}	:design wind speed	[m/s]
V_{e50}	:expected extreme wind speed (averaged over 3s), with a recurrence time interval of 50 years.	[m/s]
V_i	:shear force at section I of the blade	[N]
V_{ref}	:reference wind speed averaged over 10 minutes	[m/s]
X_0	:radial load factor for the bearing	[N]
Y_0	:axial load factor for the bearing	[N]
z	:reference height above ground	[m]
z_{hub}	:hub height of the wind turbine	[m]
η	:efficiency of the components between the electric output and the rotor	[-]
λ_{design}	:tip speed ratio at design rotational speed	[-]
λ_{e50}	:tip speed ratio at maximum rotational speed	[-]
ρ	:air density, here assumed 1.225 (as in IEC 61400-2)	[kg/m^3]
$\omega_{n,design}$	:design rotational speed of the rotor	[rad/s]
$\omega_{n,max}$	:maximum rotational speed of rotor	[rad/s]
$\omega_{yaw,max}$	:maximum yaw rate of the turbine	[rad/s]

CHAPTER 1 INTRODUCTION

1.1 Background

In recent years, renewable energy has attracted a great deal of attention all over the world. However, it is necessary to apply it in such a manner that the burning of fossil fuels and carbon dioxide emissions are minimised. The effects that the burning of fossils fuels and carbon dioxide emissions have on the planet could be seen in the environmental changes in terms of climate and weather. Drastic action should be taken to avoid the harsh consequences that could result if not taken seriously (Banks & Schäffler, 2006).

Wind as a form of renewable energy has attracted a great deal of attention over the past few years, with wind turbines being the main source of converting this wind energy to electricity. There are thousands of wind turbines currently in operation in various countries around the world, all of which are only generating power to make up about 1% of the total power generated in the world. Of all the wind turbines installed globally, 80% are centred in just four countries, which proves that most other countries fail to use wind as a renewable energy source (Patnaik, 2009).

Renewable energy, more specifically wind energy, is not yet sufficiently utilised in South Africa considering the great amount of wind energy that is available, especially in the coastal regions as well as the lowland and Highveld escarpment (Banks & Schäffler, 2006). According to international standards as referred to in Banks and Schäffler (2006), South Africa has fair to reasonable wind resources. This could also be validated by the first verified numerical Wind Atlas for South Africa as seen in Figure 1-1 (Wind Atlas for South Africa, 2013).

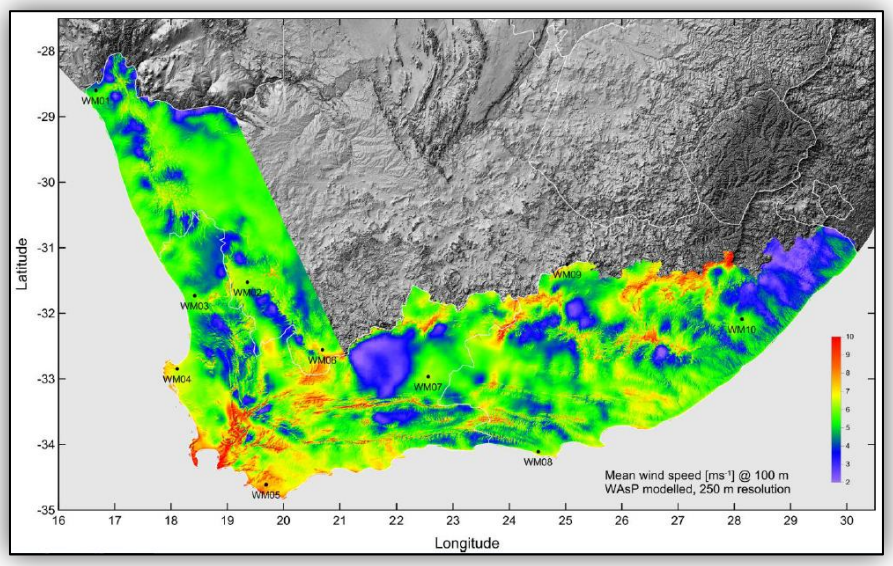

Figure 1-1: The Wind Atlas for South Africa displaying the mean wind speed distribution along the coastal regions of South Africa (Source: Wind Atlas for South Africa)

South Africa's main energy production source consists of coal-burning power stations, however, the use of wind turbines is starting to increase, according to studies by Teske *et al.* (2011). Benton (2006) stated that South Africa does not have many wind farms which supply the national grid but noted that there are numerous projects in progress attempting to solve this problem. Wind turbines that are currently used in South Africa are mainly small-scale wind turbines used for applications such as water pumping and battery charging (van der Linde, 1996).

Considering the wind turbine as a whole, the rotor blade is generally regarded as the most important component as it comprises 15 to 20% of the total production cost of the turbine (Jureczko *et al.*, 2005). The cost of the wind turbine blade is mainly owed to the materials in the blade, hence the materials that form the blade's shape and structure, providing strength and stability. The cost of the blade is therefore directly proportional to its weight, which is obtained from its structural materials. The optimisation of the blade's structure is consequently necessary to minimise its weight, hence cost, but still achieve sufficient strength and stability. In other words, a balance between cost and structural strength is needed to allow cost-effective operation of the blade (Liao *et al.*, 2011).

Jureczko *et al.* (2005) stated that the expenses in designing the wind turbine blade represent only a small amount of the overall cost of production and therefore it is necessary to apply numerical modelling and optimisation techniques to design a better structural model with suitable materials and better manufacturing methods to ensure that the manufacturing of the blade is cost effective.

Composite materials are used in wind turbine blades due to their high strength-to-weight ratio. Composite materials consist of fibre-reinforced polymers that are normally stacked in a number of layers. Each layer consists of fibres that are bonded together with resin to form a laminate (Gurit, 2011). The combination of these two or more materials in a laminate results in a material with better properties than those of the individual components used alone (Campbell, 2010).

The use of composites is optimised when each layer in a laminate is ordered in specific directions to provide high stiffness in the loading directions and lower stiffness in other directions. The weight of a blade can therefore be minimised by applying the least amount of layers possible, each orientated to provide sufficient strength and stiffness in the loading directions. This would ensure that no redundant fibres or material is applied to non-loaded areas, hence avoiding unnecessary weight (Stegmann & Lund, 2005).

The structural design process of a wind turbine blade consists of finding the above-mentioned loaded or stressed areas and applying enough composite materials to sufficiently withstand external loads. The structural design therefore consists of determining the topology of the subcomponents of

the blade that forms its structure and arranging the material in each component to provide sufficient strength and stiffness as shown in Figure 1-2 (Bottasso *et al.*, 2012). The subcomponents of a blade usually consist of the spar caps, shear webs and the outer skin (Bottasso *et al.*, 2012). The above-mentioned subcomponents are also shown in Figure 1-2.

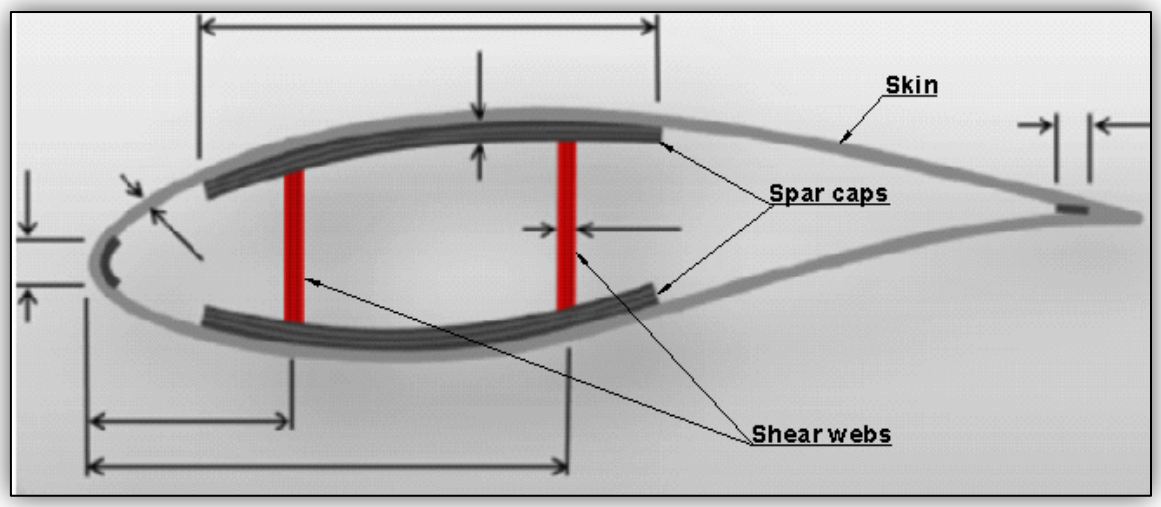

Figure 1-2: The subcomponents of a section of a wind turbine blade illustrating the topology of the design variables

According to Gurit (2011), the design of a wind turbine blade consists of finding the best compromise between the structural and aerodynamic efficiency. The choice of materials, material orientation, thickness distribution and internal structure are essential to the structural design process to construct a blade that will be strong and stiff enough to withstand ultimate and fatigue loads. However, all of the above-mentioned factors will influence the weight, hence aerodynamic efficiency and production cost of the blade (Gurit, 2011). This thesis will only commit to the structural design and analysis stages as the aerodynamic design, hence aerodynamic shape and optimisation is already completed.

Aero Energy, in conjunction with the North-West University (NWU) and Stellenbosch University, is supplying small-scale wind turbines with power capacities of 1kW, 3kW and 10kW. The design of a 50kW blade is intended to serve as the next logical step in the process ladder to design even larger wind turbines, and at the end, reach the goal to design and manufacture wind turbines in the megawatt range.

The design of the 50kW blade is thought to be rational as it lies near the boundary in distinguishing between small- and large-scale wind turbines. According to IEC 61400-2 (2006), the design requirements of a large wind turbine include that the wind turbine should have a swept area of at least 200m^2 and small wind turbines an area of up to 200m^2 (IEC, 2006). The swept area of the blade that will be designed in this project will be close to the 200m^2 mark.

This thesis will comply with the necessary studies to understand and optimise the structural design aspects of a 50kW wind turbine blade.

1.2 Problem statement

The structural dimensions of the 50kW Aero Energy wind turbine blade are unknown as a structural analysis has not yet been performed.

1.3 Objectives

The following objectives have been identified for this project:

1. Calculate external loads.
2. Design blade root end.
3. Calculate preliminary layup schedule of all subcomponents for validation of FEA model.
4. Set up finite element model.
5. Complete structural design and finite element analysis.
6. Obtain final layup schedule and subcomponent topology.
7. Verify structural design and analysis method.
8. Draw conclusions and recommendations.

1.4 Chapter breakdown

Chapter 2 provides a review of the published literature on the topics related to the objectives of this research. The aspects that influence the structural design of the blade will be discussed, particularly the cross-section design, fibre orientation and thickness distribution.

Chapter 3 presents the calculation of all the load cases as described in IEC 61400-2. The blade is divided into 10 elements or sections. The calculated loads are distributed over the length of the blade by applying a proportion of the load to each section of the blade. The magnitude of the proportion of the load applied to each section is derived from the ratio of each section's projected area to the projected area of the entire blade. Thus, the loads calculated are applied to the blade similar to the BEM method. With the loads distributed over the length of the blade and thus having loads at each section, bending moment- and shear force-distribution diagrams are plotted for all the load cases.

Overlay plots of all the loads in the same directions are generated to obtain the maximum loading the blade would experience when considering all the load cases. These maximum loadings in the principle direction would thus be used to perform the structural design of the blade in the following

chapters. Chapter 3 also includes the design/ selection of the pitch bearing where the root of the blade will be connected to the hub of the wind turbine. This bearing selection process is only performed to obtain the dimensions of the circular root end of the blade as this part was not designed in the aerodynamic geometry design phase of the blade. The aerodynamic shape/ geometry of the blade was designed prior to this project and does not form part of this thesis.

Chapter 4 includes the cross-section structural modelling of the blade as a composite beam structure to determine the thickness distribution and internal configuration, hence topology, of the subcomponents of the blade. The structural modelling of the blade is based on the maximum stress criterion, and the design stresses are calculated with the use of the partial safety factors as prescribed by IEC61400-2. This chapter thus consists of the mathematical modelling of the blade's subcomponents to obtain its thickness distribution and topology over the length of the blade. The subcomponents consist of the blade outer skin, the spar caps and the shear webs.

The thickness distribution and topology results obtained from this structural modelling serve as a preliminary design measurement, only to obtain approximate initial values. The blade is modelled with these preliminary design values for the thickness distribution and topology of the spar caps and an FEA is performed. The preliminary design is thus performed to obtain initial thickness distribution and topology values and to validate the FEA results that are used in the detailed structural design in the next chapter.

Chapter 5 covers the detailed structural design of the blade. The thickness distribution and topology of the blade's subcomponents is modified in the finite element analysis as each subcomponent was respectively designed in the previous chapter for a certain load while not taking the other subcomponents into account. This chapter therefore includes the setup of the finite element model, a description of how the load cases are applied to the blade and a detailed analysis of the FEA results to complete the structural design and therefore the topology of the subcomponents of the blade.

The topology and layup schedule of each subcomponent are therefore changed to comply with the predetermined design requirements, which are the safety factor and the tip displacement. The methodology for the structural design is based on adding or subtracting the number of layers in each of the subcomponents in order to obtain the required design safety factor in each subcomponent. After the required safety factor is obtained over whole length of the blade, the tip deflection of the blade is checked and adjustments are made to the layup schedule to obtain the required maximum tip deflection. The topology of the subcomponents is also modified to minimise stress concentration regions which was not accounted for in the mathematical design calculations in the previous chapter. This chapter also includes the verification of the results by comparing the

results of an FEA and a full scale test performed on an existing propeller blade. The existing blade is modelled in the same procedure as the blade designed in the thesis.

Chapter 6 is the conclusion to this research project and summarises the results obtained in comparison to the predictions and objectives set for this project. A proposal for future work will also be presented.

CHAPTER 2 LITERATURE REVIEW

2.1 Introduction

The structural design and manufacturing stages of a wind turbine consist of several aspects that influence the structural integrity and/or efficiency of the blade. In this chapter a literature survey is conducted to review the methods of previous research studies in terms of all the above-mentioned influencing aspects.

2.2 Design loads

The design loads that will be studied in this thesis will only include ultimate loads, as fatigue loads will exceed the scope of the project. There are different ways to predict and calculate the loads that a wind turbine blade would experience, but research has shown that the most common method of doing so is by using the Blade Element Momentum (BEM) method. Duan and Zhao (2010) stated that the current methods of calculating aerodynamic loads on a wind turbine blade include the BEM method as previously mentioned, Computational Fluid Dynamics (CFD) and wind tunnel testing (Duan & Zhao, 2010).

A fundamental step in the structural design stage of the blade is calculating the loads that the wind turbine blade would experience. It is the initial step in designing a blade to ensure sufficient stiffness, strength and stability to endure the most extreme wind conditions possible. Duan and Zhao (2010) created an aerodynamic mathematical model based on the BEM theory and considered the relationship between the gravity, centrifugal force and aerodynamic force in each blade element, as these three forces could be considered the principal load factors on the blade (Duan & Zhao, 2010).

Jiao and Sun (2011) used the BEM method as a theoretical basis to derive a formula to calculate the loads on a wind turbine blade and its components taking various factors into account, and finally created a software program to provide data support for future strength analysis of wind turbine blades (Jiao & Sun, 2011). Ingram (2011) also used the BEM theory with an iterative spreadsheet to calculate the axial and tangential induction factors. Together with the use of the lift and drag curves of the appropriate airfoils, the author calculated the loads acting on the blade (Ingram, 2011).

Wu and Young (2011) developed a graphical user interface (GUI) to design the blade model used for the stress analysis with the finite element analysis program ANSYS. In terms of the design loads the authors used the IEC 61400-1 standard to calculate the extreme wind speed that the blade should face in the parking stated. The authors then used this extreme wind speed to calculate the

lift and drag forces acting on the blade by using three different methods of which the BEM method was a part. The results of the study showed that the BEM method was an efficient method to calculate the wind loads on a wind turbine blade with certain accuracy (Wu & Young, 2011).

The IEC 61400-2 standards that state the design requirements for small wind turbines comprise three methods for calculating the design loads on the wind turbine. These include simplified equations to calculate the loads for wind turbines with certain configurations, the use of a structural dynamics model with design test data and limited full-scale load measurements to verify the model, and finally a full-scale load measurement of the conditions that the wind turbine would experience together with load extrapolation. The design requirements for the wind turbines in the IEC 61400-2 regulation apply only to wind turbines with a rotor swept area smaller than 200m^2.

The method for calculating the design loads used in this thesis is based on the IEC 61400-2 simplified load calculations. This method was chosen for its simplicity over the BEM, where a iteration process is needed to calculate the effective angle of attack at each blade element. The loads, however, are applied to the blade model similar to that of the BEM, where the loads are calculated and applied to each blade section.

2.3 Partial safety factors

Wind turbine blade design is normally based on a deterministic approach where the reliability of the component is predetermined. The blade design comprises several influencing variables, therefore the reliability of the blade can only be determined if all of these variables are considered. Partial safety factors are used to assure a safe and reliable design by accounting for the uncertainties and variability of these variables.

The IEC 61400-1 (IEC, 2005) standard defined these variables as the blade loads, materials, analysis methods and the importance of structural components with respect to the consequences of failure. The minimum clearance limit between the blade tip and the tower wall is also governed with partial safety factors.

Kong *et al.* (2005) specified the structural design requirements of the blade with the use of IEC1400-1 international specification and the GL regulations. The design requirements consisted of the strain limits along the fibre direction, minimum clearnace limit between blade tip and tower wall, surface stress limit and fatigue life. All of the aforementioned requirements were determined with partial safety factors (IEC, 2005; Kong *et al.*, 2005; Lloyd, 2010).

Wu and Young (2011) did not mention the use of any partial safety factors. The authors employed the failure criterion of the maximum principal stress for the blade and a safety factor was set as a

design goal. Details on how the safety factor design goal was determined were not specified. The authors also mentioned that the blade deflection was not constrained in the optimisation of the blade design (Wu & Young, 2011).

Ronold and Larsen (2000) presented a probabilistic model to analyse the safety of a wind turbine blade against failure in ultimate loading. The only failure condition considered was the flapwise bending during normal operation. The model consisted of an extreme-value analysis of the load response process together with a stochastic representation of the principal tensile strength of the blade material.

The model was used to analyse the reliability of a site-specific wind turbine with a prescribed make. The probability of flapwise bending failure was determined with a first order reliability method. A method to calibrate the partial safety factors for load and resistance with the use of the reliability analysis results was demonstrated. The authors prescribed this method for conventional deterministic design (Ronold & Larsen, 2000).

Different methods to calculate the partial safety factors are presented in literature as seen in the IEC61400-1 design specifications and the Germanischer Lloyd ceritification guidelines (IEC, 2005), (Lloyd, 2010). The IEC 61400-2 calculates a safety factor by considering the materials used in the blade and the loads calculated for the design of the blade. Each of the aforementioned considerations is used to calculate partial safety factors. The partial safety factor for materials is used to adjust the blade's strength to account for the uncertainty of the estimated material properties, with specified probalility and confidence limits. The safety factors for loads are used to account for the uncertainty in the load estimation process.

This thesis will implement the partial safety factors of the IEC61400-2 specifications as the load calculations are also based on this method. The partial safety factors permit a predefined reliability for the blade structure and could therefore be used to define the root design, thickness distribution, and cross-section design variables.

2.4 Root design

The design of the root region of a wind turbine blade can be considered a critical aspect in the structural design of the blade as the root end has to resist the maximum moments and torques developed by the aerodynamic loads and carried through the blade to the rotor shaft. The stresses and strains are therefore concentrated in the root section of the blade, which explains why the thickness of the composite materials is much thicker at the root end than the thickness at the tip of the blade.

The shape or geometry of the root end of a wind turbine blade cannot be designed with the use of simple design rules, criteria or rules of construction. The design of the root end is very complex and therefore the only design criteria of the geometry of the root end is that the airfoil shape should only be continuously and smoothly coalesced to the circular shape that connects the root to the hub flange (Habali & Saleh, 1999).

The authors calculated the thrust load on the swept area of the blades to calculate the moment at the root of the blade. They also calculated the stress within the root section and then with the use of the flexure formula they iterated to find the inner and outer diameter of the root, thus the thickness of the root (Habali & Saleh, 1999).

Wu and Young (2011) simplified the geometry of the wind turbine blade into two kinds of cross sections. They simplified the root section of the blade by analysing it as a cylindrical shape and the airfoil section of the blade as two parallel plates. They calculated the dimensions of the root by using the normal bending stress equation to determine the moment of inertia of the simplified cylindrical shape. The thickness and diameter of the root section was calculated and the process was iterated to optimise this section with the use of the failure criterion of the materials and a predetermined safety factor as a design goal (Wu & Young, 2011).

In this thesis, the moments at the root of the blade will be calculated and a pitch bearing will be designed to withstand the reaction forces. The diameter and thickness of the root section will be determined after the dimension (inner diameter) of the pitch bearing is known and a safety factor is calculated. The circular shape will then be smoothly and continuously coalesced with the airfoil shapes to avoid any stress concentration points on the blade.

2.5 Cross-section design

The cross-section design of a wind turbine blade is better described as the process in which the subcomponents or internal blade structure is designed, in other words, the load carrying beam which consists of spar caps and shear webs. According to Liao *et al.* (2012), the spar caps are the major load carrying components in the wind turbine blade structure, while the shell or outer skin of the blade provides for the minor shear stresses and aerodynamic shape (Liao *et al.*, 2011). The issues in the design of the blade's internal structure comprise the beam type (Box-beam, I-beam, D-spar etc.) and the topology of the materials used in the beam to withstand different load cases.

A cross-sectional analysis code was developed by Visweswaraiah (2010) for the preliminary analysis and structural optimisation stages in composite rotor blade design. The author presented various parametric studies to emphasise the effect of internal geometry changes on the structural stiffness and coupling stiffness of the blade. The changes in the internal geometry used in

Visweswaraiah's study included the web inclination angle of the spar and the distance of the shear web from the leading edge. The author also performed a multi-objective optimisation process on a helicopter rotor blade using the min-max approach. The results of the blades with and without the internal geometry changes were compared to emphasise the role of the internal geometry variables in the structural design of composite rotor blades (Visweswaraiah, 2010).

De Goeij *et al.* (1999) investigated the implementation of bending-torsion coupling of a composite wind turbine blade to provide passive pitch-control. The authors realised that the passive torsion deformation in a constant speed rotor blade is limited with a structural coupling between flapwise bending and elastic twist. They also discovered that the conventional blade configuration where the complete blade with shell, spar caps, and shear webs is modelled and analysed together had some disadvantages. These disadvantages encouraged the authors to review different design concepts, where the coupling plies are only utilised in the load carrying spars, while the softer skin material provides the aerodynamic shape.

De Goeij *et al.* (1999) compared different spar web configurations in terms of structural and manufacturing advantages and disadvantages. The authors found that box beams are more effective and strain incompatibilities at the joints are bypassed. Further studies by these authors proved the coupled double box spar to be the most efficient internal structure to accommodate passive pitch control (de Goeij *et al.*, 1999).

Blasques and Stolpe (2012) presented a framework where the topology and laminate properties are simultaneously optimised in the structural design of laminated composite beam cross-sections. They used a beam finite element model and a cross-section analysis tool, suitable for the analysis of anisotropic and inhomogeneous sections of arbitrary geometry, to evaluate the structural response of the beam. The amount of the given materials in the cross-section represented the design variables used in their multi-material topology optimisation model. They also extended the model to accommodate any amount of anisotropic materials by extending existing material interpolation, penalisation and filtering schemes. Their methodology was applied to several composite beams with different cross-sections and solutions to a maximum stiffness problem with constraints on weight, shear- and mass centre positions presented (Blasques & Stolpe, 2012).

Liao *et al.* (2012) developed and programmed a multi-criteria optimum design model for wind turbine blades, based on the blade layers. The aim of the model was to attain minimum blade mass and reduce the cost of wind turbine production. The thickness and location of the layers on the spar caps was the chosen optimisation variables as they are the main parts to endure the loads. The maximum tip deflection was highlighted as a major design criterion to be satisfied. An improved

particle swarm optimisation (PSO) algorithm was used to find the optimum solution (Liao *et al.*, 2011).

The cross-section design of composite laminate wind turbine blades and/or beams has become a major subject for the optimisation of the blades. The review of different researchers' studies provided various methods for the cross-section design, each focussing on different aspects. Some studies focused on the formulation of the beam model while others studied the beam topology or the topology of the beam materials. However, the cross-section design approaches of various researchers differed, they all used some sort of optimisation method that required different criteria to be satisfied with different design variables.

In this thesis the cross-section of the wind turbine blade will be designed using an optimisation model with predetermined design criteria and variables. The details on the optimisation method will be reviewed in chapter 2.8

2.6 Thickness distribution

Considering the previous chapter the thickness distribution also forms part of the blade's cross-section. However, this chapter is aimed at the distribution of the outer skin or shell materials, which as previously mentioned only, endure the shear loads and provide the aerodynamic shape.

The thickness of the laminates that a wind turbine blade consists of varies continuously from root to tip, as the moments and torques transmitted by aerodynamic loads decrease from the root to the tip of the blade. The maximum moments and torque that the blade experiences occur in the root section and therefore the laminate thickness will be a maximum to withstand the resultant maximum stresses and strains as also stated by Habali and Saleh (1999).

Wu and Young (2011) set a goal to sufficiently arrange the materials in a 3.5m blade to reach the optimal utilisation of the material strength in order to withstand various load cases in operation and parking state, thus reducing the weight of the blade. The authors based their design on the failure criterion of the materials used in the blade. They simplified the blade as previously mentioned (section 2.4) into two types of cross sections which consisted of the root section and the airfoil section. The root section was simplified as a cylindrical shape and the airfoil section of the blade was simplified as two parallel plates. The authors made use of an iterative process in which the thickness of each element was determined according to a predetermined safety factor (Wu & Young, 2011).

Lanting (2012) determined four different lay-up schemes according to the loading characteristics and stress relationship of the composite blade. The author calculated the stress relationship of

different cross-sections and thereby calculated the main ratio between positive stress and shear stress. With the use of these ratios the author determined four different lay-up schemes by varying the fibre orientation to resist different stresses. The author used the maximum stress criterion in his study to find the lay-up scheme that permits maximum strength and stiffness (Lanting, 2012).

Liao *et al.* (2012) optimised their lay-up scheme by developing a multi-criteria constrained design model. The aim of their study was to minimise the weight of the blade to reduce its cost and with the use of an improved PSO algorithm they determined the thickness distribution and layer location in the spar caps as this was selected as the design variables (Liao *et al.*, 2011).

Kong *et al.* (2005) used a finite element method (FEM) to determine the optimal structural configuration through a parametric study. The design variables, which included the thickness distribution of the composite material and many others, was varied until the design criteria was satisfied. The design criteria that the blade had to satisfy included minimum clearance limit between the blade tip and the tower wall, the strain limits along the fibre direction, surface stress limit and fatigue life time of over 20 years (Kong *et al.*, 2005).

The process of determining the thickness distribution of the wind turbine blade skin is very similar to that of the beam design. Both these components in the wind turbine blade are designed with the use of different variables and constraints to satisfy predetermined optimisation criteria. The literature shows that blade weight and structural requirements such as blade tip deflection, maximum stress limits and fatigue life are the most common design goals to validate the thickness distribution of the materials in a wind turbine blade.

The thickness distribution of the blade designed in this thesis was determined with the use of the maximum-stress criterion. The blade was divided into 10 sections and the thickness of each section was determined to satisfy the maximum-stress criterion. This resulted in a thickness distribution along the entire blade. This procedure is similar to the one used in Wu and Young's (2011) study. This thickness distribution will then only be used as a preliminary or initial input parameter for the FEA. The thickness distribution is then adjusted and modified until the design constraints are satisfied.

2.7 Fibre orientation

The costs of a wind turbine blade make up about 15 to 20% of the total production cost of the entire wind turbine (Jureczko *et al.*, 2005). The costs of the blade are directly proportional to the blade weight and therefore the material quantity of which the blade consists. Thus, the cost of the blade will decrease as the material quantity decreases, hence the laminate thickness or ply amount decreases. It is possible to minimise the blade weight with the use of fewer composite materials by

arranging the materials in a sufficient way so the fibres are directed in the loaded areas to utilise optimal material strength (Wu & Young, 2011).

One of the key concepts to optimise matertial strength is to apply aeroelastic tailoring. Aeroelastic tailoring has been defined as “the (incorporation) of directional stiffness into an aircraft’s structural design to control aeroelastic deformation, whether static or dynamic, in such a fashion as to affect the aerodynamic and structural performances of that aircraft in a beneficial way” (Weisshaar, 1987). De Goeij *et al.* (1999) stated that aeroelastic tailoring is a method used to avoid typical design problems, such as the necessity to add material, hence weight, in order to satisfy certain design criteria such as strength and stiffness requirements.

Stegmann and Lund (2004) presented a method to solve the orientation and selection of orthotropic material problems, as well as the problems involving both. The method utilised a combination of gradient information with mathematical programming to solve a discrete optimisation problem. It is therefore labelled as a Discrete Material Optimisation (DMO) method.

The last-mentioned method was based on the ideas from multi-topology optimisation. This enabled the method to achieve a general parameterisation that reduced the risk of obtaining a local optimum solution for the tested configurations. The authors demonstrated the applicability of the DMO method by optimising the fibre orientations of a cantilever beam (Stegmann & Lund, 2005).

Liu *et al.* (2012) proposed a solution for the simultaneous optimisation of the layup configuration and fibre distribution of laminated plates to obtain a maximum stiffness design. It was found that the optimal lamination parameters for maximum stiffness could be obtained by using the ply thickness, fibre orientation angle and fibre volume fraction in a laminated plate of least ply groups as design variables. The optimal lamination parameters were set as the design objective followed by the implementation of the optimised detailed layup design regarding predetermined manufacturing limitations. These limitations consisted of preset ply thickness, fibre orientation angles and the limit of consecutive plies with the same fibre orientation (Liu *et al.*, 2012).

The litarature available containing studies in the design or tailoring of the fibre orientation angles can be summarised in different categories. These categories are the design criteria, constraints and the method of finding the optimum point that satisfy the design criteria and constraints. The maximum stiffness criterion and failure criteria such as the maximum stress, Tsai-Wu, and failure mechanism based (FMB) are examples of the design criteria category as employed by Liu *et al.* (2012) and Narayana Naik *et al.* (2011) respectively.

The constraints in the design of fibre ply angles are based on the minimisation of the blade weight and/or elastic deformation, in other words, maximum ply thickness, laminate thickness and tip deflection as described by Liu *et al* (2012) and Liao *et al.* (2012). The different methods of determining the optimium point that satisfies the criteria and constraints can be seen in the work of Lund (2009), Luo and Gea (1998), Narayana Naik *et al.* (2011) and Liao *et al.* (2012). The last-mentioned authors used the DMO method, energy-based method, VEPSO and GA methods and PSO method respectively.

The fibre orientations used in the subcomponents of the wind turbine blade designed in this study will be based on the type of loading that it should resist as presented by Mishnaevsky (2011). According to Mishnaevsky (2011), the shell (or skin as it is refered to in this thesis) has to maintain the blade shape and resist the the wind and gravitational loads. Thus, the shear forces are the main loading that the shell/skin has to resist due to torsional loading on the blade. Bi-directional fibreglass angled at 45° is utilised in the skin to withstand these shear forces.

The spar caps are designed with unidirectional fibreglass oriented in the 0º direction along the length of the blade to withstand the flapwise bending loads and axial centrifugal loads. The shear webs are self explanatory in name and have to withstand the shear stresses caused by the flapwise bending. The shear webs, similar to the shell/skin, are designed with bi-directional fibreglass angled at 45º. The layup schemes from the different stress situations will then be added together and the resultant scheme will be optimised in terms of bending stiffness and tip deflection.

2.8 Optimisation

The literature in Chapter 2, sections 2.2.4 - 2.2.6 shows that the thickness distribution, cross-section or beam design and laminate fibre orientation are the most popular subjects in wind turbine blade optimisation. The main objective of the optimisation of a wind turbine blade is to minimise its weight while maintaining structural strength and stiffness to withstand the design loads without failure. In the preceding chapters the optimisation methods of different researchers were explained. Each of these methods has different design criteria and constraints. The similarity in the methods is in the variables, which consist either of the thickness distibution of the spar caps and blade skin, or the orientation of the laminate fibres.

Optimisation of the blade is not considered a focal point in this thesis. Thus, no methods using algorithms focused on blade optimisation are used. However, a method for determining an optimum spar cap topology to minimise the weight of the spar caps is performed in the preliminary design stage. This method involves selecting the spar cap topology with a width and thickness combination that provides the smallest cross-section area that satisfies the design strength requirements.

2.9 Finite element analysis

In the design phases prior to manufacturing the wind turbine blade model is usually subjected to a finite element analysis. During the finite element analysis the blade is modelled to simulate the loading and structural properties and to predict or verify the stress and deformation results.

Duan and Zhao (2010) applied a finite element numerical analysis on a blade to obtain the stress distribution in the blade. The finite element analysis was thereby used for strength checking of the blade.

Benchly and Clausen (1997) wrote a program to create a detailed finite element mesh of a 2.5-metre-long fibreglass composite wind turbine blade. The design data from the blade element theory and panel code predictions was used to write this program, which was written in a suitable format to be imported into a commercially available finite element software program. The results from the finite element program compared well with static test deflections and the fisrt two natural frequencies of vibration (Benchly & Clausen, 1997).

Jensen *et al.* (2006) measured the ovalisation of the load carrying box girder in a 34-metre composite wind turbine blade. The measurement was done in a full-scale test and was simulated in non-linear finite element calculations. The ovalisation was caused by a crushing pressure that characterised the non-linear Brazzier effect. Non-linear finite element analyses at different scales were employed on different scales to capture the effect. A non-linear finite element model of the blade was used to extract the boundaries to a more detailed sub-model. The finite element model was calibrated based on the full-scale measurements (Jensen *et al.*, 2006).

Lanting (2012) used a finite element analysis software package ANSYS for stress-strain analysis of a 1.2MW wind turbine blade. The analysis was used to verify that the designed blade structure was safe under extreme load conditions (Lanting, 2012). Jureczko *et al.* (2005) also made use of finite element analysis software for performing multi-criteria discrete-continuous optimisation of a wind turbine blade.

The commercially available finite element analysis software package MSC Patran is used in this thesis to determine the final structural dimensions of the wind turbine blade. Linear elastic analyses were performed to obtain the safety factor distribution and tip deflection results. The blade simulation is verified by comparing the finite element and test results of an existing wind turbine blade.

2.10 Summary

The structural design stage of the wind turbine blade can be summarised as the design and optimisation of all the subcomponents of which the blade consists. These subcomponents comprise the blade skin materials and the internal load carrying structure, in other words, the spar caps and shear web. The literature showed different concepts and methods for the structural design of the blade, although the methods that will be used in this thesis are summarised in the paragraph which follows.

The external loads acting on the blade were determined using the IEC 61400-2 simplified load calculation method and applied to the blade similar to the BEM method. The design required safety factors were also determined as prescribed by IEC 61400-2. Since the root of the blade does not consist of a circular shape that could be connected to a variable pitch hub, bearings at the root end will be selected. The selection of the root bearings will thus only be performed to obtain the diameter of the root end of the blade that could therefore be smoothly coalesced into the airfoil shape of the blade.

The thickness distribution and topology of the subcomponents of the blade, hence its cross-section, will be designed in a preliminary design where initial thicknesses and topologies are calculated with the use of the maximum stress criterion. The fibre orientation of the materials in the respective subcomponents will be aligned at 0 degrees along the blade length for the spar caps and 45 degrees for the skin and shear webs. The topology of the spar caps will be optimised by determining a width-and thickness combination that provides the small cross-section area in order to minimise the weight of the blade.

The thickness distribution and topology design values obtained from the preliminary design will then be used as initial values to perform the detailed structural design. The detailed structural design is performed through several FEA runs where the thickness distribution and topology of the blade's subcomponents are adjusted to satisfy the design requirements while exposed to the maximum load.

CHAPTER 3 DESIGN LOADS

According to Habali and Saleh (1999), enormous amounts of data are required for the design and construction of sophisticated wind turbine blades, especially the components describing its geometry and structural characteristics. The geometry or aerodynamic shape of the blade in this thesis was already designed and thus the structural design could be initiated.

The first step in the structural design phase is to calculate and determine the external loads that the wind turbine blade should withstand. This thesis only considers ultimate loads and therefore fatigue loads are not considered. The loads are calculated according to the simplified load calculation method of the IEC 61400-2 design requirements (IEC, 2006).

To avoid confusion, the symbols, subscripts, terms and abbreviations of the variables in the design equations in this thesis are used similar to those used in the IEC 61400-2 design requirements. Therefore, the same coordinate system to define the direction of the loads is used, as illustrated in Figure 3-1.

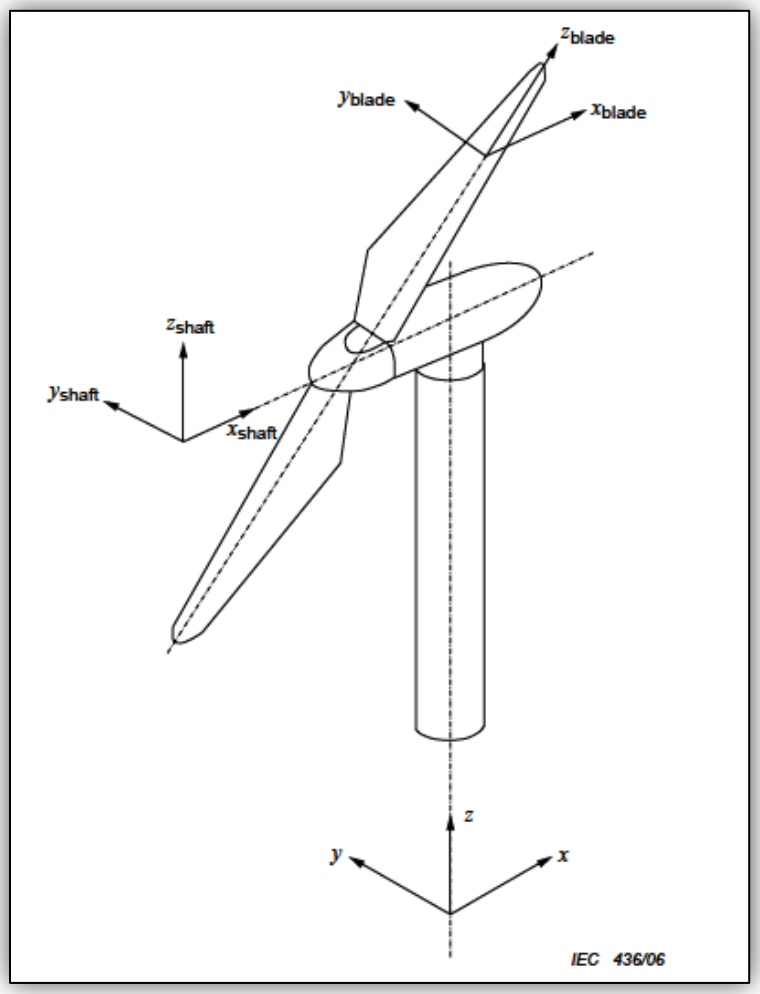

Figure 3-1 : The coordinate system defining the directions of the loads

IEC 61400-2 presents 10 load cases for the design of a wind turbine blade. The load case that complies with transportation, assembly, maintenance and repair, referring to “Load case J”, is eliminated from the list of design load cases used in this thesis. The equations for the design of the shaft of the wind turbine are also eliminated as only the equations for the loads on the blade are significant for this thesis.

The load equations used in this thesis therefore could be listed as load case B to load case I, with the addition of an extra load case that considers the torsion on the blade (moment about the z-axis). It is not included in IEC61400-2. The last-mentioned load case is added as it is required for the design of the thickness distribution of the blade’s outer skin.

3.1 Design load case equations

Load case B: Yawing

This load case calculates the ultimate loads on the blade caused by gyroscopic forces and moments, assuming it operates at maximum yaw speed $\omega_{yaw,max}$ and design rotor speed n_{design}.

$$M_{yB} = m_B \omega_{yaw,max}^2 L_{rt} R_{cog} + 2\omega_{yaw,max} I_B \omega_{n,design} + \frac{R}{9} \Delta F_{x-shaft} \qquad (3\text{-}1)$$

where,

$$\Delta F_{x-shaft} = \frac{3}{2} \frac{\lambda_{design} Q_{design}}{R} \qquad (3\text{-}2)$$

and for a wind turbine with a passive yaw system the maximum yaw rate is given by Equation (3-3).

$$\omega_{yaw,max} = 3 - 0.01(\pi R^2 - 2) \qquad (3\text{-}3)$$

Load case C: Yaw error

According to IEC (2006), all wind turbines operate with a certain yaw error. A yaw error of 30^o is assumed for this load case as prescribed in IEC (2006). Therefore, the flapwise bending moment (moment about y-axis) caused by the yaw error is given by equation (3-4).

$$M_{yB} = \frac{1}{8} \rho A_{proj.B} C_{l,max} R^3 \omega_{n,design}^2 \left[1 + \frac{4}{3\lambda_{design}} + \left(\frac{1}{\lambda_{design}} \right)^2 \right] \qquad (3\text{-}4)$$

Load case D: Maximum thrust

This load case describes the thrust load on the rotor shaft and, as previously mentioned, the loads on the shaft are eliminated. However, this load case is used to determine the maximum thrust load

on the blades by dividing the load on the shaft by the number of blades on the turbine, hence three. The maximum value for the thrust load is given by Equation (3-5).

$$F_{x,B} = (C_T \, \mathbf{3.125} \, \rho V_{ave}^2 \, \pi R^2)/B \tag{3-5}$$

where,

C_T is the thrust coefficient and according to (IEC, 2006) has a value of 0,5.

Load case E: Maximum rotational speed

The following Equation (3-6) gives the load due to the centrifugal forces on the blade when rotating at maximum rotation speed.

$$F_{z,B} = m_B \omega_{n,max}^2 R_{cog} \tag{3-6}$$

Load case F: Short at load connection

This load case is caused by an electrical short at the output of the wind turbine or internal short in the generator. A moment is created about the rotor shaft due to the short circuit torque of the alternator.

$$M_{x,B} = \frac{M_{x-shaft}}{B} \tag{3-7}$$

where,

$$M_{x-shaft} = GQ_{design} \tag{3-8}$$

Load case G: Shutdown (braking)

According to IEC (2006), a mechanical or electrical brake system in a wind turbine can cause a high breaking moment. The moment caused by the braking system on the wind turbine blade is given by Equation (3-8). Note that the $M_{x\text{-shaft}}$ in equation (3-10) is not the same as used in Equation (3-8) as the cause of the moments differs.

$$M_{x,B} = \frac{M_{x-shaft}}{B} + m_B g R_{cog} \tag{3-9}$$

where,

$$M_{x-shaft} = M_{brake} + Q_{design} \tag{3-10}$$

Load case H: Parked wind loading

The load on the blades in this load case is calculated for a parked wind turbine exposed to a wind speed of V_{e50}. This load case consists of two scenarios.

The first scenario is for a parked wind turbine which, according to IEC (2006), will experience an out of plane root bending moment that will be dominated by drag, thus giving Equation (3-11).

$$M_{y,B} = C_d \frac{\mathbf{1}}{\mathbf{4}} \rho V_{e\mathbf{50}}^{\mathbf{2}} A_{proj,B} R \tag{3-11}$$

where,

C_d is the drag coefficient and shall be taken as 1,5, and

$A_{proj,B}$ is the planform area of the blade.

The second scenario is for a wind turbine with its rotor spinning at V_{e50}. According to IEC (2006), it is expected that at some location on one of the blades, maximum lift will occur. Thus, the blade root bending moment is:

$$M_{y,B} = C_{l,max} \frac{1}{6} \rho V_{e50}^2 A_{proj,B} R \tag{3-12}$$

where,

$C_{l,max}$ is the maximum lift coefficient with a value of 2,0 according to IEC (2006), if no data is available as it is in this case.

Load case I: Parked wind loading (maximum exposure)

This load case considers a scenario of a possible failed yaw mechanism. In such a case the wind turbine blade can be exposed to wind from all directions. Thus, for design purposes, the forces on the blade should be calculated for all possible wind exposures. In this study only flapwise exposure to the wind will be calculated for this load case, as it will cause the maximum bending stress in comparison to other exposure scenarios.

The flapwise load on the blade is given by:

$$F_{x,B} = C_f \frac{1}{2} \rho V_{ref}^2 A_{proj,B} \tag{3-13}$$

where,

C_f is the force coefficient which may result from lift or drag. A value of 2 is given to C_f according to IEC (2006).

Load case J: Maximum torsion load (not included in IEC 61400-2)

An additional load case is created to consider the torsion load that the blade would experience at maximum rotational speeds. This is necessary as it is used to design the blade skin thickness as the skin is the main component that withstands this load.

The torsion load at maximum rotational speed is given by:

$$M_{z,B} = C_m \frac{1}{2} \rho V_{max}^2 A_{proj,B} L_c \quad (3\text{-}14)$$

where,

C_m is the torsion moment coefficient

V_{max} is the velocity of the fluid (air) over the blade at maximum rotational speed

L_c is the chord length of the blade.

(Note that the blade is divided into 10 sections in order to calculate the torsion at each section.)

The calculation of the values of each of the variables used in the equations shown in Chapter 3, section 3.1 is presented in Appendix A, while the calculated load cases are presented in Appendix B.

3.2 Load distribution

The loads calculated in Chapter 3, section 3.1 are distributed over the blade surface to determine a layup thickness distribution and to perform a preliminary structural design of the blade. Therefore, the blade is divided into 10 sections and the loads calculated in Chapter 3, section 3.1 are distributed over the length of the blade in terms of the projected area of each section. The distributed loads are used directly in the structural analysis of the blade, where these loads at each section are applied to the blade surface in the finite element analysis.

Figure 3-2 shows the original blade geometry as it was obtained after the aerodynamic design was completed. Note that this blade does not comprise a circular root section that could be connected to the hub of the wind turbine, as this section of the blade still has to be designed. The design of the root section is covered in Chapter 3, section 3.4.

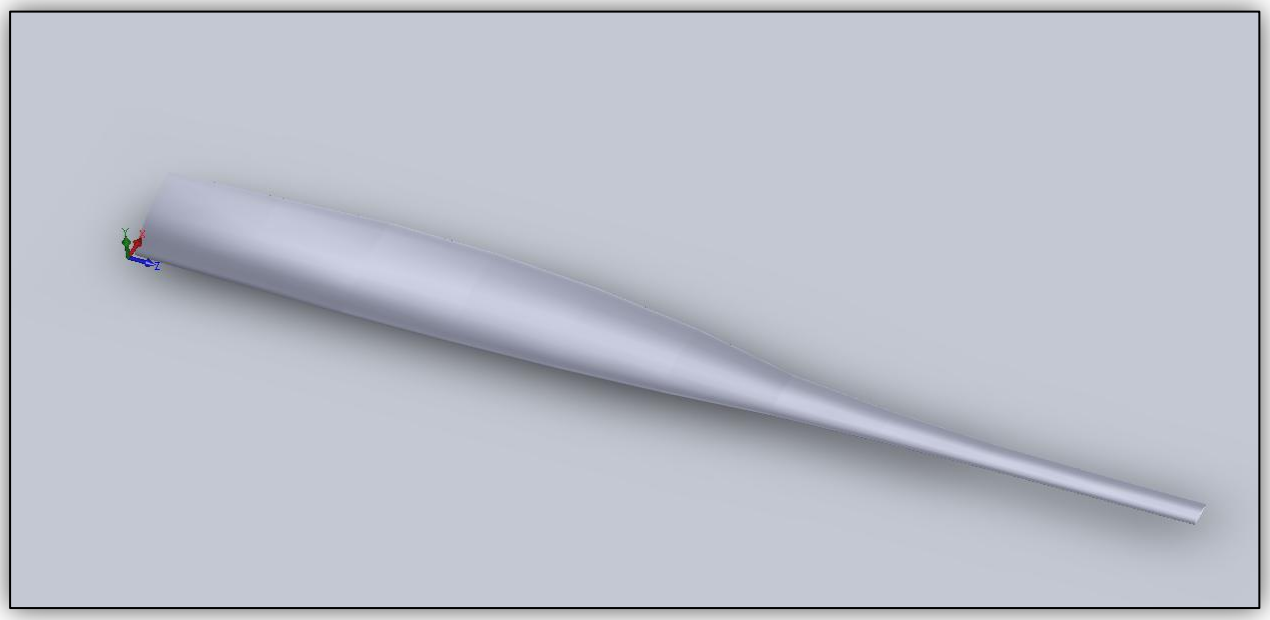

Figure 3-2: The original blade geometry as obtained after aerodynamic design was completed

Figure 3-3 shows the blade divided into 10 equal sections over the length of the blade. Figure 3-4 shows the projected areas of each section of the blade.

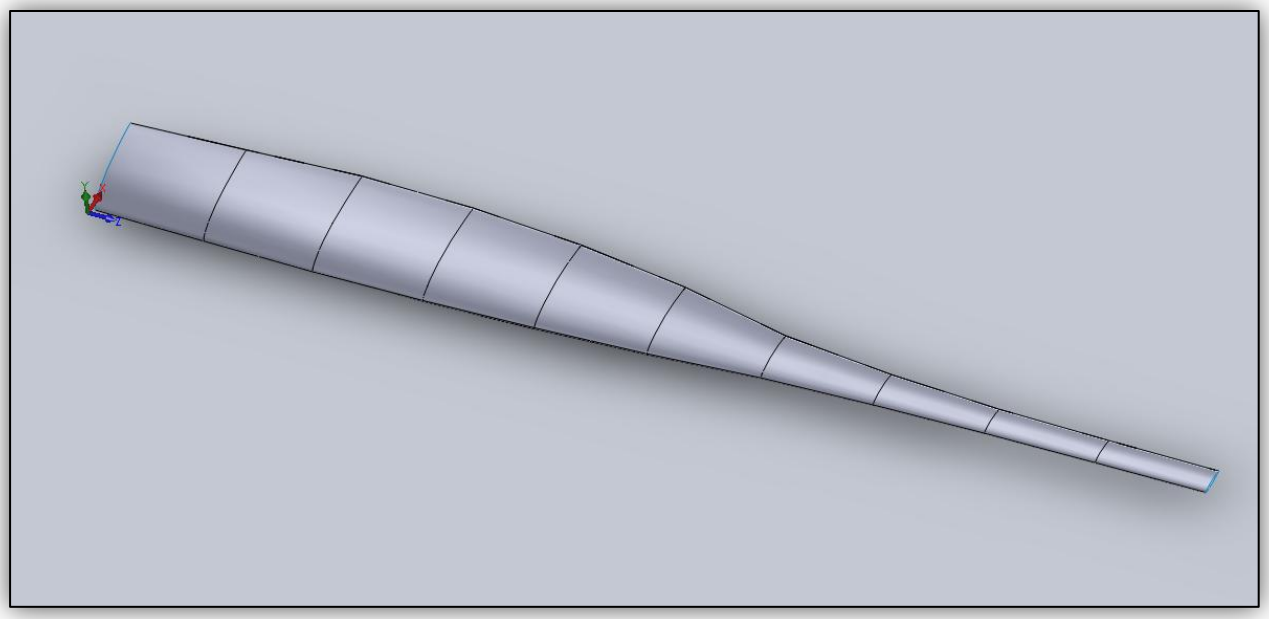

Figure 3-3: The blade divided into 10 sections

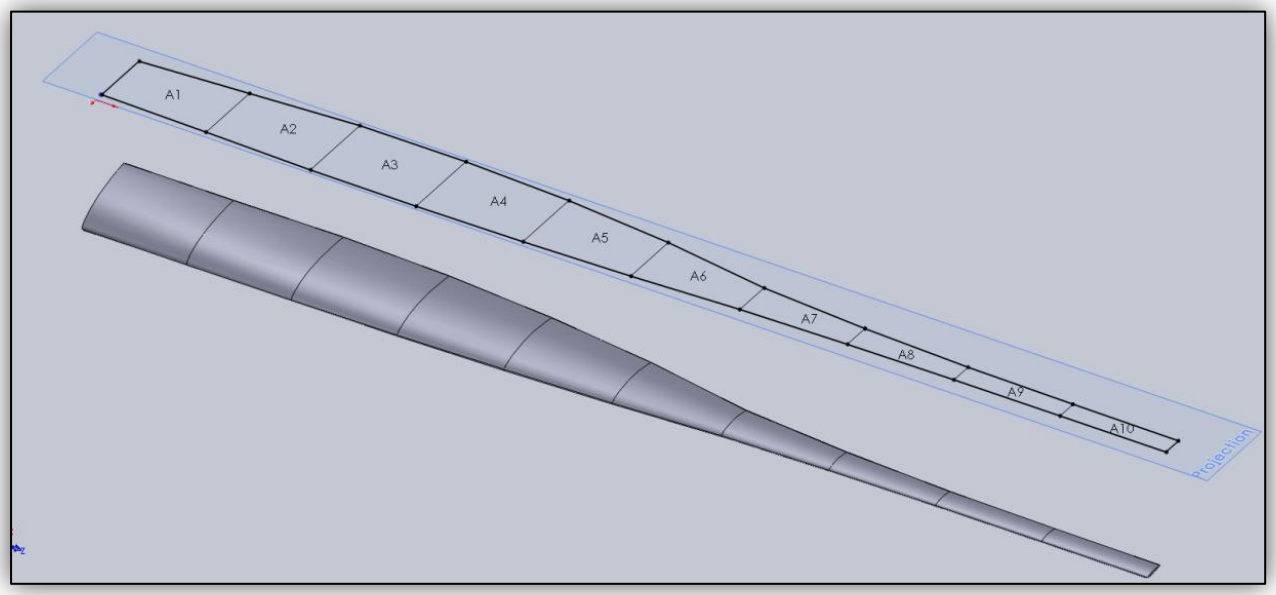

Figure 3-4: The projected areas of the blade sections

The loads are distributed over the length of the blade surface by dividing the loads calculated in Chapter 3, section 3.1 by the proportion of the projected area of each section to the total projected area of the blade. Note that design load cases D, E and I provides forces acting on the blade whereas B, C, F, G, H, and J provide bending moments. Equation (3-15) shows the calculation of the force at each section of the blade for the design load cases that provide forces.

$$F_i = F_T \frac{A_{proj,i}}{A_{proj,T}} \tag{3-15}$$

where

F_i is the force calculated for section i

F_T is the total force as calculated in the design load cases in Chapter 3.1. (D, E, and I)

$A_{proj,i}$ is the projected area of section i

$A_{proj,T}$ is the total projected area of the blade.

The bending moment distribution for the load cases that provides force is determined with the distance of each section from the root of the blade. Note the blade is modelled as a cantilever beam with the root end as a fixed constraint. The bending moment at each section of the blade is needed in order to obtain the bending moment distribution graphs. Therefore, the bending moment at each section is calculated in Equation (3-16).

$$M_i = F_i d_i \tag{3-16}$$

where

M_i is the bending moment about axis x, y or z (depending on the orientation of the applied load case) at section i.

d_i is the displacement of section i from the root of the blade. (Figure 3-5 shows the distances at which each force and moment was calculated.)

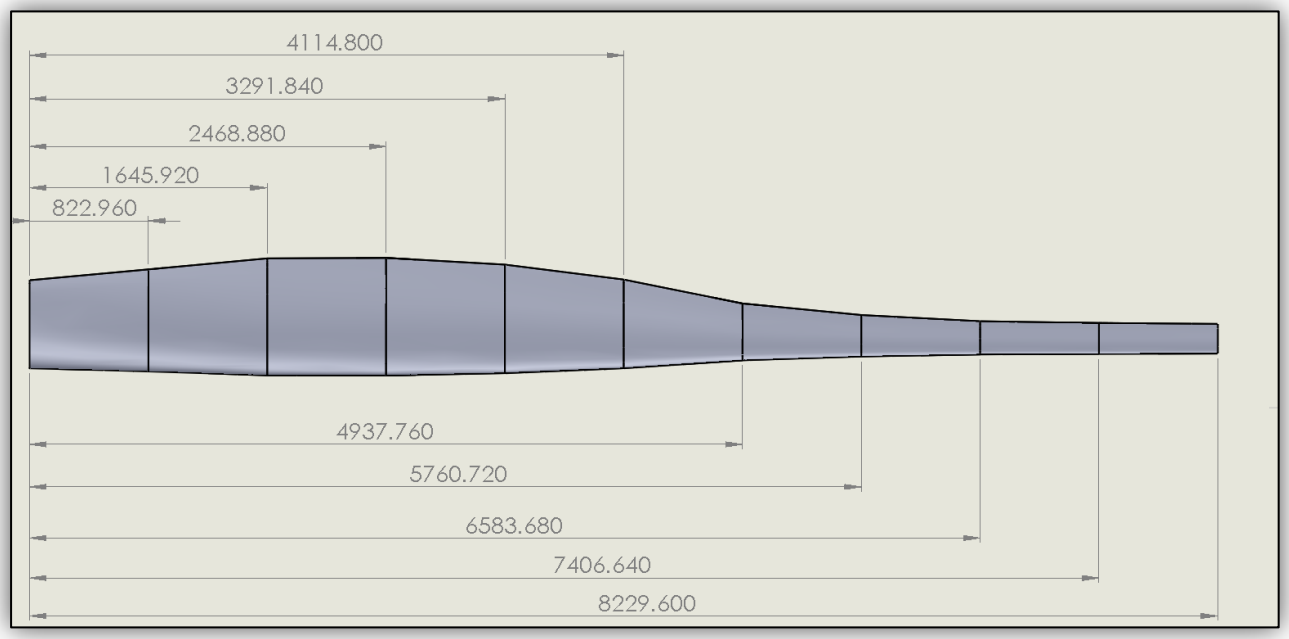

Figure 3-5: The displacements of all the blade sections from the fixed root end of the blade

The moments and forces at each section of the blade calculated from the design load cases in Chapter 3, section 3.1 that provide bending moments are also calculated in this way, except the moments are now multiplied by the proportion ratio of the section's projected area to the total projected area. Thus, for the design load cases providing bending moments, the moments at the root of the blade are determined with Equation (3-17).

$$M_i = M_T \frac{A_i}{A_T} \tag{3-17}$$

where

M_i is the bending moment about axis x ,y or z at section i as divided by the proportion ratio of the projected area

M_T is the total bending moment as calculated in the design load cases. (B, C, F, G, H and J).

The calculation of the forces acting at each section of the blade for the load cases that provided bending moments are therefore determined with Equation (3-18).

$$F_i = \frac{M_i}{d_i} \tag{3-18}$$

where,

F_i is the force acting on section i calculated from the bending moment.

Appendix B shows the results of the forces and moments calculated from the design load equations. These values can now be used to plot the shear and moment diagrams. Note that load case J is calculated differently to the load cases from IEC 61400-2, and is presented in Appendix B.

3.3 Shear and moment distribution diagrams

The shear and moment diagrams are plotted from the data calculated in the previous chapter. The shear force and bending moment diagrams of each load case are calculated and an overlay plot of all of these forces and moments in the same direction and about the same axis respectively is determined. This is necessary to obtain the highest values for shear and bending moments in each direction at each section of the blade. The largest values are used to calculate the thickness distribution of the blade's subcomponents.

The blade is modelled as a cantilever beam and the forces and moments calculated in Chapter 3, section 3.2 are used to determine the shear force and bending moment distribution diagrams. Figure 3-6 presents the modelling of the blade as a cantilever beam with the root end fixed and the forces acting at each section of the blade.

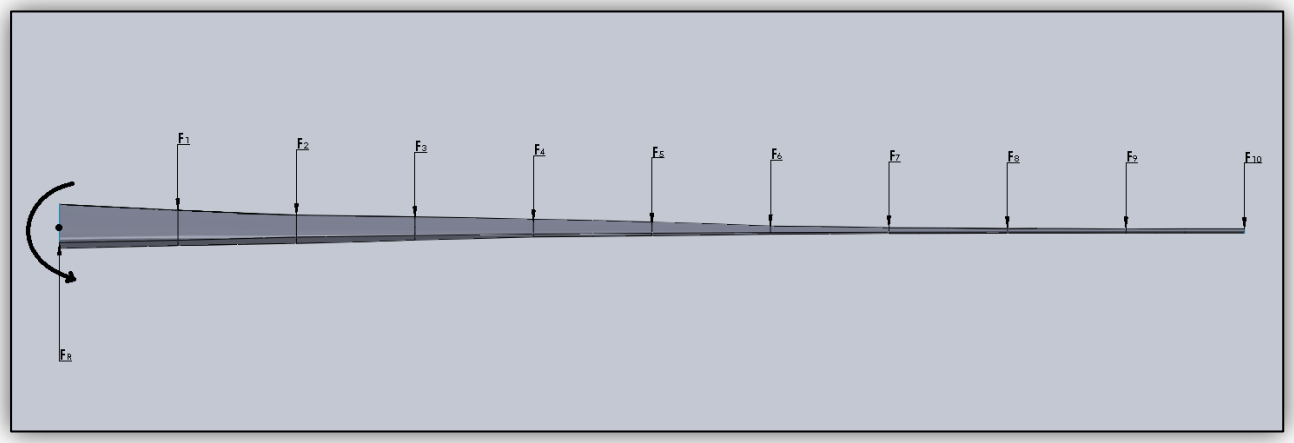

Figure 3-6: The blade modelled as a cantilever beam with the flapwise bending forces distributed over the length of the blade and the root end fixed

The shear force distribution diagrams were plotted by calculating the shear force at each section of the blade, using Equation (3-19).

$$V_i = F_R - \left(\sum_{k=1}^{i} F_k\right) \quad ; F_0 = 0 \tag{3-19}$$

where

V_i is the shear force at section i

F_r is the reaction force at the root of the blade due to the forces on the blade

F_k is the forces acting on the blade at each section as calculated in Chapter 3, section 3.2.

The moment distribution diagrams were also plotted by calculating the bending moment at the root of the blade for the forces acting at each of the blade sections. Equation (3-20) was used to determine the moment values at each section/station for the bending moment distribution graph.

$$M_i = F_R(x_i) + \sum_{k=0}^{i} F_k\,(x_i - x_k) + M_R \qquad ; x_0 \; and \; F_0 = 0 \qquad (3\text{-}20)$$

where,

M_i is the moment at section i when considering all the forces from point x=0 at the root of the blade to x=i at section i

F_R is the reaction force at the root of the blade due to all the forces at the blade sections.

Figure 3-7 shows the overlay plot of the shear force distribution of all the load cases in the x-direction. Figure 3-8 shows the shear force distribution of the forces acting in the y-direction. Note that only a single line is visible in Figure 3-8. This is due to load cases F and G having the same values. Figure 3-9 shows the flapwise bending moment distribution about the y-axis.

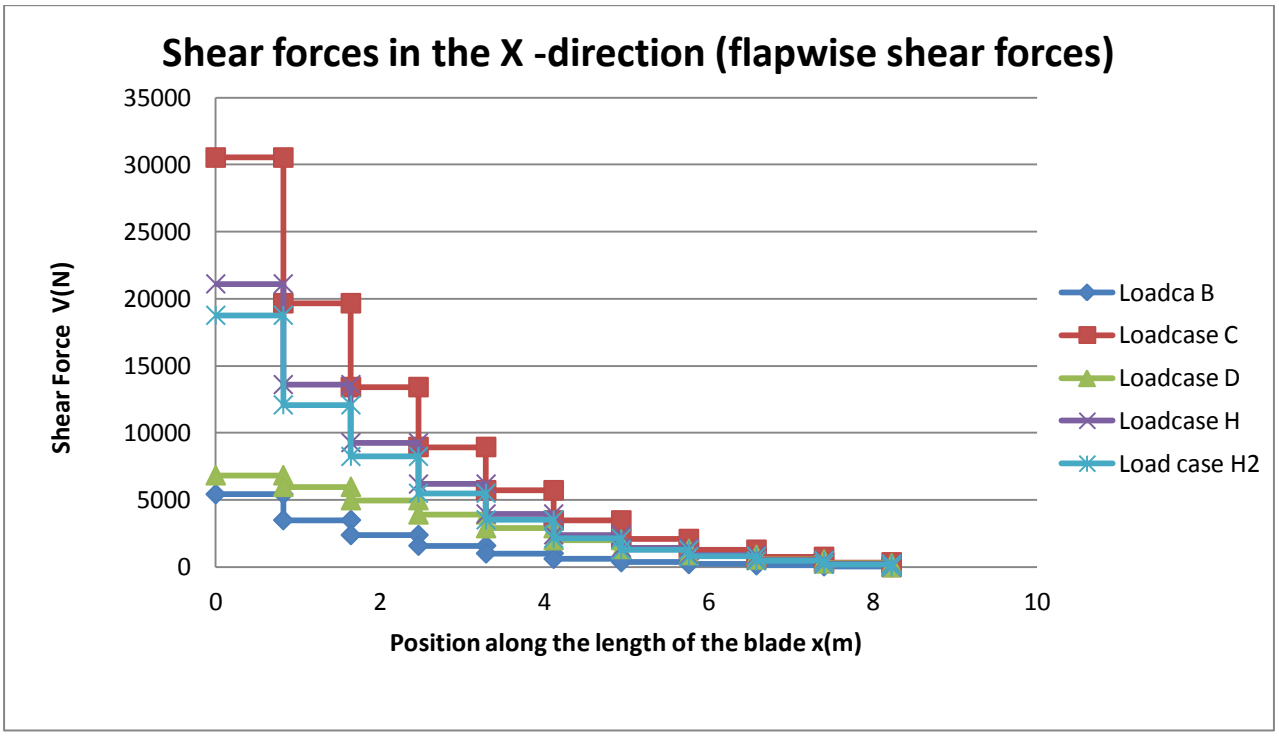

Figure 3-7: Shear force distribution diagram for forces acting in the x-direction (flapwise forces)

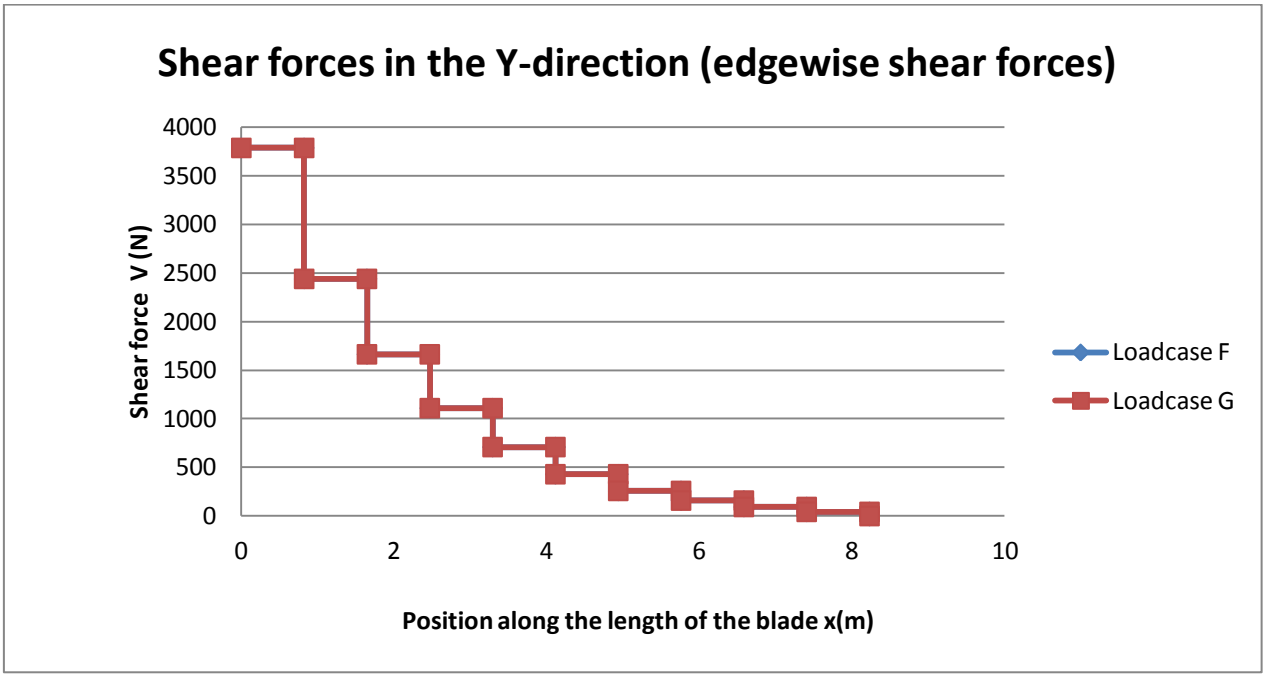

Figure 3-8: Shear force distribution diagram for forces acting in the y-direction (edgewise forces)

Figure 3-9 shows the overlay plot of the bending moment distribution about the y-axis for flapwise bending of the blade.

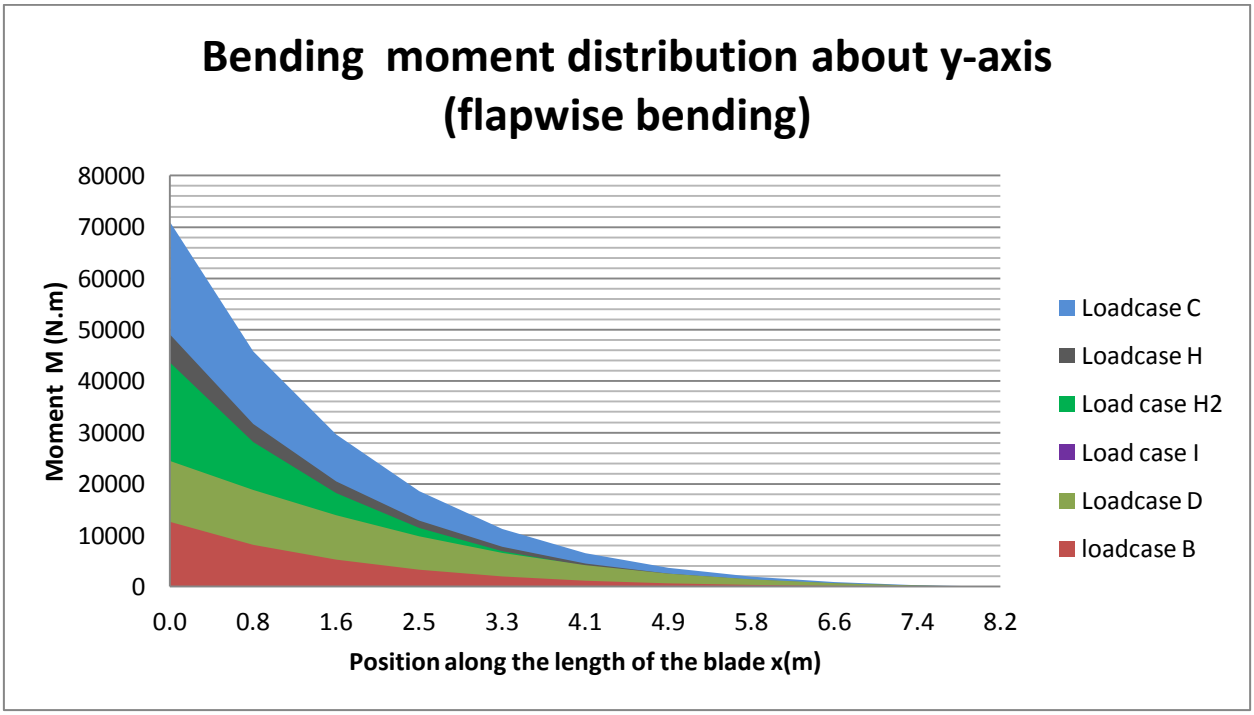

Figure 3-9: Bending moment distribution about the y-axis (flapwise bending)

Figure 3-10 shows the bending moment distribution for edgewise bending and again it is clear that only one graph is visible, as load cases F and G have the same values. The torsion moment distribution about the z-axis graph as calculated for the extra added torsion load case can be seen in Figure 3-11.

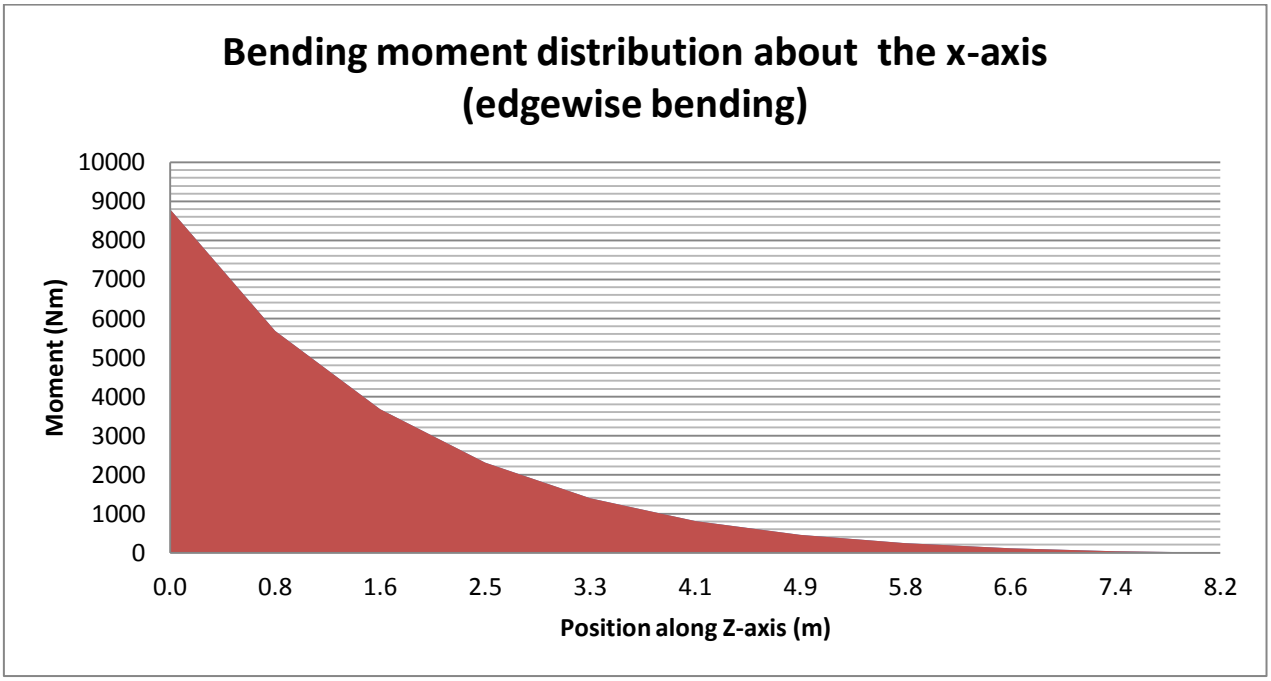

Figure 3-10: Bending moment distribution about the x-axis (edgewise bending)

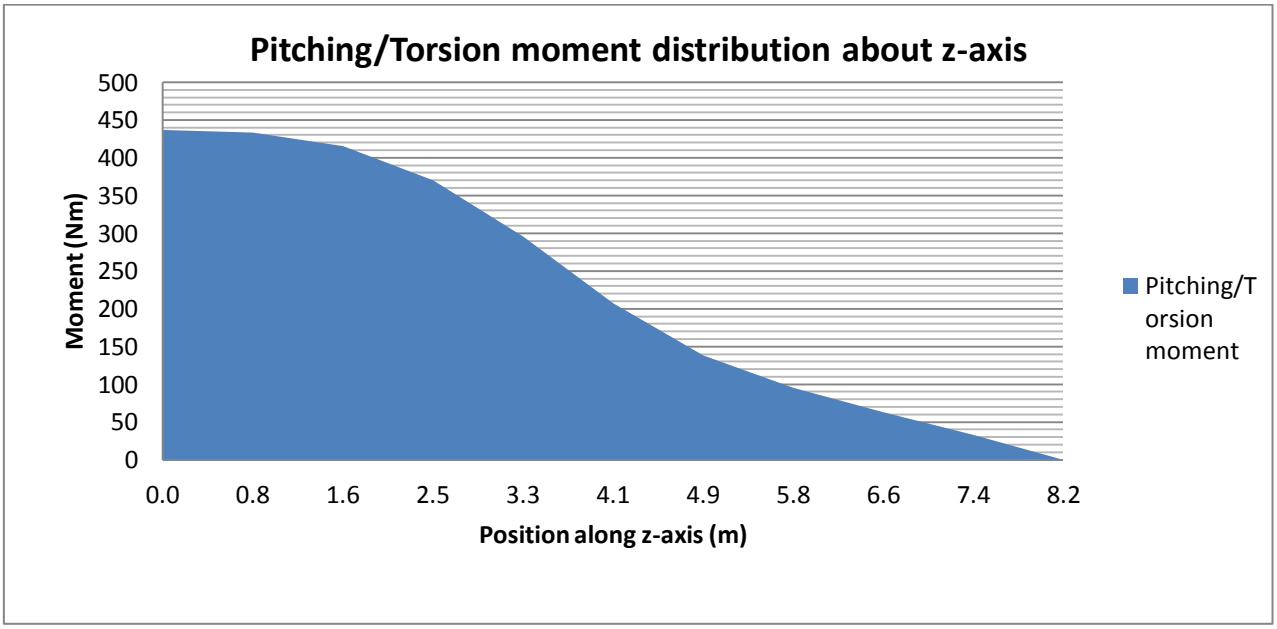

Figure 3-11: Pitching or torsion moment distribution about the z-axis as calculated in the load case that was added to the list of IEC 61400-2's load cases

More detail on the calculation of the shear and bending moment distribution graphs can be seen in Appendix C.

3.4 Root bearing design

The design of the blade root bearing is necessary to obtain the circular shaped root end that could be connected to the hub of the turbine that has active pitch control. The selection of the root bearing is possible as all the loads acting on the blade are known. The reaction forces from the greatest

axial and shear and radial loads determined from the shear and moment diagrams are used to design the root bearing. Apart from the design equations that are used to select the bearing size, criteria such as fitting into a 1-metre-diameter hub cone, the distance between the bearings and the ability of the blade root to be smoothly coalesced from a circular shape to the airfoil shape without creating stress concentration regions is considered.

The design of the root bearing firstly consists of selecting the appropriate bearing type. The bearings required at the root of the blade have to withstand both axial loads due to the centrifugal loads on the blade as well as radial loads due to the bending of the blade. Spherical roller bearings are chosen for this application due to their excellent rating for combined axial and radial loading, according to SKF (2008). Although there are other bearing types capable of withstanding both axial and radial loads, the spherical roller bearings are chosen due to their availability in larger sizes, which will be required to withstand the great bending moments and centrifugal forces.

Recent wind turbine blade roots are designed to connect to the hub of the wind turbine with a slewing bearing. The root of the blade is then designed with T-bolts infused in the laminated material. This root and bearing configuration simplifies the assembly and maintenance of the wind turbine. Slewing bearings can accommodate axial, radial and moment loads acting either singly or in combination and in any direction (SKF, 2008). Despite these bearings having a low profile and excellent weight/performance ratio and being ideal for wind turbine blade root applications, they are expensive. Thus, for this project, two spherical roller bearings will be used at the root section of the blade, as seen in Figure 3-12.

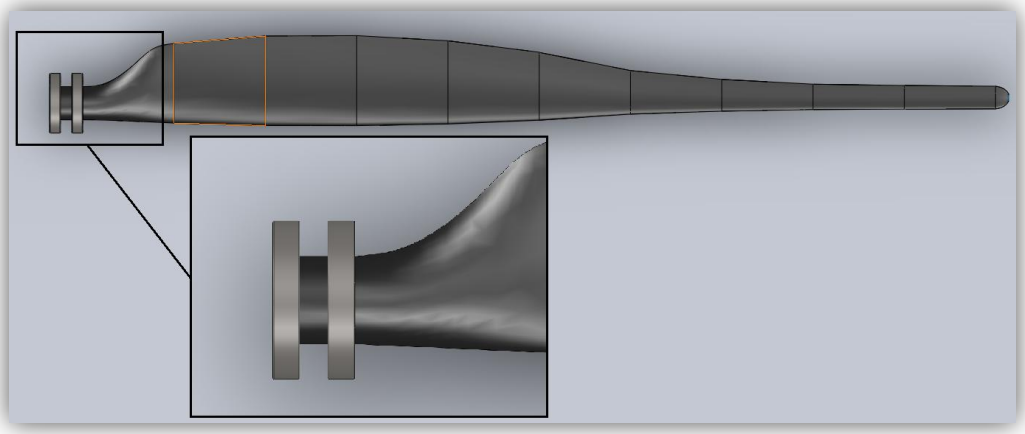

Figure 3-12: A representation of the positioning of the root bearings and the conversion of the root to a circular shape to accommodate the bearings

According to SKF (2008), the bearing size is selected on the basis of static load carrying capacity rather than on bearing life, when one of the following conditions exist:

- Bearing is stationary and subjected to continuous intermittent (shock) loads.
- The bearing makes slow oscillating or alignment movements under load.

- The bearing rotates under load at very slow speeds (n < 10r/min) and is only required to have a short life (the life equation in this case, for a given equivalent load P would give such a low requisite basic dynamic loading C, that the bearing selected on a life basis would be seriously overloaded in service).
- The bearing rotates and, in addition to the normal operating loads, has to sustain heavy shock loads.

The pitch bearings in the root of the blade in this project will experience three of the above-mentioned conditions, and thus the bearing size is selected using the static load carrying capacity C_0 and by calculating the equivalent static bearing load. In order to calculate the equivalent static bearing load for the bearings, the axial and radial reaction forces on both bearings are calculated as presented in Figure 3-13. The static load carrying capacity C_0 is given for each bearing in the SKF catalogue. The static load rating is used to calculate the static safety factor that is used as a guideline for the selection of the root bearings.

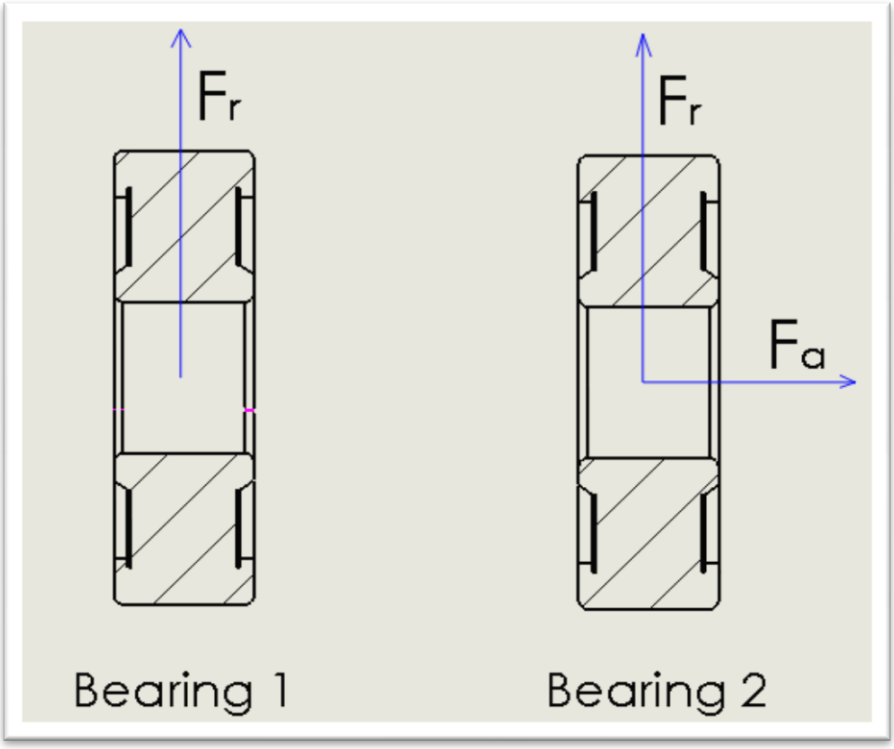

Figure 3-13: The actual radial and axial loads as calculated for the two root bearings

The details on the design calculations of the root bearings are presented in Appendix D. The bearing selection calculations provided spherical roller bearings with an inner diameter of 300mm. Thus, the outer diameter of the circular shape of the root of the blade is 300mm and is smoothly coalesced into the airfoil shape of the blade at section 1. See Appendix C for the description of the root end of the blade.

3.5 Summary

This chapter comprised the calculations of the design loads that the blade should withstand during operation. The loads, and the variables used to calculate these loads, are determined according to the IEC 61400-2 design guideline using the simplified load calculation method. The blade is divided into 10 sections of equal lengths in order to distribute the above-mentioned loads over the blade surface. The loads are distributed over the length of the blade by dividing the total blade load by the proportion ratio of each section's surface area to the total surface area of the blade and applying these load proportions to its relevant section.

The bending moment and shear force for each load case is determined at each section of the blade and therefore the bending moment and shear force distribution diagrams are drawn for each load case. The results of the shear force and bending moment distribution graphs proved that load case C causes the greatest shear forces and bending moments over the length of the blade in the flapwise direction. Load cases F and G provided loads of equivalent magnitude and caused the greatest edgewise loads. Load case J is a load case that was not included in IEC61400-2 design guideline. This load case was added to account for the torsion loads that the blade should withstand. The root bearings are designed to obtain the circular dimensions at the root end of the blade. The bearings are designed using the SKF bearing selection guide (SKF, 2008) and using the maximum load values obtained from the calculated design loads.

The dimensions of the root circle are obtained from the bearing design and therefore the root of the blade is coalesced from an airfoil shape into the circular shape where it will be connected to the hub of the wind turbine. The loads that equated to the greatest shear force and bending moments in the principal directions as determined from the graphs plotted in this chapter are used in the preliminary cross-section topology design or thickness distribution of the blade's subcomponents.

CHAPTER 4 PRELIMINARY CROSS-SECTION DESIGN

The cross-section design of a wind turbine blade is better described as the process in which the subcomponents or internal blade structure is designed – in other words, the load carrying beam which consists of spar caps and shear webs (Liao *et al.*, 2011). Also, according to Liao *et al.* (2012), the spar caps are the major load carrying components in the wind turbine blade structure, while the shell or outer skin of the blade provides for the minor shear stresses and aerodynamic shape. The issues in the design of the blade's internal structure comprise the beam type (Box-beam, I-beam, D-spar etc.) and the topology of the materials used in the beam to withstand different load cases.

This chapter includes the structural topology modelling and cross-section design of the blade as a composite beam structure to determine the thickness distribution and internal configuration, hence topology, of the subcomponents of the blade. The structural modelling of the blade is based on the maximum stress criterion which is calculated from the partial safety factors as prescribed by IEC 61400-2. The results from this structural topology modelling serve as a preliminary design measurement, only to obtain approximate initial layup values for the subcomponents to be used in the detailed structural design through FEA.

The results are also used for validation of the detailed structural design model where the stresses from the mathematical model are compared to those obtained from the FEA results by modelling the preliminary design model. This chapter also includes the optimisation of the blade in terms of minimising the area of the spar caps at each section to minimise the weight of the blade. The cross-section topology chosen for the blade in this thesis consists of the outer blade skin layers and a box-beam configuration which consists of the spar caps and shear webs as seen in Figure 4-1. A foam core material is also used to improve the rigidity of the blade.

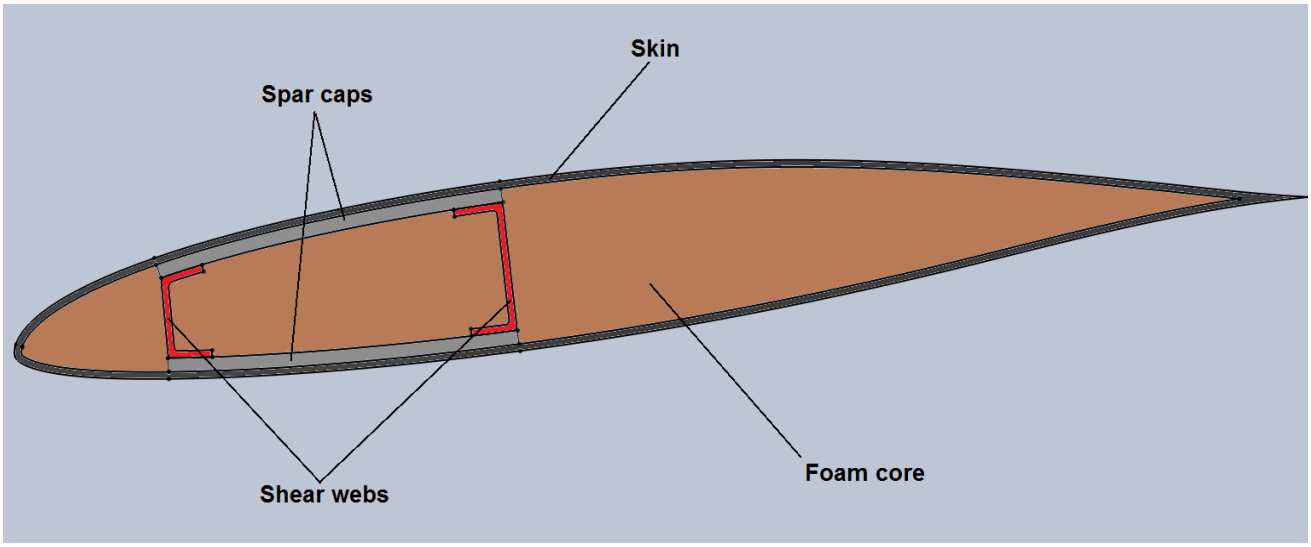

Figure 4-1: Illustration of the cross-section topology of the blade containing the box-beam, which consists of the outer skin spar caps and shear webs

Each of the subcomponents as presented in Figure 4-1 is designed according to the loads that it should withstand, in other words, the shell or outer skin of the blade is designed to withstand the shear loads due to the torsion load on the blade. The spar caps are designed to withstand the bending moments, while the shear webs have to withstand the shear forces on the blade. Thus, to summarise, the skin is designed using the torsion load case, the spar caps are designed using the load case causing the greatest bending moments and the maximum centrifugal forces, and the shear webs are designed using the load case causing the greatest shear forces. The foam core is not modelled in the calculations but is considered in the calculation of the mass of the blade.

To calculate the thickness distribution/ layup design, a criterion is set so the blade could meet the structural requirements as prescribed by IEC61400-2. The maximum stress criterion is therefore used to set the stress limit of the blade's subcomponents. This maximum stress of each of the subcomponents is determined from the partial safety factor requirements presented in IEC61400-2. Therefore, the partial safety factors are firstly determined in order to calculate the maximum design stresses for each subcomponent.

4.1 Partial safety factors and maximum design stress

The partial safety factors presented in this chapter are determined according to IEC 61400-2 design requirements. IEC 61400-2 presents two partial safety factors to account for the uncertainty involved in the structural design of the blade. Thus, a safety factor for the materials used in the blade and a safety factor for the loads is presented.

The partial safety factor for the materials presented in IEC61400-2 is divided in two groups based on the probability and confidence limits of the materials used in the blade. These two groups are labelled the full characterisation and minimal characterisation as seen in Table 4-1. The safety factor under full characterisation is used when five prescribed factors are adequately considered when the material properties are determined.

As presented by IEC (2006), the factors to be considered are:

1. Materials and material configurations shall be representative of the full-scale structure.
2. Manufacturing method of the test samples that are typical of the full-scale structure.
3. Static, fatigue and spectrum load testing (including rate effects).
4. Environmental effects (for example, corrosion, UV degradation, humidity, temperature etc.)
5. Geometry effects as they affect material properties (for example material orientation for injection moulded blades, ply drops in composites and wood, material orientation from forging of metals etc.)

The safety factor for material under minimal characterisation is used when the material properties are based solely on coupon testing and do not consider the above-mentioned factors. Table 4-1 presents the partial safety factors for the fatigue strength and ultimate strength of the materials under the two above-mentioned groups. Note that since only ultimate loads are considered in this project, the material safety factor for fatigue strength is not applicable.

The partial safety factor for materials under full characterisation is used in this project as the material properties were determined from tests performed by NWU.

Table 4-1: Partial safety factors for material as presented in IEC (2006)

Condition	Full characterisation	Minimal characterisation
Fatigue strength	1.25	10.0
Ultimate strength	1.1	3.0

The partial safety factor for loads as previously mentioned accounts for the uncertainty in the load estimation process and varies for the different load determination methods. IEC 61400-2 presents safety factors for three different load determination methods as seen in Table 4-2. Since the loads calculated in this project are based on the simplified load calculation method, a partial safety factor of 3 will be used for the loads according to Table 4-2.

Table 4-2: Partial safety factors for loads as presented by IEC (2006)

Load determination method	Safety factor for ultimate loads
Simple load calculation	3.0
Aeroelastic modelling	1.35
Load measurements with extrapolation	3.0

The partial safety factors as presented above are used to determine the required design stress. According to IEC 61400-2, the ultimate design strength required is calculated as presented in Equation (4-1).

$$\sigma_d = \frac{f_k}{\gamma_m \gamma_f} \tag{4-1}$$

where

f_k is the characteristic material strength

γ_m is the partial safety factor for materials

γ_f is the partial safety factor for loads.

From the above-presented equation it is calculated that a safety factor of 3.3 is used to determine the maximum design stress. The material properties are required to determine this maximum design stress.

4.2 Material selection and properties

The choice of materials used in the 50kW wind turbine blade are based on the strength and stiffness-to-weight ratio to minimise the weight of the blade and thus make it more aerodynamically efficient and reduce the cost of the blade. The reduction of the blade weight and cost should, however, be performed while simultaneously ensuring that the strength and stiffness of the blade are sufficient to withstand the operating loads that it will experience.

Fibre-reinforced plastics are the most common materials used in wind turbine blades due to their high strength and stiffness-to-weight ratio. According to Gurit (2011), glass and carbon are the two most popular fibres used in fibre-reinforced plastics. Gurit (2011) also states that carbon fibres, although almost twice as strong and three times as stiff as glass fibres, are much more expensive and are tended to be used only where these superior properties are essential. This means that carbon fibre is only used on some of the largest wind turbine blades. Therefore, glass fibre-reinforced plastics are used in the wind turbine blade designed in this project, as the blade is not even near the large scale mark for wind turbine sizes.

Two types of glass fibres are used in the blade designed in this project, namely unidirectional fibres and bi-directional fibres. The unidirectional fibres will be used in the spar caps to withstand the bending loads on the blade and will be oriented along the blade length (0^o along the z-axis) as that is the direction of the bending loads. The bi-directional fibres are used in the blade skin to provide stiffness and maintain the blade shape and to withstand the torsion load on the blade. Bi-directional fibres are also used in the shear webs to prevent the spar caps form sliding or shearing relative to each other. The bi-directional fibres are oriented at approximately $+45^o$ or -45^o along the z-axis.

The orthotropic material properties for the above-mentioned glass fibres as determined by NWU are presented in Table 4-3 (Naude & Jonker, 2008).

Table 4-3: Orthotropic material properties of the unidirectional and bi-directional fibres used in the blade designed in this project

Material	E_{11} (MPa)	E_{22} (MPa)	G_{12} (MPa)	v	$S_{11}T$ (MPa)	$S_{22}T$ (MPa)	$S_{11}C$ (MPa)	$S_{22}C$ (MPa)	S12 (MPa)
Glass Unidirectional	32000	8000	3200	0.25	480	50	300	50	40
Glass Bi-directional	22500	22500	4200	0.28	223	223	180	180	60

The safety factors presented in Chapter 4, section 4.1 are applied to these material properties and the maximum design stress is calculated.

Thus, the maximum design bending stress for unidirectional glass fibre is presented in Equation (4-2):

$$\sigma_d = \frac{480}{3.3} = 145.45\ MPa \tag{4-2}$$

The shear stress is not calculated with the shear stress formula but with the shear flow formula as presented in the next chapter. Therefore, the maximum stress criterion is not used to calculate the design shear stresses in the blade skin and the shear webs. However, a safety factor of 3.3 is still applied to these shear stresses.

From the above-presented data it is possible to initiate the layup design/thickness distribution modelling of the subcomponents, in other words, skin, spar caps and shear webs, of the blade. The following sub-clauses cover the layup design modelling of the blade's subcomponents starting from the outermost component (skin) and working inward to the shear webs, as the outer geometry of the blade is already set and could not be changed and the topology of the subcomponents directly affects each other and the strength of the blade.

4.3 Skin layup design

The thickness distribution/ layup of the skin is determined by calculating the number of bi-directional fibreglass layers needed to withstand the torsion load on each section of the blade. Thus, the results of load case J will be used to model the skin thickness distribution over the length of the blade. The shear flow for torsion formula is used to determine the number of bi-directional glass fibre layers at each section of the blade as mentioned in the previous sub-clause.

The shear flow at each section of the blade is determined and the shear flow that a single BID glass fibre layer could withstand is determined. Since the shear flow a single layer could withstand is then known, the number of layers required to withstand the shear flow at each section is determined. This calculation is an iterative process as the thickness of the skin is not known and thus an initial skin thickness value of 1mm is chosen.

The shear flow in the skin with a thickness of 1mm under the torsion moment at that section is determined. The number of layers required for this shear flow is then determined with the value of shear flow that a single layer could withstand with the use of Equation (4-3).

$$number\ of\ layers\ to\ withstand\ shear\ flow = \frac{shear\ flow\ calculated\ for\ a\ certain\ skin\ tickness}{shear\ flow\ that\ a\ single\ layer\ of\ BID\ glass\ fibre\ could\ withstand}$$

(4-3)

The number of layers is then converted to a thickness (thickness of one layer of BID glass fibre is 0.28mm) and this thickness is then used for the second step in the iteration process. This process is iterated until the value for the skin thickness converges. The shear flow formula used is presented in Equation (4-4). The converged number of layers calculated to withstand the torsion moment is multiplied by 3.3 to obtain the required design strength.

$$q_i = \frac{T_i}{2A_{mi}} \tag{4-4}$$

where,

q_i is the shear flow in the skin of section i

T_i is the torsion moment at section i

A_{mi} is the mean area enclosed within the boundary of the centreline of the skin's thickness. A_{mi} is shown shaded in Figure 4-2 for the circular root section of the blade. The CAD software Solidworks is used to determine the mean areas in every iteration step and was performed on all sections of the blade.

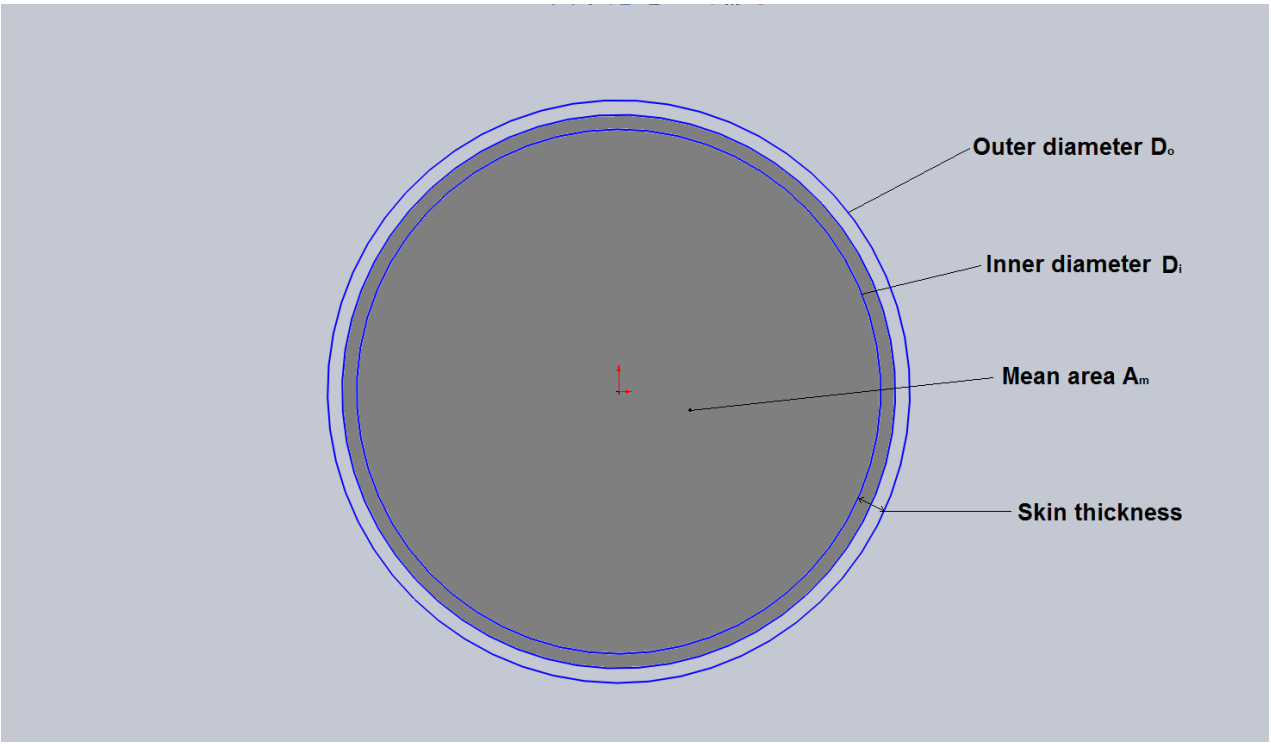

Figure 4-2: A representation of the mean area calculated for the circular root section of the blade

The shear flow which a single layer of bid glass with a thickness of 0.28mm and oriented at 45 degrees could withstand is determined by the use of a laminate analysis software package LAP (Laminate Analysis Program, 2011). Figure 4-3 shows the material data input to LAP to determine the shear flow a single BID glass fibre layer could withstand. The material properties used in Figure 4-3 are those obtained from Table 4-3 for BID glass fibre. Figure 4-4 shows the layup of only one layer of BID glass fibre of 0.28mm thickness, oriented at 45 degrees.

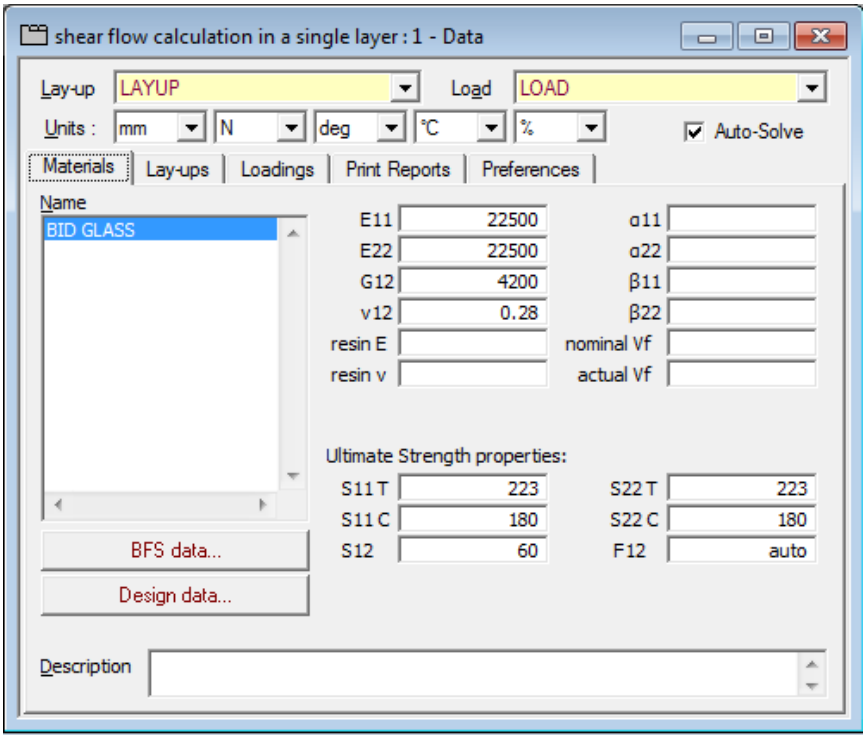

Figure 4-3: Material properties of BID glass fibre used as input values to obtain the shear flow a single layer could withstand

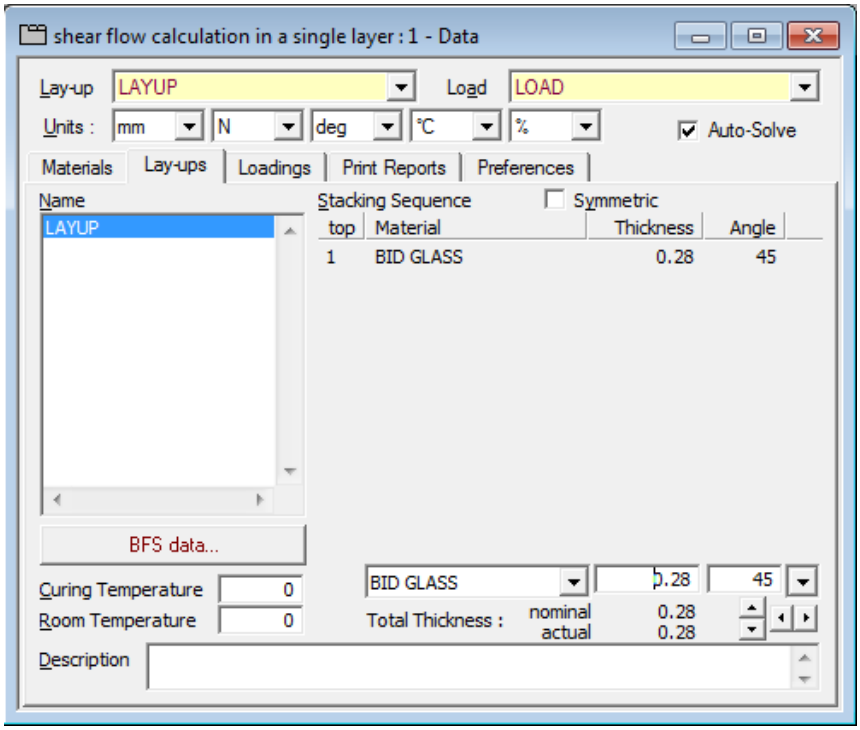

Figure 4-4: A single layer of BID glass fibre with a thickness of 0.28mm oriented at 45 degrees used as input to LAP to determine the flow this single layer could withstand

The shear flow load, $N_{xy,}$ was iterated until a safety factor of 1 was obtained under the maximum stress criterion. Figure 4-5 shows the shear flow load applied to the single layer , while Figure 4-6 shows the results obtained showing the safety factors for the different stress criteria. As previously mentioned, the maximum stress criterion is used as it is the most conservative as seen in Figure 4-6.

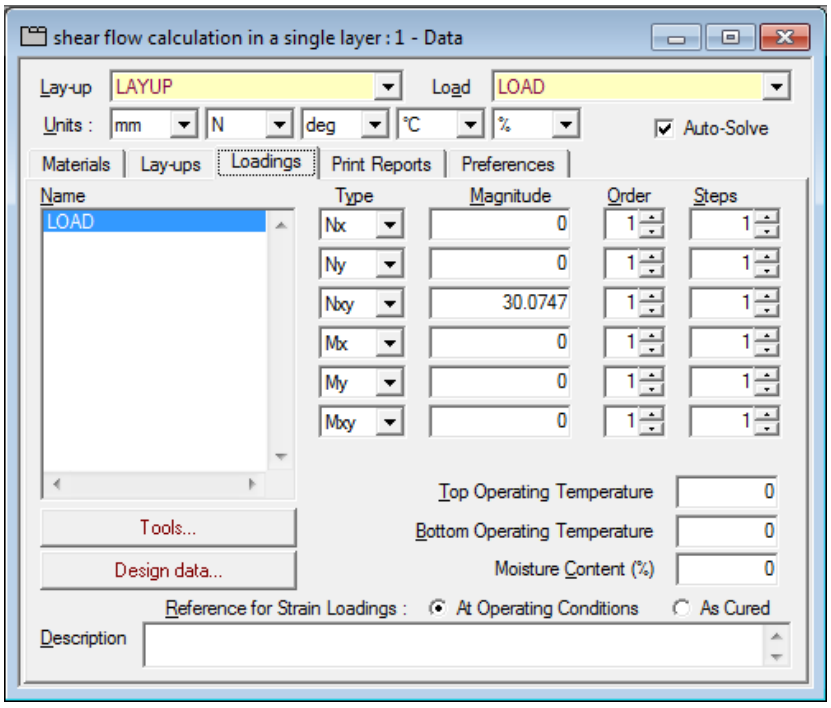

Figure 4-5: The converged shear flow load giving a safety factor of 1 in the maximum stress criterion

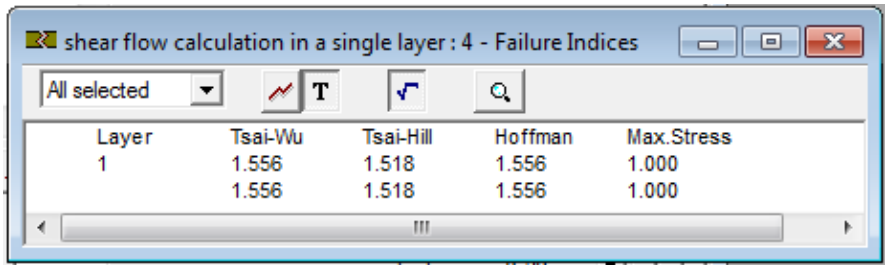

Figure 4-6: The results of a single layer BID glass fibre with a shear flow load of 30.0747N/mm resulting in a safety factor of 1 under the most conservative maximum stress criterion

The above-presented calculations prove that a single layer of BID glass fibre could flow of 30.0747 N/mm. This value is used to determine the thickness of the skin at each the blade. Table 4-4 presents the torsion load case as calculated in Chapter 3. The torsion load at each section of the blade as presented in Table 4-4 is added to the torsion loads of all the sections further away from the root of the blade. For example the pitching moment at section 6 of the blade = the sum of the pitching moments at section 6, 7, 8, 9 and 10. This is due to the fact that the skin of the blade at a certain section of the blade has to withstand not only the pitching moment at its own section but also the pitching moments of the sections further away from the root of the blade. Thus, the skin nearer to the root of the blade will be thicker than the skin at the tip of the blade.

Table 4-5 presents the pitching moments/ torsional loads at each section of the blade used for the calculations of the skin thickness at each section. Furthermore, a presentation of the pitching moment and the resulting shear flow in the skin is shown in Figure 4-7 and Figure 4-8.

Table 4-4: The pitching moments/ torsional loads at each section of the blade as calculated in chapter 3

Load case J Pitching moment (moment about 1/4 chord)	(Nm)
Pitching Moment at section 1	3.472
Pitching Moment at section 2	17.907
Pitching Moment at section 3	45.274
Pitching Moment at section 4	74.470
Pitching Moment at section 5	88.375
Pitching Moment at section 6	69.123
Pitching Moment at section 7	42.891
Pitching Moment at section 8	32.298
Pitching Moment at section 9	30.054
Pitching Moment at section 10	33.110

Table 4-5: The pitching moments/ torsional loads summed with the loads of the sections further away from the root of the blade. These values are used to calculate the skin thickness at each section of the blade

Load case J Pitching moment (moment about 1/4 chord)	(Nm)
Pitching Moment at section 1	436.974
Pitching Moment at section 2	433.501
Pitching Moment at section 3	415.595
Pitching Moment at section 4	370.320
Pitching Moment at section 5	295.850
Pitching Moment at section 6	207.475
Pitching Moment at section 7	138.353
Pitching Moment at section 8	95.462
Pitching Moment at section 9	63.164
Pitching Moment at section 10	33.110

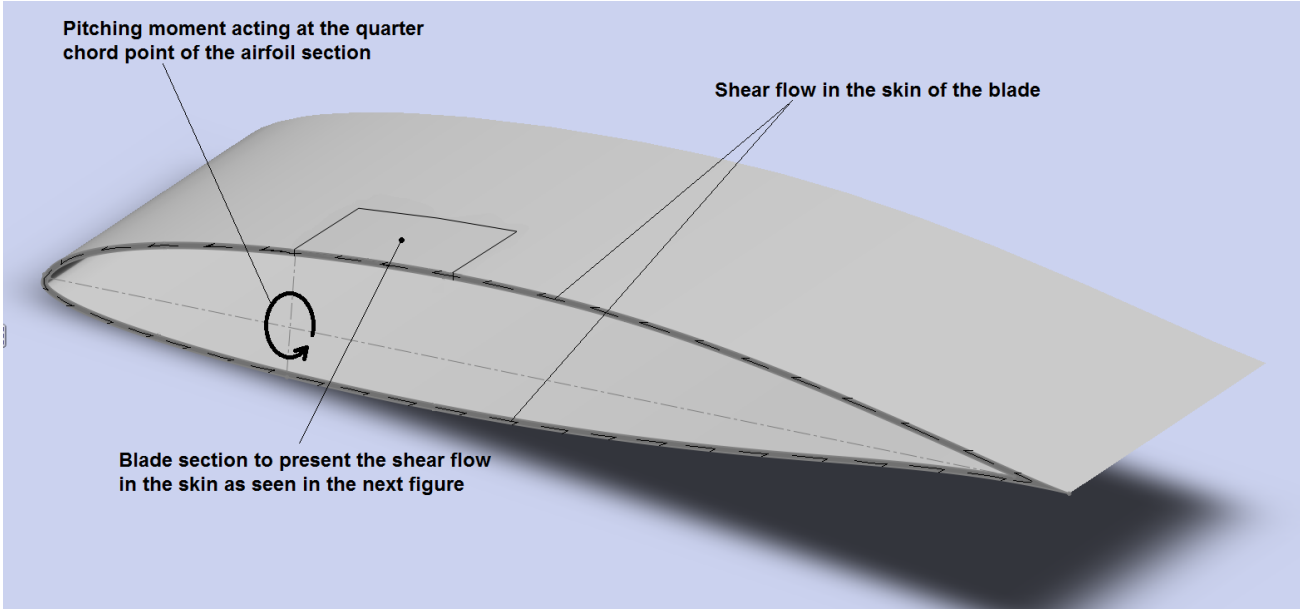

Figure 4-7: A presentation of the pitching moment and resulting shear flow in the skin of the blade

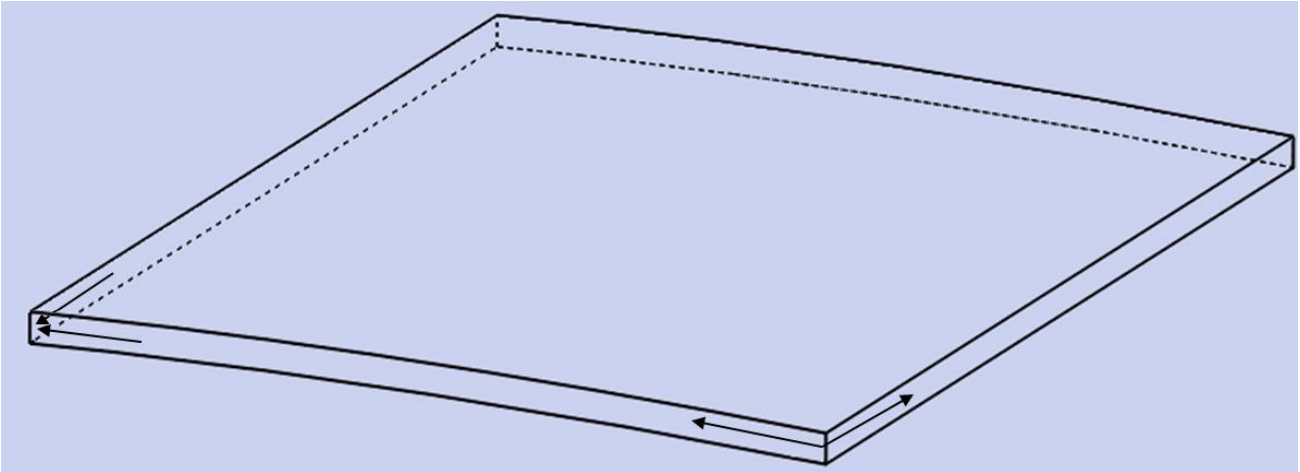

Figure 4-8: A skin section (seen in Figure 4-7) presenting the shear flow in it

A minimum design parameter was set for the skin thickness. For manufacturing purposes a value of two layers is set as the minimum for the skin of the blade. The thickness of the skin of the blade is calculated at each section of the blade and results show that even with a safety factor of 3.3 the number of layers required to withstand the pitching moment/ torsion load is less than 1. Therefore ,the minimum number of BID glass fibre layers is used at all the sections of the blade. Appendix E presents the iterative calculation of the skin thicknesses at each of the blade sections. Figure 4-9 present the steps involved in the iteration to calculate the skin thickness at each section of the blade.

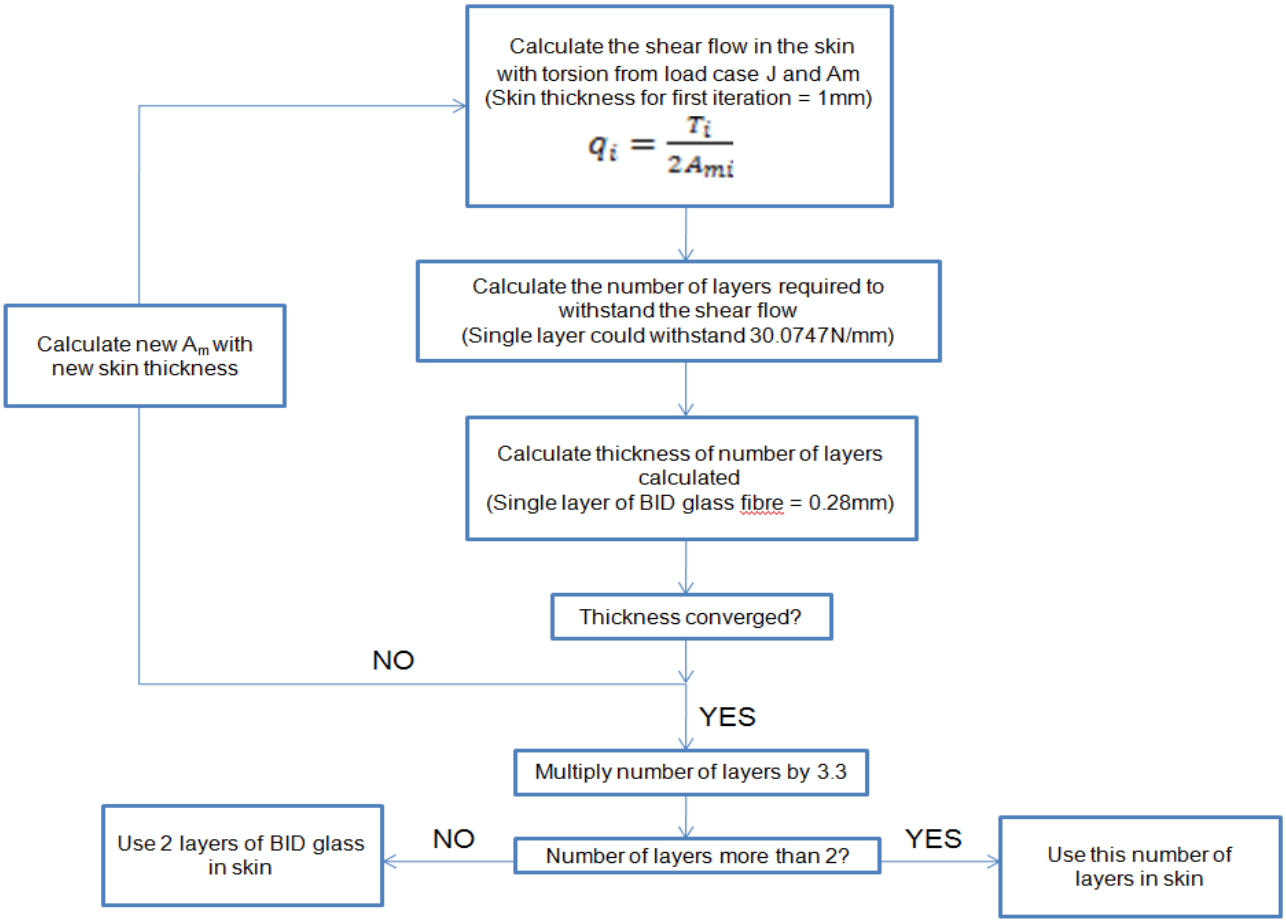

Figure 4-9: A process chart to explain the iteration steps in calculating the skin thickness at each section of the blade

4.4 Spar cap layup design

The spar caps in the wind turbine blade are designed for the purpose of withstanding the bending and centrifugal loads as previously mentioned. In this sub-clause the layup design of the spar caps only considers the bending loads as the centrifugal loads is covered in a following sub-clause. The thickness distribution of the spar caps is determined with the use of the bending stress formula as used for isotropic materials and presented in Equation (4-5).

$$\sigma_{bi} = \frac{M_i y_i}{I} \quad (4\text{-}5)$$

where,

σ_{bi} is the maximum bending stress at section i

M_i is the bending moment at section i

y_i is the perpendicular distance from the neutral axis (chord line) to a point farthest away from the neutral axis (Note that this distance is determined from the quarter chord point perpendicular to the chord line as presented in Figure 4-10)

I is the moment of inertia of the cross-section area computed about the neutral axis (chord line).

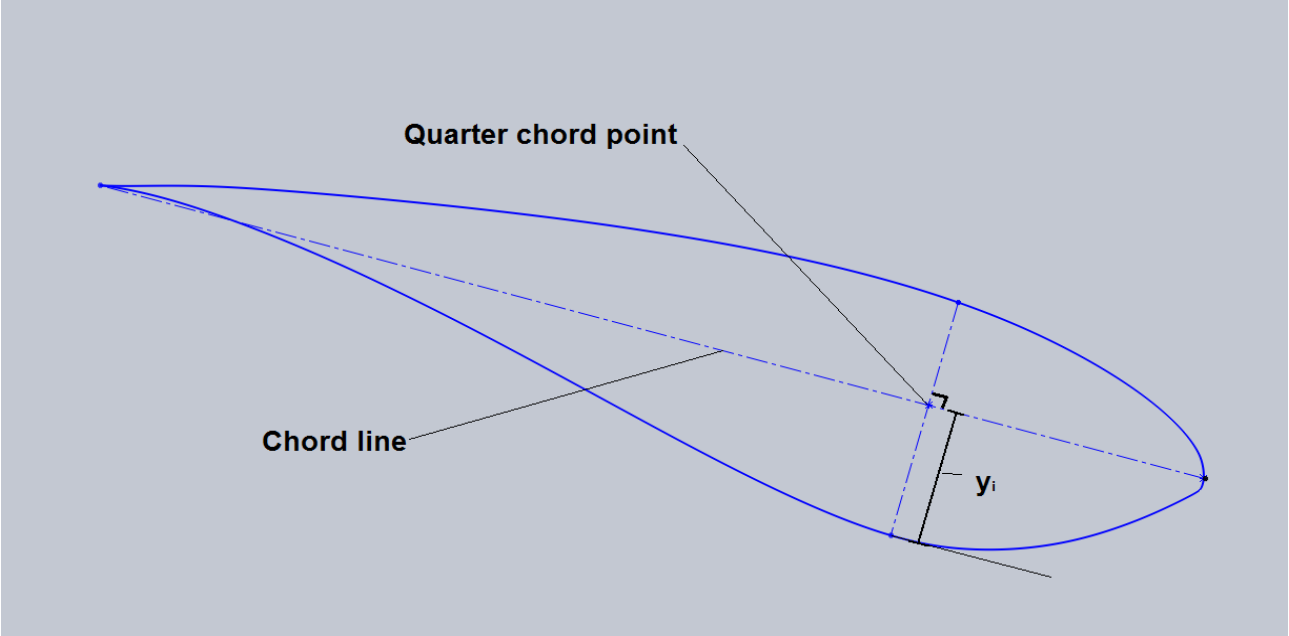

Figure 4-10: Description of how y_i is determined for the use in the bending moment formula

Equation (4-5) provides four variables of which three are known. The known variables are the maximum bending stress, the bending moment and the perpendicular distance from the neutral axis to a point farthest away from the neutral axis. The maximum bending stress is the maximum design stress calculated with the maximum stress criterion as previously presented in Equation (4-2). (Note that the spar caps are manufactured from UD glass fibre oriented at 0 degrees along the blade length.) The bending moments used are those calculated for load case C, which provided the greatest values at each section as previously shown in Chapter 3. The perpendicular distance from the neutral axis to a point farthest away from the neutral axis is determined from the CAD model in Solidworks.

Two unknown variables are present in the calculation of the moment of inertia about the neutral axis of the spar caps. These two variables are the width and thickness of the spar caps as presented in Figure 4-11.

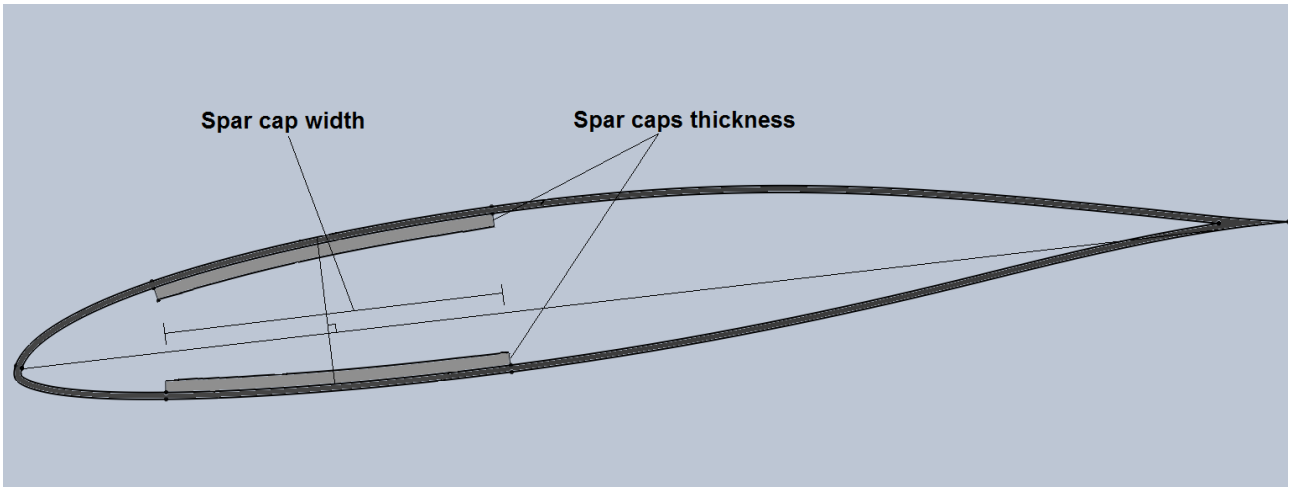

Figure 4-11: Description of the width and thickness of the spar caps

The method for calculating the width and thickness of the spar caps is by firstly calculating the required moment of inertia the spar caps should have to obtain the specified design stress from Equation (4-5). With the required moment of inertia known, the width and thickness of the spar caps can be calculated. The spar caps are modelled for different widths in order to make their thickness the only unknown variable. The widths of the spar caps vary from 20% to 30% of the chord length in 1% increments, and a thickness for each of the widths is calculated. Thus, the thickness of the spar caps is calculated for different widths to withstand the bending moment at that section and to obtain the maximum design stress.

The spar cap topology is optimised by choosing the width and thickness combination that provides the smallest spar cap area, thus minimising the area where UD glass fibre is required and so minimising the weight of the blade. As the spar caps are not rectangular plates but curved along the inner surface of the blade skin, the moment of inertia of the spar caps is determined by dividing the spar caps of a certain width (as a percentage of the chord length) into small blocks, each with a width of 0.5% of the chord length and an unknown thickness.

The moment of inertia is calculated for each block about the chord line as the neutral axis, using the parallel-axis theorem as seen in Equation (4-6). Note that the airfoil curve coordinates are used to calculate the position and dimensions of each of the small blocks.

$$I_{block} = I_x + Ad^2 \tag{4-6}$$

where,

I_x is the moment of inertia of the block about its own neutral axis (see Equation (4-7)

A is the area of the block

d is the distance between the neutral axis (chord line) and the centroid of the block.

$$I_x = \frac{1}{12} bh^3 \tag{4-7}$$

where,

b is the width of the blocks that the spar cap is divided into (0.5% of chord length)

h is the thickness of the blocks that the spar cap is divided into (unknown variable).

The moment of inertia of all the blocks in a spar cap is summed to obtain the moment of inertia of that spar cap as seen in Equation (4-8). (Note that there are two spar caps at each section of the blade, the spar cap on the high pressure side and a spar cap on the low pressure side of the airfoil.)

$$I_{spar\ cap,(Upper\ or\ lower)} = \sum I_{block} \tag{4-8}$$

The moments of inertia of these two spar caps are added to obtain the moment of inertia of the spar caps as a single part as seen in Equation (4-9).

$$I_{spar\ caps\ as\ single\ part} = I_{spar\ cap,\ upper} + I_{spar\ cap,\ lower} \tag{4-9}$$

All the above-mentioned calculations are modelled in a spreadsheet with the thickness of the spar cap as an unknown variable. An iterative solver is used to determine the thickness of the spar cap for different widths to obtain the required moment of inertia. Figure 4-12 shows how the spar caps are divided into blocks with a width of 0.5% of the chord length for a spar cap width of 20% of the chord length.

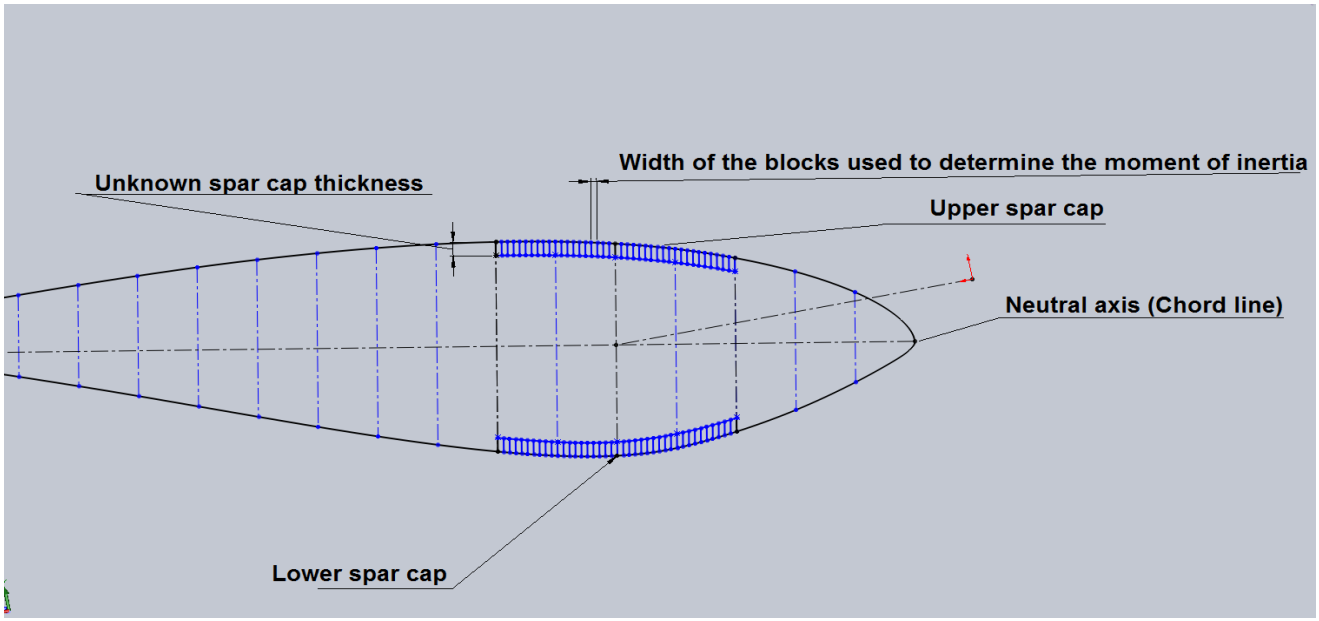

Figure 4-12: An example of the spar caps divided into blocks with a width of 0.5% of the chord length for a spar cap with a width of 20% of the chord length to determine the unknown thickness

The spar cap area obtained from the different thickness and width combinations are plotted to obtain the minimum area. The thickness of the combination (thickness and width) providing the minimum area is used to determine the number of UD glass layers at the section. This minimum thickness is therefore divided by 0.22 (as a single layer of UD glass fibre is 0.22mm thick) to obtain the number of UD glass fibre layers required to withstand the bending moment and to obtain the maximum design stress as calculated in Equation (4-2). The spar cap areas for the different widths plot of section 2 of the blade are presented in Figure 4-13. The Spar cap area versus spar cap width plots for all the sections are provided in Appendix F.

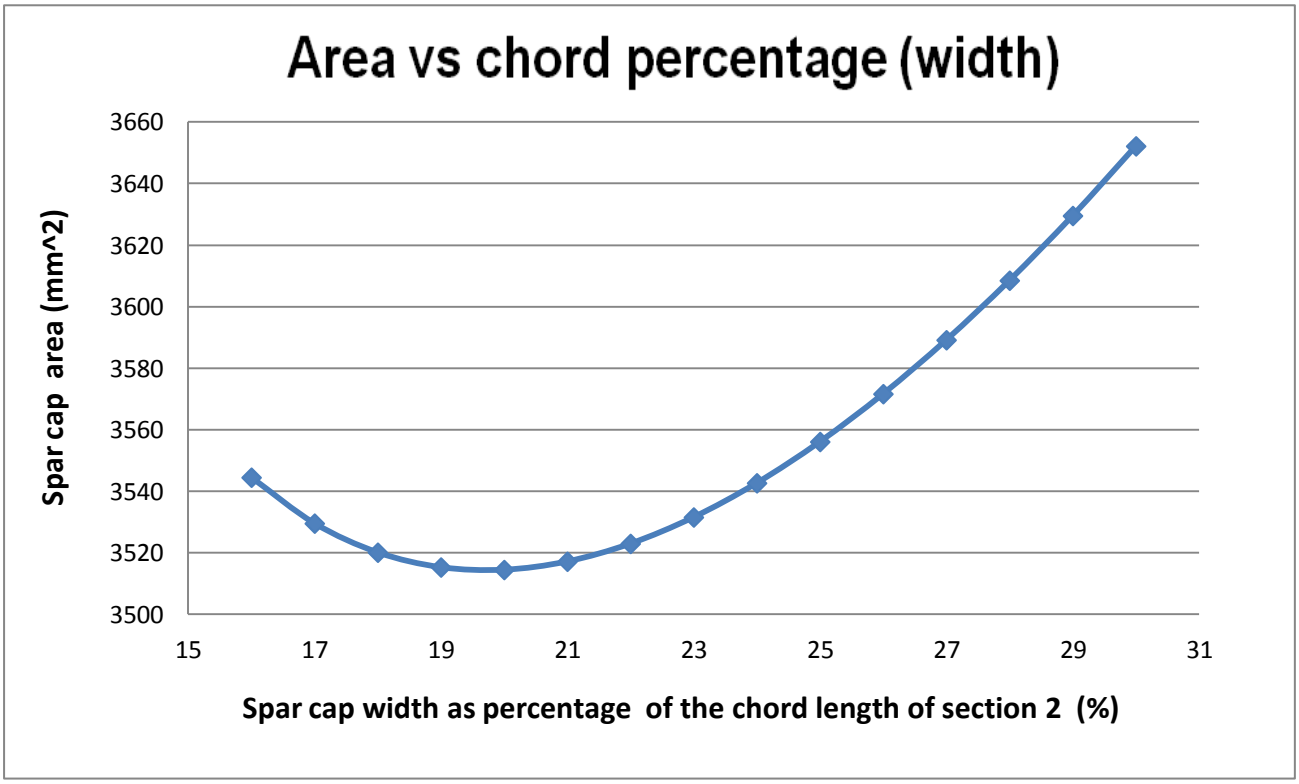

Figure 4-13: The spar cap area versus the width as a percentage of the chord length of section 2

From Figure 4-13 it is clear that the thickness of the spar cap with a width of 20% of the chord length provides the smallest area and is therefore the optimum design dimensions of the spar cap at section 2 of the blade. This procedure to calculate the thickness and width of the spar cap at section 2 was performed on all the sections of the blade. The thicknesses distribution plot of the spar caps over the length of the blade is presented in Figure 4-14. (Note that the thickness distribution of the spar caps is only determined with the bending moment, thus the centrifugal loads are not taken into account yet. The centrifugal load is calculated after the layups for all the

subcomponents of the blade are calculated. Extra layers are then added to the spar caps to account for the centrifugal loads.)

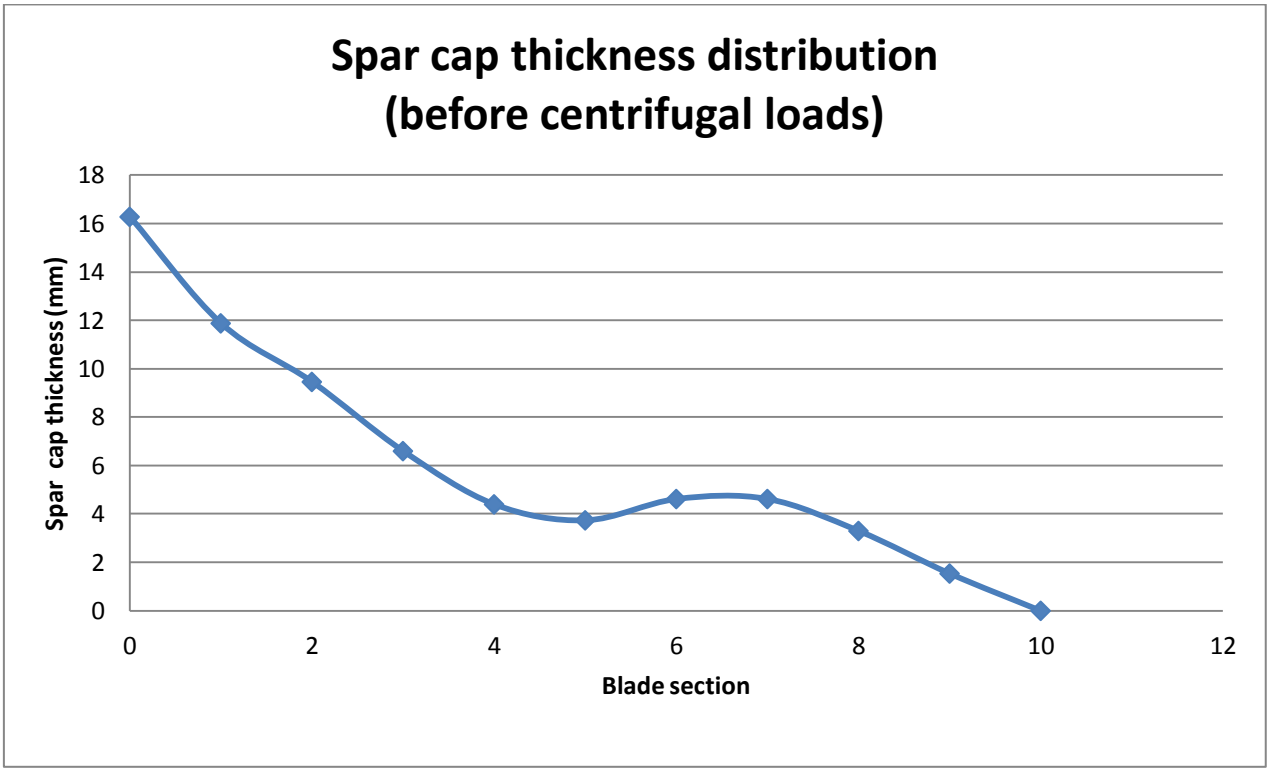

Figure 4-14: The thickness distribution over the length of the blade

4.5 Shear web layup design

The thickness distribution/layup design of the shear webs are calculated in the same iterative process as the skin thickness, except that the shear flow formula for a shear force is used and not for torsion as in the case of the skin. The shear webs are also designed with bi-directional glass fibres oriented at approximately 45 degrees along the blade length. Therefore, the shear flow that a single layer of these bi-directional glass fibres could withstand is the same as calculated in Chapter 4, section 4.3. The shear forces used for the calculation of the shear flow at each section of the blade is that obtained from load case C. The shear flow formula for shear forces is presented in Equation (4-10).

$$q_{shear\ web,i} = \frac{V_i \bar{y}' A'}{I_i} \qquad (4\text{-}10)$$

where,

$q_{shear\ web}$ is the shear flow in the shear web at the neutral axis of section i

V is the shear force as calculated in load case C for section i

A' is the cross-sectional area of the segment that is connected to the beam at the neutral axis

$\bar{y}'$ is the distance from the neutral axis to the centroid of A'

I_i is the moment of inertia of the entire cross-sectional area of sections i about the neutral axis.

Figure 4-15 shows the spar cap and shear web model in Solidworks to calculate the geometric variables ex. centroid distance, area and moment of inertia. Similar models are created for every cross-section at each section of the blade for the calculation of the shear web thickness distribution.

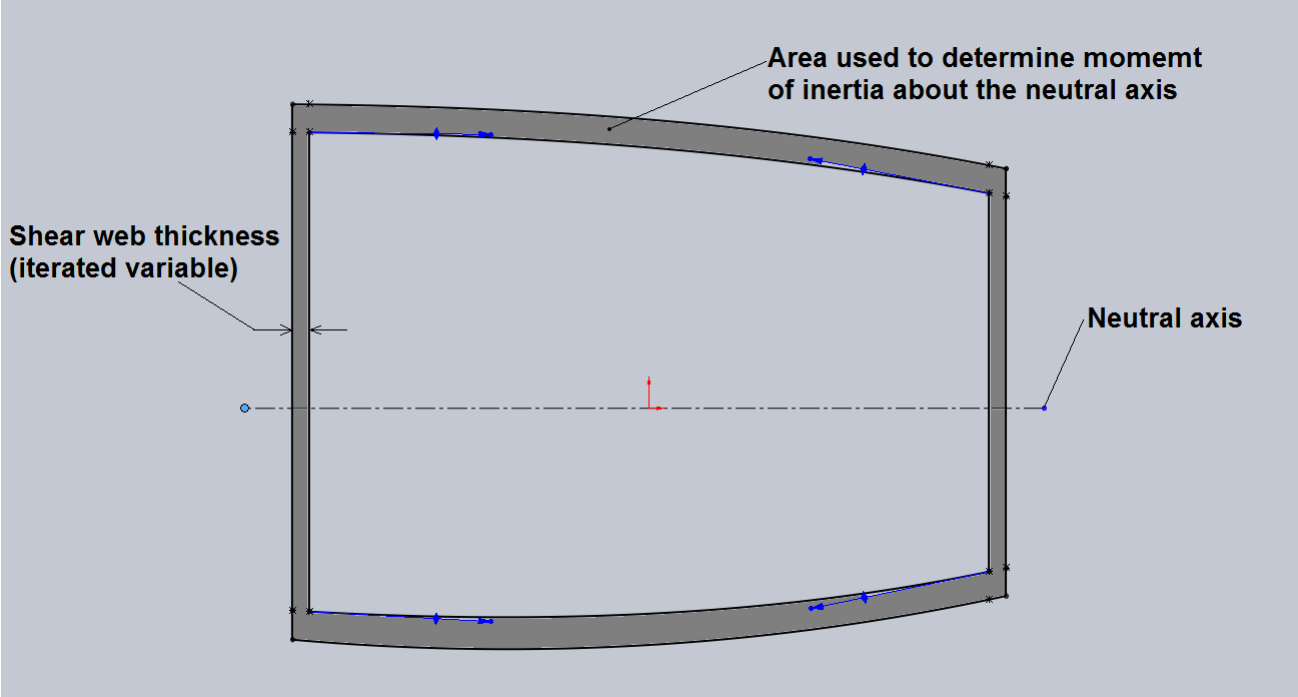

Figure 4-15: Cross-section topology of the spar caps and shear webs modelled for the calculation of the shear web thickness (Note that this is only a presentation of the spar caps and shear webs at one of the blade's sections)

Thus, an initial shear web thickness of 1mm is also used to calculate the shear flow. (Note that the CAD model in Solidworks is used in every step of the iteration process to determine the cross-sectional areas and centroid distances at all sections.) The number of layers needed to withstand this initial shear flow value is determined in the same way as in Equation (4-3). This number of layers is converted to a thickness, which is used in the next iteration step for the calculation of the shear flow in the shear webs. This iteration process is repeated until the thickness of the shear webs converges. The converged shear web thickness or number of layers is multiplied by 3.3 to obtain the required design strength. The thickness distribution of the shear webs is presented in Figure 4-16. See Appendix G for the tables showing the iteration steps for the calculation of the shear web thicknesses.

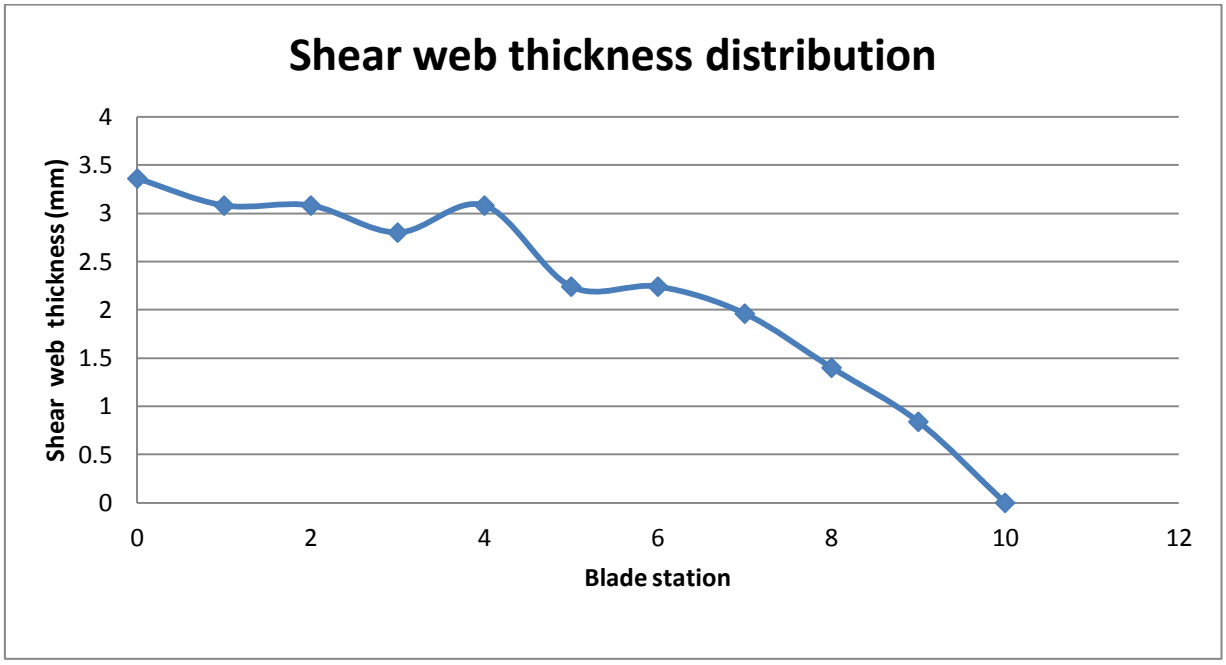

Figure 4-16: The thickness distribution of the shear webs at each section of the blade

4.6 Spar cap adjustment for centrifugal load

Now that the layup schedule for all the subcomponents is designed over the whole length of the blade, the mass of the blade is calculated to determine the centrifugal load at maximum rotational speed. The centrifugal load is calculated to determine the number of layers to be added to the spar caps to account for the centrifugal loads as Chapter 4, section 4.4 only considered the bending loads. The centrifugal load at each section of the blade is calculated with the mass of each section. This centrifugal load at each section of the blade is calculated in Equation (4-11) and used to determine the number of layers to be added to the spar caps at the respective sections.

$$F_{z,i} = m_i \omega_{n,max}^2 R_{cog,i} \tag{4-11}$$

where,

m_i is the mass of section i, where m_i is the sum of the mass of all the subcomponents in section i (see Equation (4-12)

$\omega_{n,max}$ is the maximum rotational speed of the blade

$R_{cog,i}$ is the distance from the centre of rotation to the centre of gravity of section i.

$$m_i = (\sum m_{sc,i}) + m_{foam,i} \tag{4-12}$$

where,

$m_{sc,i}$ is the mass of the subcomponents at section i (subcomponents consist of the skin, spar caps and the shear webs)

m_{foam} is the mass of the foam core at section i.

The CAD model of the blade in Solidworks is used to determine the surface area of each sub-component at each section of the blade. Figure 4-17 shows an example of how Solidworks is used to determine the surface areas of the different subcomponents at each section. In Figure 4-17 the surface area of the upper spar cap at section 1 is presented.

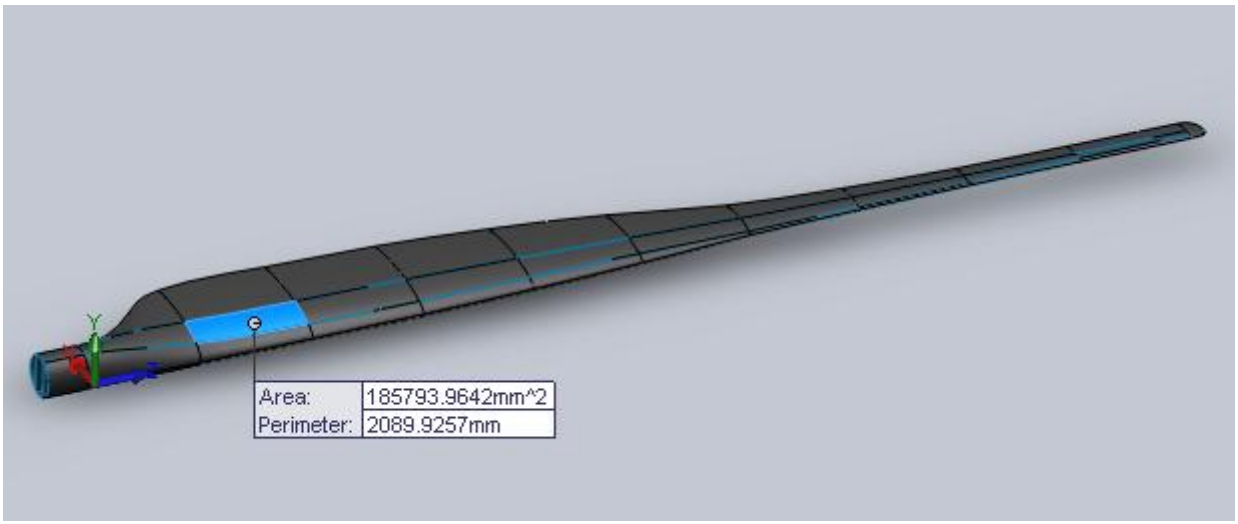

Figure 4-17: Example of how Solidworks is used to determine the surface area of each subcomponent of each section of the blade

The density of the glass fibre materials used is presented in kg/mm^2, as the thickness of the glass fibre layers is constant for each type of glass fibre type, in other words, unidirectional or bi-directional. The mass of each subcomponent at each section of the blade is therefore calculated with the use of Equation (4-13).

$$m_{sc,i} = \rho_m A_{sc,i} n_{layers} \tag{4-13}$$

where,

ρ_m is the density of the applicable material used in the subcomponent in this case in kg/mm^2

$A_{sc,i}$ is the surface area of the subcomponent at section i

n_{layers} is the number of layers as calculated for the subcomponent.

The core of the blade is conceptually designed to be filled with a foam material to improve the rigidity of the blade. This foam core material has no significant contribution to the blade structure in terms of bending or axial strength, however, it contributes to the rigidity and stiffness of the blade structure. This foam core in the blade thus also contributes to the weight of the blade and is considered in the calculation of the centrifugal load. The mass of the foam core at each section of the blade is calculated with the volume that it has to fill and its density in kg/mm^3. The density of the foam used is 60 kg/m^3 and thus 60 x 10^{-9}kg/mm^2. The volume of the foam is determined by

subtracting the volume of the glass fibre materials in the blade from the blade as a solid volume as described in Figure 4-18.

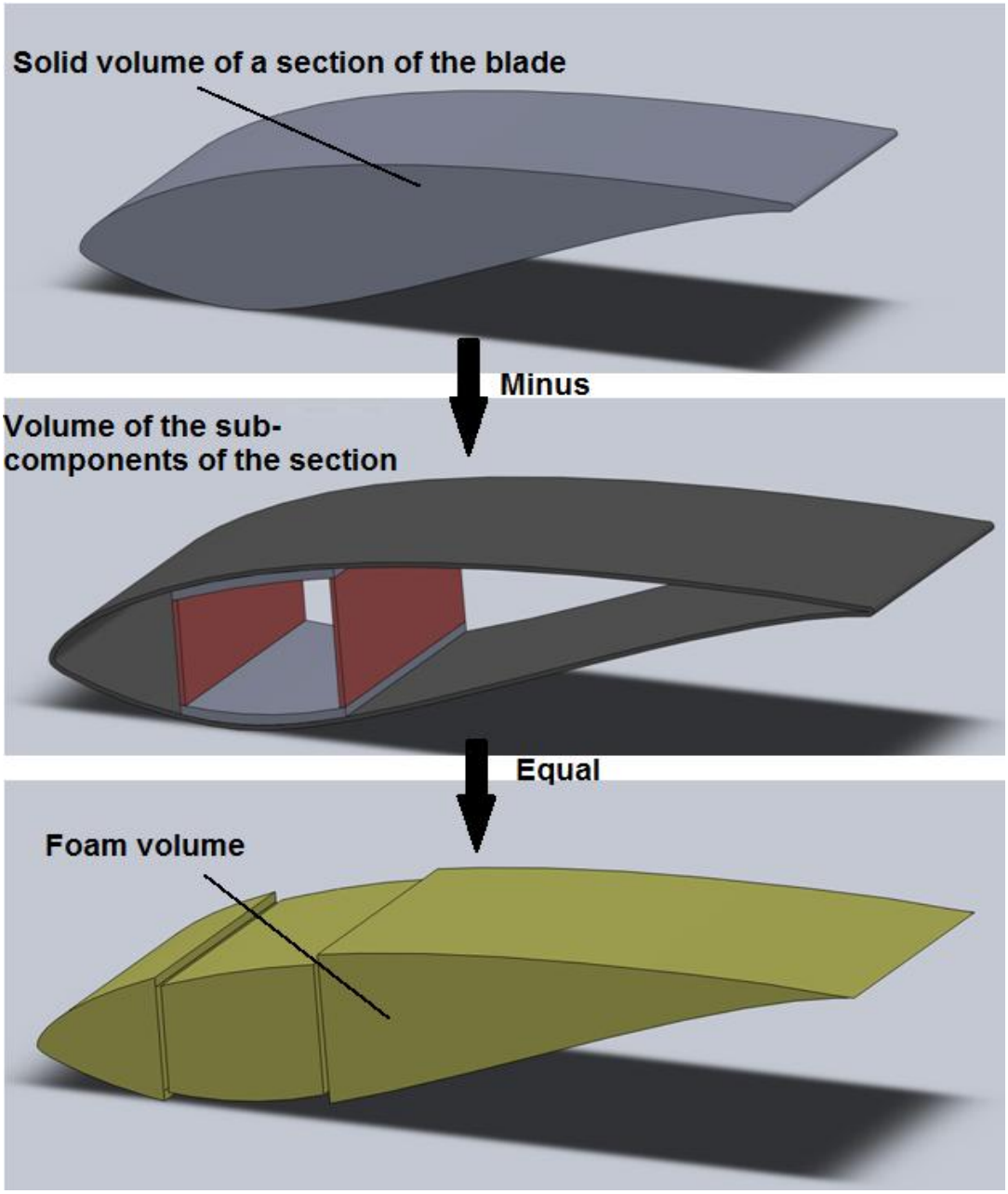

Figure 4-18: A description of how the volume of the foam in each section of the blade is determined

Thus, the mass of the foam in each section is calculated with Equation (4-14).

$$m_{foam.i} = \rho_{foam} V_{foam,i} \tag{4-14}$$

where,

ρ_{foam} is the density of the foam

$V_{foam,i}$ is the volume of the foam in section i.

The material density, layer thickness and name specifications are given in Table 4-6. The mass of the subcomponents and the foam at each section of the blade is calculated and presented in Table 4-7.

Table 4-6: Specifications of all the materials used in the blade

Material specification name	Density	Style number	Specification number	Weave pattern	Thickness
Unidirectional Glass filament fabric (Spar Caps)	220g/m^2	92145	MIL-Y-1140H	Plain	0.22mm
Bidirectional Glass twill filament fabric (shear webs and skin)	280g/m^2	92125	MIL-Y-1140H	2 x 2 Twill	0.28mm
Foam Core (Core)	60kg/m^3				

Table 4-7: The mass in kg calculated for each subcomponent at each section of the blade

Section	Spar Caps	Skin	Shear webs	foam	Total mass of section
1	4.84	0.66	1.88	4.93	12.30
2	3.15	2.95	0.82	3.77	10.70
3	2.99	0.78	0.65	3.38	7.80
4	2.26	0.75	0.45	2.73	6.19
5	1.38	0.65	0.38	1.92	4.34
6	0.98	0.47	0.20	1.02	2.68
7	1.00	0.31	0.12	0.40	1.83
8	0.79	0.24	0.08	0.22	1.33
9	0.42	0.21	0.05	0.17	0.84
10	0.14	0.22	0.03	0.19	0.59
Total mass of sub-comp.	17.95	7.25	4.67	18.75	48.61(total blade weight)

The mass of the blade does not, however, only consist of the mass of the subcomponents and the mass of the foam, it also consists of the resin used in the manufacturing of the blade. The mass of the resin is taken into account by multiplying the mass of all the glass fibre components of the blade by two, as the blade is manufactured with a resin-to-composite volume ratio of 1:1. Therefore, the mass of the resin is equal to the mass of the glass fibre material. This resulted in a mass table including the mass of the resin as seen in Table 4-8.

Table 4-8: The mass in kg calculated for each subcomponent at each section of the blade with the mass of the resin also taken into consideration

WITH RESIN = fibre weight x2					
Section	**Spar Caps x2**	**Skin x2**	**Shear webs x2**	**foam x1**	**Total mass of section**
Root	9.67	1.31	3.75	4.93	19.67
1	6.30	5.90	1.65	3.77	17.62
2	5.97	1.57	1.29	3.38	12.22
3	4.52	1.50	0.90	2.73	9.65
4	2.76	1.31	0.77	1.92	6.76
5	1.97	0.95	0.40	1.02	4.34
6	2.00	0.63	0.24	0.40	3.26
7	1.59	0.48	0.16	0.22	2.45
8	0.83	0.41	0.10	0.17	1.52
9	0.28	0.45	0.07	0.19	0.99
Total mass of sub-comp.	35.89	14.50	9.33	18.75	78.47(total blade weight)

With the mass of all the sections known, the centrifugal force at each section is calculated as previously mentioned with Equation (4-12). The centrifugal forces at each section of the blade are used to determine the number of unidirectional glass fibre layers to be added to the spar caps with the use of the axial stress equation as seen in Equation (4-15), with the design stress as previously determined for unidirectional glass fibre. The area obtained from this equation is the cross-section area of the layers to be added to the spar caps and since the width of the spar caps is known from Chapter 4, section 4.4, the thickness is calculated to determine this number of layers.

$$A_{added,i} = \frac{F_{z,i}}{\sigma_d} \tag{4-15}$$

where,

$A_{added,i}$ is the cross-section area of unidirectional glass fibre to be added

F_i is the centrifugal force as calculated for section i

σ_d is the design stress for unidirectional glass fibre as previously calculated in Chapter 4, section 4.2.

Table 4-9 shows the calculation of the spar cap cross-section area to be added at each section of the blade. Note that the mass used for the calculation of the centrifugal force at each section increases from the tip of the blade to the root end (section 10 to section 1). This is due to the centrifugal force that is calculated not only for the mass of a single section, but also for the mass of all the sections further away from the root of the blade. Hence, the spar cap at a certain section of

the blade should withstand not only the centrifugal force due to its own weight but also the centrifugal force caused by the mass of the sections further away from the centre of rotation.

Table 4-9: Calculation of the spar cap cross-section areas to be added

Section	Mass (kg)	Radius (m) from center of rotation	Rotational speed (rad/s)	Centrifugal force (N)	Spar cap Area (mm^2) to be added
Root	78.47	0.888454	12.566	11009.2	75.69
1	58.80	1.711424	12.566	15890.3	109.25
2	41.18	2.534394	12.566	16479.2	113.29
3	28.96	3.357364	12.566	15354.6	105.56
4	19.31	4.180334	12.566	12746.2	87.63
5	12.55	5.003304	12.566	9917.5	68.18
6	8.21	5.826274	12.566	7557.0	51.95
7	4.95	6.649244	12.566	5199.3	35.75
8	2.50	7.472214	12.566	2954.7	20.31
9	0.99	8.295184	12.566	1290.7	8.87

The areas obtained from Table 4-9 are added to the area as calculated of the spar caps in the previous sub-clause. This total area is used in same mathematical model used to calculate the thickness of the spar caps but the total spar cap area is set as the target value and not the moment of inertia as in the previous case. Therefore, a new spar cap thickness is determined for each section and the number of layers in the spar caps at each section is determined. Table 4-10 shows the number of layers added to the spar caps. (Note that if the area added to the spar cap resulted in a thickness less than that of a single unidirectional glass fibre layer, no extra layers are added, in other words, section 9 and 10.)

Table 4-10: The number of layers added to each section of the blade to allow for the centrifugal load

blade section	number of layers added
1	2
2	2
3	2
4	2
5	1
6	1
7	1
8	1
9	0
10	0

4.7 Test for subcomponent strength against edgewise bending and shear

The subcomponents of the blade are designed in the previous sub-clauses to withstand the maximum flapwise bending and shear loads. Thus, the maximum loads from Chapter 3 in the edgewise bending direction (bending about the x axis and shear in the y-direction) are not used in the layup design of the blade's subcomponents. Therefore, the topology of the subcomponents as designed in the previous sub-clauses is tested against edgewise loading to determine if it could withstand these loads with the prescribed safety factor or if extra layers are needed. The maximum edgewise loads (load case F) are applied to the blade with the subcomponent topology as calculated in the previous sub-clauses and a safety factor according to the maximum stress criterion is determined. This safety factor is compared to the design safety factor of 3.3 as determined in Chapter 4, section 4.1 and the number of layers in the subcomponents is increased if the safety factor does not meet the design requirement.

The spar caps are influenced by the edgewise bending and shear loads are therefore tested for strength against these loads. The edgewise bending stress in the spar caps is also determined with the bending stress formula as in Chapter 4, section 4.4 ,but the moment of inertia is calculated about the x-axis as presented in Figure 4-19.

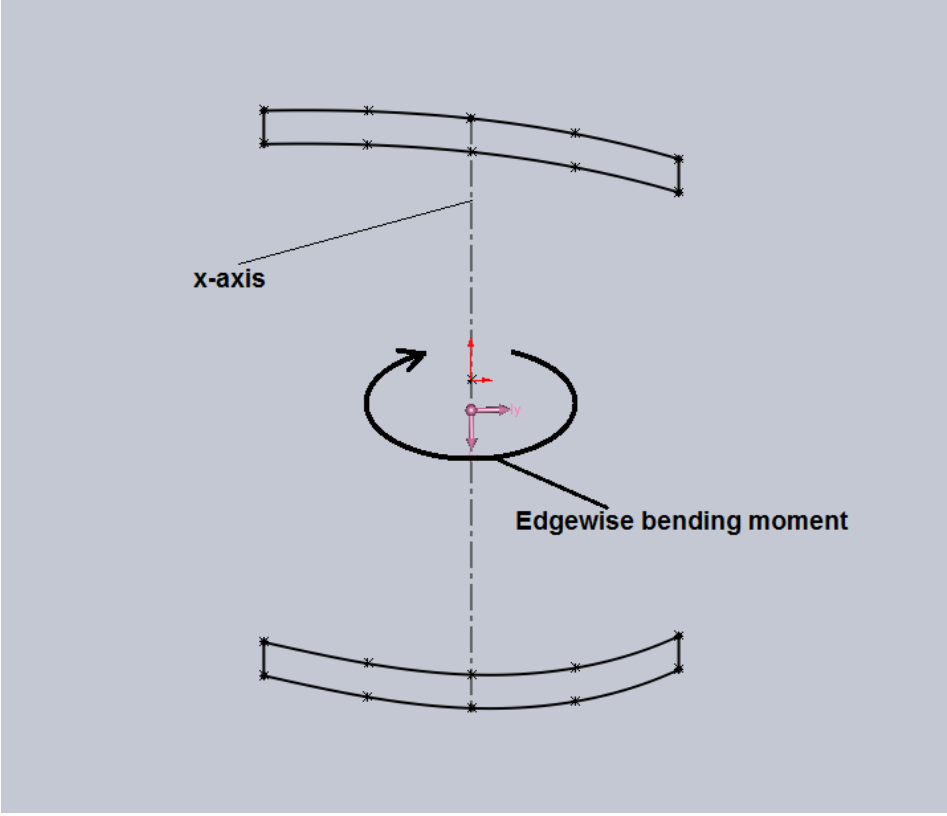

Figure 4-19: The edgewise bending stress calculated for the spar caps about the x-axis. The topology of the spar caps used is as calculated in the previous sub-clauses

The safety factor of the spar caps for edgewise bending is calculated for each section of the blade and is presented in Table 4-11. From Table 4-11 it is clear that the safety factor of the spar car caps for edgewise bending at all the sections of the blade is above the required design safety factor of 3.3 and thus no layers are added to the spar caps.

Table 4-11: The safety factors of the spar caps for edgewise bending loads

blade section	SF for edgewise bending
1	5.2
2	7.4
3	11.3
4	14.0
5	21.2
6	23.0
7	33.2
8	40.9
9	41.1
10	25.4

The skin and the spar caps are tested for strength against the edgewise shear loads. The shear flow is calculated for the skin and the spar caps in the edgewise direction (in the y-direction). The shear flow that a single layer of unidirectional and bi-directional glass fibre could withstand is then determined in the same way as in Chapter 4, section 4.3, and therefore the number of layers needed to withstand the calculated shear flow in the skin and spar caps is calculated. This number of layers required to withstand the shear flow in the skin and the spar caps is compared to the number of layers currently in the skin and spar caps and thus a safety factor is calculated. Table 4-12 presents the safety factors of the skin and the spar caps for edgewise shear. From Table 4-12 it is also clear that the safety factors of the above-mentioned subcomponents are above the required design safety factor of 3.3 and therefore no extra layers are added to the skin or spar caps.

Table 4-12: The safety factor of the spar caps and shear webs for shear loading

blade section	spar caps SF for edgewise shear	skin SF for edgewise shear
1	16.7	3.7
2	22.7	11.4
3	24.9	21.5
4	32.4	27.9
5	32.2	44.0
6	47.4	65.5
7	61.3	64.4
8	86.7	77.7
9	83.3	101.0
10	55.8	204.9

4.8 Summary

In this chapter the topology of the blade was mathematically modelled to determine the layup/ thickness distribution of the subcomponents of the blade. The calculation of the subcomponent thicknesses is based on the maximum stress criterion, with the design stresses calculated with the partial safety factors as described by IEC61400-2 design guideline. The subcomponents of the blade comprise the skin, spar caps and shear webs, as well as a foam core. The skin and shear webs of the blade are designed with bi-directional glass fibres oriented at ±45º along the length of the blade. The spar caps are designed with unidirectional glass fibres oriented at 0º along the blade length.

The thickness distribution of the blade skin is determined by applying the torsion load case (load case J) to the shear flow formula. The shear flow that a single layer of BID glass could withstand is calculated with LAP and thus a number of layers to withstand the torsion load with the predetermined safety factor of 3.3 are calculated. The calculation of the skin thickness distribution is an iterated process using a spreadsheet and the blade model in Solidworks to obtain the geometric variables. A minimum of 2 BID glass fibre layers are set as a design minimum.

The thickness distribution and topology of the spar caps is calculated with the maximum flapwise bending load (load case C) and the use of the bending stress formula. As the design stress and the bending moment at each section of the blade are known (already calculated), the variable to be solved in the bending stress formula is the moment of inertia. Thus, the moment of inertia is used as the target value to determine the width and thickness of the spar caps. The thicknesses of the spar caps are calculated for different widths varied in 1% increments of the chord length of each section. The topology of the spar caps are then optimised by choosing the spar cap width and thickness combination providing the smallest area, thus minimising the weight of the blade.

The thickness distribution of the shear webs is performed with the same iteration procedure as with the skin of the blade. The shear formula is also used in the shear web layup design, however, the shear formula for shear forces is used and not the shear formula for torsion as in the case of the blade skin. The calculation also consists of an iteration process where the thickness of the shear webs is used as the iteration variable to determine the shear flow in the shear webs. The CAD model in Solidworks is used to model the cross-section topology of the shear webs and to determine the geometric variables used in the shear flow formula.

After all the above-mentioned subcomponents are designed at each section of the blade, the mass of each section is calculated to determine the centrifugal force on the blade. This centrifugal force is then used to calculate the number of unidirectional glass fibre layers to be added to the spar caps to withstand this centrifugal load. The mass of the blade is determined with the surface area of each

of the subcomponents as obtained from the CAD model in Solidworks, the density of the materials used in the different subcomponents and the number of layers as calculated for each section of the blade.

The blade also includes a foam core for the purpose of increasing its rigidity. This foam core is not modelled in the subcomponent topology modelling as it does not significantly contribute to the bending, torsion and shear strength of the blade but increases the rigidity of the blade as will be seen in the finite element analysis of the blade. The mass of the foam core, however, contributes significantly to the total mass of the blade and is therefore considered in the calculation of the blade mass. The resin used in the manufacturing of the blade is also considered in the calculation of the blade mass and is modelled with a glass-fibre-to resin mass ratio of 1:1. Thus, the mass of the resin is modelled as equal to the mass of the glass fibres used in the blade. This gives a fibre-to-resin ratio which can conservatively be obtained using hand lay-up methods.

The mass of each section of the blade is calculated and thus the centrifugal forces at each section are calculated. These centrifugal forces are used in the axial stress formula and the number of layers to be added to the spar cap are calculated based on the area obtained from the axial stress formula. Table 4-13 presents a summary of the number of layers of each subcomponent at each section of the blade as calculated in this chapter. The blade model with the layup schedule as presented in Table 4-13 is used as preliminary values for the structural design and finite element analysis of the blade in the FEM modeller program Patran in the next chapter. Therefore, the thickness distribution of the subcomponents as calculated in this chapter is prone to adjustment and is not the final values for the layup schedule of the blade.

Table 4-13: A summary of the layup schedule (number of layers) of each subcomponent at each section in the blade as calculated in Chapter 4

Section	Skin (BID Glass +-45^o)	Spar caps (UD Glass 0^o)	Shear webs (BID Glass +- 45^o)
1	2	76	12
2	2	56	11
3	2	45	11
4	2	32	11
5	2	22	11
6	2	22	8
7	2	22	8
8	2	22	7
9	2	15	5
10	2	7	3

CHAPTER 5 DETAILED STRUCTURAL DESIGN USING FINITE ELEMENT ANALYSIS

The detailed structural design of the blade can now be initiated after the load cases are calculated and the preliminary layup schedule is determined. The layup schedule of the blade's subcomponents will, however, change during the finite element analysis as each subcomponent was respectively designed in the previous chapter for a certain load while not taking the other subcomponents into account. This chapter therefore includes the setup of the finite element model, a description of how the load cases are applied to the blade and a detailed analysis of the FEA results to complete the structural design and therefore the topology of the subcomponents of the blade.

The topology and layup schedule of each subcomponent are therefore changed to comply with the predetermined design requirements – the safety factor and the tip displacement. The methodology for the structural design is based on adding or subtracting the number of layers in each of the subcomponents in order to obtain the required design safety factor in each subcomponent. After the required safety factor is obtained over whole length of the blade, the tip deflection of the blade is checked and adjustments are made to the layup schedule to obtain the required maximum tip deflection. The topology of the subcomponents is also modified to minimise stress concentration regions. This was not accounted for in the mathematical design calculations in the previous chapter.

5.1 Finite element model

The CAD model of the blade is modelled in the 3D modelling software package Solidworks. The blade and all of its subcomponents are modelled as 2D surfaces, while the topology of the subcomponents is modelled as calculated in the previous chapter. Thus, no thicknesses are applied to any of the subcomponents in the CAD model as the thicknesses are applied in the FEM modeller Patran, where the layup schedule for each subcomponent in each section is applied. The finite element model is presented with all the surfaces that represent all the subcomponents at each section of the blade. Figure 5-1 shows the blade modelled as 2D surfaces for the use in the finite element analysis. Figure 5-2 is a cross-section of the blade model to present the topology of the shear webs. Note that the shear webs are presented in red.

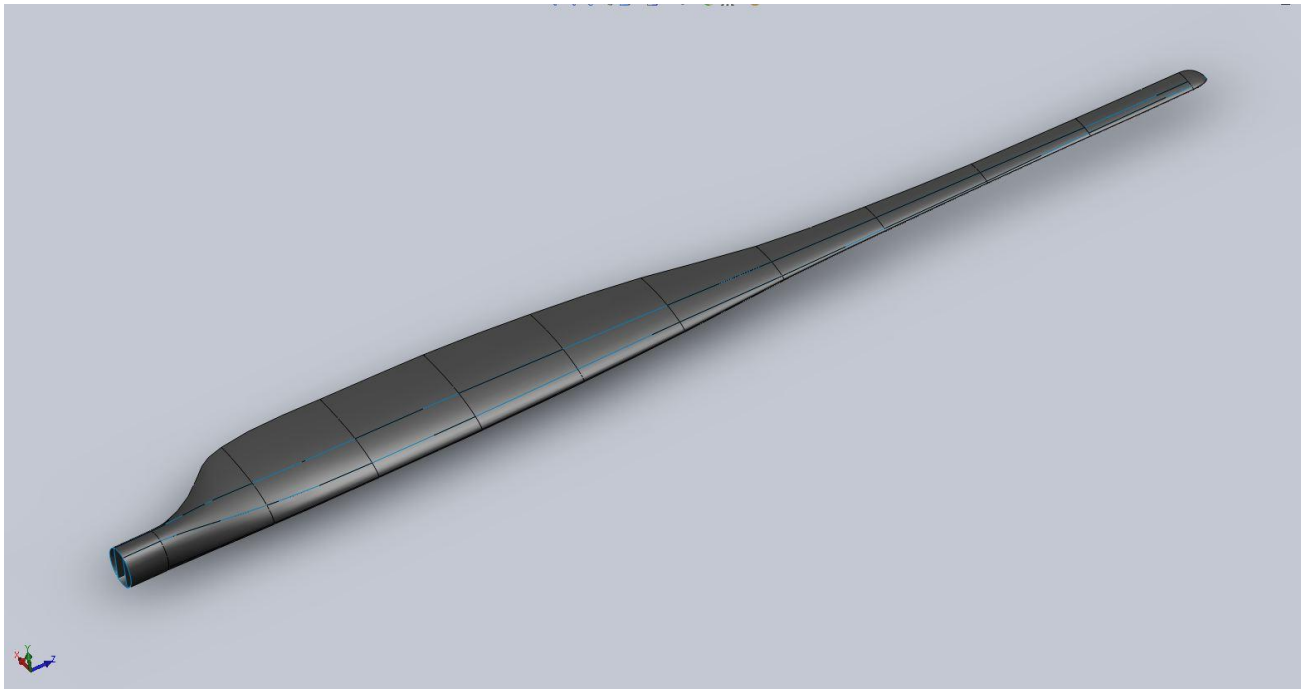

Figure 5-1: The blade modelled from 2D surfaces showing the topology of the subcomponents of the blade

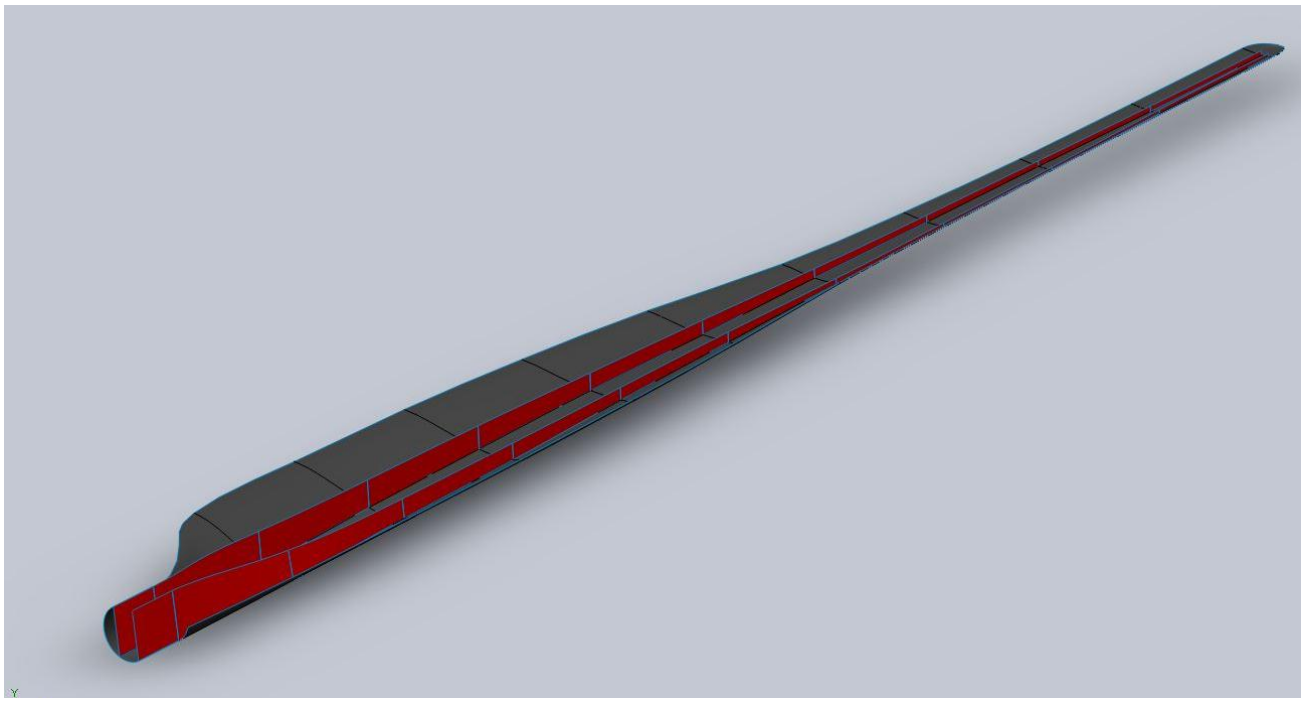

Figure 5-2: A cross-section of the FEM blade model presenting the shear web topology

5.2 Computational mesh

The 2D blade model is imported to Patran and a mesh with 10x10mm elements is applied to the blade geometry. This mesh resulted in 117 653 elements and 115 953 nodes. Mesh refinement studies are performed on the model to determine whether the mesh density is appropriate for this model. The results proved a variance of less than 4% in the maximum stress results when the density of the mesh is made finer. The finer mesh used in the refinement studies consisted of

5x5mm elements, while the coarser elements consisted of 20x20mm elements. The 10x10mm elements are chosen to maintain accuracy in the blade geometry as the coarser mesh produces a less smooth blade geometry especially at the leading and trailing-edge regions.

This mesh is also chosen before the 5x5mm meshes to save calculation time,as the 5x5mm mesh provides more than double the amount of elements which would increase the solving time significantly. A magnified view of the meshed blade model is presented in Figure 5-3. Note that Figure 5-3 is a magnified view of the root end to show the mesh.

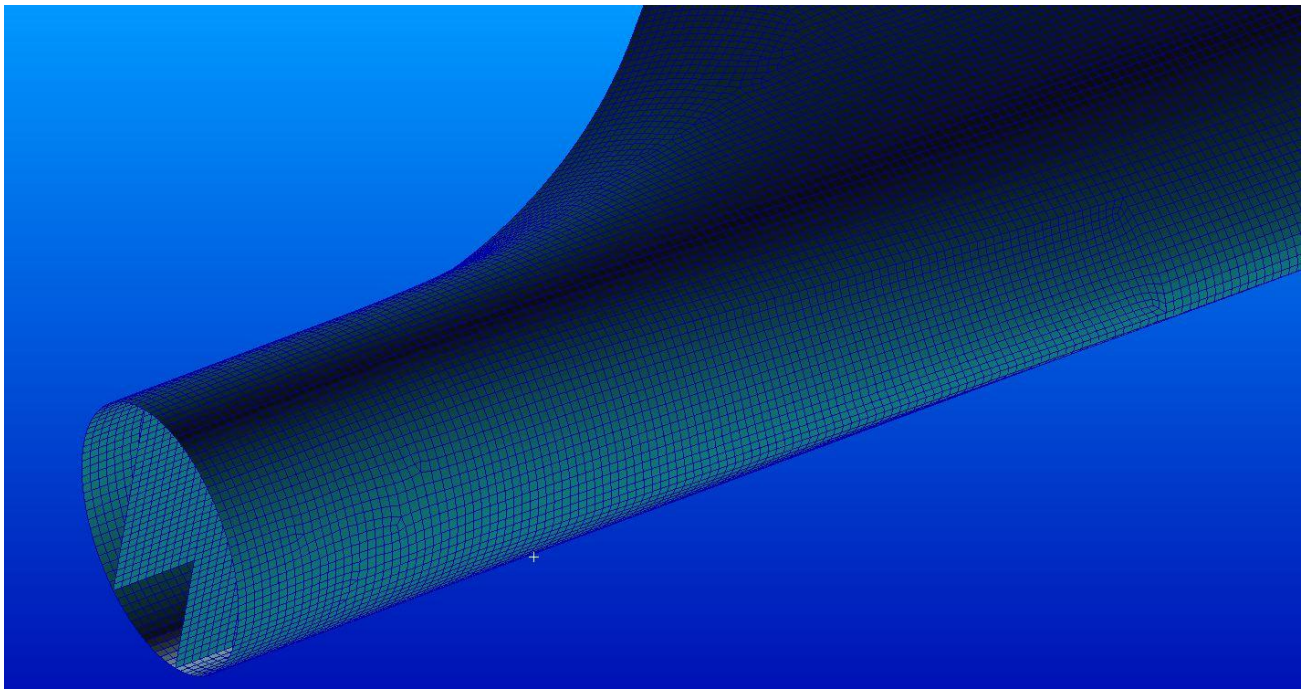

Figure 5-3:The meshed model of the blade geometry for the use in the FEA

5.3 Material properties and layup orientation

The materials are defined as orthotropic with the properties as previously presented in Chapter 4, section 4.2. As previously mentioned, the skin and shear web material are orientated at 45^{o} along the longitudinal axis of the blade while the spar caps' UD glass fibres are orientated in the 0^{0} direction. Figure 5-4 shows the layup orientations of the material in their respective subcomponents in a single section of the blade.

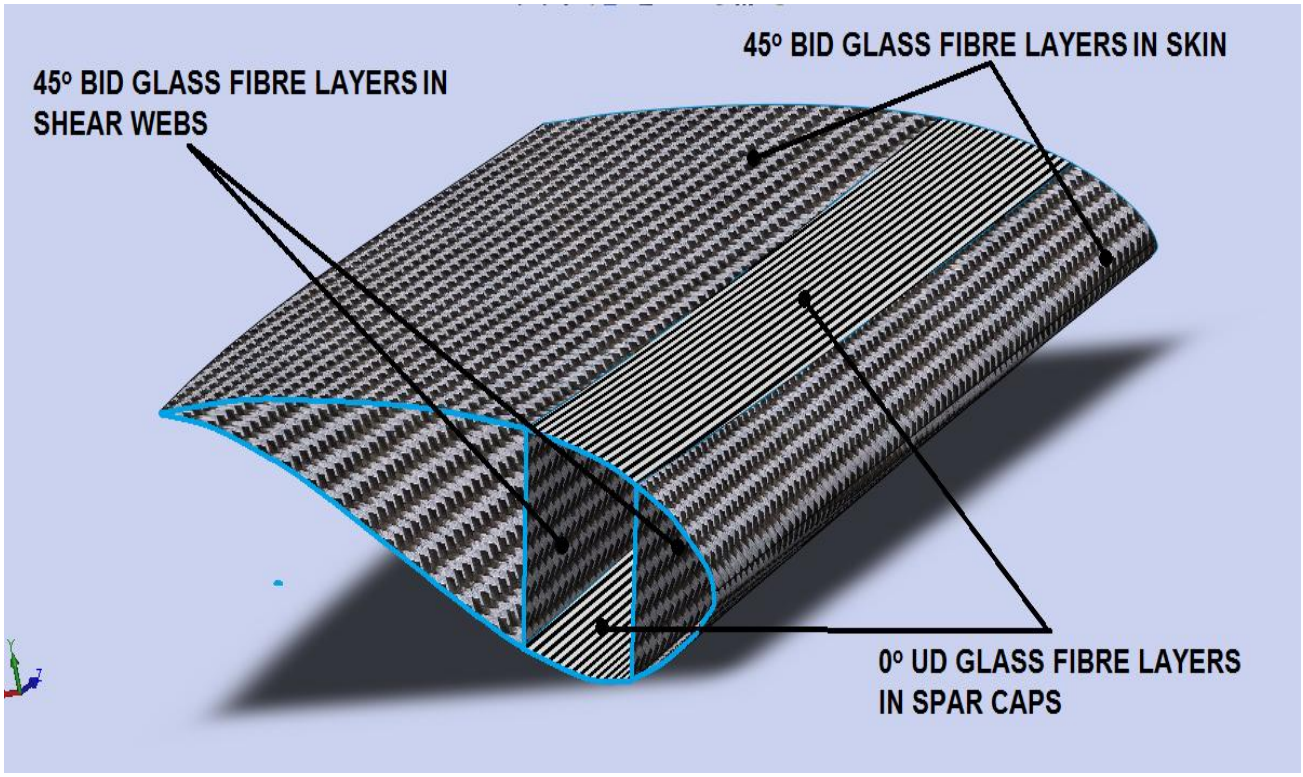

Figure 5-4: A representation of the orientation of the two materials applied to the respective subcomponents

5.4 Loads and boundary conditions

The load cases applied to the FEM model are those calculated in Chapter 3, however, some load cases are adjusted to account for the centrifugal and torsional load at the specified rotational speed of each load case. Therefore, the load cases applied to the FEM model are summarised in Table 5-1.

Table 5-1: The load cases as applied to the finite element model

Load case B	**Description**
Flapwise bending	Bending forces as calculated at each section for load case B
Centrifugal load	Calculated at each section @ $\omega_{n,design}$
Torsion load	Calculated at each section @ $\omega_{n,design}$
Load case C	
Flapwise bending	Bending forces as calculated at each section for load case C
Centrifugal load	Calculated at each section @ $\omega_{n,design}$
Torsion load	Calculated at each section @ $\omega_{n,design}$
Load case D	
Flapwise bending	Bending forces as calculated at each section for load case D
Load case E	
Centrifugal load	Centrifugal load calculated @ $\omega_{n,max}$ with mass as calculated in preliminary layup schedule

Load case F=G	
Edgewise bending	Bending forces as calculated at each section for load case F or G (load case F = G)
Load case H1 (for stationary hub)	
Flapwise bending	Bending forces as calculated at each section for load case H1
Load case H2 (for hub rotating at $\omega_{n,max}$)	
Flapwise bending	Bending forces as calculated at each section for load case H1
Centrifugal load	Centrifugal load calculated @ $\omega_{n,max}$ with mass as calculated in preliminary layup schedule
Torsion load	Calculated at each section @ $\omega_{n,max}$

5.4.1 Flapwise bending forces

The flapwise bending forces as calculated for load cases B, C, D, H1 and H2 are distributed over the length of the blade by dividing the force at each section by the number of nodes on the high-pressure side of the blade surface as seen in Figure 5-5. Figure 5-5 shows the flapwise bending forces at each section of the blade as calculated for load case B. Note that all flapwise bending forces are applied in the same manner, only the magnitude of the forces for the different load cases change. Figure 5-6 is a magnified view of the flapwise bending forces at section 1 of the blade for clarity purposes.

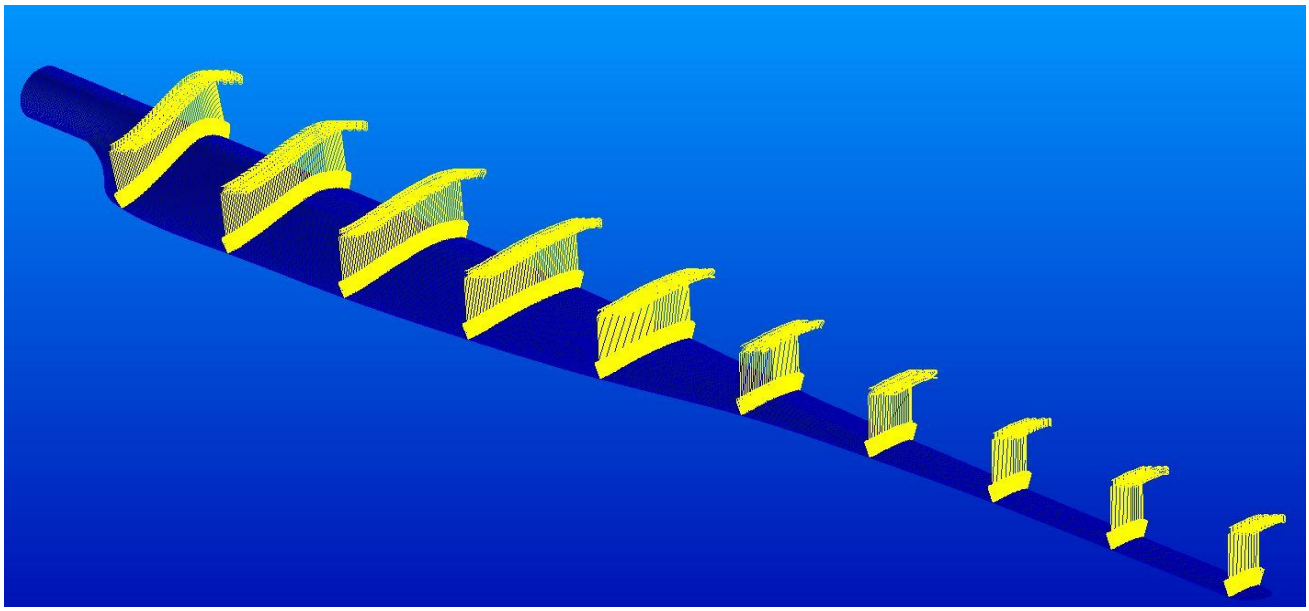

Figure 5-5: The flapwise bending forces applied to the FEM model of the blade

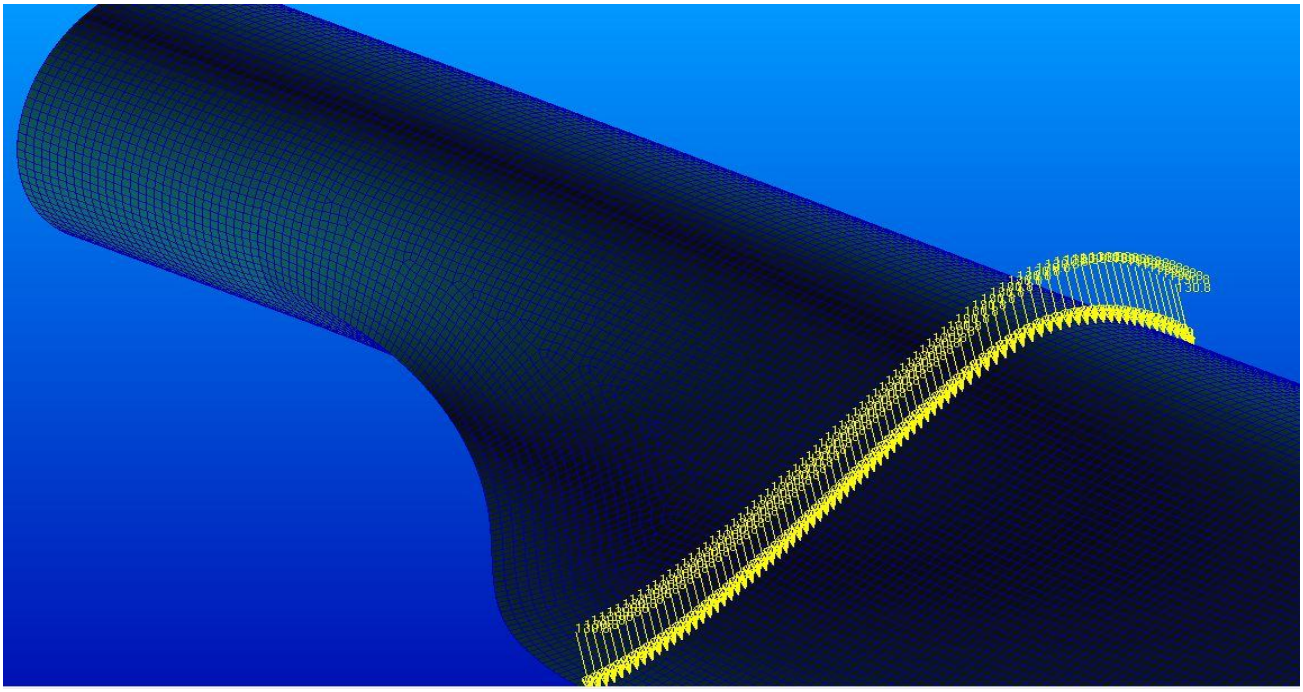

Figure 5-6: A magnified view of the flapwise bending forces applied to the nodes at section 1 of the blade

5.4.2 Centrifugal forces

The centrifugal loads for load cases B, C, D and H2 are applied in the same manner as the flapwise loads where the forces at each section are divided by the number of nodes at their respective sections. The centrifugal force at each section, now divided by the number of nodes at that section, are applied to these nodes. Figure 5-7 shows the centrifugal forces at each section of the blade as calculated for load case C. All centrifugal loads for the different load cases are applied in the same manner, only the magnitude of the forces are subjected to change for the different load cases. Note that the magnitude of the centrifugal loads is adjusted as the topology of the blade's subcomponents and thus its weight changes throughout the structural design phase of the project.

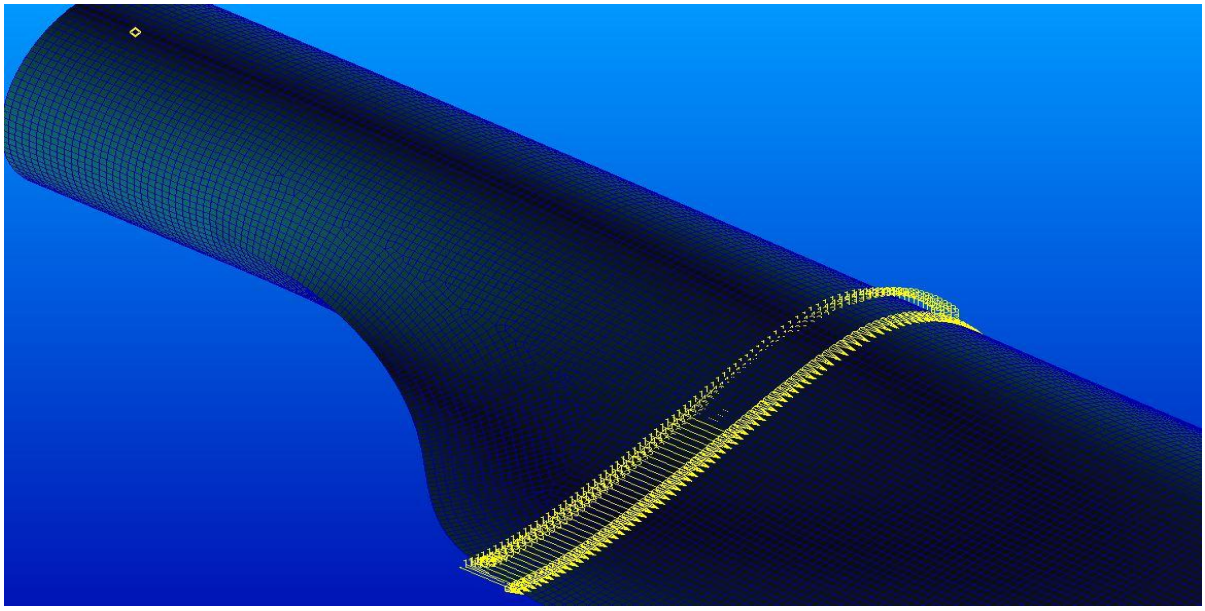

Figure 5-7: A magnified view of the centrifugal forces applied to the nodes at section 1

5.4.3 Torsion moments

The torsion loads for load cases B, C, D and H2 are applied by adding forces to the leading and trailing edges at each section. These forces at the leading and trailing edge of each section are calculated to produce a couple moment at the quarter chord point of each section to represent the torsion moment as calculated about the quarter chord point of each section. The magnitude of the forces at the leading and trailing edge of each section is calculated as in equation 5-1 and equation 5-2. See Figure 5-8 for the description of the variables.

$$F_{leading\ edge,i} = \frac{T_i}{2d_{leading\ edge,i}} \tag{5-1}$$

and

$$F_{trailing\ edge} = \frac{T_i}{2d_{trailing\ edge,i}} \tag{5-2}$$

where,

T_i is the torsion moment about the quarter chord as calculated for section i

$d_{leading\ edge}$ is the perpendicular distance from the quarter chord point of section i to its leading edge

$d_{trailing\ edge}$ is the perpendicular distance from the quarter chord point of section i to its trailing edge.

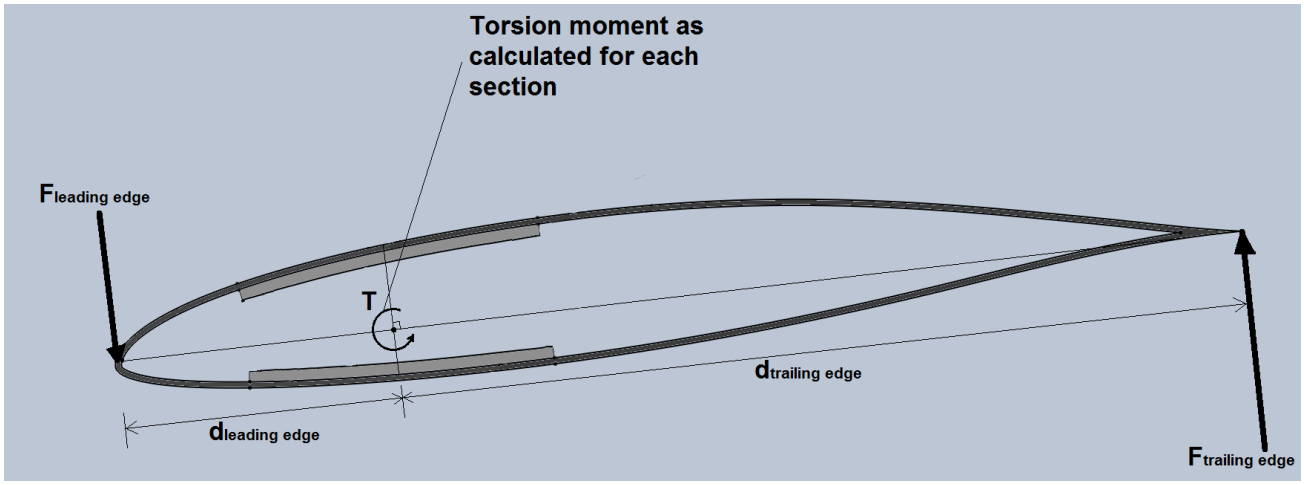

Figure 5-8: Description of the forces on the leading and trailing edges to obtain the torsion moment about the quarter chord point of each section of the blade

Figure 5-9 shows the torsion forces at the leading and trailing edges applied to the FEM model.

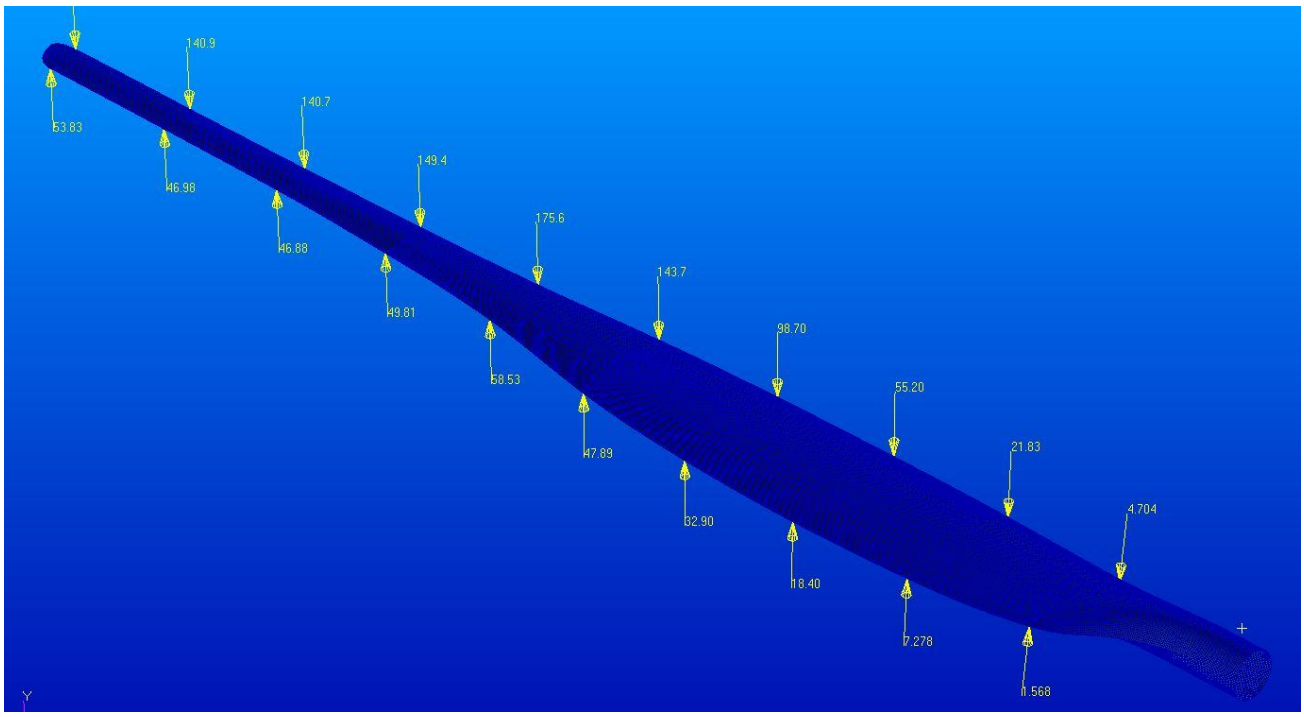

Figure 5-9: The forces applied to the leading and trailing edges at each section of the blade to obtain the torsion moment about the quarter chord point of each section

5.4.4 Edgewise bending forces

The edgewise bending forces are applied to the blade similar to the centrifugal load but oriented in the edgewise direction. The edgewise bending forces of load case F and G are also divided by the number of nodes at each section and then applied to these nodes. Figure 5-10 shows the edgewise bending forces applied to the FEM model. Figure 5-11 shows a magnified view of the edgewise bending forces at section 10 of the blade.

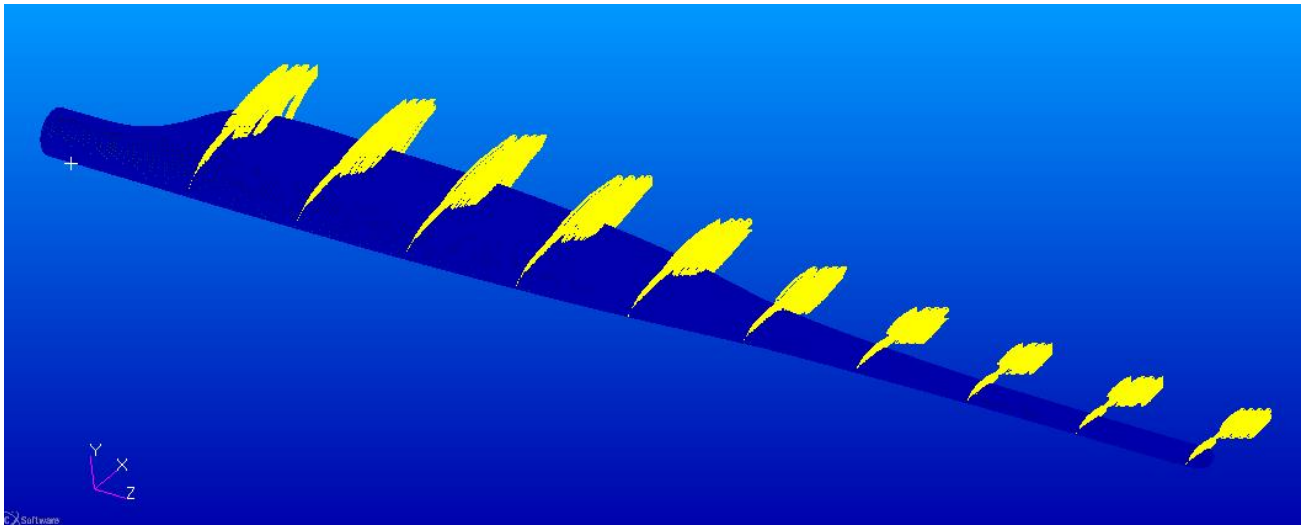

Figure 5-10: The edgewise bending forces applied to the FEM model of the blade

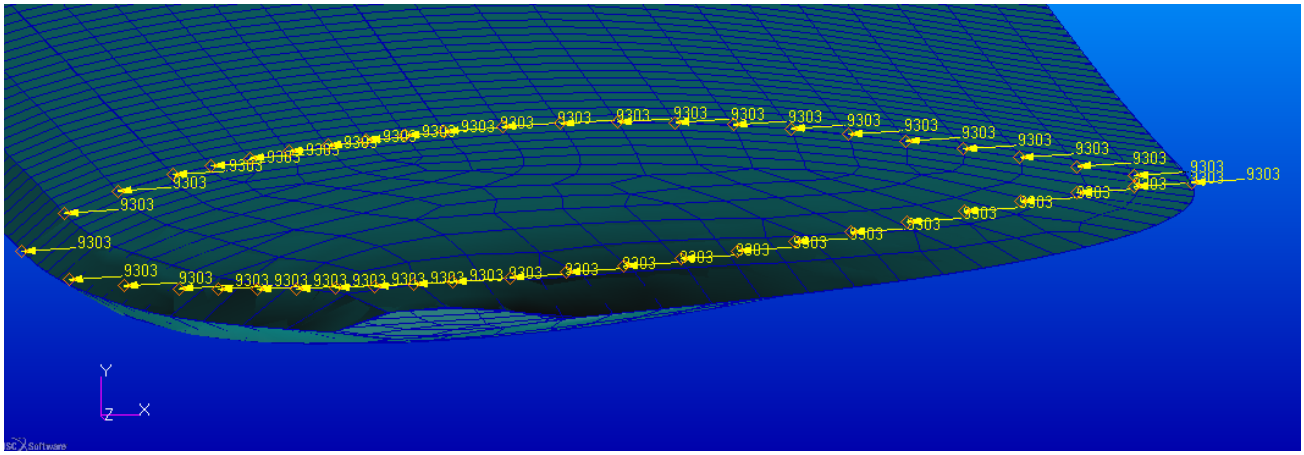

Figure 5-11: A magnified view of the edgewise bending forces applied to the nodes at section 10 of the blade

5.4.5 Root constraints

The root section of the blade is constrained in the FEM model as if it is connected to the hub of the wind turbine. The constraint is applied by constraining all the nodes in the circular root section that will be inserted into the hub of the wind turbine. The nodes are totally constrained for all translational and rotational movement, thus constraining all degrees of freedom. Figure 5-12 shows the constrained root end of the blade.

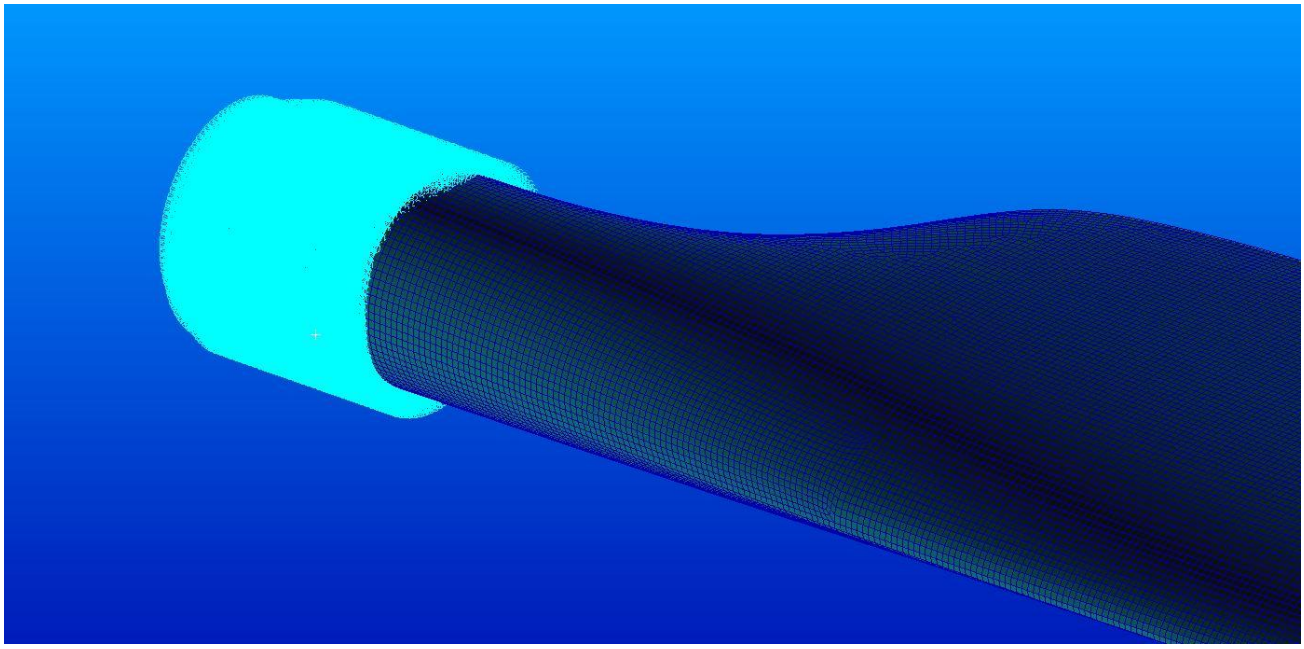

Figure 5-12: The root end of the blade constrained by constraining all the nodes in all degrees of freedom

5.5 Verification of the FEA design model

The layup thickness distribution and topology of the blade's subcomponents as determined previously in Chapter 4, the preliminary design, are used to verify the FEA model. The verification of the FEA model is performed to ensure that the material properties, loads, layup sequence, layup orientation and mesh are applied correctly and that the FEA of the model provides significant results compared to the preliminary design values.

The safety factor results obtained from analysing the blade with this preliminary layup as calculated through hand calculations are compared to the predetermined design safety factor as calculated in Chapter 4. Thus, the FEA is set up to simulate the blade in the same method the preliminary design calculations were applied to determine the layup distribution and topology of the subcomponents. The blade's skin is therefore loaded with the torsion load only, as this was the load case used to calculate the skin thickness at each section of the blade. The spar caps and shear webs are exposed to load case C's flapwise bending forces as this load is used to determine the thickness distributions of these subcomponents.

The safety factor distribution results showed a good correlation to that of the calculated design requirement from the preliminary design chapter, and therefore the FEA model is accepted as verified. The verification simulation results of the FEA model is presented in Appendix H.

5.6 Detailed structural design

The detailed structural design of the blade as previously mentioned is performed by adjusting the layup schedule of the subcomponents of the blade in the finite element analysis until the design requirements are met. These design requirements are the safety factor and the tip deflection of the blade. The required safety factor for all the subcomponents at all the sections of the blade is 3.3 as previously calculated according to the IEC 61400-2 design guidelines. The maximum stress criterion was used in the preliminary design phase of the blade, although the Tsai Wu criterion is used in the detailed structural design due to it conservatism and applicability to composite materials. The maximum stress criterion was thus only used due to its simplicity in its calculation to validate the FEA model.

Analysis of the blade under all the load cases respectively showed that load case C causes the highest stress and lowest safety factor distributions. Therefore, the blade is designed to satisfy the design requirements while exposed to load case C. When the design requirements are met for the blade exposed to this load case, the safety factor and tip deflection results are checked for all the other load cases.

The structural design is performed by analysing the stress distributions and thus the safety factor distributions for each subcomponent over the length of the blade. Initial linear elastic FEA runs of the blade with the subcomponent layup schedules as determined in the preliminary design phase showed low safety factors in all the subcomponents which do not meet the design required safety factor of 3.3. This is due to the combined loads applied to the FEA model whereas the preliminary calculations only considered single loads for each subcomponent respectively. Thus, the subcomponents are exposed to a greater load due to the combination of bending, centrifugal and torsion, hence the higher stress and lower safety factor distributions. The preliminary design calculations also did not consider stress concentrations due to the geometry of the blade and its subcomponents. Layers are therefore added to the different subcomponents to decrease the stress distributions and increase the safety factor results, while the topology of the subcomponents is modified to minimise stress concentration regions.

Analyses of the skin of the blade showed safety factor distributions which are far lower than the design requirement, namely 0.125 as presented in Figure 5-13. This occurrence is due to the skin that is designed for torsion only and not accounting for the bending of the blade. Thus, the skin of the blade might be strong enough to withstand the torsion shear but is unable to withstand bending. According to Gurit (2011), the procedure of solving these high stresses in the skin, especially in the region between the spar caps and the trailing edge, is to increase the thickness of the skin. Note that the results displayed in the FEA program Patran presents a margin of safety. The safety factor is calculated from this margin of safety with the use of equation (6-1).

$$SF = Margin\ of\ safety + 1 \quad (6\text{-}1)$$

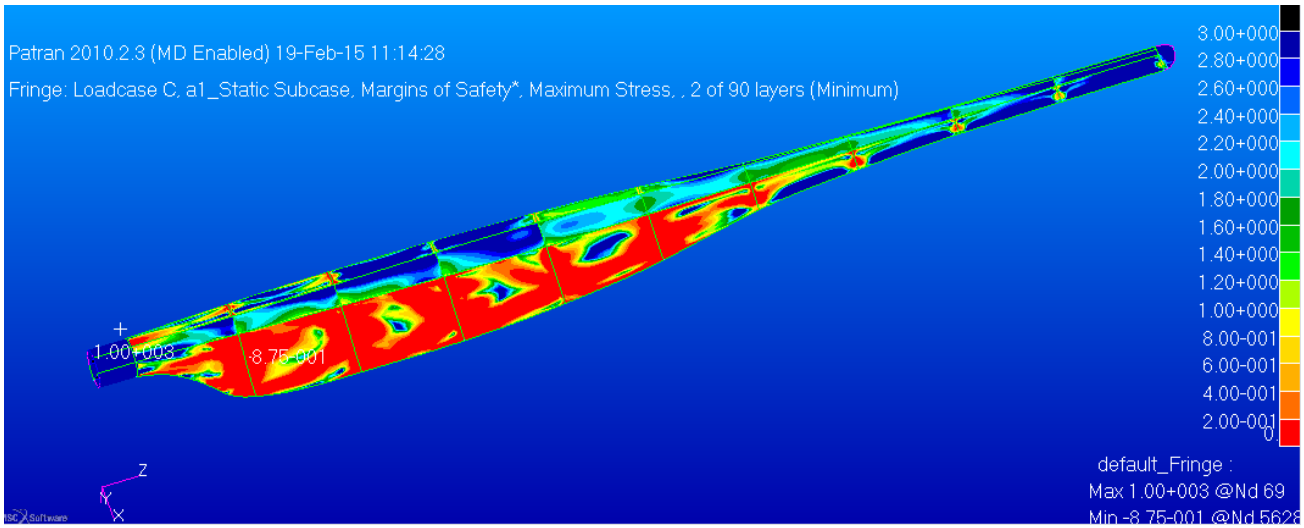

Figure 5-13: The low safety factors in the skin due to the bending of the blade

Gurit (2011) also noted that increasing the skin thickness by adding more FRP layers would make it strong enough but it would still be too flexible and would be a problem in keeping the aerodynamic shape and to resist buckling. Therefore, Gurit (2011) advised that the thickness of the shell should be increased by making it a sandwich structure with FRP skins on either side of a low density core material. The skin layup of the blade in this project is therefore changed to a sandwich structure by adding BID and UD glass layers on both sides of a standard 6mm low density foam core layer. This sandwich structure is applied to the skin regions outside the box spar region as seen in Figure 5-14.

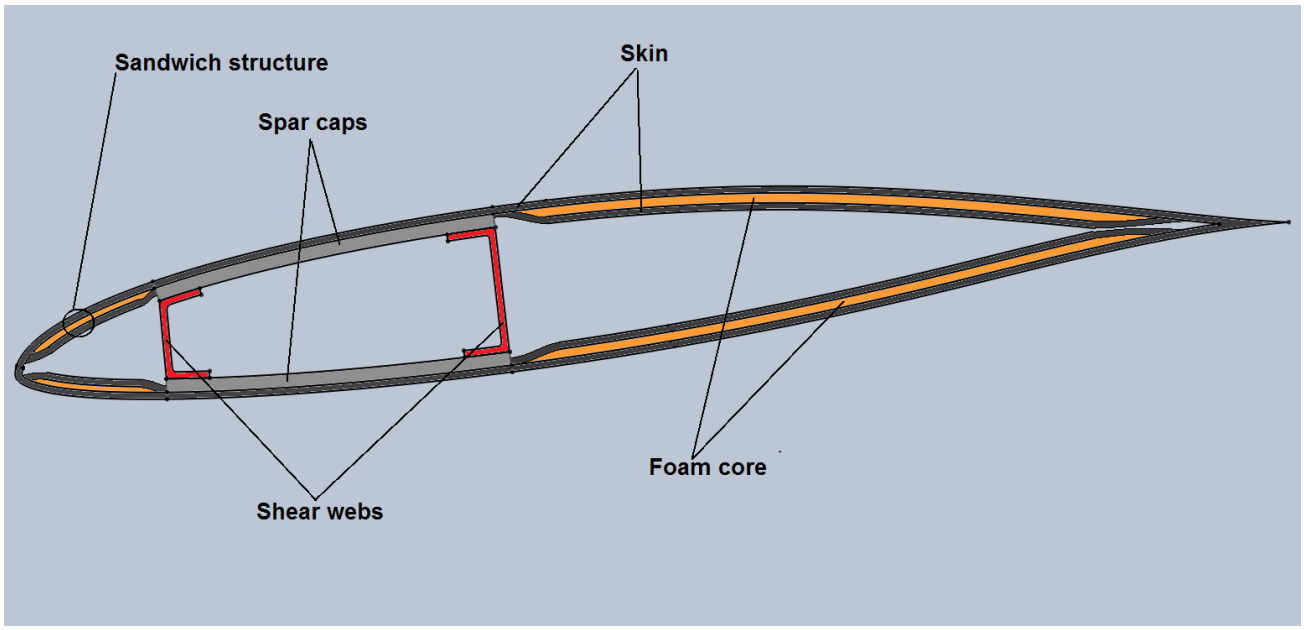

Figure 5-14: An illustration of the skin sandwich structure in the regions outside the box-spar

The spar caps also showed high stresses and did not meet the required safety factor especially in sections 1, 2 and 3, where the minimum is 1.67 as presented in Figure 5-15. The highest stresses appeared at the root end of the blade in these sections. These high stresses appeared to be caused by the topology of the spar caps near the root as it narrowed nearer to the root of the blade, causing stress concentration. The spar caps' topology is therefore changed to maintain the width of the section where it is the widest through to the root end of the blade as described in Figure 5-16. The number of layers in the spar caps is also adjusted to increase the safety factor distribution in the spar caps.

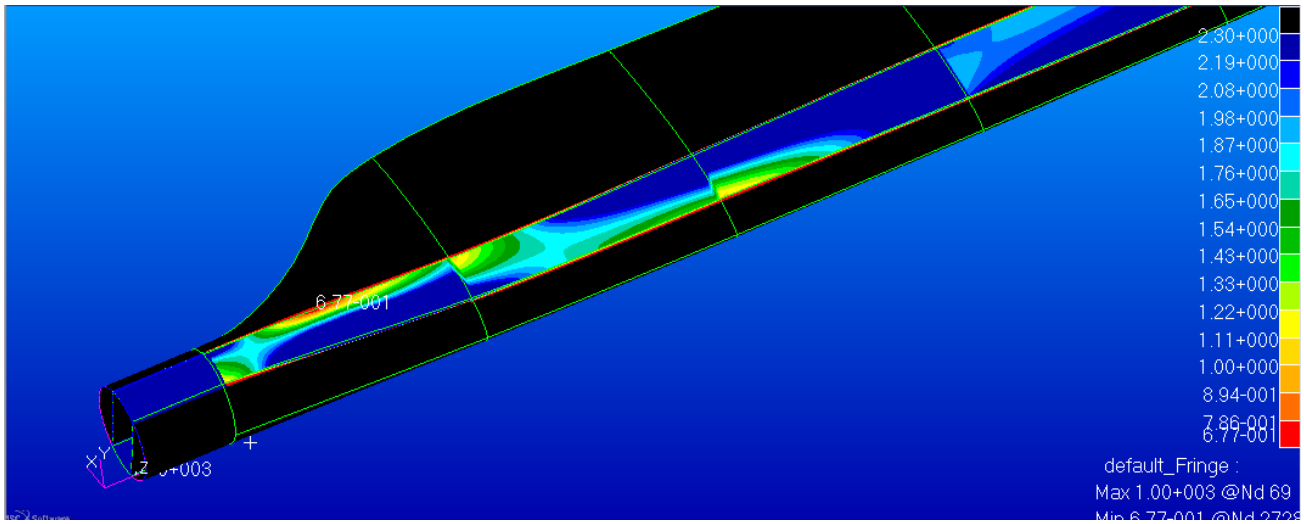

Figure 5-15: The low safety factor distribution due to the topology of the spar caps causing stress concentration

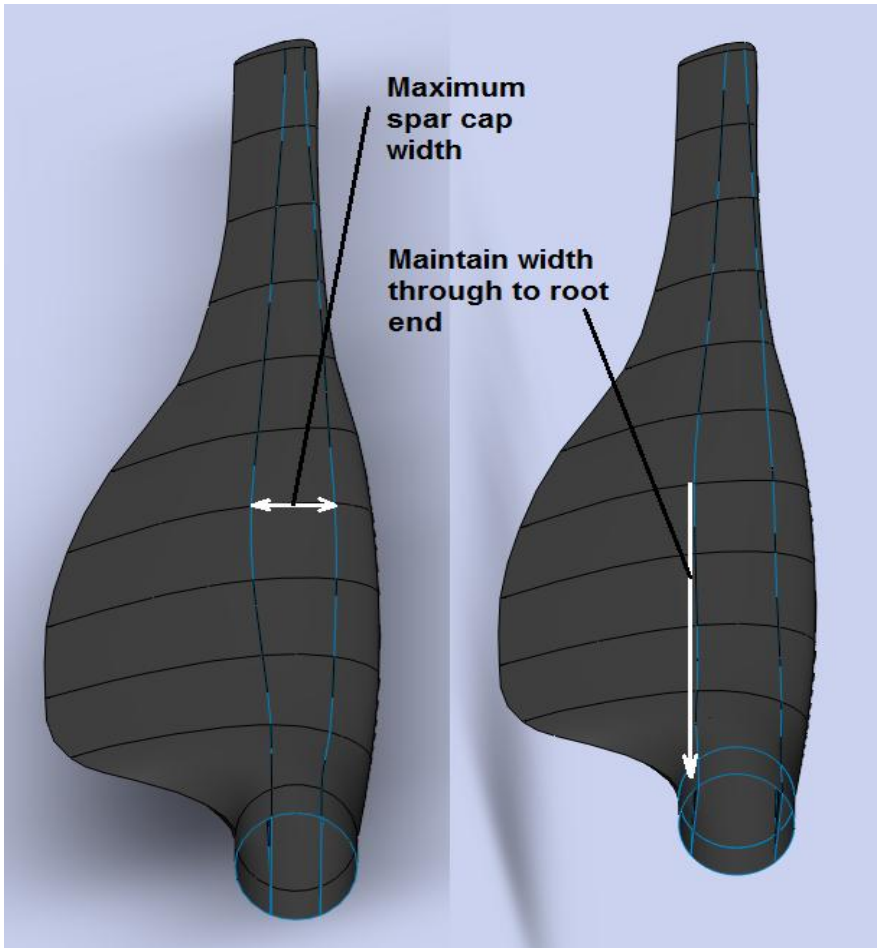

Figure 5-16: The spar cap topology changed to eliminate the stress concentrations at the root end of the blade.

The results from the first FEA run also showed high stresses and low safety factors in the shear webs. These low safety factors, 1.166 as seen in Figure 5-17, appeared to be connected to the high stressed areas in the spar caps as also seen in Figure 5-17. The low safety factor distribution in these areas is therefore also caused by the stress concentration due to the narrowing topology of the spar caps. Thus, the number of BID layers in the shear webs is increased.

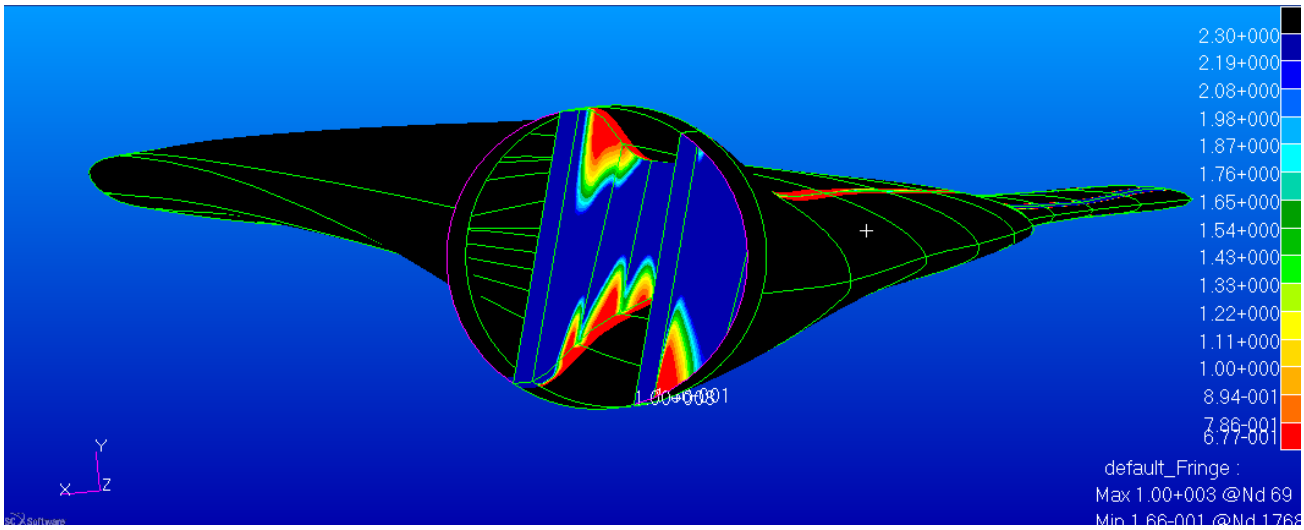

Figure 5-17: Low safety factor distribution in the shear webs due to stress concentration caused by the narrowing topology of the spar caps

The strength of the blade is the main focus point up until this point in the structural design of the 50kW wind turbine blade. This does not, however, mean that the blade is stiff enough to withstand the deflection and possibly result in a collision between the blade and the tower. Therefore, after the strength of the blade is obtained with the required safety factor, the blade structure is designed/ adjusted to meet the predetermined maximum tip deflection to avoid collision between the two structures. Thus, layers are added to the different subcomponents of the blade not only to increase the strength but also to increase its stiffness, thereby decreasing maximum tip deflection.

The deflection of the blade tip is limited to a minimum clearance between the blade tip and the tower of approximately 30% of the unloaded clearance, which is taken as 1.5m. Therefore, the maximum tip deflection that the blade tip should experience is taken as 0.5m. This minimum tip clearance limit is based on (Gurit, 2011) statement that this 30% clearance limit is typically aimed for by wind turbine designers. The design of the topology of the blade's structural subcomponents is completed at this point and therefore layers are only added to the different subcomponents to stiffen the blade to meet the design required tip deflection.

UD fibreglass layers added to the spar caps proved to be effective to stiffen the blade up to a point where the spar caps became too thick and did not contribute significantly to the stiffness of the blade. This is due to the layers closest to the centre of the bending axis having a low moment of inertia and not providing as much stiffness as the layers closer to the outer surface of the blade. UD layers are therefore rather added to the skin of the blade to utilise the maximum distance from the neutral axis of bending. This procedure resulted in stiffening the blade to obtain the required tip deflection and adding less weight to the blade compared to the weight from adding layers to the spar caps. The next section presents the results obtained from the detailed structural design.

5.7 Results and final structural layup design

This chapter presents the results obtained from performing linear elastic type FEA's on the blade with the final layup schedules as designed for all the subcomponents of the blade. Table 5-2 present the final layup schedule obtained from the detailed structural design process. The material layup in the skin of the blade consist of BID glass layers and UD glass layers.

Table 5-2: The final layup schedule of the blade presenting the number of layers in each subcomponent at each section of the blade

	Subcomponent number of layers		
SECTION	Skin	Spar caps (UD Glass @ 0.22mm per layer)	Shear webs (BID glass @ 0.28mm per layer)
1	16	154	30
2	16	113	22
3	16	85	17
4	16	66	14
5	16	54	12
6	16	46	11
7	16	41	10
8	16	38	9
9	16	37	8
10	16	35	7

Table 5-3: The final layup schedule of the blade presenting the thickness of each subcomponent at each section of the blade

	Subcomponent Thicknesses (mm)		
SECTION	Skin	Spar caps (UD Glass @ 0.22mm per layer)	Shear webs (BID glass @ 0.28mm per layer)
1	10	33.88	8.4
2	10	24.86	6.16
3	10	18.7	4.76
4	10	14.52	3.92
5	10	11.88	3.36
6	10	10.12	3.08
7	10	9.02	2.8
8	10	8.36	2.52
9	10	8.14	2.24
10	10	7.7	1.96

Figure 5-18 describes the layup schedule of this composite layup in the skin.

BID fibreglass @ 45°	0.28mm thickness	Total thickness = 10mm
BID fibreglass @ 45°	0.28mm thickness	
BID fibreglass @ 45°	0.28mm thickness	
BID fibreglass @ 45°	0.28mm thickness	
UD fibreglass @ 0°	0.22mm thickness	
UD fibreglass @ 0°	0.22mm thickness	
UD fibreglass @ 0°	0.22mm thickness	
UD fibreglass @ 0°	0.22mm thickness	
Foam core material	6mm thickness	
UD fibreglass @ 0°	0.22mm thickness	
UD fibreglass @ 0°	0.22mm thickness	
UD fibreglass @ 0°	0.22mm thickness	
UD fibreglass @ 0°	0.22mm thickness	
BID fibreglass @ 45°	0.28mm thickness	
BID fibreglass @ 45°	0.28mm thickness	
BID fibreglass @ 45°	0.28mm thickness	
BID fibreglass @ 45°	0.28mm thickness	

Figure 5-18: Description of the composite layup schedule in the skin of the blade.

The thickness distribution of the final layup of all the subcomponents is presented in Figure 5-19. Note that the skin appears very thick compared to the preliminary design value of two layers, but this is due to the 6mm foam core that is included in the calculation of the skin thickness. The skin effectively consist of two 2mm composite BID and UD glass laminate layers as previously presented, separated by the 6mm foam core to increase the blade's stiffness.

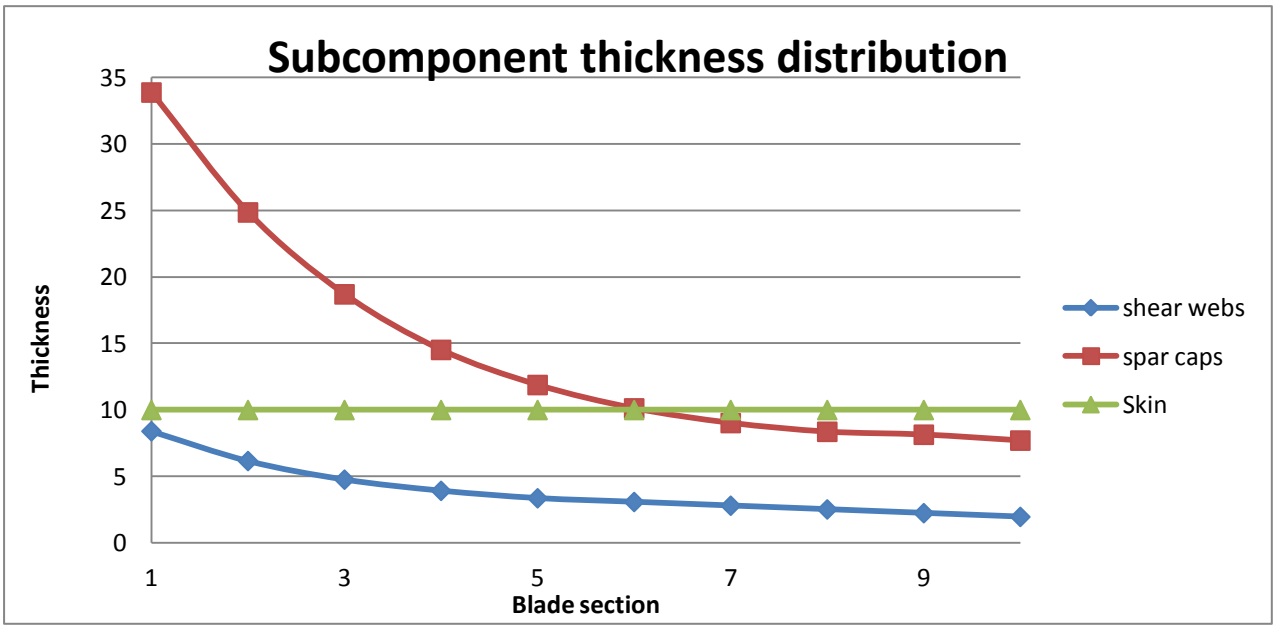

Figure 5-19: The thickness distribution of the blade's subcomponents

The mass distribution of the blade presents the mass of each section of the blade and is represented in Figure 5-20. The mass distribution from Figure 5-20 follows nearly the same trend line as the load distribution plots as calculated in Chapter 3. This shows that the amount of material

required at each section of the blade is directly correlated to the magnitude of the load that it should withstand. Factors such as the geometry of the blade and the topology of its subcomponents are the reason for the slight deviations from the load distribution's trend line. The blade with the final layup and topology obtained from the detailed structural design and analysis resulted in a calculated weight of 169.8kg.

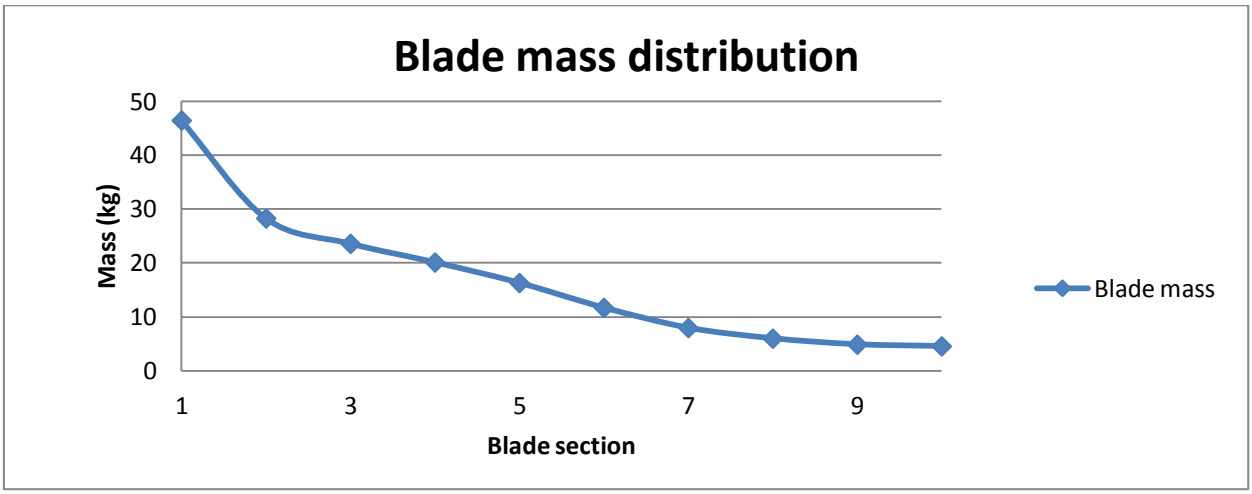

Figure 5-20: The blade mass distribution graph presenting the mass at each section of the blade

5.8 FEA results of detailed structural design under maximum flapwise bending load

Safety factor distribution results in the skin layup present a minimum safety factor of 3.4 in section 1 on the tension side (high-pressure surface) of the blade presented in Figure 5-21.

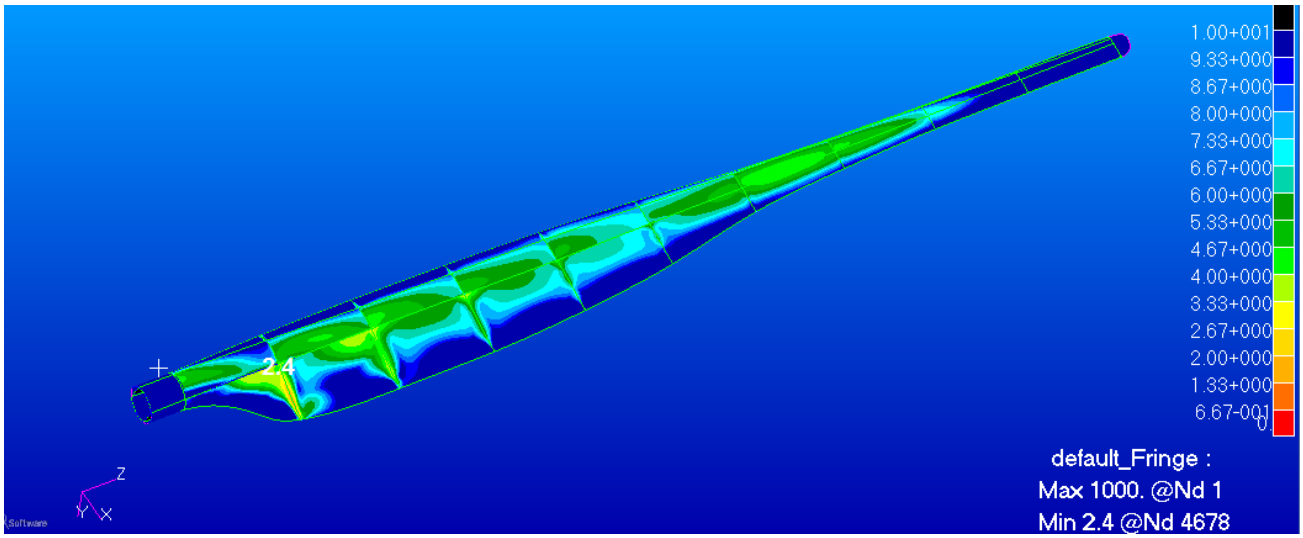

Figure 5-21: The margin of safety distribution results of the skin of the blade under the maximum flapwise bending load, load case C

The safety factor distribution results in the spar caps are presented in Figure 5-22. It is clear from Figure 5-22 that the minimum safety factor in the spar caps is 4.9 when calculated from the margin

of safety as previously mentioned. The minimum safety factor is at section 2 of the blade on the compression side (low pressure surface) of the spar caps. This minimum safety factor is significantly higher than the design required safety factor of 3.3. This is due to the fact that layers were added to the spar caps to stiffen the blade to obtain the maximum required tip deflection after the required strength was obtained. Thus, the strength of the spar caps also increased with the extra layers added to the spar caps to stiffen the blade.

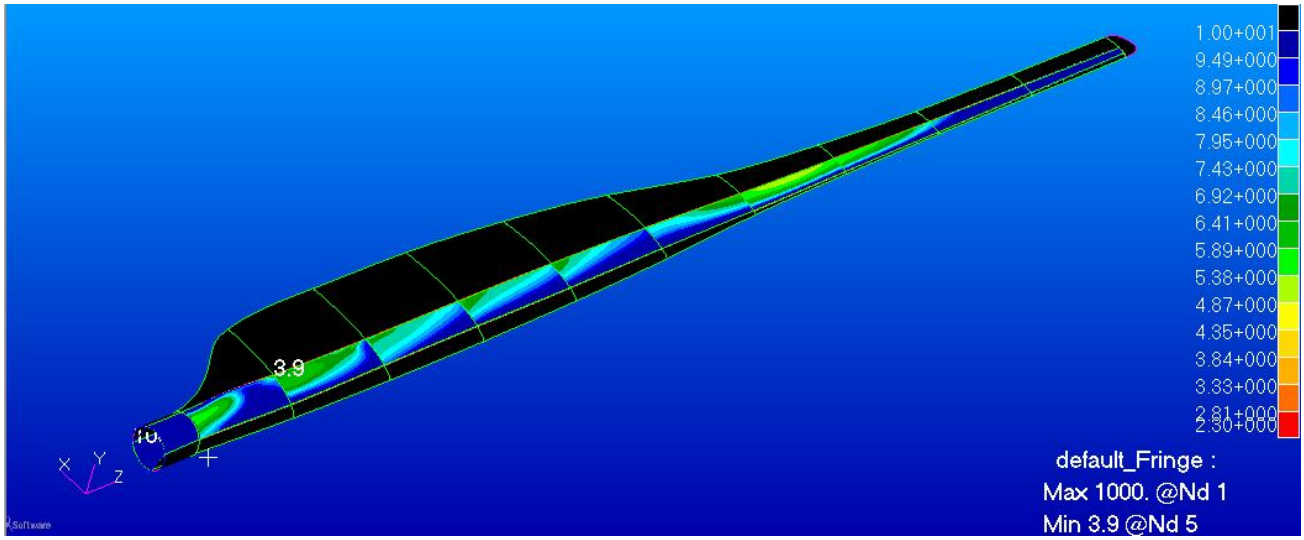

Figure 5-22: The margin of safety distribution results in the blade's spar caps presenting a minimum safety factor of 4.9

The margin of safety distribution results for the shear webs shows a localised minimum of 2.7. This equates to a minimum safety factor of 3.7, thus above the required minimum. The locality of this minimum safety factor is due to the point loads applied to the FEA model causing high localised stresses. The safety factor result should therefore rather be interpreted in the areas away from these localised stresses caused by the applied point loads to obtain a more global and accurate value. The safety factors distribution in areas away from the stress concentration regions show a safety factor well above the design requirement.

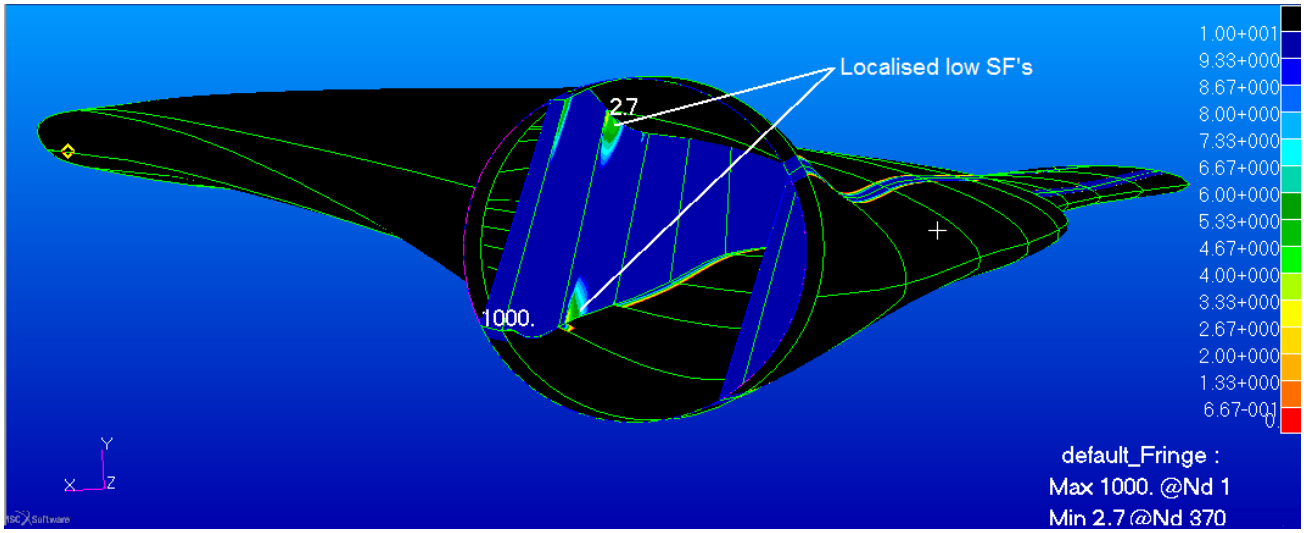

Figure 5-23: The margin of safety distribution results of the shear webs showing a localised minimum safety factor of 3.7

The deflection distribution results showed a maximum of 504mm at the tip of the blade as presented in Figure 5-24. This is significantly close to the design required 500mm mark. The 4mm over the design requirement is acceptable as the tip of the blade will still be 1m (996mm exactly) from the tower, which is set as the design requirement.

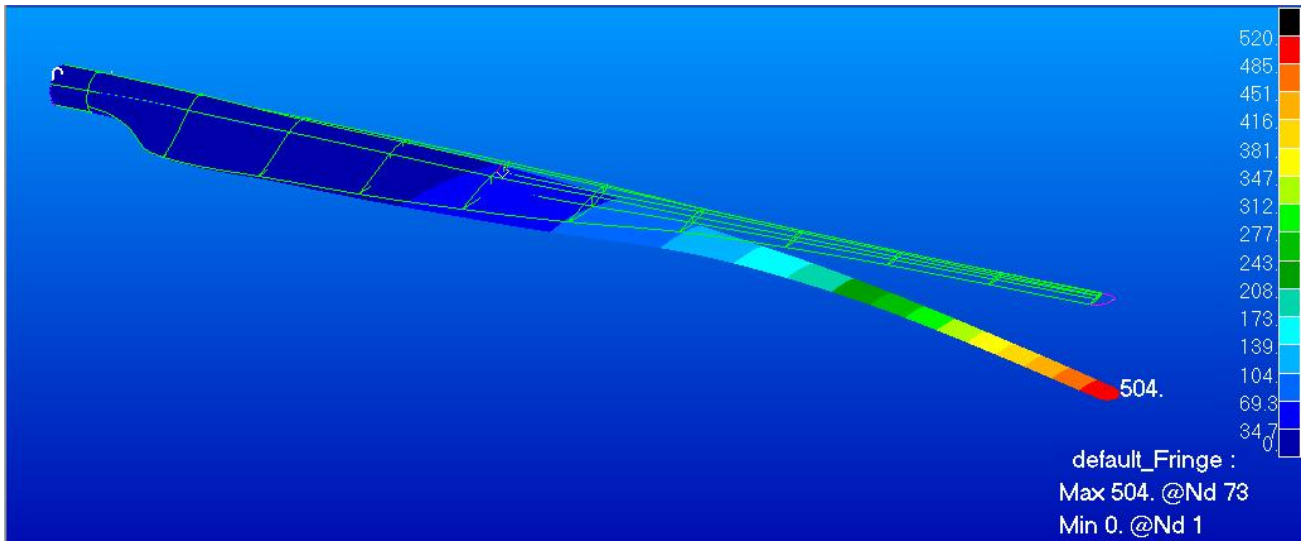

Figure 5-24: The deflection distribution results showing a maximum tip deflection of 0.504m

5.9 FEA results of detailed structural design under maximum edgewise bending load

The safety factor distribution results for the blade under maximum edgewise loading are obtained to determine whether the current layup distribution, which is only determined from flapwise loading, also meets the design required safety factor for this loading. The margin of safety distribution results obtained from applying the maximum edgewise bending load to the blade showed a minimum safety factor of 13.5 in the skin of the blade as presented in Figure 5-25.

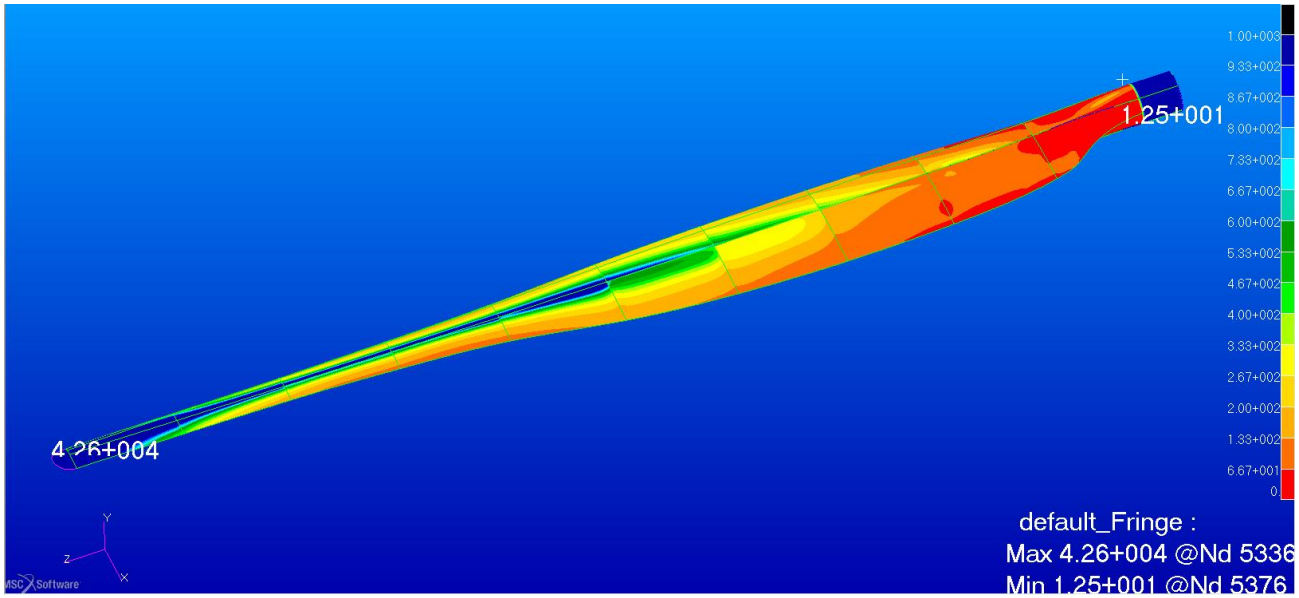

Figure 5-25: The safety factor distribution results of the blade skin under the maximum edgewise bending load (load case C)

The margin of safety distribution results in the spar caps with the blade under edgewise bending presented a minimum safety factor of 24.3 as presented in Figure 5-26.

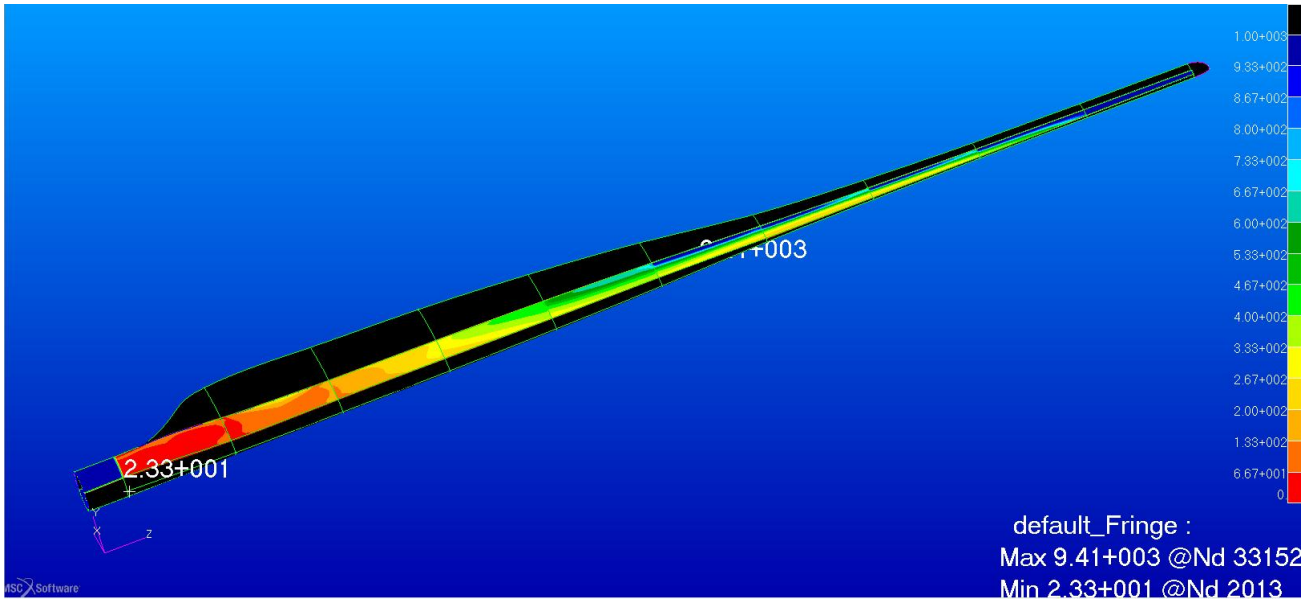

Figure 5-26: The safety factor distribution results of the spar caps under the maximum edgewise bending load

The margin of safety distribution results in the shear webs under maximum edgewise bending load shows a minimum safety factor of 9.22 as presented in Figure 5-27.

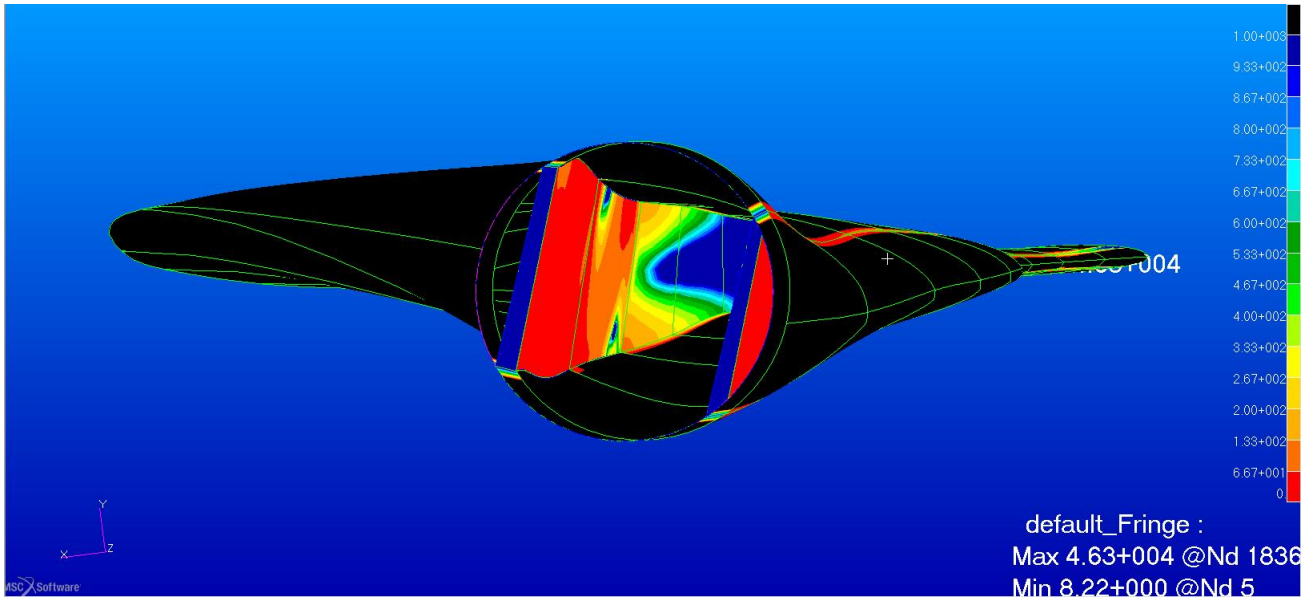

Figure 5-27: The safety factor distribution results in the shear webs under maximum edgewise load.

From the results of the blade under the maximum edgewise bending load, load case C, it is clear that the layup schedule that is initially determined from the flapwise bending loads is structurally sufficient to withstand the edgewise loads. The safety factor distribution results in all of the blade's subcomponents are significantly higher than the design required 3.3 safety factor. The current thickness distribution and topology of all of the blade subcomponents as obtained from the detailed structural design are thus structurally sufficient, as the minimum design required safety factor is obtained in all the subcomponents over the entire length of the blade with the maximum loads considered in all directions.

Appendix I presents the setup of the FEA and full-scale test for the verification of the structural design method used in this thesis. An existing composite propeller blade is modelled in an FEA and used in a full-scale test to verify that the methods used to perform the structural design and analysis of the 50kW wind turbine blade are valid. The methods used to perform an analysis on the propeller blade presented accurate results compared to the full-scale tests' results. Therefore, it is accepted that the methods used in the structural design and analysis process of the 50kW wind turbine blade in this thesis is verified.

5.10 Summary

This chapter included the setup of the finite element model, a description of how the load cases were applied to the blade and a detailed analysis of the FEA results to complete the structural design and therefore the topology of the subcomponents of the blade. A 2D model was created of the blade with the subcomponent topology as determined in the preliminary design phase. The finite element model was presented with all the surfaces that represent all the subcomponents at each

section of the blade. A 10x10mm mesh was applied to the model after mesh refinement studies were performed.

The material properties, load cases and boundary conditions were applied to the model in the FEA software package Patran. The load cases applied are those calculated in Chapter 3, however, the loads applied to the model consisted of a combination of the load case's forces, centrifugal load and a torsion load. This combination of loads applied for each load case was done to simulate a more realistic load model. The validation of the FEA model was performed to ensure that the material properties, loads, layup sequence, layup orientation and mesh were applied correctly and that the FEA of the model provided significant results compared to the preliminary design values.

The safety factor results obtained from analysing the blade with this preliminary layup were compared to the predetermined design safety factor as calculated in Chapter 4. The safety factor distribution results showed a good correlation to that of the calculated design requirement from the preliminary design chapter and therefore the FEA model was accepted as validated.

With the FEA model validated, the detailed structural design phase was initiated. The detailed structural design of the blade was performed by adjusting the topology and layup schedule of the subcomponents of the blade in the finite element analysis until the design requirements were met. These design requirements included the safety factor and the tip deflection of the blade. Analysis of the blade under all the load cases respectively showed that load case C causes the highest stress and lowest safety factor distributions. Therefore, the blade was designed to satisfy the design requirements while exposed to load case C. Initial linear elastic FEA runs of the blade with the subcomponent layup schedules as determined in the preliminary design phase showed low safety factors in all the subcomponents which do not meet the design required safety factor of 3.3. This is due to the combined loads applied to the FEA model, whereas the preliminary calculations only considered single loads for each subcomponent. Thus, the subcomponents were exposed to a greater load due to the combination of bending, centrifugal and torsion, hence the higher stress and lower safety factor distributions. The preliminary design calculations also did not consider stress concentrations due to the geometry of the blade and its subcomponents.

The topology and layup schedule of all the subcomponents was therefore adjusted to finally meet the design required safety factor over the entire length of the blade. After the strength requirements were met, further adjustments to the subcomponents' layup were performed to meet the maximum tip deflection requirement. Final safety factor and deflection results showed the blade meeting all the required safety factor and tip deflection results.
The FEA structural design method was verified by comparing the FEA results from an existing composite propeller blade to that of a full-scale test performed on the blade. The FEA model of the

existing composite propeller blade was modelled and analysed in exactly the same way as for the blade designed in this thesis. The methods used to perform the analysis on the propeller blade presented accurate results compared to the full-scale tests' results. Therefore, it is accepted that the methods used in the structural design and analysis process of the 50kW wind turbine blade in this thesis are verified.

CHAPTER 6 CONCLUSION AND RECOMMENDATIONS

The main objective of this study was to determine the structural dimensions of a 50kW wind turbine blade to be manufactured by Aero Energy. Thus, the thickness distribution and topology of all the subcomponents that the blade consists of needed to be determined. The aerodynamic shape of the blade was designed prior to this study, hence the design of the subcomponents was performed to fit into this previously designed outer shape.

The structural design process was initiated with the calculation of the loads that it should withstand. The loads were calculated according to the IEC 61400-2 design guideline's simplified calculation method, which provides equations to calculate the different loads that the blade should withstand. All the load cases presented by this guideline are calculated and distributed over the length of the blade. The blade is divided into 10 sections and the calculated loads cases are distributed over the entire blade length by applying a fraction of the load to each section. The fraction of the load applied to each section was calculated as the ratio of the projected area of a section over the projected area of the whole blade.

With the loads distributed over the blade's length and the magnitude of the loads at each section known, shear force and bending moment distribution plots are created for each of the load cases. Overlay plots of all the load cases in the same directions were plotted to obtain the maximum loads at each section of the blade. These maximum loads are thus used to perform the structural design of the blade. A root bearing selection was performed as the aerodynamic shape obtained from the aerodynamic design did not include a circular root section. The bearing design/selection was thus only performed to obtain the dimensions of the circular root end of the blade.

A preliminary design was performed to calculate initial thickness distribution values for all the subcomponents of the blade and to validate the finite element model. The structural subcomponents of the blade consist of the skin, spar caps and shear webs. The thickness of each subcomponent at each section of the blade was calculated to withstand the maximum load as determined from the overlay plots with a determined design safety factor. The design safety factor used to calculate the thicknesses of the subcomponents at each section of the blade was calculated as prescribed by IEC 61400-2.

An optimisation method was used to determine the thickness distribution of the spar caps at each section of the blade. This optimisation method calculated the spar cap topology which provides the smallest cross-section area, so minimising the amount of material used and also minimising the weight of the blade. A finite element analysis model was created of the wind turbine blade with its thickness distribution and subcomponent topology as calculated in the preliminary design. A linear elastic analysis of this blade under the exact loading as used in the preliminary design calculation

was performed to validate the FEA model. The safety factor results of all the subcomponents compared very well with the preliminary design calculations.

With the FEA model validated the detailed structural design was initiated. The loads applied to the detailed structural design FEA model consisted of a combination of the loads used in the preliminary design calculations. Thus, the load used in the detailed structural design consisted of a combination of the maximum flapwise bending, centrifugal and torsion loads. The detailed structural design process consisted of adding layers to the blade's subcomponent to meet the design required safety factor, as prescribed by IEC 61400-2.

The maximum tip deflection of the blade was also a set design requirement. This requirement is set to ensure that the blade does not collide with the tower of the wind turbine. FEA results showed that the strength requirement was met before the tip deflection requirement was met. Thus, more layers were added and topology changes made to stiffen the blade. This required adding a foam layer between the skin layers to form a sandwich structure. The addition of the sandwich structure proved to stiffen the blade significantly and did not add too much weight to the blade compared to only adding more glass fibre layers.

The FEA results of simulating the blade under the maximum loads showed safety factor and tip deflection results that met the calculated design requirement. The blade strength and stiffness was tested in the FEA against the maximum loads in both edgewise and flapwise bending directions. The results proved significant for both cases, and presented a relatively lightweight blade compared to those currently available in the market. The structural design process was verified by comparing the results obtained from performing the same analysis procedure on an existing composite propeller blade to that obtained from full-scale tests. The results from this FEA compared well with the full-scale test results, and therefore the structural design and analysis of the 50kW wind turbine blade was assumed to be adequate.

6.1 Recommendations for future work

The blade in this project was designed with the use of IEC 61400-2 simplified load calculation method. Future work could consider the aeroelastic modelling method or load measurement method to obtain more accurate values of the loads on the blade. Using these other methods will thus provide a lower design required safety factor as presented in IEC 61400-2. The high design requirement for safety factor in this project is due to the uncertainty in the loads and thus a very conservative value was taken. The weight of the blade could possibly be decreased if a lower safety factor is used in the structural design phase.

A detailed analysis using the BEM method could also be applied to the blade to better understand the load components ,such as the lift and drag, and the locations of the aerodynamic centres. This would also provide more accurate values when applying the loads to the blade.

Further studies could focus on the root end of the blade to design a root bearing. The root bearings designed in this project are two separate spherical roller bearings placed at a calculated distance from each other on the root of the blade. The way in which these bearings were attached to the blade and the rotor hub was not researched in this thesis and therefore a study on this connection could be performed. Further studies that compare these two separate bearings and a single slewing bearing commonly used on wind turbine blades could also be performed. The comparison of these bearings could consider structural integrity, maintainability, costs and so on.

The topology blade's spar caps in this project were calculated with an optimisation method to find a width and thickness combination that provided the smallest cross-section area at each section of the blade. This process was a very time-consuming manual application. Further studies could focus on creating a script to perform this optimisation calculation automatically, with only a few inputs required.

Further studies could also consider the use of topology optimisation methods that are already available in current FEA packages, such as Patran and ANSYS. This methods could provide more accurate spar cap topologies that would decrease unnecessary material in the blade and decrease the weight of the blade.

CHAPTER 7 REFERENCES

BANKS, D. & SCHÄFFLER, J. 2006. *The potential contribution of renewable energy in South Africa*. Johannesburg.

BENCHLY, M.E. & CLAUSEN, P.D. 1997. Structural design of a composite wind turbine blade using finite element analysis. *Computers & stuctures*, 63(3):639-646.

BENTON, S. 2006. Greenlight for SA's wind farm. http://www.southafrica.info/about/sustainable/windfarm-darling.htm Date of access: 13 March 2001.

BLASQUES, José Pedro & STOLPE, Mathias. 2012. Multi-material topology optimization of laminated composite beam cross sections. *Composite Structures*, 94(11):3278-3289.

BOTTASSO, C.L., CAMPAGNOLO, F., CROCE, A., DILLI, S., GUALDONI, F. & NIELSEN, M.B. 2012. *Structural optimization of wind turbine rotor blades by multi-level sectional/ multibody/3DFEM analysis*. Lyngby.

CAMPBELL, F C. 2010. Introduction to composite materials. *In*: *Structural Composite Materials*, ASM International. 1-29 p.

DE GOEIJ, W.C., VAN TOOREN, M.J.L. & BEUKERS, A. 1999. Implementation of bending-torsion coupling in the design of a wind-turbine rotor-blade. *Applied Energy*, 63(3):191-207.

DUAN, W. & ZHAO, F. 2010. Loading analysis and strength cacluation of wind turbine blade based on blade element momentum theory and finite element method. (*In* 2010 Asia-Pacific Power and Energy Engineering Conference, APPEEC 2010 - Proceedings.)

EDKINS, Max, MARQUARD, Andrew & WINKLER, Harald. 2010. *South Africa's renewable energy policy roadmaps*. Cape Town.

GURIT. 2011. Gurit Wind Energy Handbook. Date of access: August 2013.

GURIT. 2011. Gurit wind energy handbook. Date of access: 14 February 2011. <http://www.gurit.com/gurit-wind-energy-handbook.aspx>

GURIT. Wind turbine blade structural engineering. *In*: *Gurit Wind Energy Handbook*, 8-9 p.

HABALI, S. M. & SALEH, I. A. 1999. Local design and manufacturing of small mixed airfoil wind turbine blades of glass fiber reinforced plastics Part 1: Design of the blade and root. *Energy Conversion & Management*:249-280. 16 May.

IEC, 61400-1. 2005. Wind turbine generator systems, Part 1: Safety requirements. 3rd ed.

IEC, 61400-2. 2006. *Wind turbines Part 1: Design requirements for small wind turbines*.

INGRAM, G. 2011. *Wind turbine analysis using the blade element momentum method.*

JENSEN, F.M., FALZON, B.G., ANKERSEN, J. & STANG, H. 2006. Structural testing and numerical simulation of a 34m composite wind turbine blade. *Composite structures*, 76:52-61. 12 July.

JIAO, H. & SUN, W. 2011. Full load calculation of large-scale wind turbine. (*In* Proceedings - International Conference on Computer Distributed Control and Intelligent Environmental Monitoring, CDCIEM 2011. p. 223-226.)

JURECZKO, M., PAWLAK, M. & MEZYK, A. 2005. Optimisation of wind turbine blades. *Journal of materials processing technology*:463-471.

KONG, C., BANG, J. & SUGIYAMA, Y. 2005. Structural investigation of composite wind turbine blade considering various load cases and fatigue life. *Energy*:2101-2114.

LANTING, Zhang. 2012. Research on structural lay-up optimum design of composite wind turbine blade. *Energy Procedia*, pp.637-642.

LIAO, C.C., ZHAO, X.L. & XU, J.Z. 2011. Blade layers optimization of wind turbines using FAST and improved PSO Algorithm. *Renewable Energy*:1-7.

LIU, S., HOU, Y., SUN, X. & ZANG, Y. 2012. A two-step scheme for maximum stiffness design of laminated plates based on lamination paramaters. *Composite structures*:3529-3537.

LLOYD, Germanischer. 2010. *Guideline for the certification of wind turbines*.

LTD., Anaglyph. 2011. Laminate Analysis Program. www.anaglyph.co.uk Date of access: 27 March 2011.

MISHNAEVSKY, Leon Jr. 2011. Composite materials in wind energy technology. *Thermal to Mechanical Energy Conversion:Engines and requirements*

NARAYANA NAIK, G., OMKAR, S.N., MUDIGERE, Dheevatsa & GOPALAKRISHNAN, S. 2011. Nature inspired optimization techniques for the design optimization of laminated composite structures using failure criteria. *Expert systems with applications*, 38(3):2489-2499.

NAUDE, S & JONKER, A.S. 2008. *Composite material test report*. Potchefstroom.

PATNAIK, Ishan. 2009. *Wind as a renewable source of energy*. Orissa.

RONOLD, K.O. & LARSEN, G.C. 2000. Reliability-based design of wind turbine rotor blades against failure in ultimate loading. *Engineering structures*:565-574. 28 January.

SKF. 2008. SKF General Catalogue. SKF Group.

STEGMANN, J. & LUND, E. 2005. Discrete material optimization of general composite shell structures. *International Journal for numerical methods in engineering*, 62:2009-2027. 9 February.

TESKE, Sven, ZERVOS, Arthouros, LINS, Christine, STEELE, Melita, MUSANA, Fiona, TEULE, Dr. Rianne & ADAM, Ferrial. 2011. *The advanced energy [r]evolution: Asustainable energy outlook for South Africa*.

VAN DER LINDE, H A. 1996. Wind energy in South Africa. *Renewable Energy*, 9(1-4):880-883. September-December.

VISWESWARAIAH, S.B. 2010. *Structural design and multi-objective optimization of an advanced composite rotor blade*. Montreal.

WEISSHAAR, T.A. 1987. Aeroelastic tailoring--creative use of unusual materials. (*In* Structural dynamics and materials conference. Monterey, CA.)

Wind Atlas for South Africa. 2013.

WU, W. & YOUNG, W. 2011. Structural analysis and design of the composite wind turbine blade. *Applied composite materials*:1-11.

APPENDIX A: CALCULATION OF LOAD CASE VARIABLES

A.1 General

This Appendix presents the calculation of the values for the variables used in Chapter 3, section 3.1 Note that some of the values were calculated according to IEC 61400-2 regulations and others were calculated either using test data or using assumptions made from other studies. The calculation of the variables is presented in A.3 and a table listing the calculated values of each of the variables is presented in A.4.

A.2 Symbols

$Aproj, BAproj, BV_{proj,b}$:projected area of the blade [m^2]

B	:number of blades	[-]
C_d	:drag coefficient	[-]
C_f	:force coefficient	[-]
C_{l_max}	:maximum lift coefficient	[-]
C_m	:pitching moment coefficient	[-]
C_T	:thrust coefficient	[-]
G	:ratio between rated torque and short circuit torque for a generator	[-]
g	:acceleration due to gravity 9.81	[m/s^2]
I_B	:mass moment of inertia of the blade about the blade root flap axis	[kgm^2]
L_{rt}	:distance between the rotor axis and the yaw axis	[m]
M_{brake}	:torque on the low speed shaft caused by the brake	[Nm]
$M_{x-shaft}$	:torsion moment on the rotor shaft at the first bearing	[Nm]
m_B	:mass of the blade	[kg]
n_{design}	:design rotor speed	[rpm]
n_{max}	:maximum rotor speed	[rpm]
P_{design}	:design electrical power rating	[W]
Q_{design}	:design rotor torque	[Nm]
R	:radius of the rotor	[m]
R_{cog}	:radial distance between the centre of gravity of a blade and the rotor centre	[m]
V_{ave}	:annual average wind speed at hub height	[m/s]
V_{design}	:design wind speed	[m/s]
V_{e50}	:expected extreme wind speed (averaged over 3s), with a recurrence time interval of 50 years	[m/s]
V_{ref}	:reference wind speed averaged over 10 minutes	[m/s]

z	:reference height above ground	[m]
z_{hub}	:hub height of the wind turbine	[m]
η	:efficiency of the components between the electric output and the rotor	[-]
λ_{design}	:tip speed ratio at design rotational speed	[-]
λ_{e50}	:tip speed ratio at maximum rotational speed	[-]
ρ	:air density, here assumed 1.225 (as in IEC 61400-2)	[kg/m^3]
$\omega_{n,design}$	:design rotational speed of the rotor	[rad/s]
$\omega_{n,max}$	:maximum rotational speed of rotor	[rad/s]
$\omega_{yaw,max}$	:maximum yaw rate of the turbine	[rad/s]

A.3 Calculation of variable values

A3.1 Projected area of the blade, $\mathbf{A_{proj,B}}$

The projected area of the blade was calculated with the use of the CAD model in Solidworks. The blade's surface area was projected to a plane parallel to its top plane as seen in Figure A. 1. Note that the value of the projected area is determined with an automated measuring function in Solidworks.

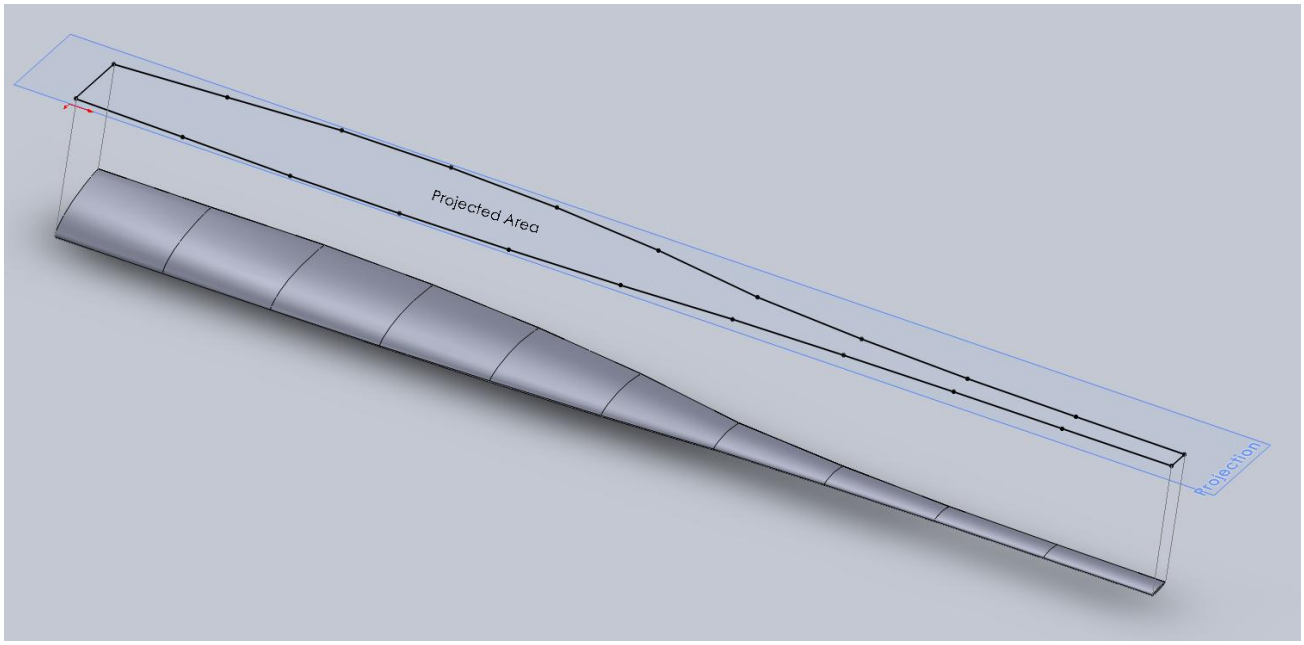

Figure A. 1: A presentation of how the projected area of the blade was determined in Solidworks

A3.2 Number of blades on the wind turbine, B

The value for B in the load calculations is taken as 3.

A3.3 Drag coefficient, force coefficient Maximum lift coefficient and thrust coefficient, C_d, C_f, C_{l_max} and C_T

According to the IEC 61400-2 design guidelines, the drag coefficient C_d used in the calculation of Load case H for parked wind turbine shall be taken as 1.5. The force coefficient C_f was chosen from a table in the IEC 61400-2 guideline and the most conservative value was chosen, namely 2. The maximum lift coefficient $C_{l,max}$ is taken as 2 as depicted in the guideline for Load case H for a spinning rotor. The thrust coefficient C_T is taken as 1.5 as depicted in the calculation of Load case D.

A3.4 Pitching moment coefficient C_m

The pitching moment coefficient C_m is used in the load case that was added to the list of load cases presented by the IEC 61400-2 design guidelines. This coefficient is used in the equation for the calculation of the torque/pitching moment about the quarter chord of the wind turbine blade. The value of this coefficient is determined with the use of XFLR 5 that is an analyses tool for airfoils, wings and planes operating at low Reynolds numbers. The input variables for the analyses of the airfoils is set as a range for the angle of attack and a range for the Reynolds number under which the airfoils will operate.

The range of angles of attack used in the analyses of the airfoils is taken as [-10;10] degrees, which proved sufficient as only the maximum value of the pitching moment coefficient obtained from the analysis would be used in the calculation of the pitching moment. The analysis proved that the maximum pitching moment coefficient is found in the above-mentioned range for angles of attack.

The range for the Reynolds numbers used in the airfoil analyses is determined with equation A-1 and equation A-2 using the design rotational speed as the lower boundary value and the maximum rotational speed as the upper boundary value.

$$Re = \frac{\rho V D}{\mu} \qquad \text{(A-1)}$$

and

$$V = \omega r \qquad \text{(A- 2)}$$

where

ρ is the air density taken as 1.225 kg/m^3

D is the chord length of the airfoil

V is the velocity of the air flowing over the airfoil

ω is rotational speed of the wind turbine blade in rad/s

r is the distance of the airfoil from the centre of rotation

μ is the dynamic viscosity of air taken as 1.806 x 10^{-5} m^2/s

The airfoils used in this analysis are NREL's s821, s819, and an airfoil that was self designed by the aerodynamic engineer. This last mentioned airfoil is called the tip airfoil for convenient purposes of this project. Figure A. 2 shows the calculation of the Reynolds numbers for each of the airfoils at their respective positions along the length of the blade (distance from the centre of rotation).

	r(m)	0.4
	chord length (m)	0.6558
	ω	Re(for S821 airfoil)
design rotational speed (rad/s)	8.9012	158379.2586
maximum rotational speed (rad/s)	12.56	223480.3721
	r (m)	1.63444
	chord length (m)	0.777
	Omega	Re (for S819 airfoil)
design rotational speed (rad/s)	8.9012	766755.5057
maximum rotational speed (rad/s)	12.56	1081927.061
	r (m)	8.6296
	chord length (m)	0.205186
	ω	Re (for TIP airfoil)
design rotational speed (rad/s)	8.9012	1069067.908
maximum rotational speed (rad/s)	12.56	1508503.677
	r (m)	3.6912
	chord length (m)	0.755
	ω	Re (for TIP airfoil)
design rotational speed (rad/s)	8.9012	1682602.116
maximum rotational speed (rad/s)	12.56	2374228.484

Figure A. 2: Calculation of the Reynolds numbers of the airfoils used in the wind turbine blade

The Reynolds number range for the s821 airfoil is therefore set as [150000; 240000] and is analysed in increments of 15000. The Reynolds number range for the s819 airfoil is [750000; 1110000] and is analysed in increments of 45000. The Tip airfoil has a wider range as it is integrated into 60% of the blade length. Thus the Reynolds number range for the tip airfoil is taken as [1000000; 2500000] and is analysed in increments of 100000. Figure A. 3, Figure A. 4 and Figure A. 5 shows the analysis graphs of airfoil s821, s819 and the tip airfoil respectively in xflr5. The graphs plot the Cm value to the angle of attack for the different Reynolds numbers.

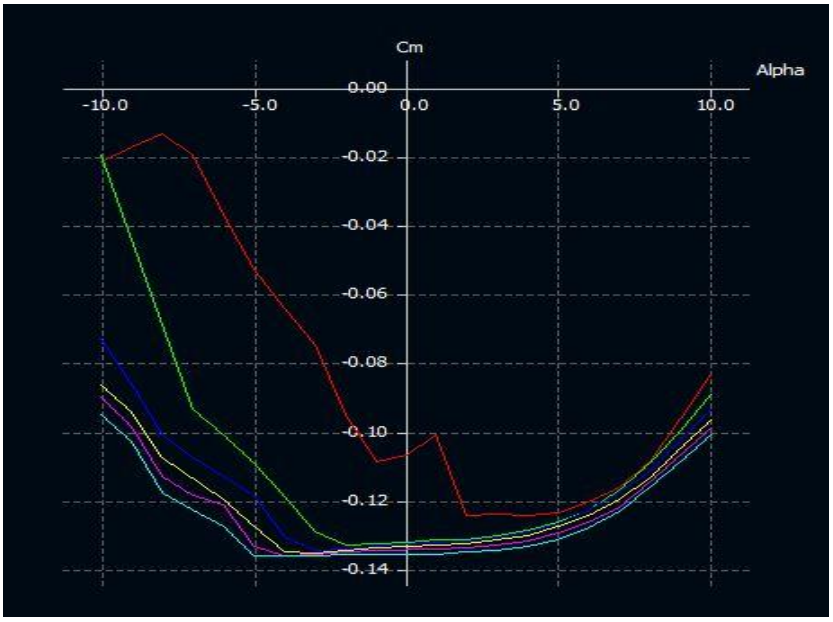

Figure A. 3: The C_m – α plot from xflr5 for the s821 airfoil showing different curves for each Reynolds number in its predetermined range

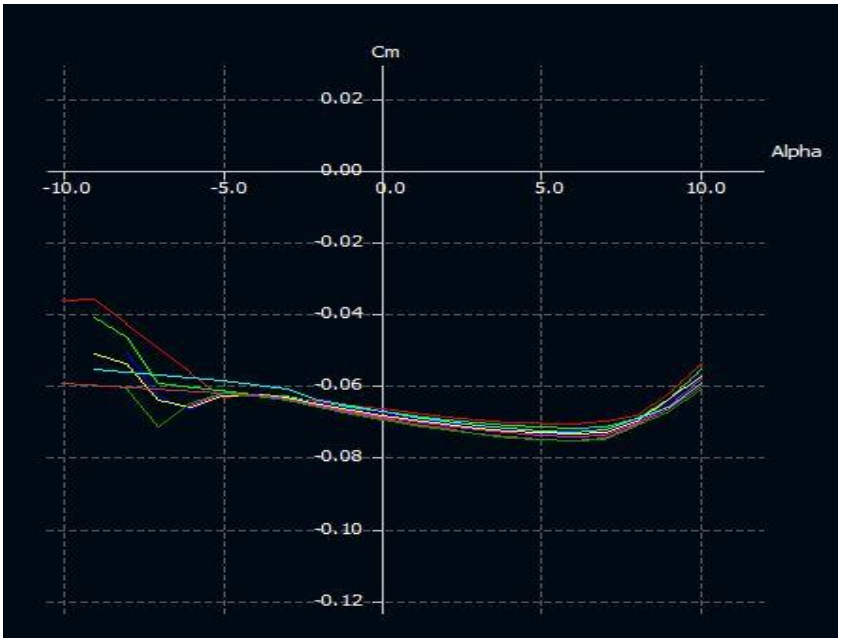

Figure A. 4: The C_m – α plot from xflr5 for the s819 airfoil showing different curves for each Reynolds number in its predetermined range

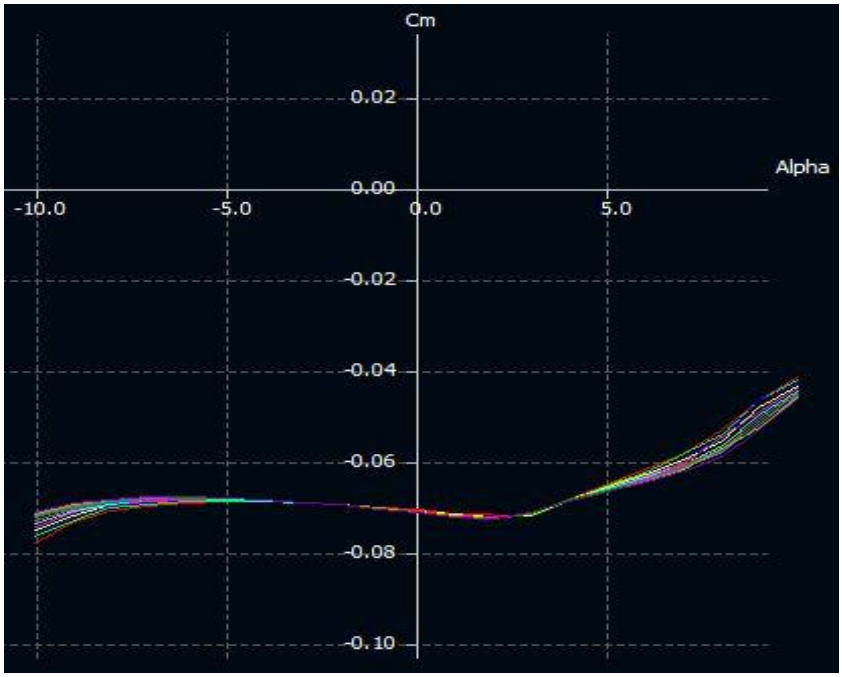

Figure A. 5: The C_m – α plot from xflr5 for the tip airfoil showing different curves for each Reynolds number in its predetermined range

The results of the airfoil analysis show a maximum pitching moment coefficient between -0.12 and -0.14 as seen in Figure A. 3. A conservative global pitching moment coefficient is therefore chosen as -0.14 that will be used in the calculation of the pitching moment at all the sections of the blade.

A3.5 Ratio between rated torque and short circuit torque for the generator, G

According to IEC 61400-2 the value of G shall be 2,0 in the absence of any proven values, which is appropriate in this thesis.

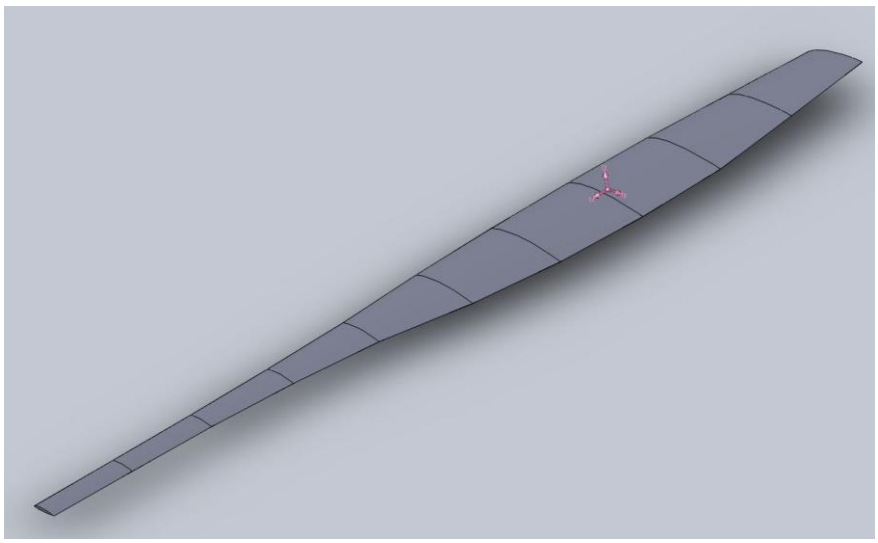

Figure A. 6: The coordinate system in Solidworks to determine the mass moment of inertia of the blade out the blade root flap axis

A3.6 The distance from the rotor axis to the yaw axis, $\mathbf{L_{rt}}$

The dimensions of the wind turbine as a whole are not known yet and thus an assumed value of 1 metre is chosen. Figure A. 7 describes the distance between the above-mentioned axes.

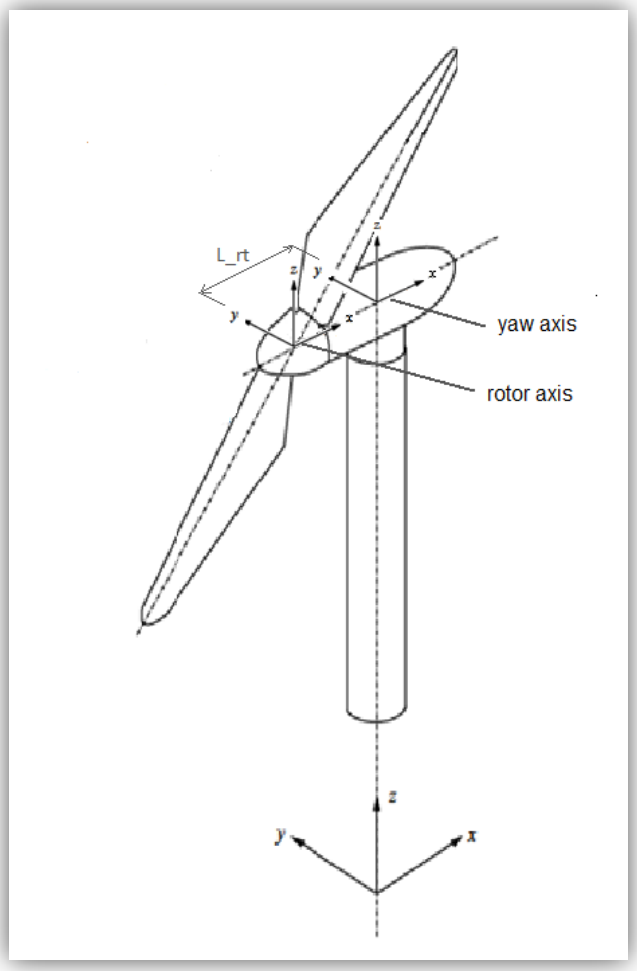

Figure A. 7: A description of the distance L_{rt}

A3.7 Torque on the low speed shaft due the brake, $\mathbf{M_{Brake}}$

The braking moment is taken as a minimum value as no proven values exist. The minimum braking moment is assumed to be equal to the driving moment of the wind turbine Q_{design} which value is determined later in this appendix.

A3.8 Torsion moment on the rotor shaft at the first bearing, $\mathbf{M_{x-shaft}}$

The torsion moment on the rotor shaft at the first bearing is calculated according to the description given in Load case F and G. Equation A-3 shows how this torsion moment is calculated as in Load case F and equation A-4 shows its calculation as in Load case G. Both these equations provide the same results due to the value that was chosen for M_{brake}.

$$M_{x-shaft} = GQ_{design} \quad \text{(A-3)}$$

$$M_{x-shaft} = M_{brake} + Q_{design} \quad \text{(A-4)}$$

The numerical value calculated for $M_{x\text{-}shaft}$ is presented in chapter A.4

A3.9 The mass of the blade, $\mathbf{m_B}$

The mass of the blade is initially taken 150kg but a more accurate value for the blade mass is determined when the material layup and thickness distribution is determined. Thus, Load case E is determined in detail after the material layup is complete. The detail calculation of the mass of the blade and therefore the centrifugal force on the blade is an iterative process. Therefore, it is a redundant task to determine an accurate mass for the blade at this stage of the structural design.

A3.10 Design rotational speed of the rotor, $\mathbf{n_{design}}$

The rotational speed of the wind turbine is determined in the aerodynamic design phase of the wind turbine. The blade was aerodynamically designed to deliver optimum power at wind speeds of 11m/s and rotating at 85rpm. Thus n_{design} is taken as 85rpm.

A3.11 Maximum rotational speed of the rotor, $\mathbf{n_{design}}$

The maximum rotational speed of the rotor is determined from both the aerodynamic design and the generator characteristics. The maximum rotational speed of the rotor is therefore set at 120rpm to accommodate the power rating and mechanical limits of both the generator and the blade.

A3.12 Design electrical power rating, $\mathbf{P_{design}}$

The wind turbine blades designed in this thesis are designed to deliver a power rating of 50kW.

A3.13 Design rotor torque, $\mathbf{Q_{design}}$

The design torque is derived from the equation provided in IEC 61400-2. Equation A-5 presents the calculation of the design rotor torque.

$$Q_{design} = \frac{30P_{design}}{\eta\pi n_{design}} \quad \text{(A-5)}$$

where

η is the drive train efficiency and,

η = 0.7 for P_{design} >20kW

A3.14 Radius of the rotor, $\mathbf{R}$

The radius of the rotor is taken as the length of the blade namely, 8.2296m

A3.15 Radial distance between the centre of gravity of the blade and the rotor centre, $\mathbf{R_{cog}}$

The distance between the centre of gravity of the blade and the rotor centre is determined in the same way that the mass moment of inertia is determined in A3.5. The value for this distance obtained from Solidworks is 2.34196m.

A3.16 Annual average wind speed at hub height, $\mathbf{V_{ave}}$

The annual average wind speed at hub height is calculated as:

$$V_{ave} = \frac{V_{design}}{1.4} \tag{A-6}$$

A3.17 Design wind speed, $\mathbf{V_{design}}$

The wind turbine blade is aerodynamically designed to operate at 11m/s winds.

A3.18 Expected extreme wind speed (averaged over 3s), with a recurrence time interval of 50 years, $\mathbf{V_{e50}}$

V_{e50} is calculated in Equation A-7 as per IEC 61400-2 guideline.

$$V_{e50} = 1.4V_{ref}(\frac{z}{z_{hub}})^{0.11} \tag{A-7}$$

With z and z_{hub} taken as 25m (assumed hub height).

A3.19 Reference wind speed averaged over 10min, $\mathbf{V_{ref}}$

The reference wind speed is calculated as:

$$V_{ref} = \frac{V_{ave}}{0.2} \tag{A-8}$$

A3.20 Tip speed ratio at design rotational speed, $\boldsymbol{\lambda_{design}}$

The tip speed ratio at design rotational speed is calculated as:

$$\lambda_{design} = \frac{R\pi n_{design}}{30V_{design}} \tag{A-9}$$

A3.21 Tip speed ratio at maximum rotational speed, $\boldsymbol{\lambda_{design}}$

The tip speed ratio at design rotational speed is calculated as:

$$\lambda_{design} = \frac{R\pi n_{design}}{30V_{e50}} \quad \text{(A-10)}$$

A3.22 Design rotational speed of the rotor, $\omega_{n,design}$

The design rotational speed of the wind turbine blade is as previously mentioned, designed to rotate at 85rpm. Thus. 8.9011rad/s.

A3.23 Maximum rotational speed of the rotor, $\omega_{n,max}$

The maximum rotational speed of the wind turbine blade is as previously mentioned, designed to rotate at a maximum of 120rpm. Thus 12.566 rad/s.

A3.24 Maximum yaw rate/speed of the rotor, $\omega_{yaw,max}$

The maximum yaw rate is determined as in Load case B of IEC 61400-2:

$$\omega_{yaw,max} = 3 - 0.01(\pi R^2 - 2) \quad \text{(A-11)}$$

A.4 Variable values

The following table presents the values as calculated in this appendix:

Variable	Value	Unit
$A_{proj,B}$	4.289	m^2
B	3	-
C_d	1.5	-
C_f	2	-
C_{l_max}	2	-
C_m	0.14	-
C_T	0.5	-
G	2	-
g	9.81	m/s^2
I_B	776.401	$kg.m^2$
L_{rt}	1	m
M_{brake}	8024.619	N.m
$M_{x-shaft}$	16049.238	N.m
m_B	150.00	kg
n_{design}	85	rpm
n_{max}	120	rpm
P_{design}	50000	W
Q_{design}	8024.619	N.m
R	8.2296	m
R_{cog}	2.342	m
V_{ave}	7.857142857	m/s

V_{design}	11	m/s
V_{e50}	55	m/s
V_{ref}	39.286	m/s
z	25	m
z_{hub}	25	m
η	0.7	-
λ_{design}	6.659	-
λ_{e50}	1.880	-
ρ	1.225	kg/m^3
$\omega_{n,design}$	8.901	rad/s
$\omega_{n,max}$	12.566	rad/s
$\omega_{yaw,max}$	0.892	rad/s

APPENDIX B: LOAD CALCULATION

B.1 General

This appendix presents the loads as calculated in Chapter 3, section 3.1 using the variables as in appendix A.

B.2 Symbols

$A_{proj,i}$	Projected area of section i of the blade as presented in Table B- 2	[mm^2]
M_{yB}	Moment at the root of the blade about the y-axis (flapwise bending moment)	[N.m]
F_{xB}	Force on the blade in the x-direction	[N]
F_{zB}	Force on the blade in the z-direction	[N]
L_c	Chord length of section i of the blade.	[m]
M_{brake}	Torque on the low speed shaft caused by the brake	[Nm]
M_{xB}	Moment at the root of the blade about the x axis (edgewise bending moment)	[Nm]
$M_{x-shaft}$	Torsion moment on the rotor shaft at the first bearing	[Nm]
M_{zB}	Moment at the root of the blade about the z axis (pitch moment about ¼ chord)	[Nm]
$M_{z,i}$	Pitching moment about the 1/4chord (z-axis) at section i of the blade	[N.m]
r_i	Axial distance from the rotational centre to section i.	[m]
V_{max}	Translational speed of the rotor rotating at maximum rotational speed where, $V_{max}=\omega_{max}r_i$	[m/s]

B.3 Design loads calculated

Table B- 1: The design load cases as calculated from the equations in chapter 3.1

Load case B: Yawing (Ultimate load)		Units
M_{yB}	12613.09	N.m

Load case C: Yaw error (Ultimate load)		Units
M_{yB}	70923.93	N.m

Load case D: Maximum thrust (Ultimate load)		Units
F_{xB}	6841.25	N

Load case E: Maximum rotational speed (Ultimate load)		Units
F_{zB}	55474.12	N

Load case F: Short at load connection (Ultimate load)		Units
$M_{x\text{-shaft}}$	16049.24	N.m
M_{xB}	8795.94	N.m

Load case G: Shutdown (Braking) (Ultimate load)		Units
M_{Brake}	8024.62	N.m
$M_{x\text{-shaft}}$	16049.24	N.m
M_{xB}	8795.94	N.m

Load case H: Parked wind loading, Survival wind (Ultimate load)		Units
M_{yB} (Parked rotor)	49047.03	N.m
M_{yB} (Spinning at V_e,50)	43597.36	N.m

Load case I: Parked wind loading, maximum exposure		Units
F_{xB}	8108.62	N

Load case J: Pitching moment (moment about 1/4 chord)		Units
M_{zB}	436.974	N.m

Note that Load case J is not calculated directly from the equation in Chapter 3, section 3.1. This load case is calculated after the blade is divided into 10 sections and the pitching moment for each section is then calculated with the formula used in Chapter 3, section 3.1. More detail on load case J is presented in the next sub-clause.

B.4 Load distribution

The loads calculated in B3. are distributed over the blade surface to determine a layup thickness distribution and to perform an accurate structural analysis of the blade. Therefore, the blade is divided into 10 sections and the loads calculated in B.3 are distributed over the length of the blade in terms of the projected area of each section. These loads at each section of the blade are used to determine the shear and moment distribution diagrams that are used to calculate each section's layup and thickness distribution. The distributed loads are also used directly in the structural analysis of the blade, where these loads at each section are applied to the blade surface in the finite element analysis.

Table B- 2 presents the projected areas of each section the blade is divided into and Table B- 3 the distances of each section from the root of the blade. These areas and distances are used as described in Chapter 3, section 3.2 to calculate the forces and moments at each section.

Table B- 2: The projected areas of each section of the blade

Area 1	0.541198972	m^2
Area 2	0.623341868	m^2
Area 3	0.667468086	m^2
Area 4	0.643404789	m^2
Area 5	0.560993135	m^2
Area 6	0.413767791	m^2
Area 7	0.279490152	m^2
Area 8	0.212301496	m^2
Area 9	0.182078287	m^2
Area 10	0.172001671	m^2
Total Area of the blade	4.296046247	m^2

Table B- 3: The distances of each section from the root of the blade

Distance of section 1	0.82296	m
Distance of section 2	1.64592	m
Distance of section 3	2.46888	m
Distance of section 4	3.29184	m
Distance of section 5	4.1148	m
Distance of section 6	4.93776	m
Distance of section 7	5.76072	m
Distance of section 8	6.58368	m
Distance of section 9	7.40664	m
Distance of section 10 (tip)	8.2296	m

The following tables show the moments and forces calculated for each section of the blade

Moments Load case B (N.m)	**12613.088**	**Forces Load case B (N)**	**5427.240**
Moment at section 1	1588.947	Force section 1	1930.771
Moment at section 2	1830.117	Force section 2	1111.911
Moment at section 3	1959.670	Force section 3	793.749
Moment at section 4	1889.021	Force section 4	573.850
Moment at section 5	1647.062	Force section 5	400.278
Moment at section 6	1214.812	Force section 6	246.025
Moment at section 7	820.576	Force section 7	142.443
Moment at section 8	623.312	Force section 8	94.675
Moment at section 9	534.577	Force section 9	72.175
Moment at section 10	504.993	Force section 10	61.363

Moments Load case C (N.m)	**70923.932**	**Forces Load case C (N)**	**30517.601**
Moment at section 1	8934.717	Force section 1	10856.806
Moment at section 2	10290.824	Force section 2	6252.323
Moment at section 3	11019.309	Force section 3	4463.283
Moment at section 4	10622.045	Force section 4	3226.781
Moment at section 5	9261.502	Force section 5	2250.778

Moment at section 6	6830.941	Force section 6	1383.409
Moment at section 7	4614.136	Force section 7	800.965
Moment at section 8	3504.910	Force section 8	532.363
Moment at section 9	3005.952	Force section 9	405.846
Moment at section 10	2839.596	Force section 10	345.047

Moments Load case D (N.m)	**24460.998**	**Forces Load case D (N)**	**6841.249**
Moment at section 1	709.255	Force section 1	861.834
Moment at section 2	1633.810	Force section 2	992.642
Moment at section 3	2624.200	Force section 3	1062.911
Moment at section 4	3372.791	Force section 4	1024.591
Moment at section 5	3675.977	Force section 5	893.355
Moment at section 6	3253.517	Force section 6	658.905
Moment at section 7	2563.951	Force section 7	445.075
Moment at section 8	2225.811	Force section 8	338.080
Moment at section 9	2147.563	Force section 9	289.951
Moment at section 10	2254.124	Force section 10	273.904

Moments Load case E (N.m)	**0.000**	**Forces Load case E (N)**	**55474.125**
Moment at section 1		Force section 1	6988.412
Moment at section 2		Force section 2	8049.109
Moment at section 3		Force section 3	8618.903
Moment at section 4		Force section 4	8308.178
Moment at section 5		Force section 5	7244.010
Moment at section 6		Force section 6	5342.914
Moment at section 7		Force section 7	3609.009
Moment at section 8		Force section 8	2741.414
Moment at section 9		Force section 9	2351.146
Moment at section 10		Force section 10	2221.029

Moments Load case F (N.m)	**8795.940**	**Forces Load case F (N)**	**3784.773**
Moment at section 1	1108.078	Force section 1	1346.454
Moment at section 2	1276.261	Force section 2	775.409
Moment at section 3	1366.608	Force section 3	553.533
Moment at section 4	1317.339	Force section 4	400.183
Moment at section 5	1148.605	Force section 5	279.140
Moment at section 6	847.169	Force section 6	171.569
Moment at section 7	572.242	Force section 7	99.335
Moment at section 8	434.677	Force section 8	66.023
Moment at section 9	372.796	Force section 9	50.333
Moment at section 10	352.165	Force section 10	42.792

Moments Load case G (N.m)	**8795.940**	**Forces Load case G (N)**	**3784.773**
Moment at section 1	1108.078	Force section 1	1346.454
Moment at section 2	1276.261	Force section 2	775.409
Moment at section 3	1366.608	Force section 3	553.533
Moment at section 4	1317.339	Force section 4	400.183
Moment at section 5	1148.605	Force section 5	279.140
Moment at section 6	847.169	Force section 6	171.569
Moment at section 7	572.242	Force section 7	99.335
Moment at section 8	434.677	Force section 8	66.023
Moment at section 9	372.796	Force section 9	50.333

Moment at section 10	352.165	Force section 10	42.792

Moments Load case H1 (parked rotor) (N.m)	**49047.035**	**Forces Load case H1 (N)**	**21104.270**
Moment at section 1	6178.752	Force section 1	7507.962
Moment at section 2	7116.560	Force section 2	4323.758
Moment at section 3	7620.339	Force section 3	3086.557
Moment at section 4	7345.614	Force section 4	2231.461
Moment at section 5	6404.738	Force section 5	1556.513
Moment at section 6	4723.898	Force section 6	956.688
Moment at section 7	3190.879	Force section 7	553.903
Moment at section 8	2423.800	Force section 8	368.153
Moment at section 9	2078.749	Force section 9	280.660
Moment at section 10	1963.706	Force section 10	238.615

Moments Load case H2 (Rotor spinning at V_{e50}) (N.m)	**43597.364**	**Forces Load case H2 (N)**	**18759.351**
Moment at section 1	5492.224	Force section 1	6673.744
Moment at section 2	6325.831	Force section 2	3843.341
Moment at section 3	6773.635	Force section 3	2743.606
Moment at section 4	6529.435	Force section 4	1983.521
Moment at section 5	5693.100	Force section 5	1383.567
Moment at section 6	4199.020	Force section 6	850.390
Moment at section 7	2836.337	Force section 7	492.358
Moment at section 8	2154.489	Force section 8	327.247
Moment at section 9	1847.777	Force section 9	249.476
Moment at section 10	1745.516	Force section 10	212.102

Moments Load case I	**28992.486**	**Forces Loadcase I**	**8108.6152**
Moment at section 1	840.647	Force section 1	1021.491
Moment at section 2	1936.479	Force section 2	1176.533
Moment at section 3	3110.343	Force section 3	1259.819
Moment at section 4	3997.613	Force section 4	1214.401
Moment at section 5	4356.964	Force section 5	1058.852
Moment at section 6	3856.243	Force section 6	780.970
Moment at section 7	3038.932	Force section 7	527.526
Moment at section 8	2638.150	Force section 8	400.711
Moment at section 9	2545.406	Force section 9	343.665
Moment at section 10	2671.709	Force section 10	324.646

Load case J is not calculated directly from an equation and distributed over the blade length calculating a force and a moment at each section as performed on Load cases B to H2. This load case is determined by calculating the torsion moment caused by each section of the blade and only then the torsion moment distribution over the blade length is calculated.

The torsion/pitching moment at each section of the blade is calculated with the use of equation B-1.

$$M_{z,i} = C_m \frac{1}{2} \rho V_{max}^2 A_{proj,i} L_c \quad \text{(B-1)}$$

where,

$M_{z,i}$ is the pitching moment about the 1/4chord (z-axis) at section i of the blade.

$A_{proj,i}$ is the projected area of section i of the blade as presented in Table B- 2

V_{max} is the translational speed of the rotor rotating at maximum rotational speed where, $V_{max}=\omega_{max} r_i$

r_i is the axial distance from the rotational centre to section i.

L_c is the chord length of section i of the blade.

Thus, for each section of the blade V_{max} is calculated and presented in Table B- 4.

Table B- 4: The maximum translational speed of the rotor at each section of the blade

V_{max} Load case J (m/s)	V=ω*r
Velocity section 1	10.342
Velocity section 2	20.683
Velocity section 3	31.025
Velocity section 4	41.366
Velocity section 5	51.708
Velocity section 6	62.050
Velocity section 7	72.391
Velocity section 8	82.733
Velocity section 9	93.075
Velocity section 10	103.416

The chord length of the blade at each section is determined with the use of the CAD model in Solidworks and presented in Table B- 5.

Table B- 5: The chord length at each section of the blade

Section #	Chord length (m)
Section 1	0.6996
Section 2	0.7831
Section 3	0.8218
Section 4	0.7888
Section 5	0.6871
Section 6	0.506
Section 7	0.3415
Section 8	0.2592

Section 9	0.2222
Section 10	0.2099

The torsion/pitch moment at each section of the blade is calculated and presented in Table B- 6.

Table B- 6: The pitching moment calculated at each section of the blade

Load case J Pitching moment (moment about 1/4 chord) (N.m)	436.974
Pitching Moment at section 1	3.472
Pitching Moment at section 2	17.907
Pitching Moment at section 3	45.274
Pitching Moment at section 4	74.470
Pitching Moment at section 5	88.375
Pitching Moment at section 6	69.123
Pitching Moment at section 7	42.891
Pitching Moment at section 8	32.298
Pitching Moment at section 9	30.054
Pitching Moment at section 10	33.110

APPENDIX C: SHEAR FORCE- AND BENDING MOMENT DISTRIBUTION GRAPHS

C.1 General

This appendix presents the calculation of values used to draw the shear and moment diagrams for all the load cases.

C.2 Symbols

F_R	Reaction force at the root of the blade due to the loads on the blade,	[N]
F_i	Force at section I of the blade in the flapwise (x) direction,	[N]
V_i	Shear force at section I of the blade in the flapwise (x) direction,	[N]
M_R	The total reaction moment at the root of the blade due to all the loads acting on the blade,	[N.m]
M_i	The flapwise bending moment at section I of the blade (about y-axis) ,	[N.m]

C.3 Shear and moment diagram data point calculations

The calculation of the data points/values of the shear forces and moments at each section of the blade was performed by modelling the blade as a cantilever beam. These forces and moments as calculated in Chapter 3, section 3.2, while Appendix B is used to model the blade as a cantilever beam as shown in Figure C-1.

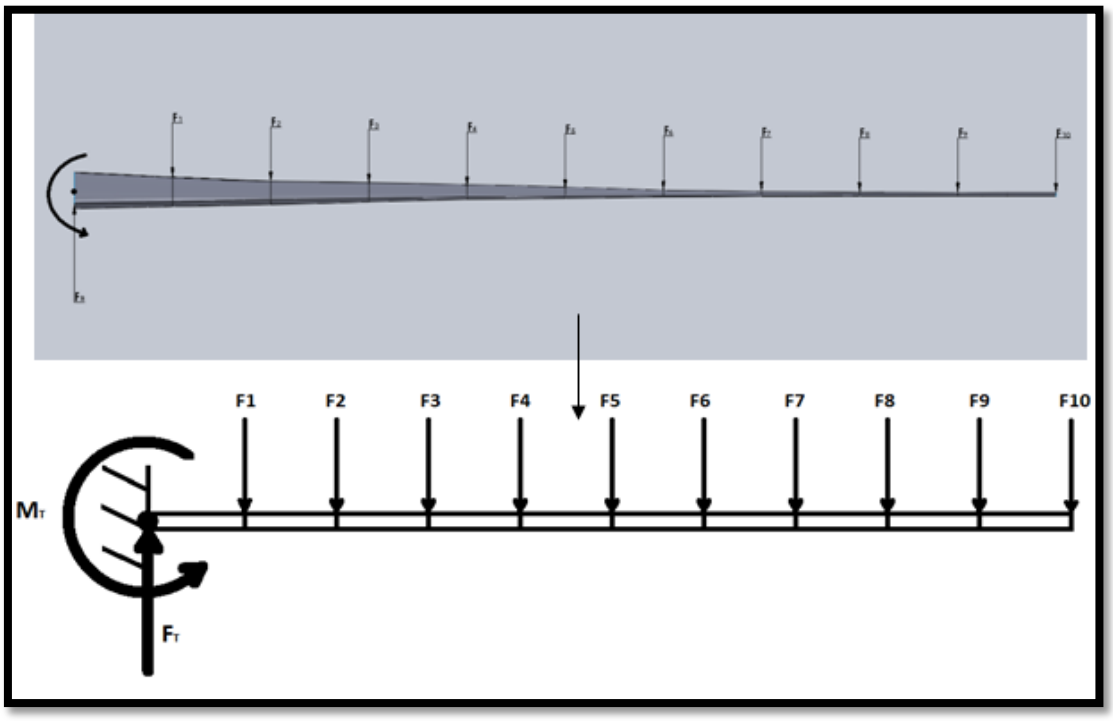

Figure C-1: The blade modelled as a cantilever beam with the root end fixed and the forces distributed over the length of the blade, acting at each section

The equations used to calculate the diagrams' data points/ values was formulated by firstly calculating the reaction force and moment at the root of the blade/cantilever beam for each load case. (Note that the equations used in this appendix are universal and were used for all the load cases – except Load case J.)

Thus, the reaction force at the fixed root end for each load case is calculated with,

$$F_R = \sum_{i=1}^{10} F_i \qquad \text{(C-1)}$$

where,

F_R the total reaction force at the root of the blade due to all the loads acting at each section of the blade

F_{xi} the force at section I of the blade in the flapwise (x) direction.

The reaction moment at the fixed root end of the blade was calculated with,

$$M_R = \sum_{i=1}^{10} M_i \qquad \text{(C-2)}$$

where,

M_R the total reaction moment at the root of the blade due to all the loads acting at each section of the blade

M_i The flapwise bending moment at section I of the blade (about y-axis).

The following three steps are performed to obtain a guideline so that a universal equation could be formulated to accommodate all the design points for shear forces and bending moments.

The first of the three steps is to calculate the shear force and the bending moment at the root of the blade. (Note that this figure is an enlarged portion of the cantilever beam at a position close to the fixed root of the beam.)

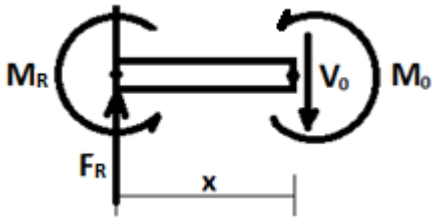

Thus, by using Newton's third law the shear force at the root of the blade is calculated. Note that the values for the root section are noted as 0. Also note that in these beam representation figures,

upwards and anti-clockwise is taken as the positive directions for the forces and moments respectively.

$$\sum F = 0 \tag{C-3}$$

Therefore,

$$F_R - V_0 = 0 \tag{C-4}$$

and

$$V_0 = F_R \tag{C-5}$$

The bending moment at the root of the blade is also calculated with this principle and is given by:

$$\sum M = 0 \tag{C-6}$$

Therefore,

$$M_R - F_R(x) + M_0 = 0 \tag{C-7}$$

Thus,

$$M_0 = M_R \tag{C-8}$$

This procedure will be performed for sections 1 and 2 until a pattern is clear and an equation can be formulated to accommodate all the sections.

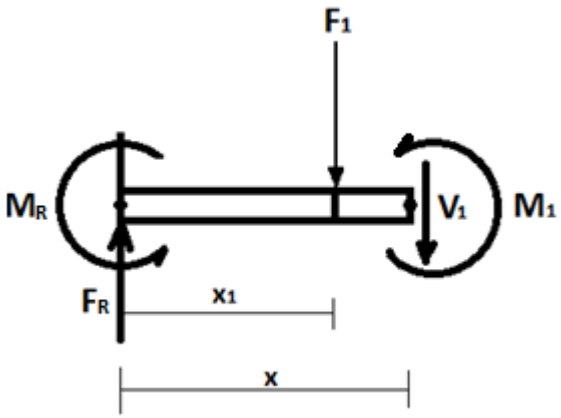

For the shear force at section 1:

$$\sum F = 0 \tag{C-9}$$

Therefore,

$$F_R - F_1 - V_1 = 0 \tag{C-10}$$

and

$$V_1 = F_R - F_1 \tag{C-11}$$

For the bending moment at section 1:

$$\sum M = 0 \tag{C-12}$$

Therefore,

$$M_R - F_R(x) + F_1(x - x_1) + M_1 = 0 \tag{C-13}$$

Thus,

$$M_1 = F_R(x) + M_R \tag{C-14}$$

as x = x_1 at section 1.

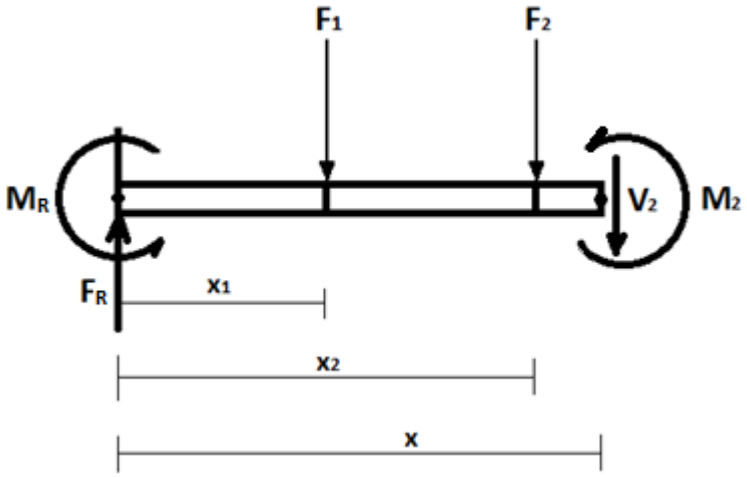

$$\sum F = 0 \tag{C-15}$$

Therefore,

$$F_R - F_1 - F_2 - V_2 = 0 \tag{C-16}$$

and

$$V_2 = F_R - F_1 - F_2 \tag{C-17}$$

For the bending moment at section 2:

$$\sum M = 0 \tag{C-18}$$

Therefore,

$$M_R - F_R(x) + F_1(x - x_1) + F_2(x - x_2) + M_2 = 0 \tag{C-19}$$

Thus,

$$M_2 = F_R(x) + F_1(x - x_1) + M_R \tag{C-20}$$

as x = x_2 at section 2.

The three steps presented prove that universal equations can be formulated for the calculation of the shear forces and moments at all the sections of the blade. Thus, from the calculation pattern found in the three steps the formula for the shear forces at each section is given by equation C-21

$$V_i = F_R - \sum_{k=0}^{i} F_k \tag{C-21}$$

Where V_i is the shear force at section i.

The formula for the calculation of the bending moments at each section is given by equation C-22.

$$M_i = F_R(x_i) + \sum_{k=0}^{i} F_k\,(x_i - x_k) + M_R \quad , x_{-1}\ and\ x_0 = 0 \qquad \text{(C-22)}$$

The values of the data points used to draw the shear force distribution graphs for all the load cases are presented in Table C-1. The values of the data points to draw the bending moment distribution diagram are presented in Table C-2. These values are calculated for each section of the blade with the use of equation C-21 and equation C-22.

Table C- 1: The shear force data points calculated for each load case at each section of the blade to draw the shear force distribution plots.

	Shear forces (N)								
	load case B	load case C	load case D	load case E	load case F	load case G	load case H	load case H2	load case I
x (position, (m))	y(in x-direction)	y(in x-direction)	y(in x-direction)	y (in z-direction)	y(in y direction)	y(in y direction)	y(in x-direction)	y(in x-direction)	y(in x-direction)
0.00	5427.24	30517.60	6841.25	55474.12	3784.77	3784.77	21104.27	18759.35	8108.62
0.82	3496.47	19660.79	5979.42	48485.71	2438.32	2438.32	13596.31	12085.61	7087.12
1.65	2384.56	13408.47	4986.77	40436.60	1662.91	1662.91	9272.55	8242.27	5910.59
2.47	1590.81	8945.19	3923.86	31817.70	1109.38	1109.38	6185.99	5498.66	4650.77
3.29	1016.96	5718.41	2899.27	23509.52	709.19	709.19	3954.53	3515.14	3436.37
4.11	616.68	3467.63	2005.92	16265.51	430.05	430.05	2398.02	2131.57	2377.52
4.94	370.66	2084.22	1347.01	10922.60	258.48	258.48	1441.33	1281.18	1596.55
5.76	228.21	1283.26	901.94	7313.59	159.15	159.15	887.43	788.82	1069.02
6.58	133.54	750.89	563.86	4572.18	93.13	93.13	519.28	461.58	668.31
7.41	61.36	345.05	273.90	2221.03	42.79	42.79	238.62	212.10	324.65
8.23	0.00	0.00	0.00	0.00	0.00	0.00	0.00	0.00	0.00

Table C- 2: The bending moment data point calculated for each load case at each section of the blade used to draw the bending moment distribution plots.

	Moments (N.m)								
	load case B	load case C	load case D	load case F	load case G	load case H	load case H2	load case I	load case J
x (position, (m))	y (about Y-axis)	y (about Y-axis)	y (about Y-axis)	y (about X-axis)	y (about X-axis)	y (about Y-axis)	y (about Y-axis)	y (about Y-axis)	y (about Z-axis)
0.00	12613.09	70923.93	24461.00	8795.94	8795.94	49047.03	43597.36	28992.49	436.97
0.82	8146.69	45809.17	18830.92	5681.22	5681.22	31679.06	28159.17	22319.42	433.50
1.65	5269.23	29629.12	13910.10	3674.58	3674.58	20489.85	18213.20	16487.00	415.59
2.47	3306.84	18594.49	9806.19	2306.08	2306.08	12858.91	11430.14	11622.82	370.32
3.29	1997.66	11232.95	6577.01	1393.10	1393.10	7768.08	6904.96	7795.42	295.85
4.11	1160.75	6526.93	4191.02	809.47	809.47	4513.66	4012.14	4967.43	207.48
4.94	653.24	3673.21	2540.24	455.55	455.55	2540.19	2257.95	3010.82	138.35
5.76	348.21	1957.98	1431.70	242.83	242.83	1354.03	1203.58	1696.93	95.46
6.58	160.40	901.91	689.44	111.85	111.85	623.71	554.41	817.16	63.16
7.41	50.50	283.96	225.41	35.22	35.22	196.37	174.55	267.17	33.11
8.23	0.00	0.00	0.00	0.00	0.00	0.00	0.00	0.00	0.00

C.4 Shear and moment diagrams

The shear force and bending moment distribution diagrams for all the load cases are drawn and presented below.

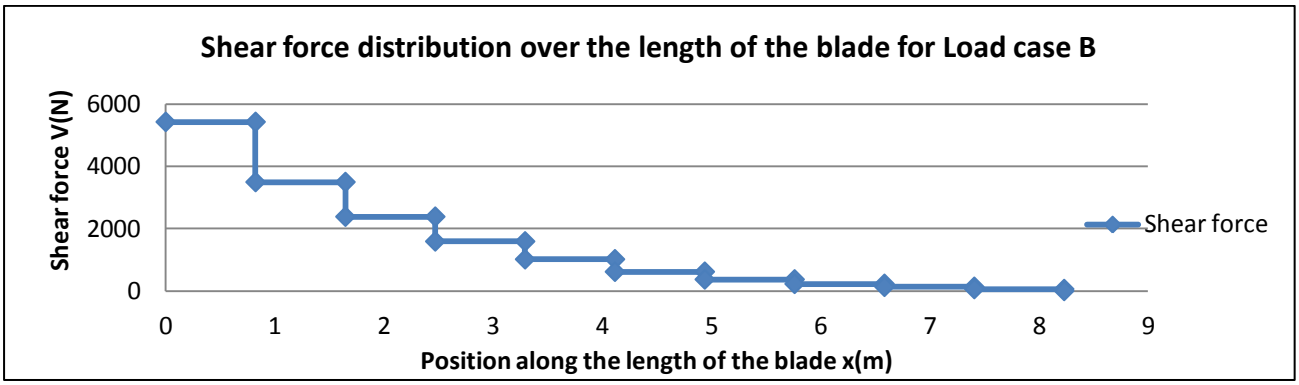

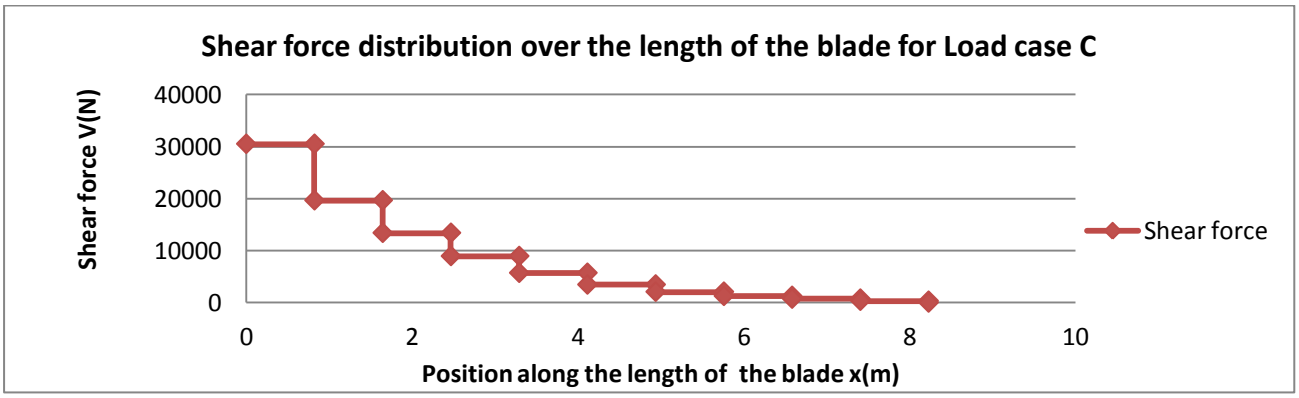

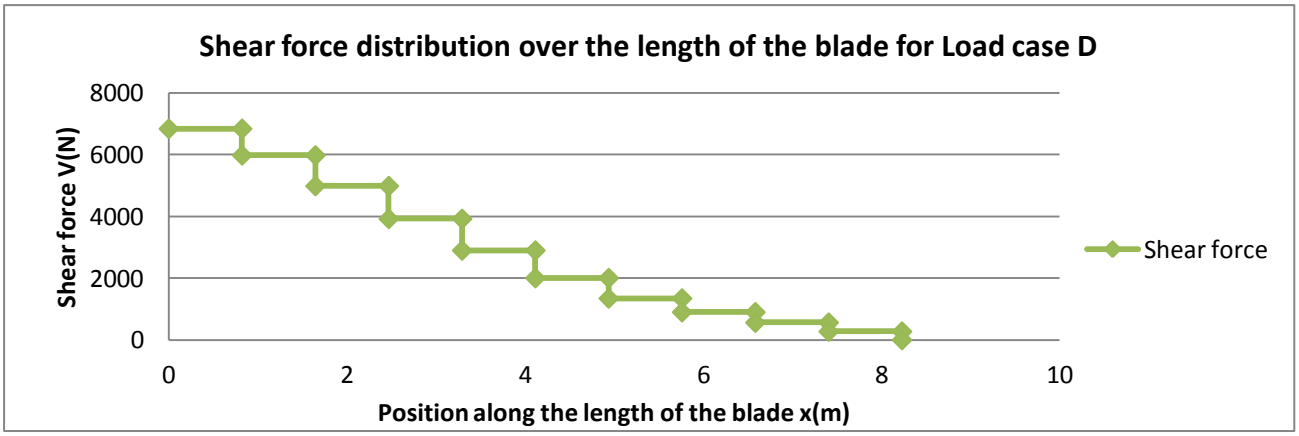

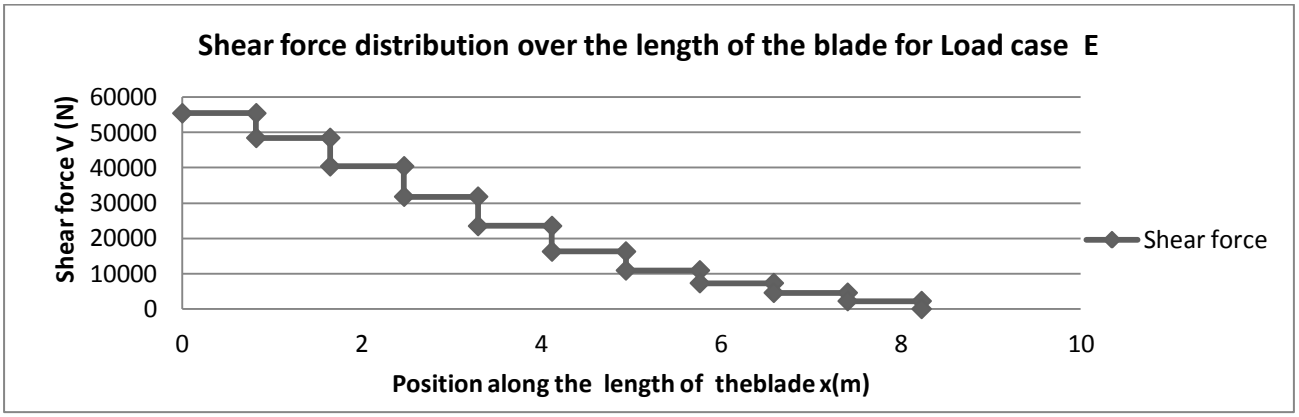
Shear force distribution over the length of the blade for Load case E
Shear force V (N)
60000
50000
40000
30000
20000
10000
0
0
2
4
6
8
10
Position along the length of theblade x(m)
Shear force

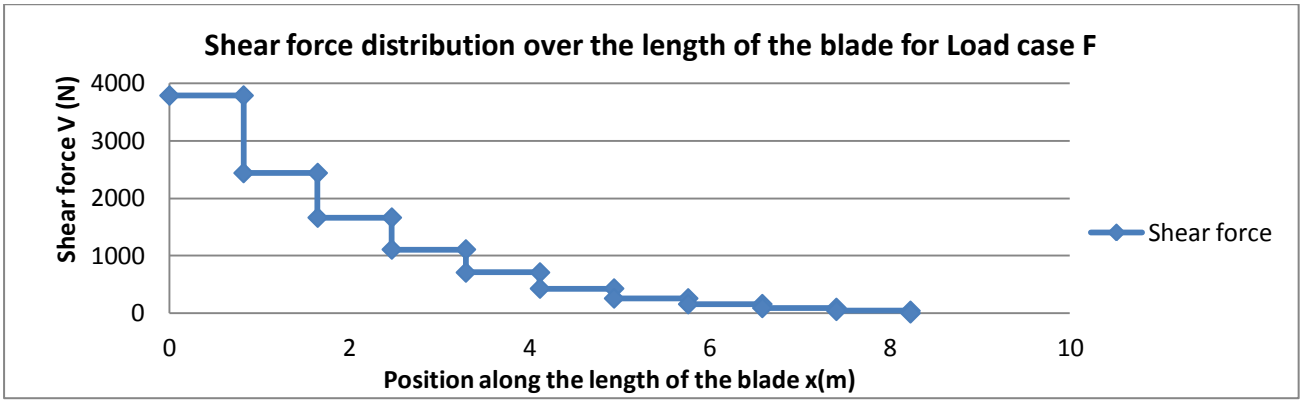
Shear force distribution over the length of the blade for Load case F
Shear force V (N)
4000
3000
2000
1000
0
0
2
4
6
8
10
Position along the length of the blade x(m)
Shear force

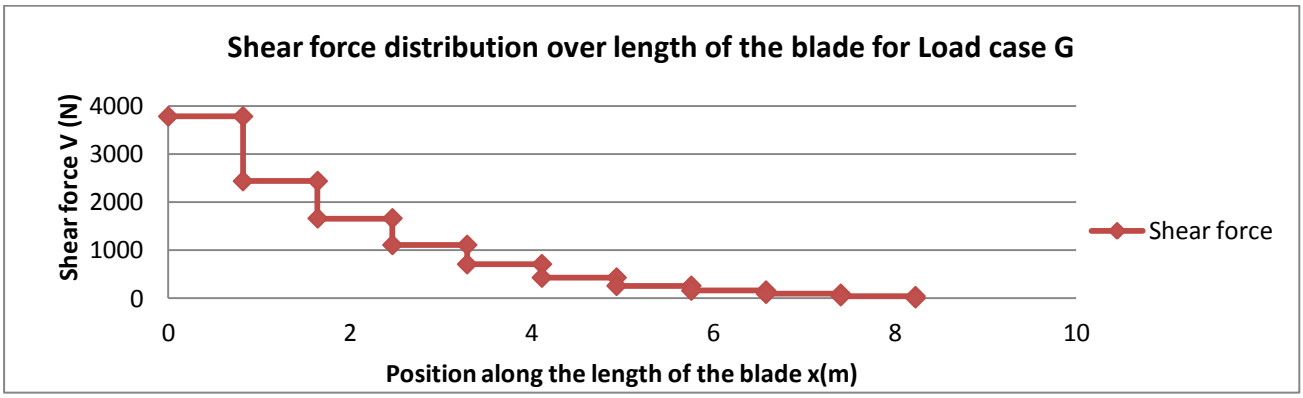
Shear force distribution over length of the blade for Load case G
Shear force V (N)
4000
3000
2000
1000
0
0
2
4
6
8
10
Position along the length of the blade x(m)
Shear force

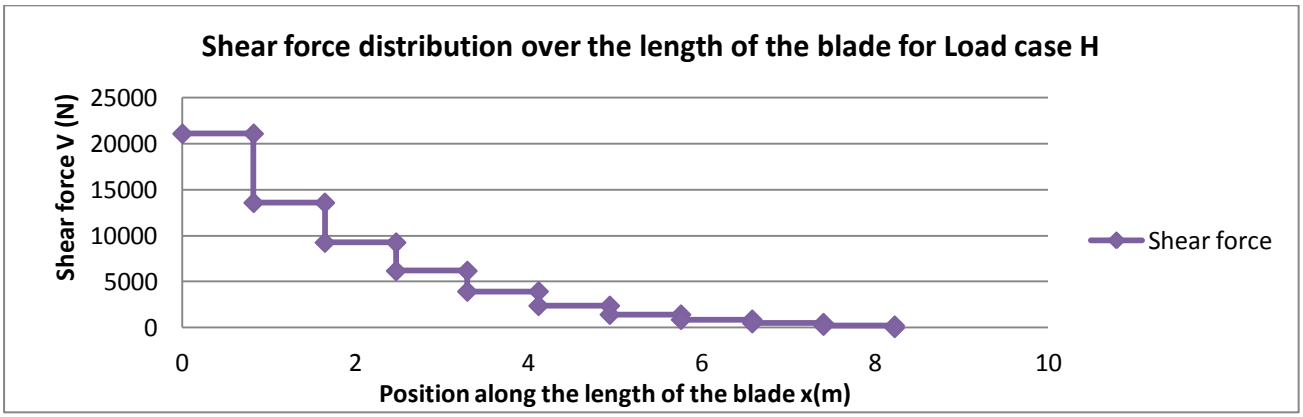
Shear force distribution over the length of the blade for Load case H
Shear force V (N)
25000
20000
15000
10000
5000
0
0
2
4
6
8
10
Position along the length of the blade x(m)
Shear force

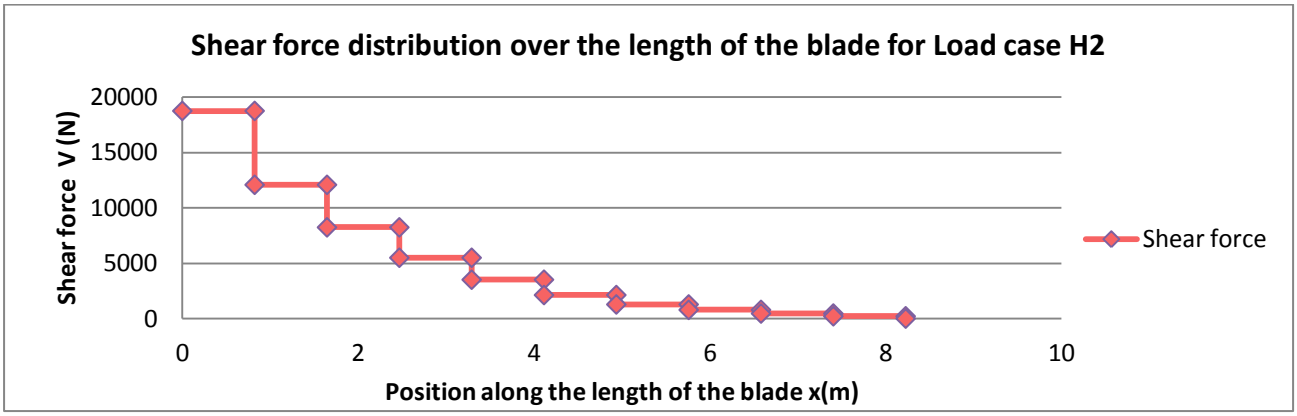
Shear force distribution over the length of the blade for Load case H2
Shear force V (N)
20000
15000
10000
5000
0
0
2
4
6
8
10
Position along the length of the blade x(m)
Shear force

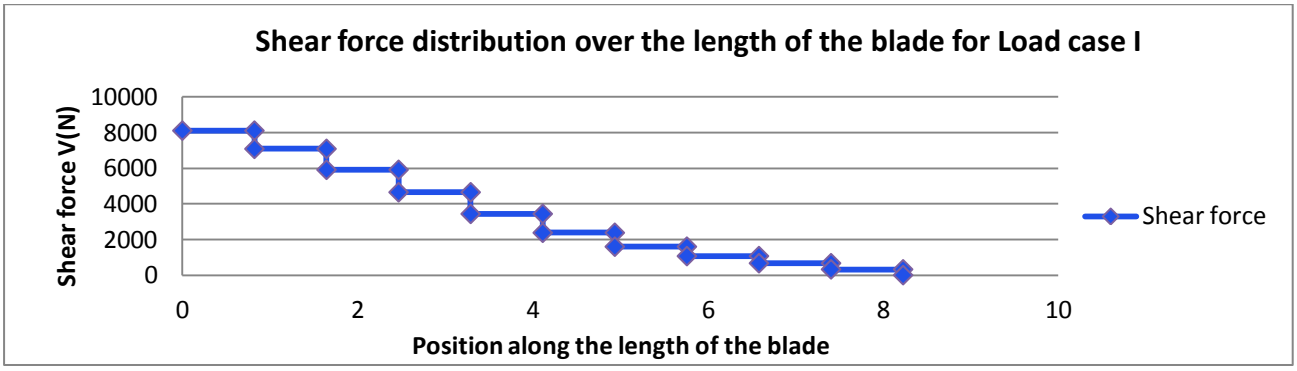
Shear force distribution over the length of the blade for Load case I
Shear force V(N)
10000
8000
6000
4000
2000
0
0
2
4
6
8
10
Position along the length of the blade
Shear force

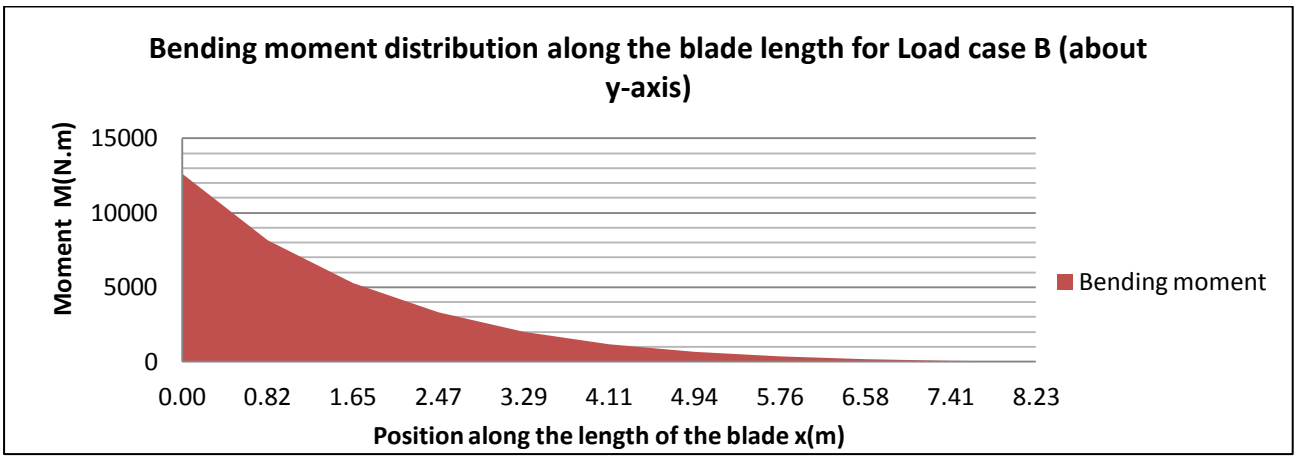
Bending moment distribution along the blade length for Load case B (about y-axis)
Moment M(N.m)
15000
10000
5000
0
0.00
0.82
1.65
2.47
3.29
4.11
4.94
5.76
6.58
7.41
8.23
Position along the length of the blade x(m)
Bending moment

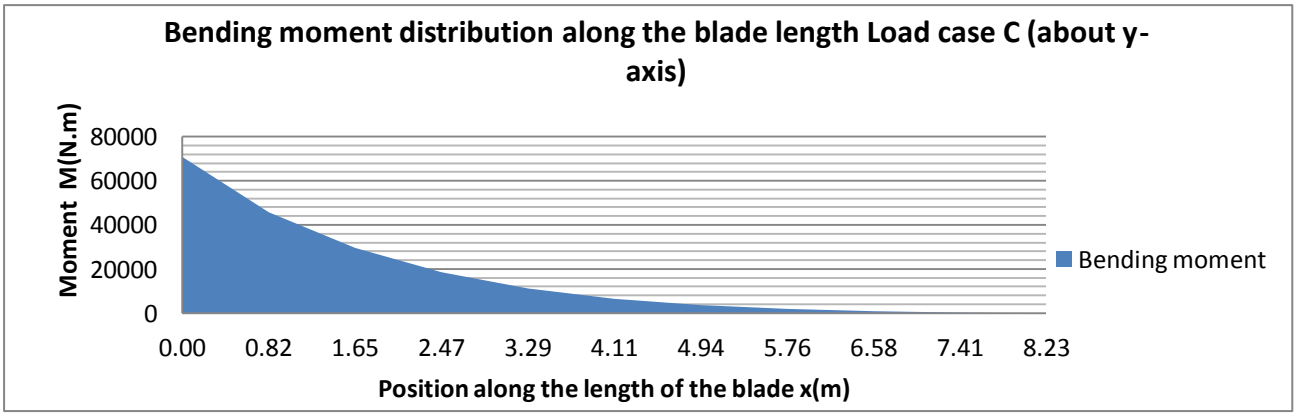
Bending moment distribution along the blade length Load case C (about y-axis)
Moment M(N.m)
80000
60000
40000
20000
0
0.00
0.82
1.65
2.47
3.29
4.11
4.94
5.76
6.58
7.41
8.23
Position along the length of the blade x(m)
Bending moment

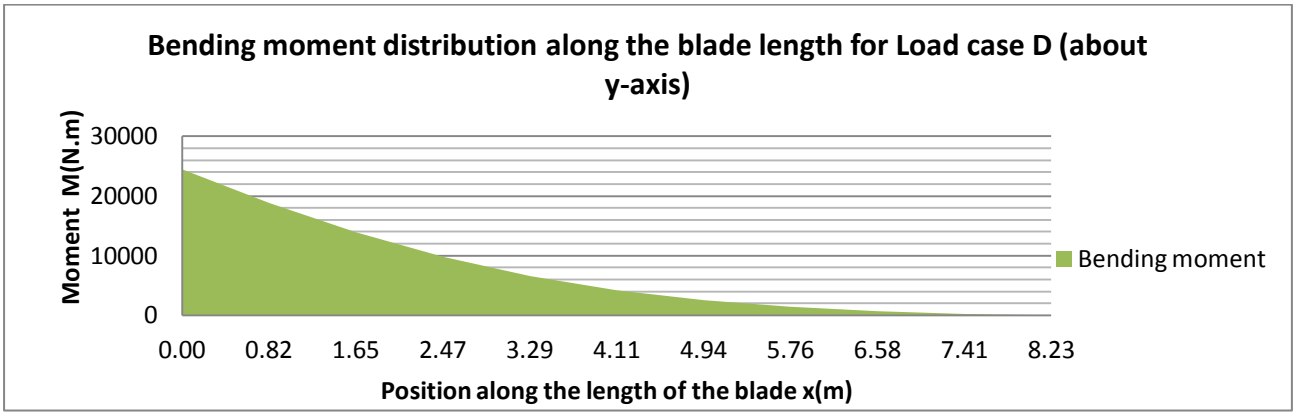
Bending moment distribution along the blade length for Load case D (about y-axis)
Moment M(N.m)
30000
20000
10000
0
0.00
0.82
1.65
2.47
3.29
4.11
4.94
5.76
6.58
7.41
8.23
Position along the length of the blade x(m)
Bending moment

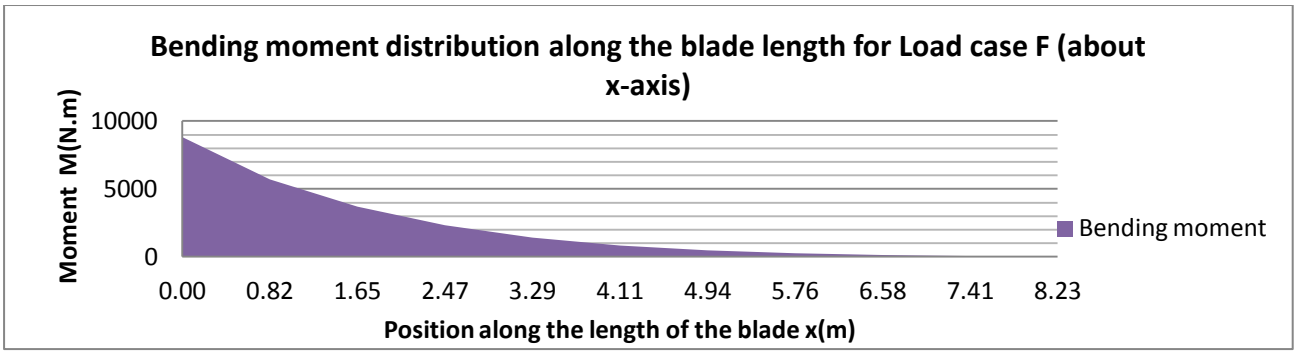
Bending moment distribution along the blade length for Load case F (about x-axis)
Moment M(N.m)
10000
5000
0
0.00
0.82
1.65
2.47
3.29
4.11
4.94
5.76
6.58
7.41
8.23
Position along the length of the blade x(m)
Bending moment

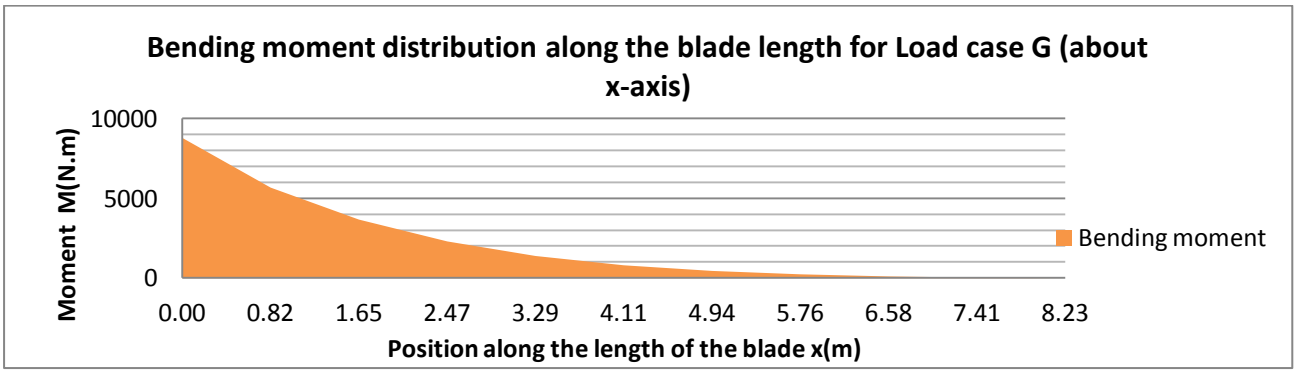
Bending moment distribution along the blade length for Load case G (about x-axis)
Moment M(N.m)
10000
5000
0
0.00
0.82
1.65
2.47
3.29
4.11
4.94
5.76
6.58
7.41
8.23
Position along the length of the blade x(m)
Bending moment

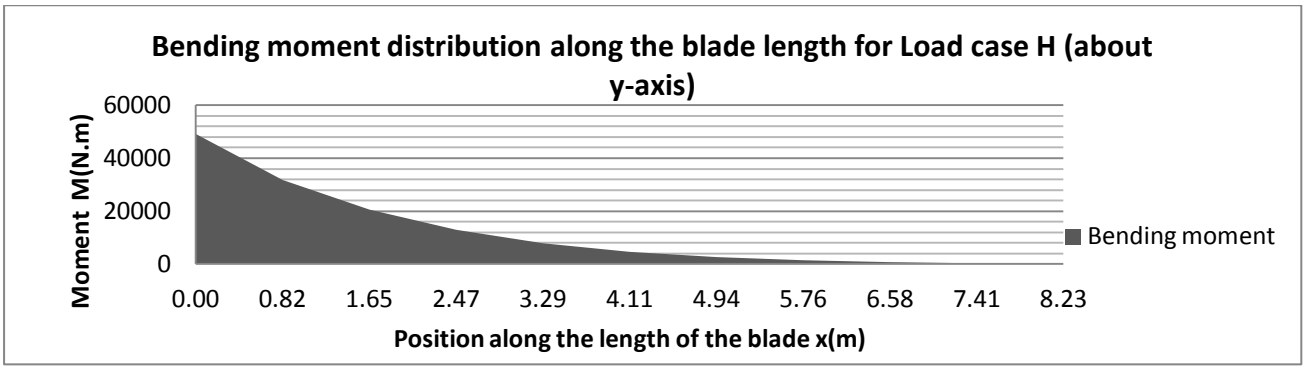
Bending moment distribution along the blade length for Load case H (about y-axis)
Moment M(N.m)
60000
40000
20000
0
0.00
0.82
1.65
2.47
3.29
4.11
4.94
5.76
6.58
7.41
8.23
Position along the length of the blade x(m)
Bending moment

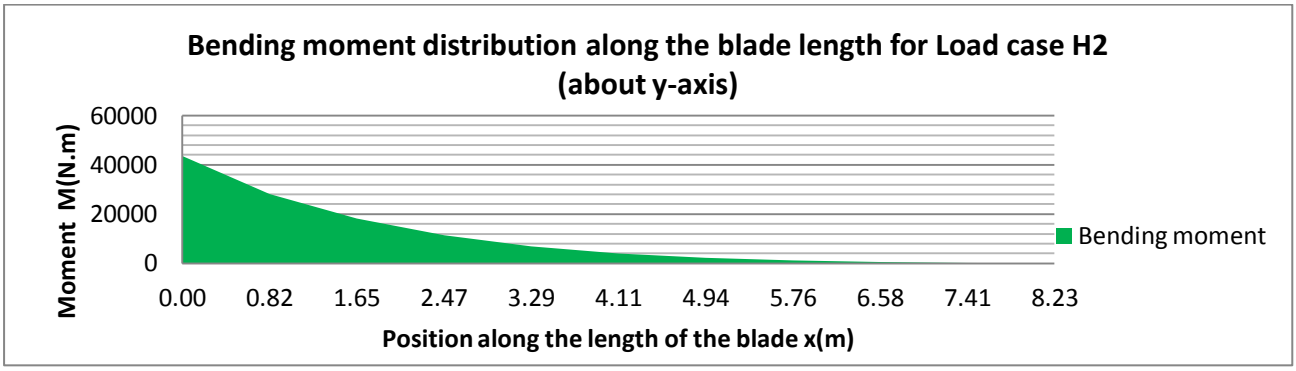
Bending moment distribution along the blade length for Load case H2 (about y-axis)
Moment M(N.m)
60000
40000
20000
0
0.00
0.82
1.65
2.47
3.29
4.11
4.94
5.76
6.58
7.41
8.23
Position along the length of the blade x(m)
Bending moment

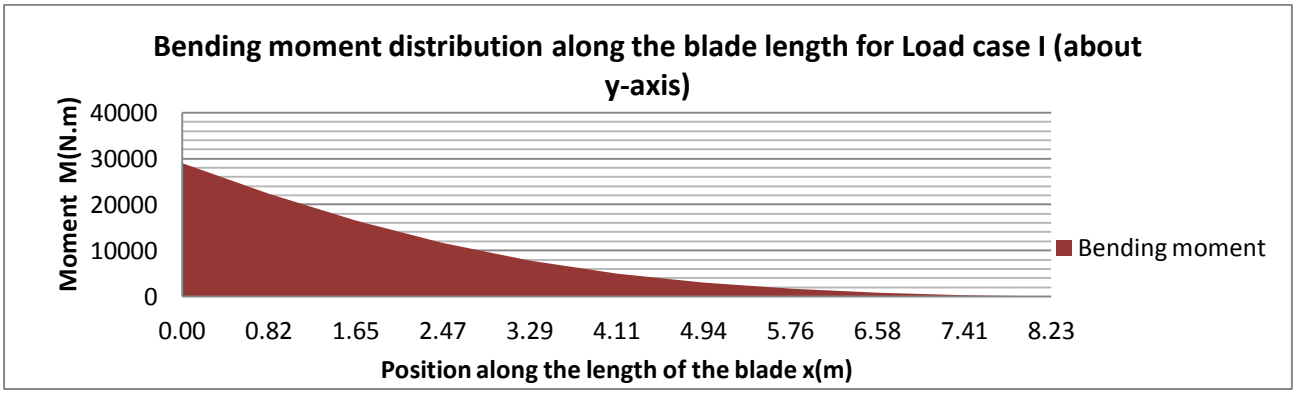
Bending moment distribution along the blade length for Load case I (about y-axis)
Moment M(N.m)
40000
30000
20000
10000
0
0.00
0.82
1.65
2.47
3.29
4.11
4.94
5.76
6.58
7.41
8.23
Position along the length of the blade x(m)
Bending moment

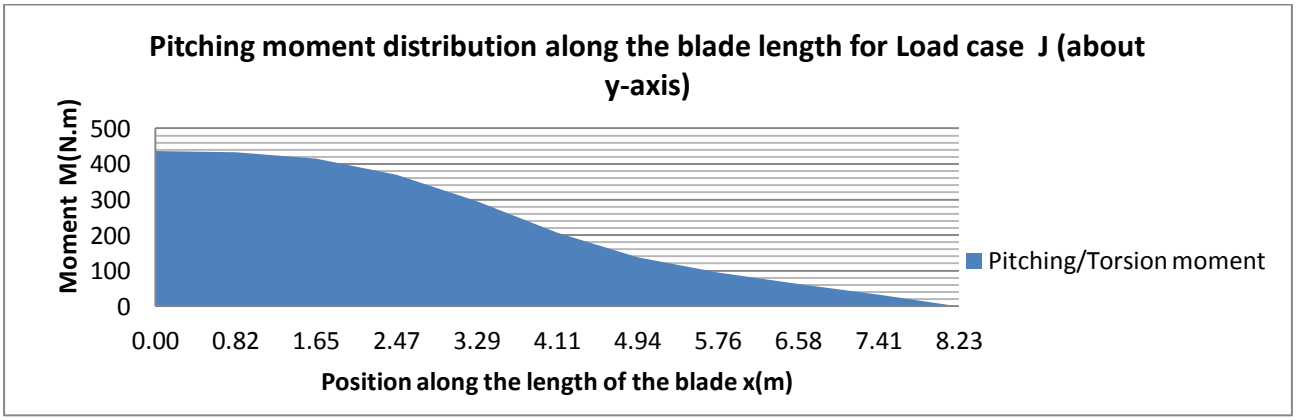
Pitching moment distribution along the blade length for Load case J (about y-axis)
Moment M(N.m)
500
400
300
200
100
0
0.00
0.82
1.65
2.47
3.29
4.11
4.94
5.76
6.58
7.41
8.23
Position along the length of the blade x(m)
Pitching/Torsion moment

APPENDIX D: BEARING DESIGN/ SELECTION

D.1 General

This appendix presents the design of the pitch bearings in the root section of the blade. The design of the root bearings is necessary to obtain the dimensions of the circular root section. The design of the bearings will be based on the guidelines for bearing selection of SKF (2008).

D.2 Symbols

P_0	equivalent static bearing load	[kN]
$F_{r,i}$	actual radial load of bearing i (see Figure D-1)	[kN]
F_a	actual axial bearing load (see Figure D-1)	[kN]
X_0	radial load factor for the bearing	[N]
Y_0	axial load factor for the bearing	[N]
M_{max}	Maximum bending moment as calculated in Chapter 3	[N.mm]
d_1	Distance from the point where the maximum bending moment is calculated to the first bearing on the blade root	[m]
$F_{shear,max}$	Maximum shear force as calculated in Chapter 3	[kN]
$F_{cent,max}$	Maximum centrifugal force as calculated in Chapter 3	[kN]

D.3 Bearing selection

The design of the root bearing firstly consists of selecting the appropriate bearing type. The bearings required at the root of the blade have to withstand both axial loads due to the centrifugal loads on the blade as well as radial loads due to the bending of the blade. Spherical roller bearings were chosen for this application as these have an excellent rating for combined axial and radial loading according to SKF (2008). Although there are other bearing types capable of withstanding both axial and radial loads, the spherical roller bearings were chosen due to their availability in larger sizes, which will be required to withstand the great bending moments and centrifugal forces.

Recent wind turbine blade roots are designed to connect to the hub of the wind turbine by a slewing bearing as shown in Figure D-1. The root of the blade is then designed with T-bolts infused in the laminated material. This root and bearing configuration simplifies the assembly and maintenance of the wind turbine. Slewing bearings can accommodate axial, radial and moment loads acting either singly or in combination and in any direction(SKF, 2008). Although these bearings have a low profile and excellent weight/performance ratio and are ideal for wind turbine blade root applications, they are very expensive. Thus, for this project, two spherical roller bearings will be used at the root section of the blade.

According to SKF (2008), the bearing size is selected on the basis of static load-carrying capacity instead of on bearing life when one of the following conditions exist:

- Bearing is stationary and is subjected to continuous intermittent (shock) loads.
- The bearing makes slow oscillating or alignment movements under load.
- The bearing rotates under load at very slow speed (n < 10r/min) and is only required to have a short life (the life equation in this case, for a given equivalent load P would give such a low requisite basic dynamic loading C that the bearing selected on a life basis would be seriously overloaded in service).
- The bearing rotates and, in addition to the normal operating loads, has to sustain heavy shock loads.

The pitch bearings in the root of the blade will experience three of the above-mentioned conditions and thus the bearing size will be selected using the static load carrying capacity C_0.

D.4 Equivalent static bearing load

Static loads comprising radial and axial components must be converted into an equivalent static bearing load (SKF, 2008). (See equation D.1.)

$$P_0 = X_0 F_r + Y_0 F_a \qquad \text{(D-1)}$$

where

$P_0 =$ equivalent static bearing load, kN

$F_r =$ actual radial bearing load (see Figure D-1), kN

$F_a =$ actual axial bearing load (see Figure D-1), kN

$X_0 =$ radial load factor for the bearing, kN

$Y_0 =$ axial load factor for the bearing, kN

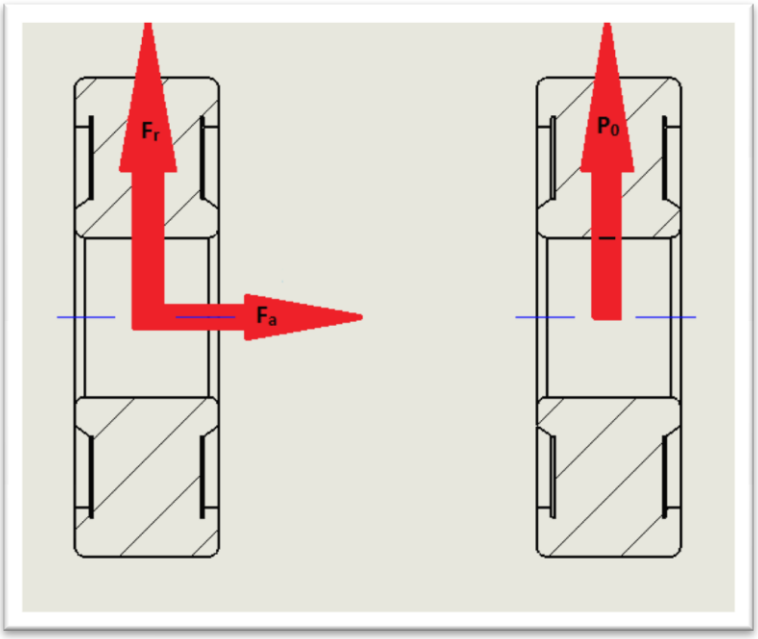

Figure D-1: The radial and axial components of the maximum load that can occur are used to calculate P_0

Thus, Table D-1 shows the maximum loads as calculated in Chapter 3 that will be used to calculate the actual radial and axial bearing loads.

Table D-1: The maximum loads as calculated in Chapter 3 for the calculation of the actual radial and –axial bearing loads

Moment and forces as calculated in chapter 3		Units
Maximum bending moment (load case C)	70923932	**N.mm**
Maximum axial force (load case E)	55474.12	**N**
Maximum shear force(load case C)	30517.6	**N**

The blade in this project does not make use of a slewing bearing as previously mentioned. Thus, two spherical bearings are used, placed at a certain distance from each other, to withstand the bending moment at the root of the blade (see Figure D-3). Note that the bearing selection process is modelled for different bearing sizes and different distances between the bearings. The bearing sizes and distances between them are calculated to fit in a nose cone on the wind turbine with a diameter of 1m as presented in Figure D-4. All the calculated values presented in this appendix are only those that were used for the final bearing selected. Figure D-2 and Figure D-3 show the conversion of the root section of the blade from the airfoil shape to the circular shape that could accommodate the root bearings.

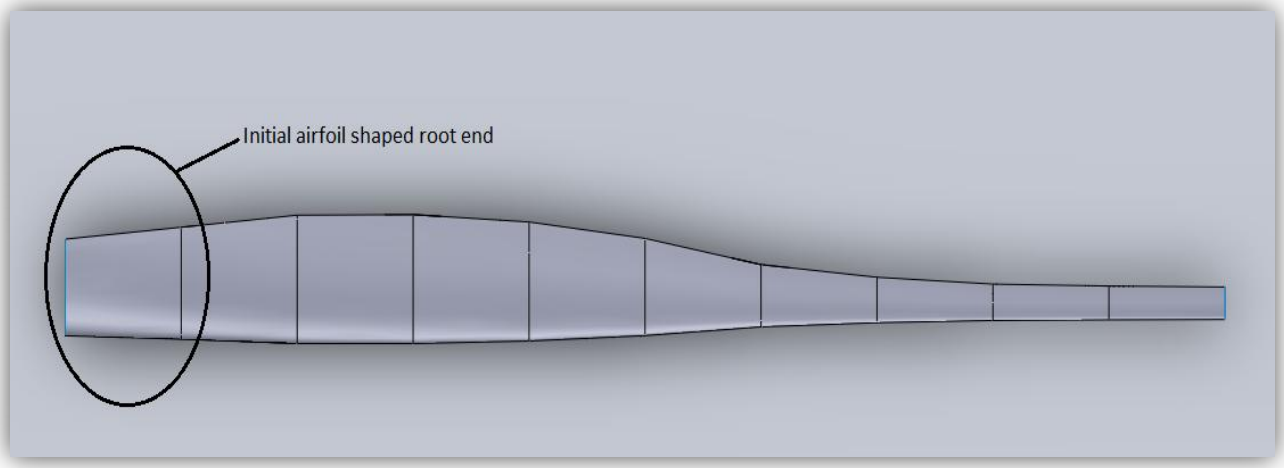

Figure D-2: The initial airfoil shape root end

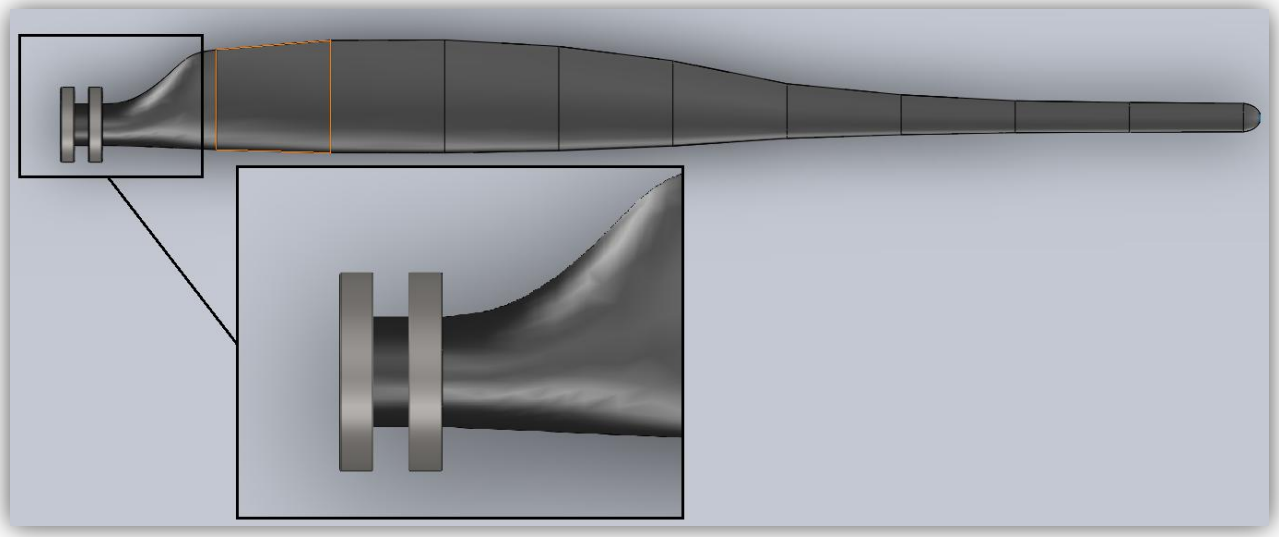

Figure D-3: A representation of the positioning of the root bearings and the conversion of the root to a circular shape to accommodate the bearings

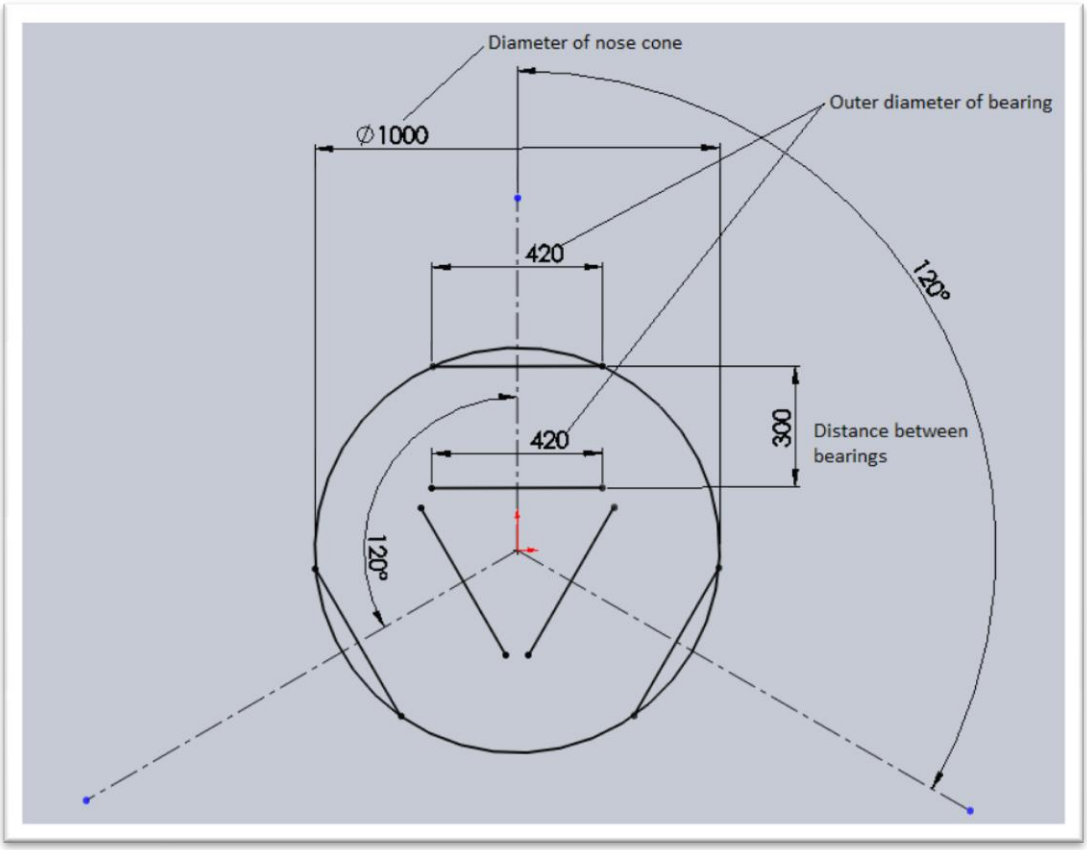

Figure D-4: A presentation of the bearing selection constraint to fit in a nose cone with a diameter of 1m

Calculation of the F_r and F_a

The axial force caused by the centrifugal load on the blade will act on only one of the two bearings as a fixed ring will be placed between the bearings to prevent axial movement of the blade inside the bearings (see Figure D-5).

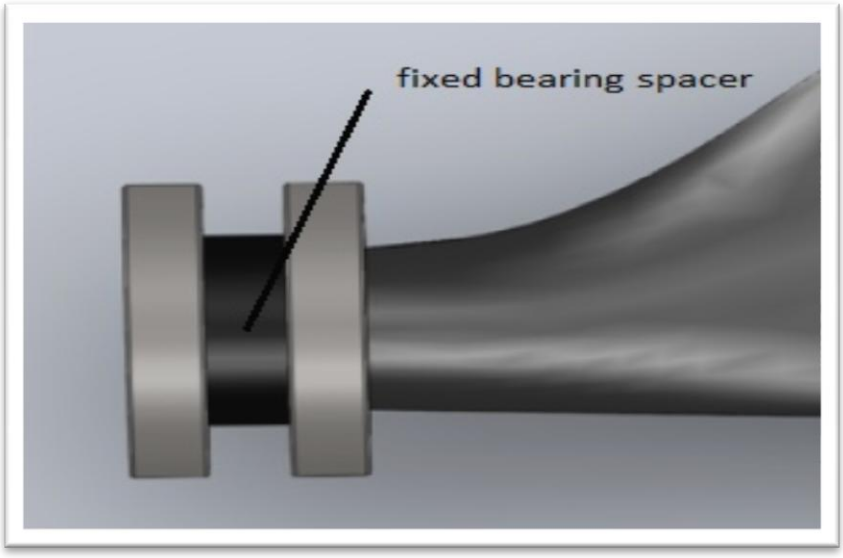

Figure D-5: The fixed spacer between the root bearings to prevent axial movement of the blade in the bearings

The actual radial load is calculated for the two bearings as follows:

For bearing 1 (see Figure D-6), the radial load is caused by the maximum bending moment as calculated at the root of the blade. Bearing 1 is positioned at a distance of 300mm from the point where the bending moment was calculated.

Thus:

$$F_{r,1} = \frac{M_{max}}{d_1} \quad \text{(D-2)}$$

and

$$F_{r,2} = F_{r,1} + F_{shear,max} \quad \text{(D-3)}$$

The actual axial force acting on bearing 2 is equal to the maximum centrifugal force that the blade will experience.

Hence,

$$F_a = F_{cent,max} \quad \text{(D-4)}$$

The radial and axial load factors (X_0 and Y_0) are given for each bearing selected. The radial load factor (X_0) is given as 1 for this type of bearings. The axial load factor (Y_0) is given for each bearing in SKF's catalogue. Table x shows the value used for Y_0 for both bearings. (Only the value for the bearing selected is shown.)

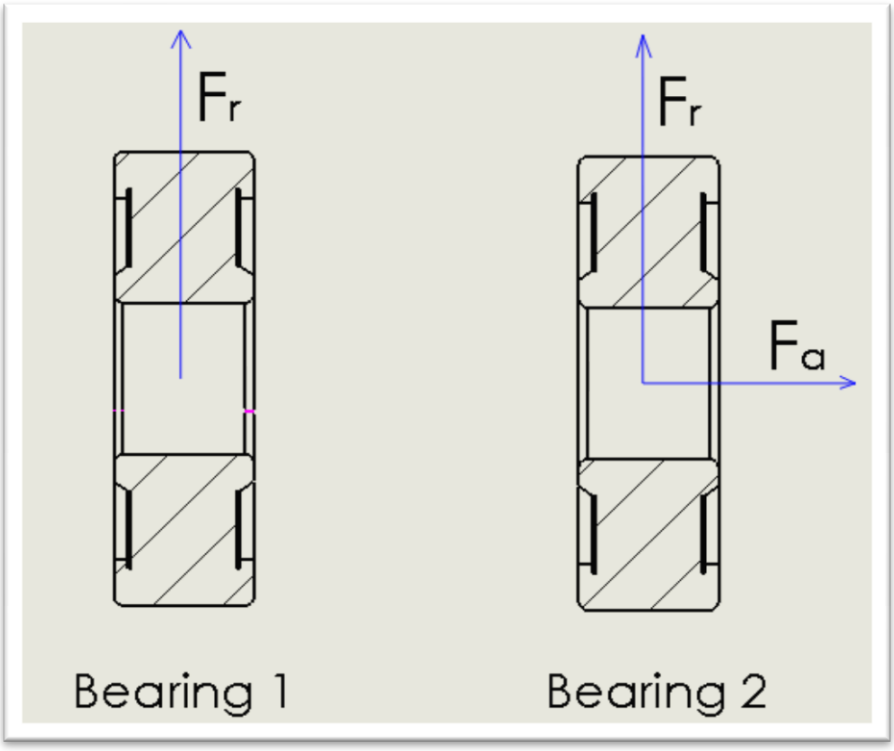

Figure D-6: The actual radial and axial loads as calculated for the two root bearings

Static load rating C_0 and static safety factor s_0

The static load rating C_0 is given for each bearing in the SKF catalogue. The static load rating is used to calculate the static safety factor that is used as a guideline for the selection of the root bearings. The equation for the calculation of the static safety factor is given by equation D-5.

$$s_0 = C_0 P_0 \tag{D-5}$$

According to SKF (2008), the required static safety factor for spherical roller bearings is 4. Thus, the bearings selected for the root of the blade were subjected to several design constraints. The previously mentioned design constraints consisted of the following:

- The bearings should fit in a nose cone with a diameter of 1m.
- The bearings should be as far apart from each other to minimise the radial loads.
- The static safety factor should be ≥ 4.
- The inner diameter of the bearing should be selected so that the root of the blade can be smoothly coalesced from a circular shape to the airfoil shape of the blade – thus not too large or too small.

Table D-2 shows the values calculated for a 23960 CC/W33 SKF bearing.

Table D-2: Results for the selection of the blade root bearings

For bearing 1		
$P_o = F_r + Y_0 F_a$		
F_r	236.4131067	**kN**
Y_0	3.6	
F_a	55.47412494	**kN**
P_o	436.1199565	**kN**
C_0	2500	
s_0	5.73236781	**satisfactory**
For bearing 2		
$P_o = F_r + Y_0 F_a$		
F_r	266.9307073	**kN**
Y_0	3.6	
F_a	55.47412494	**kN**
P_o	466.637557	**kN**
C_0	2500	
s_0	5.357477045	**satisfactory**

The selected bearing provided that the diameter of the circular blade root is 300mm. The root of the blade can therefore be smoothly coalesced from the 300mm circle into the airfoil shape of the first blade section.

APPENDIX E: SKIN THICKNESS CALCULATION FOR PRELIMINARY DESIGN

E.1 General

This appendix provides the calculation of skin thickness at each section of the blade. Note that the pitching moment/ torsion load are presented in N.mm and not in N.m as calculated in Chapter 3. The values presented in the green cells are to show that the number of layers and the thickness has converged. The cells presented in yellow are the values of the number of layers and skin thickness after a safety factor of 3.3 was applied.

E.2 Skin thickness calculations for each section

Skin thickness calculation for section 1:

Iteration	T (N.mm)	Am (mm2)	q (N/mm)	n(# of layers)	t(thickness @0.28mm per layer)	Safety factor for torsion in skin
0 (initial value)	436973.61	70215.38 (calculated for 1mm skin thickness)	3.111665945	0.1035	0.02897008	19.45607063
1	436973.61	70672.18	3.091553081	0.1028	0.028782826	
2	436973.61	70672.27	3.091549222	0.1028	0.02878279	
3	436973.61	70672.27	3.091549221	0.1028	0.02878279	<----- this is for a safety factor of 1
			X 3.3	0.3392	0.094983208	<----- this is for a safety factor of 3.3

Skin thickness calculation for section 2:

Iteration	T (N.mm)	Am (mm2)	q (N/mm)	n (# of layers)	t (thickness @0.28mm per layer)	Safety factor for torsion in skin
0	433501.31	90762.33	2.3881	0.0794	0.0222	**25.40538553**
1	433501.31	91536.39	2.3679	0.0787	0.0220	
2	433501.31	91549.27	2.3676	0.0787	0.0220	
3	433501.31	91549.27	2.3676	0.0787	0.0220	<----- this is for a safety factor of 1
			X 3.3	0.2597	0.0727	<----- this is for a safety factor of 3.3

Skin thickness calculation for section 3:

Iteration	T (N.mm)	Am (mm2)	q (N/mm)	n (# of layers)	t (thickness @0.28mm per layer)	Safety factor for torsion in skin
0	415594.64	77262.22	2.6895	0.089	0.0250	**22.61068534**
1	415594.64	78092.25	2.6609	0.088	0.0247	
2	415594.64	78112.83	2.6602	0.088	0.0247	
3	415594.64	78112.83	2.6602	0.088	0.0247	<----- this is for a safety factor of 1
			X 3.3	0.292	0.0817	<----- this is for a safety factor of 3.3

Skin thickness calculation for section 4:

Iteration	T (N.mm)	Am (mm2)	q (N/mm)	n (# of layers)	t (thickness @0.28mm per layer)	Safety factor for torsion in skin
0	370320.47	67873.24	2.7280	0.0907	0.0254	**22.31421833**
1	370320.47	68690.45	2.6955	0.0896	0.0251	
2	370320.47	68690.72	2.6955	0.0896	0.0251	
3	370320.47	68690.72	2.6955	0.0896	0.0251	<----- this is for a safety factor of 1
			X 3.3	0.2958	0.0828	<----- this is for a safety factor of 3.3

Skin thickness calculation for section 5:

Iteration	T (N.mm)	Am (mm2)	q (N/mm)	n (# of layers)	t (thickness @0.28mm per layer)	Safety factor for torsion in skin
0	295850.27	49410.62	2.9937	0.100	0.0278	**20.37249207**
1	295850.27	50100.91	2.9525	0.098	0.0274	
2	295850.27	50102.63	2.9524	0.098	0.0274	
3	295850.27	50101.97	2.9524	0.098	0.0274	<----- this is for a safety factor of 1
			X 3.3	0.324	0.0907	<----- this is for a safety factor of 3.3

Skin thickness calculation for section 6:

Iteration	T (N.mm)	Am (mm2)	q (N/mm)	n (# of layers)	t (thickness @0.28mm per layer)	Safety factor for torsion in skin
0	207475.40	32723.00	3.1701	0.1054	0.0295	**19.30955338**
1	207475.40	33301.92	3.1150	0.1035	0.0290	
2	207475.40	33302.55	3.1150	0.1035	0.0290	
3	207475.40	33302.55	3.1150	0.1035	0.0290	<----- this is for a safety factor of 1
			X 3.3	0.3418	0.096	<----- this is for a safety factor of 3.3

Skin thickness calculation for section 7:

Iteration	T (N.mm)	Am (mm2)	q (N/mm)	n (# of layers)	t (thickness @0.28mm per layer)	Safety factor for torsion in skin
0	138352.65	13261.598	5.21628885	0.173	0.0485	**11.84704371**
1	138352.65	13624.0543	5.077513952	0.169	0.0472	
2	138352.65	13624.9873	5.077166258	0.169	0.0472	
3	138352.65	13624.9897	5.077165364	0.169	0.0472	
4	138352.65	13624.9897	5.077165364	0.169	0.0472	<----- this is for a safety factor of 1
			X 3.3	0.557	0.1559	<----- this is for a safety factor of 3.3

Skin thickness calculation for section 8:

Iteration	T (N.mm)	Am (mm2)	q (N/mm)	n (# of layers)	t (thickness @0.28mm per layer)	Safety factor for torsion in skin
0	95461.80	6972.75	6.8453	0.2276	0.0637	**9.121750091**
1	95461.80	7237.54	6.5949	0.2192	0.0613	

2	95461.80	7238.46	6.5940	0.2192	0.0613	
3	95461.80	7238.46	6.5940	0.2192	0.0613	
4	95461.80	7238.46	6.5940	0.2192	0.0613	<----- this is for a safety factor of 1
			X 3.3	0.7235	0.2025	<----- this is for a safety factor of 3.3

Skin thickness calculation for section 9:

Iteration	T (N.mm)	Am (mm2)	q (N/mm)	n (# of layers)	t (thickness @0.28mm per layer)	Safety factor for torsion in skin
0	63163.53	4416.87	7.1502	0.2377	0.0665	**8.812813288**
1	63163.53	4626.22	6.8266	0.2269	0.0635	
2	63163.53	4627.21	6.8252	0.2269	0.0635	
3	63163.53	4627.21	6.8252	0.2269	0.0635	
4	63163.53	4627.21	6.8252	0.2269	0.0635	<----- this is for a safety factor of 1
			X 3.3	0.7489	0.2096	<----- this is for a safety factor of 3.3

Skin thickness calculation for section 10:

Iteration	T (N.mm)	Am (mm2)	q (N/mm)	n (# of layers)	t (thickness @0.28mm per layer)	Safety factor for torsion in skin
0	33109.79	3793.94	4.3635	0.1450	0.0406	**14.51014566**
1	33109.79	3992.83	4.1461	0.1378	0.0386	
2	33109.79	3993.61	4.1453	0.1378	0.0385	
3	33109.79	3993.62	4.1453	0.1378	0.0385	
4	33109.79	3993.62	4.1453	0.1378	0.0385	<----- this is for a safety factor of 1
			X 3.3	0.4548	0.1273	<----- this is for a safety factor of 3.3

APPENDIX F: SPAR CAP OPTIMISATION PLOTS

F.1 General

This appendix presents the plots of the spar cap as calculated in Chapter 4, section 4.4. The plots presented are those used to determine the thickness and width combination that provide the smallest area of spar cap at each section of the blade. From the plots it is possible to see the width (as percentage of the chord length) that provides the smallest area. These width and thickness combinations are then used to describe the topology of the spar caps at each section of the blade.

F.2 Spar cap area vs. width as percentage of chord length plots

Note that the spar cap width for section 1 is not presented as a percentage of the chord length as all the other sections. Since section 1 is the circular root section of the blade, the spar cap width is calculated for different sector angles as presented in Figure F-1.

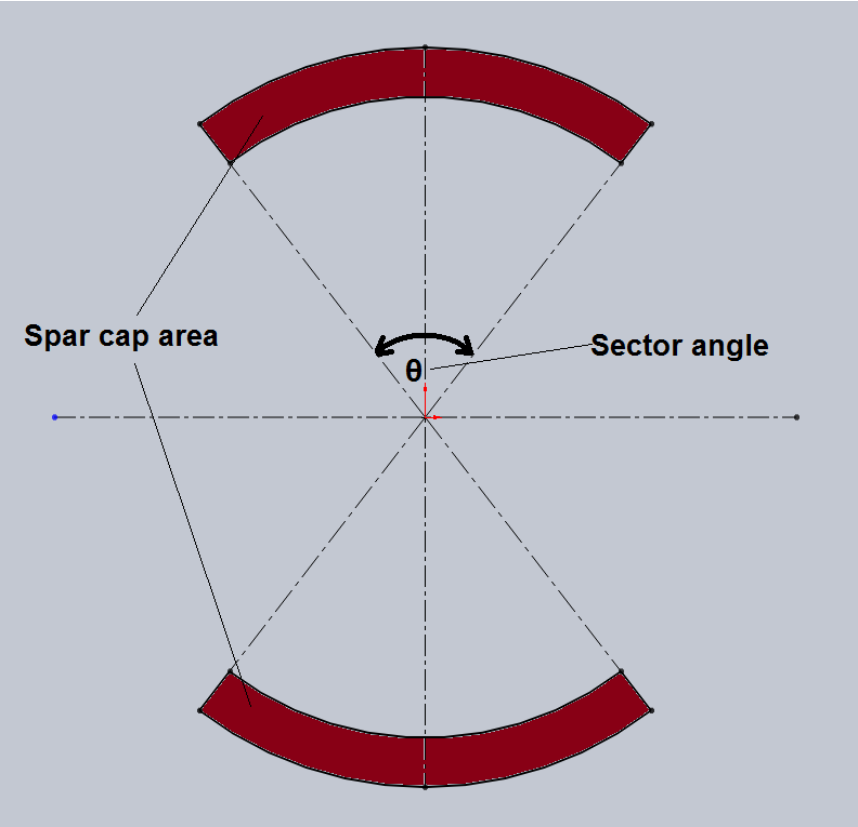

Figure F-1: The spar cap of the circular root section is modelled for different sector angles and not for different lengths as percentage of the chord length as with the other sections

Spar cap area vs. spar cap width in sector angle for section 1 (root).

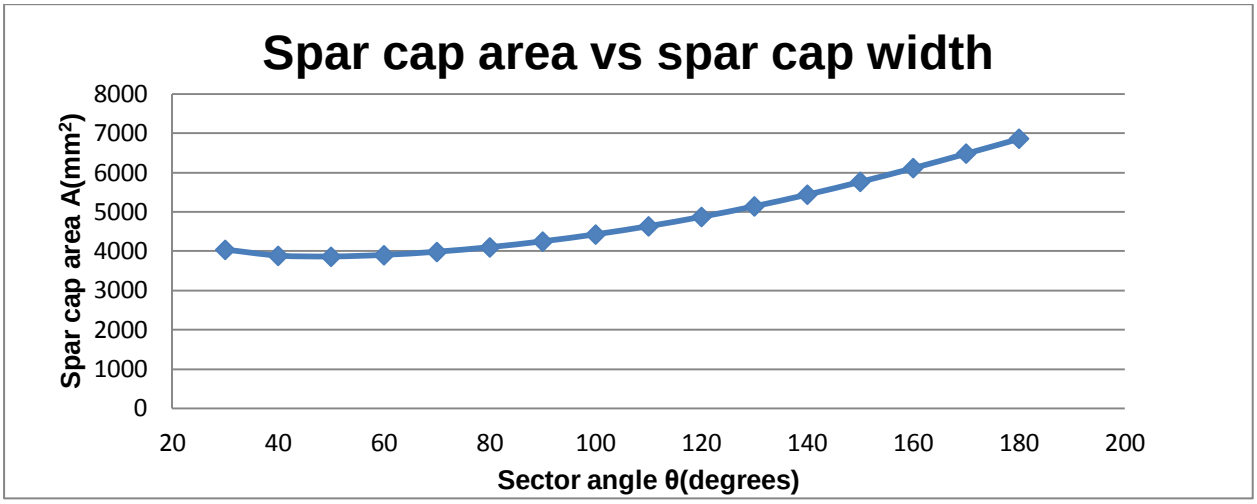

Spar cap area vs. spar cap width as percentage of chord length of section 2 plot.

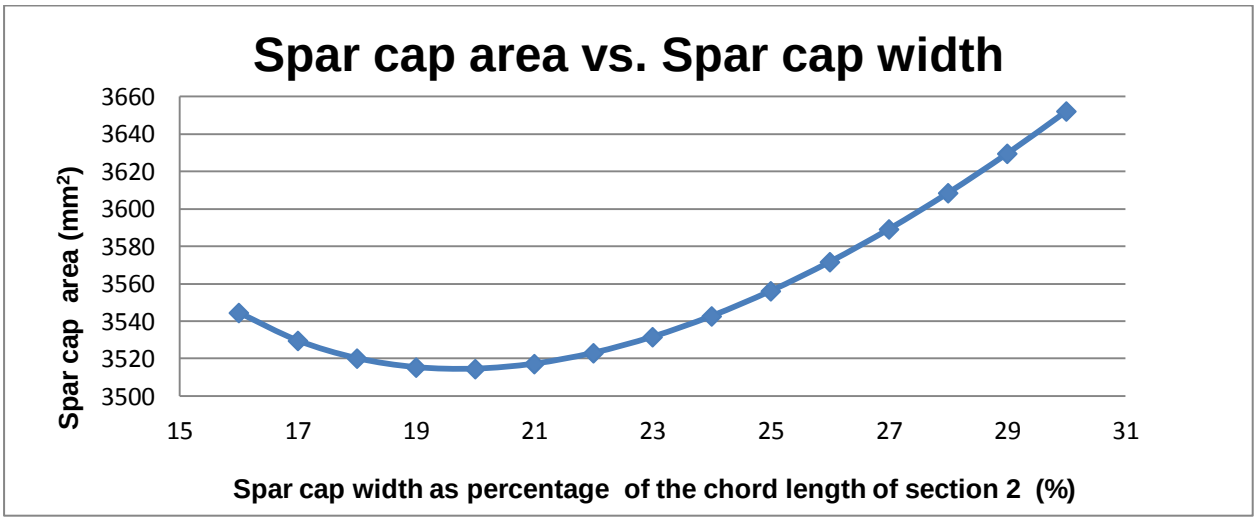

Spar cap area vs. spar cap width as percentage of chord length of section 3 plot.

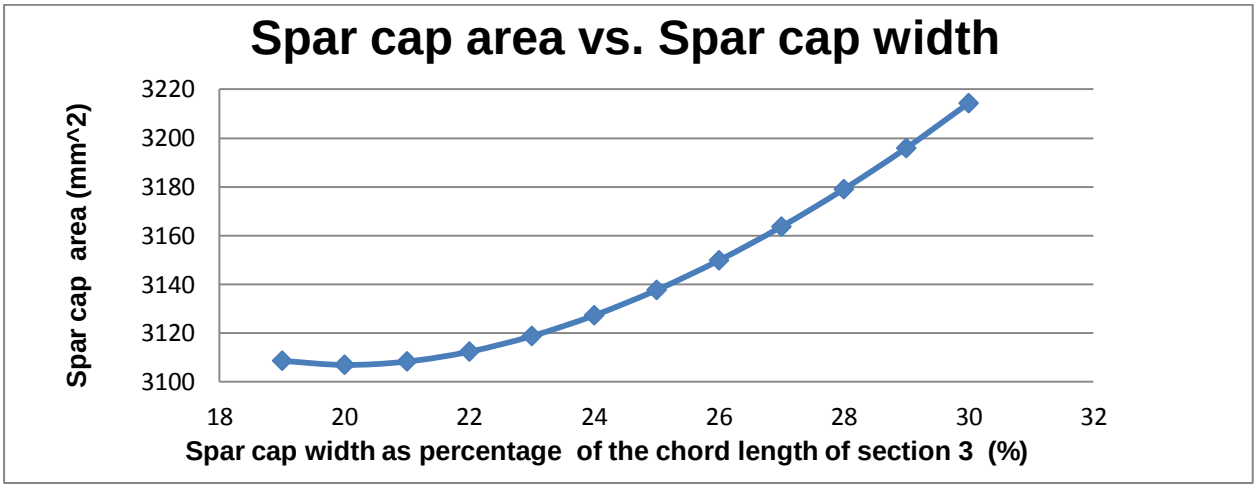

Spar cap area vs. spar cap width as percentage of chord length of section 4 plot.

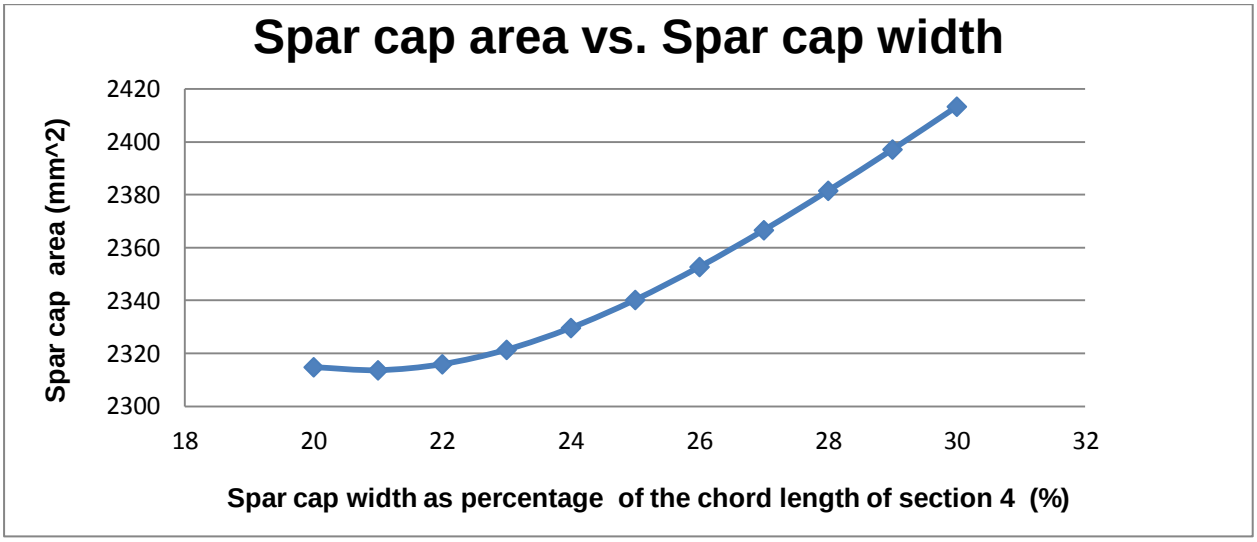

Spar cap area vs. spar cap width as percentage of chord length of section 5 plot.

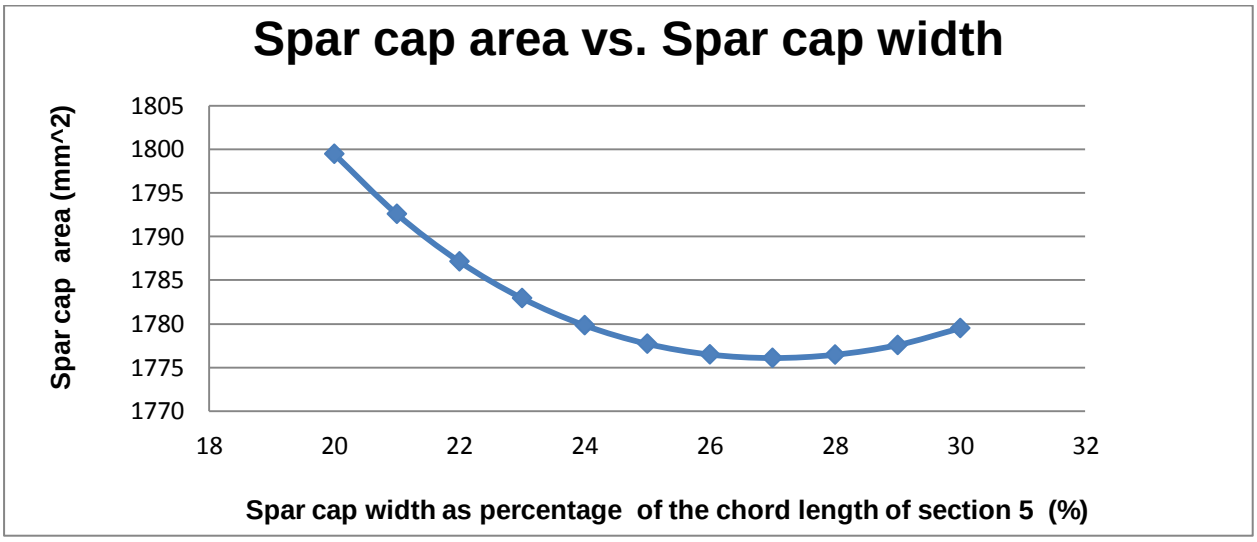

Spar cap area vs. spar cap width as percentage of chord length of section 6 plot.

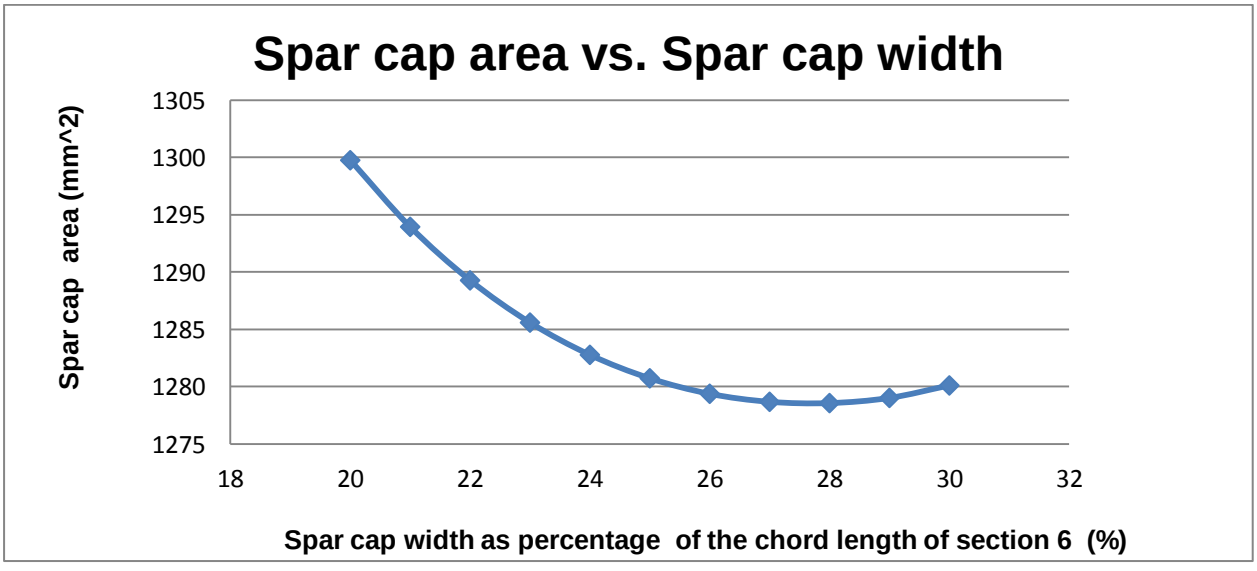

Spar cap area vs. spar cap width as percentage of chord length of section 7 plot.

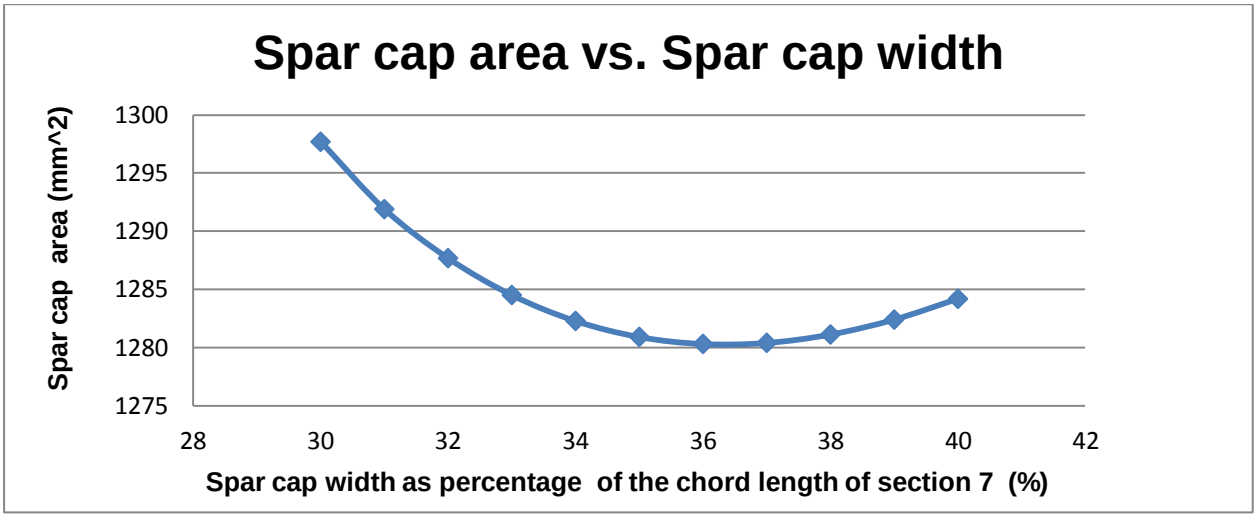

Spar cap area vs. spar cap width as percentage of chord length of section 8 plot.

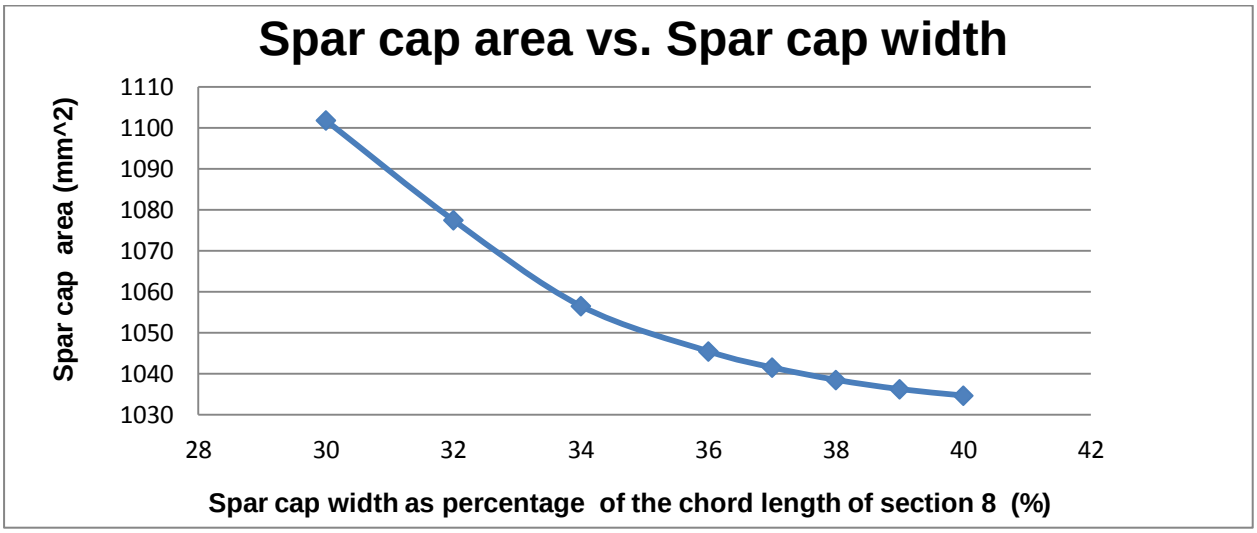

Spar cap area vs. spar cap width as percentage of chord length of section 9 plot.

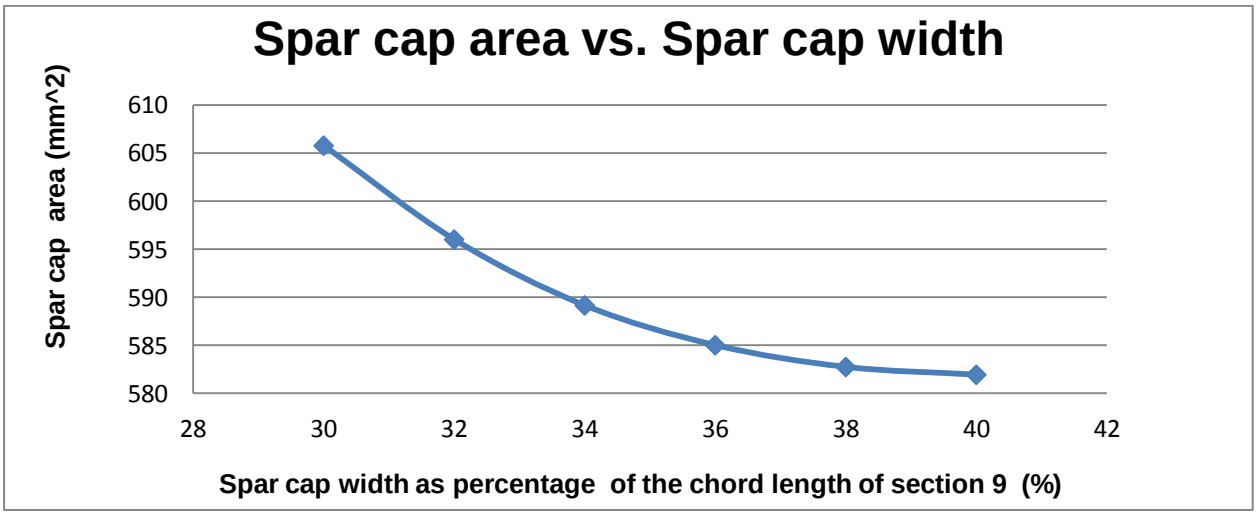

Spar cap area vs. spar cap width as percentage of chord length of section 10 plot.

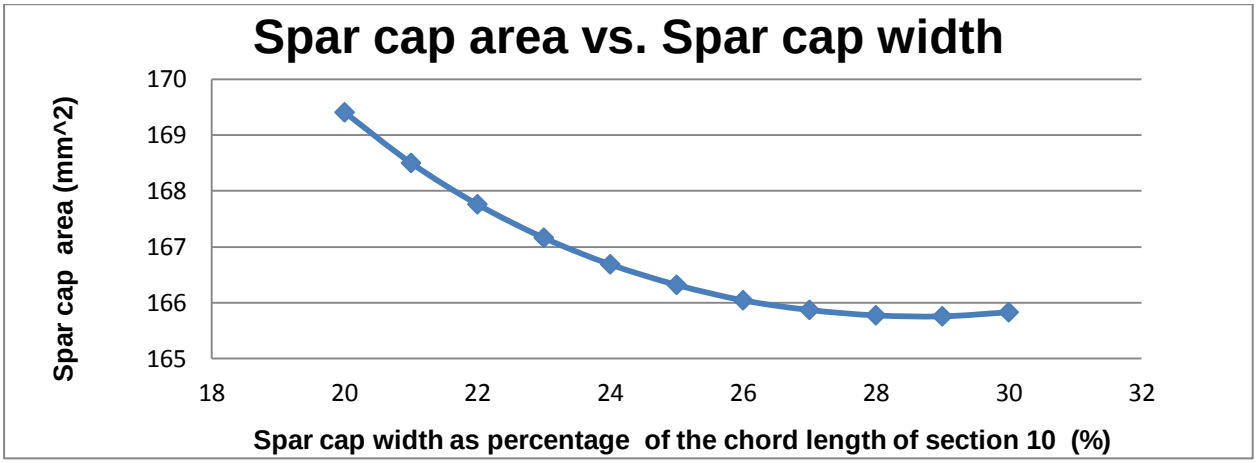

Table F-1 summarises the spar cap topology in terms of its width and the thickness for each section of the blade.

Table F-1: A summary of the spar cap width as a percentage of the chord length and thickness at each section of the blade as calculated in the preliminary design

blade section	spar cap width (%)	spar cap thickness (mm)
1	48°	19.8
2	20.0	12.3
3	20.0	9.9
4	21.0	7.0
5	27.0	4.6
6	28.0	4.0
7	36.0	4.8
8	40.0	4.8
9	40.0	3.3
10	28.0	1.5

APPENDIX G: SHEAR WEB THICKNESS CALCULATION FOR PRELIMINARY DESIGN

G.1 General

This appendix presents the tables containing the data for the iteration of the shear web thickness. The cells filled with green represent the converged shear web number of layers and thickness. The yellow-filled cells are for the applied safety factor of 3.3, while the red filled cells are the number of layers rounded up.

G.2 Shear web iteration for each section of the blade

Shear web thickness iteration for section 1.

Iteration	V (N)	y (mm)	A (mm^2)	I (mm^4)	q (N/mm)	n (# of layers)	t @ (0.26mm per layer)
1	30517.6	128.7	2283.46	86055409.15	104.1940499	3.46	0.901
2	30517.6	129.4	2259.85	85834787.83	103.9602635	3.46	0.899
3	30517.6	129.4	2259.42	85830848.45	103.9532862	3.46	0.899
4	30517.6	129.4	2259.42	85830848.45	103.9532862	3.46	0.899
						11.41	3.194
						12	3.36

Shear web thickness iteration for section 2.

Iteration	V (N)	y (mm)	A (mm^2)	I (mm^4)	q (N/mm)	n (# of layers)	t @ (0.26mm per layer)
1	19660.8	81.8	1922.99	33744333.46	91.6607950	3.05	0.853
2	19660.8	82.5	1890.50	33552712.37	91.43544176	3.04	0.851
3	19660.8	82.6	1890.12	33550476.52	91.43423116	3.04	0.851
4	19660.8	82.6	1890.12	33550476.52	91.43423116	3.04	0.851
						10.03	2.809
						11	3.08

Shear web thickness iteration for section 3.

Iteration	V (N)	y (mm)	A (mm^2)	I (mm^4)	q (N/mm)	n (# of layers)	t @ (0.26mm per layer)
1	13408.5	66.7	1706.16	16417473.42	92.9712606	3.09	0.866
2	13408.5	67.2	1681.17	16344963.1	92.71927909	3.08	0.863
3	13408.5	67.2	1680.9	16344188.07	92.72257392	3.08	0.863
4	13408.5	67.2	1680.9	16344188.07	92.72257392	3.08	0.863
5	13408.5	67.2	1680.9	16344188.07	92.72257392	3.08	0.863
6	13408.5	67.2	1680.9	16344188.07	92.72257392	3.08	0.863
						10.17	2.849
						11	3.08

Shear web thickness iteration for section 4.

Iteration	V (N)	y (mm)	A (mm^2)	I (mm^4)	q (N/mm)	n (# of layers)	t @ (0.26mm per layer)
1	8945.2	61.8	1286.4	8184792.06	86.8571881	2.89	0.809
2	8945.2	62.5	1259.66	8152473.06	86.3840307	2.87	0.804
3	8945.2	62.5	1259.22	8151945.51	86.3732626	2.87	0.804
4	8945.2	62.5	1259.21	8151933.52	86.3727037	2.87	0.804
5	8945.2	62.5	1259.21	8151932.87	86.3727106	2.87	0.804
6	8945.2	62.5	1259.21	8151932.87	86.3727106	2.87	0.804
7	8945.2	62.5	1259.21	8151932.87	86.3727106	2.87	0.804
8	8945.2	62.5	1259.21	8151932.87	86.3727106	2.872	0.804143
						9.477	2.653672
						10	2.8

Shear web thickness iteration for section 5.

Iteration	V (N)	y (mm)	A (mm^2)	I (mm^4)	q (N/mm)	n (# of layers)	t @ (0.26mm per layer)
1	5718.4	52.4	1003.71	3259768.03	92.3159033	3.07	0.859
2	5718.4	53.0	983.16	3244020.43	91.8179697	3.05	0.855
3	5718.4	53.0	982.73	3243684.68	91.8046364	3.05	0.855
4	5718.4	53.0	982.75	3243701.90	91.8060174	3.05	0.855
5	5718.4	53.0	982.75	3243701.90	91.8060174	3.05	0.855
6	5718.4	53.0	982.75	3243701.90	91.8060174	3.05	0.855
7	5718.4	53.0	982.75	3243701.90	91.8060174	3.053	0.855
						10.074	2.821
						11	3.08

Shear web thickness iteration for section 6.

Iteration	V (N)	y (mm)	A (mm^2)	I (mm^4)	q (N/mm)	n (# of layers)	t @ (0.26mm per layer)
1	3467.6	42.3	754.29	1589907.41	69.5065815	2.31	0.647
2	3467.6	43.2	721.6	1573725.02	68.7044141	2.28	0.640
3	3467.6	43.2	721.03	1573441.09	68.6943126	2.28	0.640
4	3467.6	43.2	721.03	1573441.09	68.6943126	2.28	0.640
5	3467.6	43.2	721.03	1573441.09	68.6943126	2.28	0.640
6	3467.6	43.2	721.03	1573441.09	68.6943126	2.28	0.640
7	3467.6	43.2	721.03	1573441.09	68.6943126	2.28	0.640
						7.54	2.111
						8	2.24

Shear web thickness iteration for section 7.

Iteration	V (N)	y (mm)	A (mm^2)	I (mm^4)	q (N/mm)	n (# of layers)	t @ (0.26mm per layer)
1	2084.2	25.9	688.5	533327.32	69.7141973	2.32	0.649
2	2084.2	26.3	671.1	530654.09	69.2435779	2.30	0.645
3	2084.2	26.3	670.93	530627.16	69.2295507	2.30	0.645
4	2084.2	26.3	670.93	530627.16	69.2295507	2.30	0.645
5	2084.2	26.3	670.93	530627.16	69.2295507	2.30	0.645
6	2084.2	26.3	670.93	530627.16	69.2295507	2.30	0.645

7	2084.2	26.3	670.93	530627.16	69.2295507	2.302	0.645
						7.596	2.127
						8	2.24

Shear web thickness iteration for section 8.

Iteration	V (N)	y (mm)	A (mm^2)	I (mm^4)	q (N/mm)	n (# of layers)	t @ (0.26mm per layer)
1	1283.3	18.2	566.01	214345.75	61.7744745	2.05	0.575
2	1283.3	18.5	552.67	213457.19	61.4002633	2.04	0.572
3	1283.3	18.5	552.58	213451.46	61.3919125	2.04	0.572
4	1283.3	18.5	552.58	213451.46	61.3919125	2.04	0.572
5	1283.3	18.5	552.58	213451.46	61.3919125	2.041	0.572
						6.736	1.886
						7	1.96

Shear web thickness iteration for section 9.

Iteration	V (N)	y (mm)	A (mm^2)	I (mm^4)	q (N/mm)	n (# of layers)	t @ (0.26mm per layer)
1	750.9	14.6	333.63	81290.84	44.8706581	1.49	0.418
2	750.9	14.9	319.21	80654.31	44.3102429	1.47	0.413
3	750.9	14.9	319.09	80649.11	44.3261506	1.47	0.413
4	750.9	14.9	319.09	80649.11	44.3261506	1.47	0.413
5	750.9	14.9	319.09	80649.11	44.3261506	1.47	0.413
6	750.9	14.9	319.09	80649.11	44.3261506	1.474	0.413
						4.864	1.362
						5	1.4

Shear web thickness iteration for section 10.

Iteration	V (N)	y (mm)	A (mm^2)	I (mm^4)	q (N/mm)	n (# of layers)	t @ (0.26mm per layer)
1	345.0	13.3	120.26	25358.80	21.7304326	0.72	0.202
2	345.0	14.7	98.05	24174.16	20.5587070	0.68	0.191
3	345.0	14.7	97.77	24159.56	20.5403133	0.68	0.191
4	345.0	14.7	97.77	24159.56	20.5403133	0.68	0.191
						2.254	0.631
						3	0.840

APPENDIX H: VERIFICATION OF FEA DESIGN RESULTS

H.1 General

This appendix presents the verification of the FEA results that were used to perform the detail design on the wind turbine blade. Hand calculations were used in the preliminary design stage to determine the topology of the subcomponents of the blade. These hand calculations comprised the torsional shear flow formula to calculate the skin thickness at each section of the blade, the bending stress formula for the spar caps' thickness and width and the shear flow formula for shear forces to determine the thicknesses of the shear webs at each section of the blade. Equations represent the equations used to calculate the thicknesses of the respective subcomponents of the blade.

The torsion shear flow formula to calculate the skin thickness:

$$q_i = \frac{T_i}{2A_{mi}} \tag{H-1}$$

The bending stress formula to calculate the thickness and width of the spar caps:

$$\sigma_{bi} = \frac{M_i y_i}{I} \tag{H-2}$$

The shear flow formula for shear forces to calculate the thickness of the shear webs:

$$q_{shear\ web,i} = \frac{V_i \bar{y}' A'}{I_i} \tag{H-3}$$

The methods that the above-shown formulas used to determine the thicknesses of the respective subcomponents to obtain the design safety factor of 3.3 are shown in detail in Chapter 4. All of the above-mentioned hand calculations were performed to obtain a thickness for the respective subcomponents to produce a safety factor of 3.3, the design safety factor, at each section of the blade when loaded under the maximum loads as determined in Chapter 3. The skin, spar caps and shear web calculations are performed to meet the design safety factor when loaded under torsion, bending and shear forces respectively. Therefore, each of these subcomponents' topologies is only calculated for a single load, hence preliminary topologies.

These preliminary subcomponents topologies and respective loads are now used to verify the FEA model's results. Each of the subcomponents is modelled separately with the thickness distributions as determine in the hand calculations and FEAs are performed on each of them loaded under the previously mentioned respective loads. The fundamentals of this verification are to simulate the FEA exactly as performed in the hand calculations. The safety factor distribution results from the FEAs on each of the subcomponents are compared to that of the hand calculations which is the

design safety factor of 3.3. Figure H- 1 shows a layout to better explain the comparison of the hand calculations' safety factors with that of the FEA's.

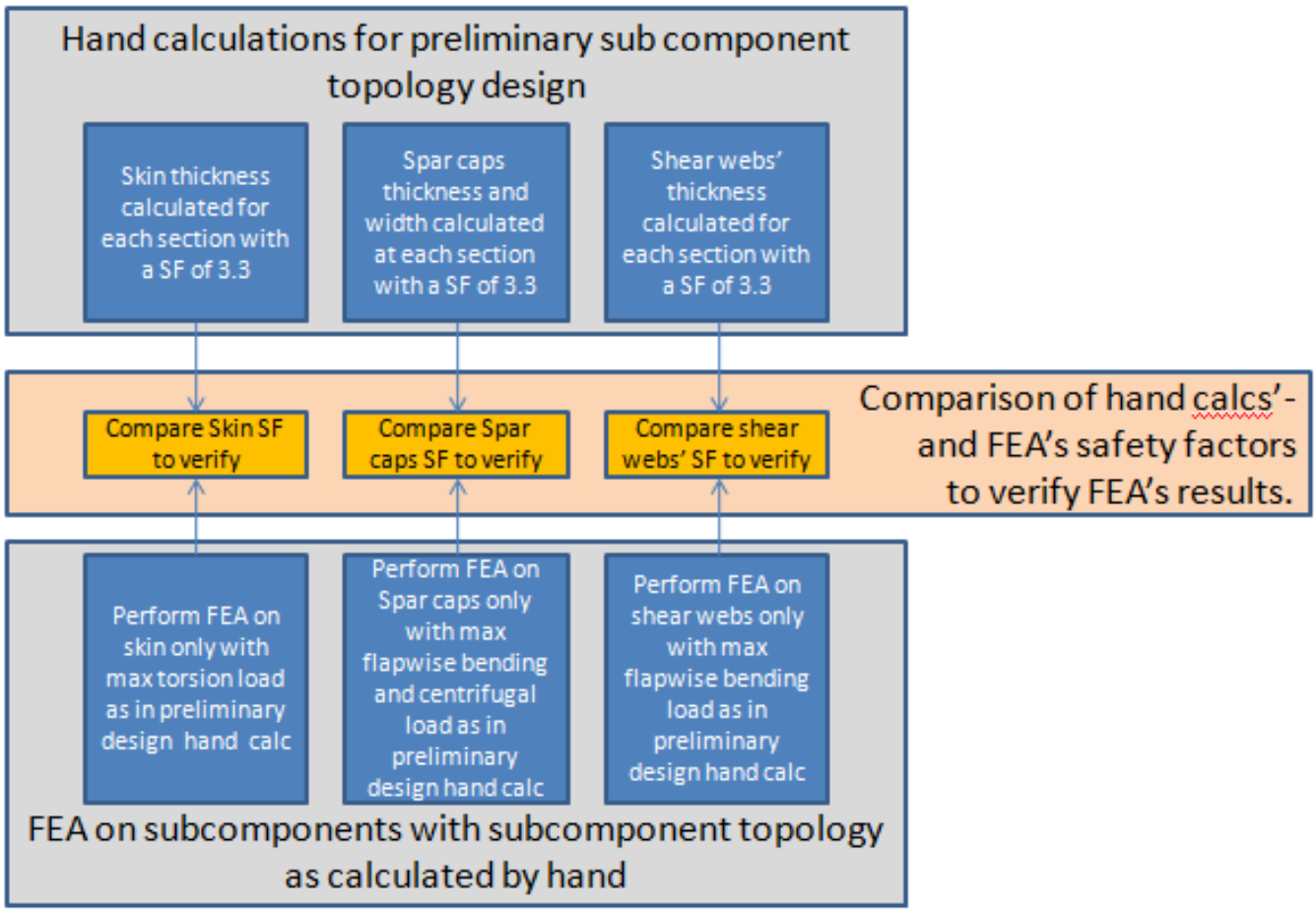

Figure H- 1: A representation of the design procedure to illustrate how the verification of the FEA results is performed

H.2 Verification results

The safety factor distributions results obtained from applying the torsion load to the skin of the blade proved be close to that of the hand calculations of 3.3 as presented in Figure H- 2. The small deviations in the FEA's= safety factor from that of the hand calculations is caused by the drastic geometric variations between the sections which was not accounted for in the calculations. This occurrence is seen at section 7 where the airfoil thickness drastically decreases from that of section 6. High stress concentrations are also visible at the root of the blade due to the drastic geometry change.

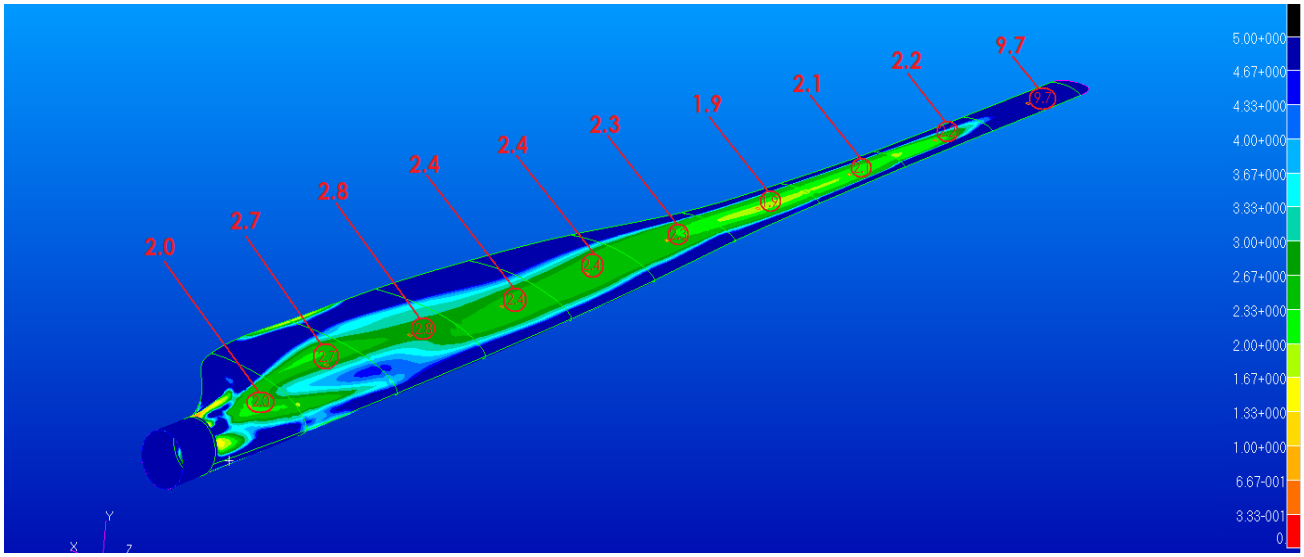

Figure H- 2: The preliminary design's safety factor distribution results in the blade's skin

The safety factor distribution results for the spar caps exposed to Load case C's flapwise bending forces also closely correlated to that of the hand calculations' safety factor of 3.3 as seen in Figure H- 3. Note that the spar caps' thickness at each section was determined at the point on the inner surface of the blade's skin perpendicular to the chord line at the quarter chord point as presented in Figure H- 4. Therefore, the safety factor results from the FEA only match that of the calculated value at this point due to the variation of the airfoil thickness from the leading to the trailing edge.

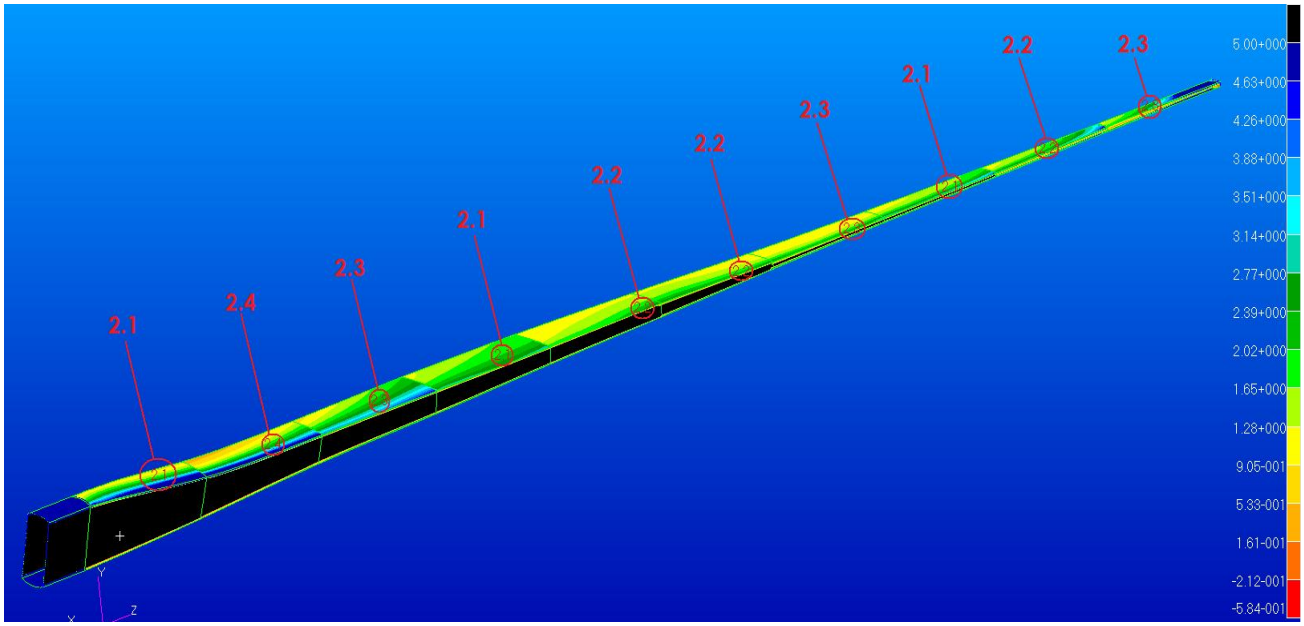

Figure H- 3: The safety factor distribution result of the spar caps under Load case C's flapwise bending forces

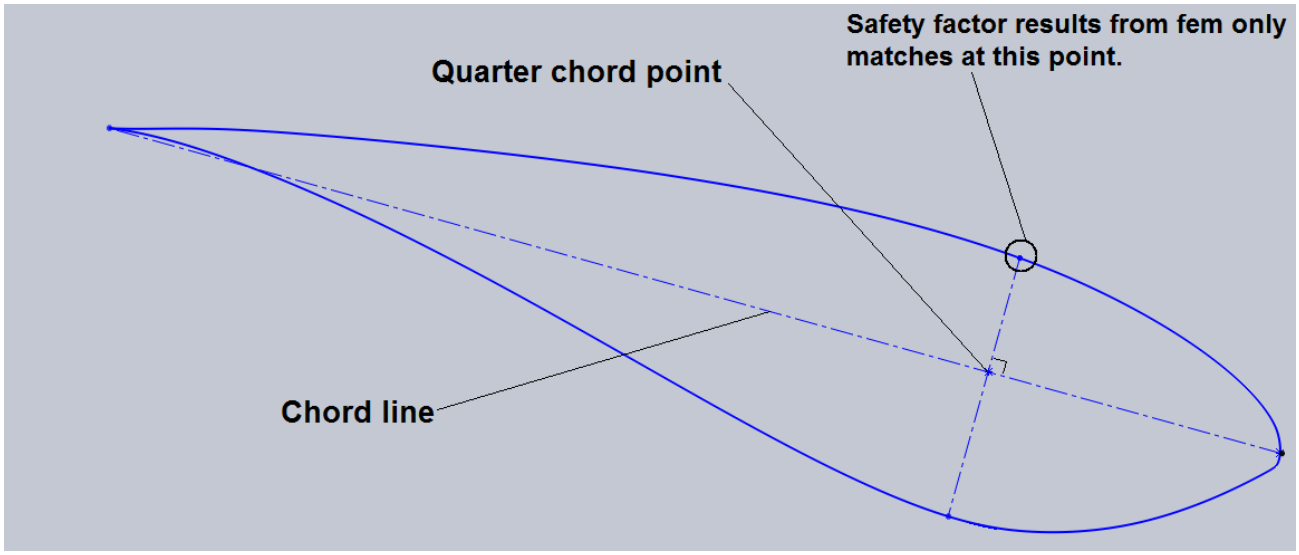

Figure H- 4: A presentation of the point where the bending stress was used to determine the spar caps' thickness at each section of the blade and thus the point where the FEA's safety factor matches that of the calculated design safety factor

The shear webs also shows a correlation to the calculated design safety factor as per hand calculations. However, the safety factor distribution results show low values at the root section, though this could be sourced to the drastic geometry change at the root end of the blade causing stress concentrations as seen in Figure H- 5.

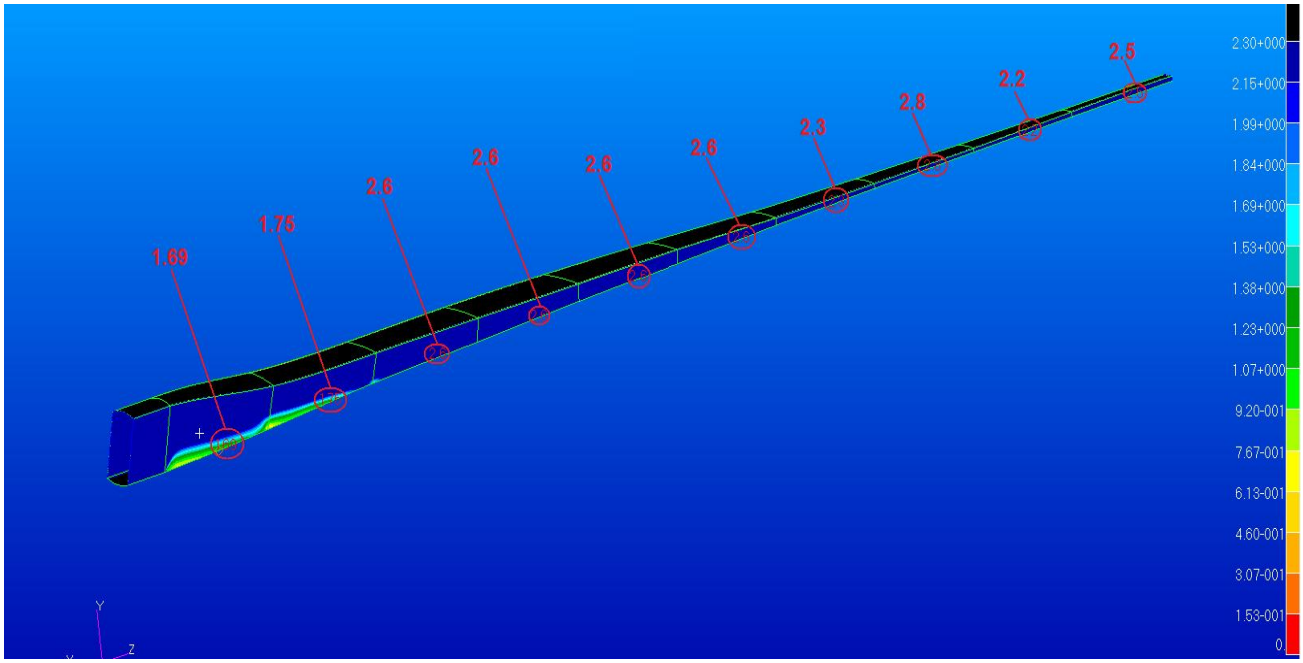

Figure H- 5: The safety factor distribution results of the shear webs

The safety factor distribution results of all the structural subcomponents of the blade thus showed a good correlation with that of the hand calculations and the design safety factor of 3.3. It is therefore accepted that the FEA results are verified and that the material properties, loads, layup sequence,

layup orientation and mesh are applied correctly and that the FEA of the model provides acceptable results.

APPENDIX I: VALIDATION OF FEA DESIGN METHOD

I.1 General

The FEM method used to design the structure of the wind turbine blade in this thesis is validated here. The method followed was to model an existing propeller blade using the same FEM methods, after which the propeller was structurally loaded and the deflection results compared with the FEM results.

I.2 FEA model

The model of the existing composite propeller blade was constructed in Solidworks and the blade divided into a finite number of sections similar to that of the wind turbine blade model as seen in Figure I- 1.

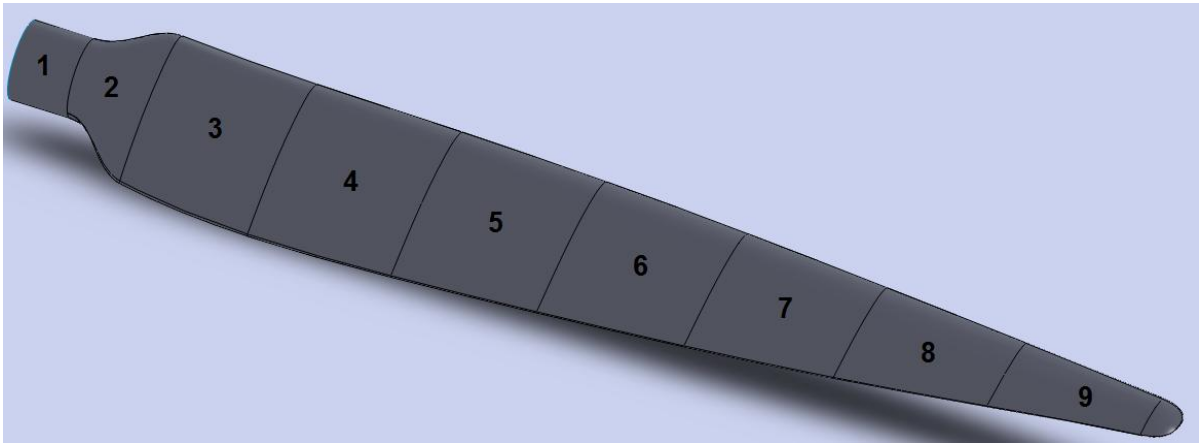

Figure I- 1: The propeller blade divided into a finite amount of sections similar to the wind turbine blade

Material properties, layup, orientation and thicknesses are applied to the propeller in the same manner as in the design of the wind turbine blade. The layup schedule of the propeller is known and is presented in Table I- 1.

Table I- 1: The layup schedule and surface area of each section of the composite propeller blade

PROELLER LAYUP SCHEDULE			
Section	**Area(mm^2)**	**BID CARBON (# of layers)**	**UD CARBON (# of layers)**
1	17987.32	5	4
2	24685.49	5	4
3	27160.21	4	4
4	26530.15	4	4
5	24880.61	4	3
6	12013.56	4	3
7	17754.21	4	2
8	11814.29	4	2
9	1633.74	4	2

The displacement constraints and flapwise bending load applied to the verification model were applied similarly to those applied to the wind turbine blade. Thus, the root end of the propeller is also constrained by applying a zero degrees of freedom constraint to all the nodes in the root of the blade. The flapwise bending load is also applied by dividing the load magnitude by the number of nodes at the application region. Forces with a magnitude of this divided load are then applied to each of the nodes at the application region. The FEA model of the propeller showing the constrained root end and the flapwise bending load is presented in Figure I- 2.

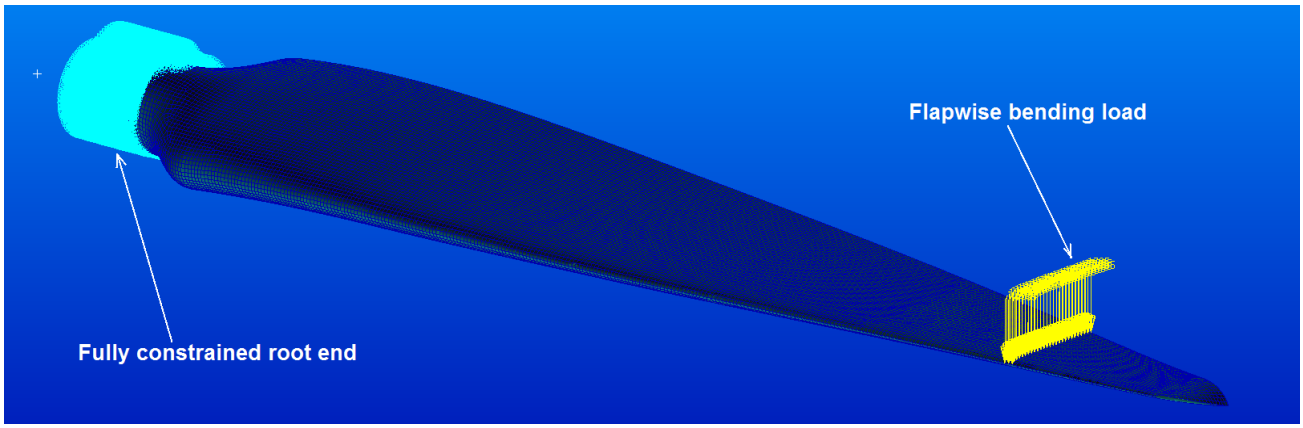

Figure I- 2: The FEA model of the propeller blade showing the root constraint and the flapwise bending load

I.3 Full-scale test setup and results

The full-scale test is set up to simulate the FEA model. The root end of the blade is thus constrained in a hub which is bolted to a fixed platform. The flapwise bending load is applied to the blade by hanging the weights on the blade at the same region as the loads applied to the FEA model. A clamp was manufactured to be fixed to the blade at the application region. The weights

are thus suspended from this clamp, applying the load in the desired direction. The setup of the blade with the constrained root and the weight suspended from the clamp at the application region is presented in Figure I- 3. Figure I- 3 also presents the setup of the micrometer used to measure the tip deflection of the blade.

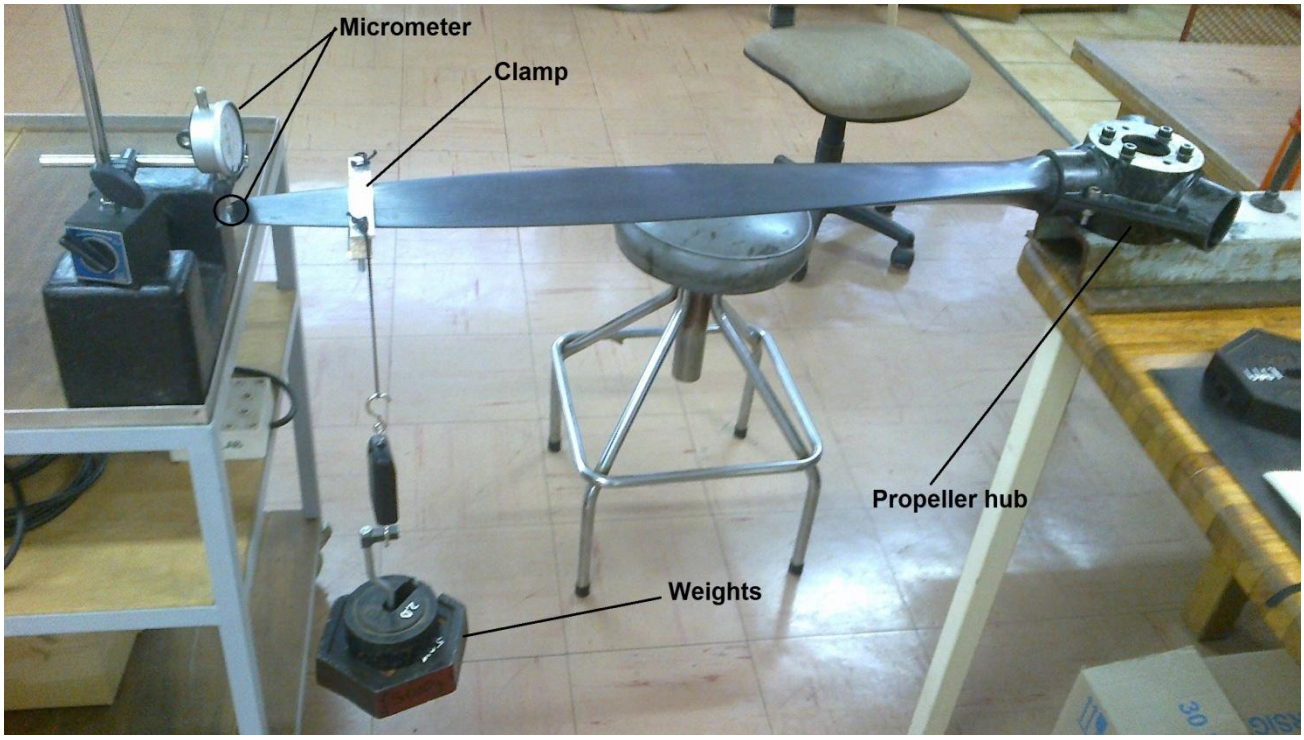

Figure I- 3: A presentation of the full-scale test setup of the composite propeller blade

The mass of all the test components that contributed to the weight applied to the blade were measured with a certified scale. The scale provided the mass to four decimal numbers as presented in Figure I- 4.

Figure I- 4: Weighing all the components that contribute to the mass applied to the blade

The tip displacement was measured initially with all the components suspended from the blade, except the steel weights. This displacement is noted as the base displacement as all five tests included these components. Additional weights were added to the setup to simulate five different loads applied to the blade. The mass of the all the components except the steel weights are presented in Table I- 2. The initial tip displacement caused by these weights is also shown.

Table I- 2: The mass of each of the base components and the initial tip deflection caused by these weights

Base components	Mass [kg]
Clamp	0.076
Steel Mass suspender	0.249
Pull scale	0.1079
Total	0.4329
Tip deflection due to base components' weight	0.22 mm

The micrometer was zeroed after the base deflection was measured. Thus, the five different weights were added after the micrometer was zeroed and the tip deflections for each of these weights were measured from zero. Table I- 3 presents the tip deflections measured twice for each of the five different weight scenarios. The tip deflection results simulated for the combination of the base mass added to the five different weights are also presented in Table I- 3. The percentage

differences for all five loading scenarios are logged and an average difference considering all the scenarios is determined.

Table I- 3: The tip deflection results obtained from the FEA and the full-scale tests

Tip deflection results						
Scenario	Mass of steel weight applied [kg]	Tip deflection test 1 [mm]	Tip deflection test 2 [mm]	Avg. of two tests + Base [mm]	FEA result[mm]	Difference [%]
1	1	0.67	0.67	0.89	0.95	6.32
2	2	1.36	1.38	1.59	1.62	1.85
3	3	2.09	2.08	2.305	2.29	0.66
4	5	3.54	3.55	3.765	3.63	3.72
5	7	4.65	4.99	5.04	4.96	1.61
					Average difference %	2.83

The tip deflection results for the FEA and the full-scale test are therefore plotted on a graph as seen in Figure I- 5. The results plotted in Figure I- 5 shows a close correlation between the FEA and practical results as both methods follow the same trend line in the tip deflection under the different loads. This correlation therefore proves that the methods applied to perform the structural design and analysis of the wind turbine blade in this thesis is valid.

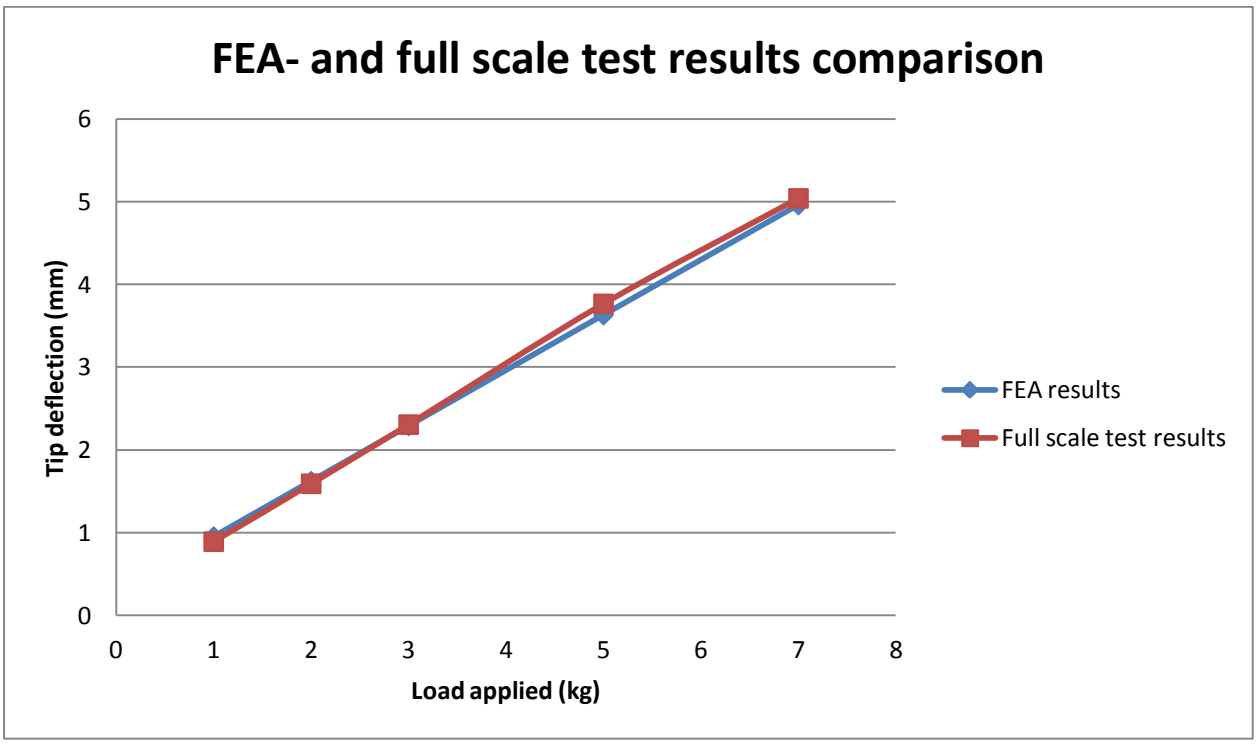

Figure I- 5: Graph showing the tip deflection results comparison between the FEA and the full-scale tests

I.4 Validation of mass calculation method

The method for calculating the mass of the blade designed in this thesis was validated by comparing the calculated weight, using the same methods as in Chapter 4, section 4.6, with that obtained from weighing the existing propeller blade. The propeller blade is also divided into a finite number of sections, nine in this case, as presented in Figure I- 6. Note that section 9 includes the tip of the blade.

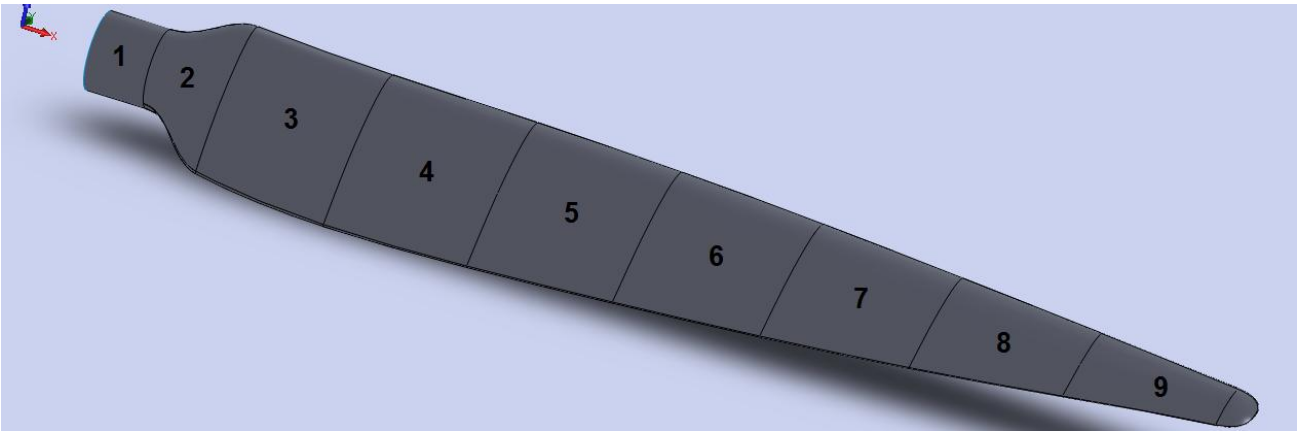

Figure I- 6: The propeller blade divided into a finite amount of sections similar to the wind turbine blade

The layup schedule for each section of the propeller is presented in Table I- 4. The surface area of each section is also provided in Table I- 4.

Table I- 4: The layup schedule for each section of the existing composite propeller blade

PROELLER LAYUP SCHEDULE			
Section	**Area(mm^2)**	**BID CARBON (# of layers)**	**UD CARBON (# of layers)**
1	17987.32	5	4
2	24685.49	5	4
3	27160.21	4	4
4	26530.15	4	4
5	24880.61	4	3
6	12013.56	4	3
7	17754.21	4	2
8	11814.29	4	2
9	1633.74	4	2

The mass of each section is thus calculated with equation (5-4), which is the same as equation 32 in Chapter 4, section 4.6.

$$m_i = \rho_m A_i n_i \qquad (6\text{-}2)$$

where,

ρ_m is the density of the material (UD or BID carbon fibre) per unit area (kg/mm^2)

A_i is the surface area of section i (mm^2)

n_i is the number of layers of the respective material in section i.

The propeller blade also consists of a solid foam core and its mass is calculated from the density of the foam and the solid volume of each section as performed in Chapter 4, section 4.6. The mass of the resin is also included as for the wind turbine blade. The mass of the resin is applied by multiplying the mass of the fibre layers with a factor of 2. The propeller blade also contains a carbon fibre insert in the root of the blade to increase the strength of this part of the blade. The mass of this component is not calculated but the measured mass of it was included in the calculation of the total mass of the blade. The calculated mass of the blade is presented in Table I- 5.

Table I- 5: The mass calculated of the existing composite propeller blade

PROPELLER MASS (KG)				
Section	**BID LAYERS WEIGHT**	**UD LAYERS WEIGHT**	**FOAM WEIGHT**	**Total**
1	0.05	0.03	0.01	0.10
2	0.08	0.04	0.02	0.14
3	0.07	0.05	0.02	0.13
4	0.06	0.04	0.01	0.12
5	0.06	0.03	0.01	0.10
6	0.03	0.02	0.01	0.05
7	0.04	0.01	0.00	0.06
8	0.03	0.01	0.00	0.04
9	0.00	0.00	0.00	0.01
			Root insert mass	0.086
			Total blade mass	**0.826**

The mass of the composite blade was measured and its mass proved to match the calculated results. The measured mass of the blade is 0.82 kg. Thus, the method for calculating the mass of the blade is validated as the results from the mathematical calculation and the practical measurements correlate with a 1% deviation.